Remote Sensing of Water Quality Parameters in Zeekoevlei, a Hypertrophic, Cyanobacteria-Dominated Lake, Cape Town, South Africa

Mark William Matthews

Thesis Presented for the Degree of

MASTER OF SCIENCE

In Environmental and Geographical Science

UNIVERSITY OF CAPE TOWN

February 2009

Acknowledgements

My God and Father and the Lord Jesus Christ for lots of little, and big, breakthroughs. Lauren, my lovely wife, for continual love, prayer and support. Stewart Bernard for excellent advice, invaluable suggestions, and help organising the fieldwork and MERIS data. Kevin Winter for initial conception of the thesis, funding money, and helpful guidance. My parents, Geoff and Shelagh, for encouragement and supporting me financially. Dr. Trevor Probyn, Andre Du Randt and others at the Marine and Coastal Management laboratories for generously providing labspace and equipment to conduct my analysis at short notice. Trey Smith, Assief Khan and the interns at the Zeekoevlei Nature Reserve for assistance with fieldwork. Candice Haskins and the City of Cape Town Scientific Services for the long-term water quality data for Zeekoevlei. Annick Bricaud for the Chl *a* specific absorption/backscattering spectra. Others whom I have not mentioned who helped with various tasks.

For funding: The Harry Crossley Postgraduate Fund, the Twalmley Postgraduate Bursary and the KW Johnstone Research Scholarships.

Abstract

Globally widespread eutrophication and harmful cyanobacterial algal blooms have degraded the condition of many of the earth's freshwater resources. In water scarce South Africa, many recreational and water supplying reservoirs are increasingly at risk from these threats. Zeekoevlei Lake, situated south of the City of Cape Town, is an archetype of a severely degraded, permanently hypertrophic and cyanobacteria dominated lake. This study aims to use satellite remote sensing to monitor and provide information on water quality parameters and cyanobacterial algal blooms in Zeekeovlei. Development of remote sensing tools will contribute towards understanding system processes and improving management of cyanobacterial algal blooms which may be toxic. The primary challenges for remote sensing in Zeekoevlei are the extremely high concentrations of covariant water constituents and its very small size (2.6Ha). This presents difficulties with algorithm development, especially differentiating between water constituents, and atmospheric correction. The study combines multispectral MERIS and Landsat 7 ETM+ data with *in situ* measurements of Chl a; total suspended solids; organic/inorganic suspended solids; absorption by CDOM; and Secchi Disk depth. Upwelling radiance and downwelling irradiance were measured *in situ* with a hyperspectral radiometer. Empirical algorithms for estimating the variation in water quality parameters generated from simultaneous field and remote measurements had significant correlation coefficients. The MERIS Level 2 Product and Eutrophic Lakes Processor Neural Network algorithms produced erroneous and invalid results. Maps produced from the satellite images reveal the synoptic variability and temporal trends of the parameters. The maps gave more accurate estimates of the mean spatial water quality parameters than the small number of *in situ* sample sites. The results indicate that MERIS, being designed for water applications, is far better suited than Landsat, and similar sensors, for frequent monitoring and change detection in Zeekoevlei. This is due to MERIS's higher acquisition frequency, free data availability, spectral arrangement, and higher signal-to-noise ratio. The study's success is not without consideration of the limitations of the small data set. Recommendations concerning future requirements for algorithm development, and the integration of real-time/operational remote water quality monitoring systems in southern Africa, are made.

Table of Contents

Chapter 1 Introduction

Water quality in almost all regions of the world has deteriorated through intensifying agriculture and the growth of urban and industrial areas (Revenga et al., 2000). Major problems related to hydromorphological alterations, eutrophication, turbidity, and the input of sewage are found in freshwater resources worldwide (Sondergaard & Jeppesen, 2007). Water scarcity is a problem experienced by an estimated more than 2 billion people worldwide, despite increasing water extraction from thousands of large dams. Without water in sufficient quantity and of acceptable quality, the future existence of both humankind and wildlife is threatened (Lozan et al., 2007). One of the most critical and greatest challenges of the 21st century will be meeting the world's growing demand for water while maintaining the health and functioning of aquatic systems (Postel, 2000).

Eutrophication is defined as an enhancement of the natural process of biological production in water resources resulting from increased concentrations of nutrients, usually phosphorus and nitrogen compounds (Vollenweider, 1968). Eutrophication stimulates the rapid growth of algae and aquatic plants which leads to anoxia and fish kills, causes turbid water conditions with unpleasant tastes and odours, increases accumulation of organically rich sedimentation and promotes the dominance of certain algal or macrophyte species. Eutrophication also has dramatic effects on the composition and structure of food webs and causes significant alterations in biogeochemical cycling over space and time. There is clear evidence that eutrophication stimulates some types of Harmful Algal Blooms (HABs) which have deleterious effects on ecosystem functions through accumulated biomass or toxin production (Hasler, 1947, Anderson et al., 2002, Smith et al., 2006). Hyper-eutrophication, or hypertrophy, exists where there is severe impairment of normal water uses resulting from these ill effects (Janus & Vollenweider, 1981).

Algae belonging to the class cyanophyceae, commonly known as cyanobacteria or blue-green algae, often make up an increasing percentage of the phytoplankton population in eutrophic conditions (Bartram et al., 1999, Downing et al., 2001). Blooms of cyanobacteria are known as the "scourge of water management" because of the dense cell accumulations that form thick surface scums or mats and because of their production of toxins (Visser et al., 2005 p.109). Poisonings by cyanotoxins, the name given to toxins produced by cyanobacteria, have resulted in animal kills and when ingested by humans in drinking water, have been shown to affect both morbidity (illness) and mortality (Falconer, 2001). Thus eutrophic lakes exhibiting dominance by

cyanobacterial species of algae pose a serious health risk to humans and animals that use the water for drinking or recreation.

In South Africa surface freshwater is limited because of the semi-arid climate. The deterioration in quality of surface water is "one of the major threats to South Africa's capability to provide sufficient water… to meet its needs and to ensure environmental sustainability" (DWAF, 2004a p.20). Eutrophication has long been recognised as a threat throughout South Africa, severely degrading and affecting the fitness for use of certain water resources (du Plessis & van Veelen, 1991, DWAF, 2003, de Villiers & Thiart, 2007). Along with eutrophication, toxic cyanobacterial algal blooms found in many of South Africa's freshwater impoundments are "a threat to the supply of safe drinking water to the whole population of South Africa" (Van Ginkel, 2004 p.41) with reported incidence of animal poisonings in almost all regions (Harding & Paxton, 2001, Oberholster et al., 2005). These problems can be controlled by reducing nutrient input from anthropogenic sources, such as sewage and agricultural runoff (Carpenter et al., 1998). However, interim measures need to be taken to improve knowledge and understanding of system processes, and to minimise the risks through better management, prediction and observation.

South Africa's policy on water states that "ongoing monitoring and assessment [is] critical to our ability to manage and protect [water] resources on the basis of sound scientific and technical information and understanding. Adequate information is essential for effective resource management and protection" (DWAF, 1997 p.6.8). Consequently, more resource quality information and sophisticated information products are required to determine the status of water resources, and to achieve quality objectives (Grobler & Ntsaba, 2004). The recent launch of many new satellite instruments, and advances in computer technologies, has greatly increased the range of successful water-related remote sensing applications, and improved real-time monitoring of water quality and the rapid detection of environmental threats from eutrophication and HABs (Mertes, 2002, Glasgow et al., 2004). Remote sensing provides an estimation of the geo/biophysical properties of the earth's surface features through analysis of the intensity and spectral distribution of the upwelling electromagnetic radiation, and has substantial advantages over traditional natural resources management monitoring methods, mainly because of the synoptic coverage and temporal consistency of the data (Navalgund et al., 2007). Remote sensing applications have immense potential benefits for the developing world, particularly in Africa, where conventional natural resource management and water quality monitoring programmes are either lacking or unsatisfactory. South Africa, like many developing countries, has lagged behind advances in remote sensing when compared to the developed world.

While water remote sensing studies have concentrated largely on the marine environment, particularly chlorophyll *a* (Chl *a*) retrieval in the oceans, comparatively little attention has been given to inland water bodies, especially freshwater lakes. These inland lakes belong to the so-called 'Case 2' waters which are optically more complex than 'Case 1' waters which typically exist in the open ocean[*] (Morel & Prieur, 1977). There are significant challenges for remote sensing in inland and nearshore coastal areas, especially concerning sensor requirements and water and atmospheric properties retrieval algorithms. There is also a need for calibration and validiation systems, *in situ* databases, and increased data access, disemmination and useability (GEO, 2007). The two approaches for deriving water quality products from remotely sensed data are the empirical and semi-analytical approaches (Lindell et al., 1999, Sathyendranath et al., 2000). The empirical approach relies on experimental data sets and statistical regression techniques to derive algorithms for estimating water quality from the remotely sensed signal. This requires the simultaneous acquisition of limnological, atmospheric, and remotely sensed data. The semi-analytical approach is more complex and uses mathematical models that generate combined water constituent and atmospheric properties retrieval algorithms based on radiative transfer simulations of light propagation through the water and atmosphere. A variety of mathematical procedures are used to solve the inverse model which derives water constituent and atmospheric properties from the remotely sensed signal independent of simultaneous *in situ* data (Neumann et al., 2000).

This study mainly uses the empirical approach, with data from a hyperspectral radiometer, and the multispectral Medium Resolution Imaging Spectrometer (MERIS) and Landsat Enhanced Thematic Mapper (ETM+) satellite sensors, to monitor eutrophication, cyanobacterial algal blooms, and water quality, in a small inland freshwater lake. Image-based techniques and a radiative transfer model are used to correct for atmospheric effects, which contribute significantly to the radiance measured outside the atmosphere. Fieldwork measurements of the main substances affecting the water-leaving radiation coincided with remote measurements. Water constituents and atmospheric properties retrieved by the MERIS Case 2 water semi-analytical algorithm (Schiller & Doerffer, 2005) were tested using comparisons with field measurements. Although the study uses both empirical and semi-analytical procedures, the empirical approach

[*] In Case 1 waters phytoplankton is the major contributor to the optical properties while in Case 2 waters there are significant contributions from dissolved organic matter and/or *tripton* as well as phytoplankton.

was used primarily, as a full development of semi-analytical procedures was deemed beyond the scope of a Masters research thesis.

The site of investigation is Zeekoevlei, a small freshwater lake situated on the Cape Flats south of the City of Cape Town in the Western Cape Province, South Africa. Zeekoevlei, literally translated from Dutch meaning "Hippo Lake", is an important local recreational and conservational resource for the City. However it is severely impaired with extensive loss of natural habitats and basic ecosystem functions (Southern Waters Ecological Research and Consulting, 2000). Nutrient enrichment from domestic and agricultural sources means that the lake is hypertrophic and displays year-round near-permanent dense blooms of cyanobacteria algae, dominated by the species *Microcystis aeruginosa* (Harding, 1992). The lake is among the most productive in the world with very high rates of primary production and extremely high algal biomass (Harding, 1996). The reported death of a dog by cyanotoxin poisoning in 1995 may suggest that Zeekoevlei presents an environmental heath threat to humans using the lake for recreation (Harding et al., 1995). Rehabilitation measures are already underway to reduce the input of nutrients from internal and external sources. The severe hypertrophic and cyanobacteria dominated conditions make Zeekoevlei an ideal study area for developing remote sensing methods to better observe and increase understanding of these environmental threats. However, its small size presents significant challenges related to the sensor spatial resolutions and atmospheric contributions from the adjacency effect.

The rationale for this thesis hinges on two major water resource problems faced in southern Africa and around the world. These are: 1) the deterioration in the quality of freshwater surface resources, including widespread eutrophication and cyanobacterial algal blooms, which present risks to human and animal health; and 2) the need for more advanced information products concerning the state of freshwater resources. The research question is as follows:

"Are current operational earth observation satellites able to monitor water quality, hyper-eutrophication and cyanobacterial algal blooms in a small inland freshwater lake with a degree of confidence?"

The aim of the research is to enhance understanding and monitoring of the dual threats of eutrophication and cyanobacterial algal blooms in Zeekoevlei Lake, by providing progressive remote sensing information products. The project is an initial investigation of techniques that

could in future be used for routine monitoring of inland freshwater resources using remote sensing in southern Africa. The specific project objectives are:

1 Determine the suitability of various multispectral satellite sensors for monitoring eutrophication, cyanobacterial algal blooms, and other water quality parameters in Zeekoevlei
2 Assess the water quality conditions in Zeekoevlei and determine the influence of water constituents on the water-leaving reflectance
3 Derive empirical algorithms and assess the performance of Case 2 semi-analytical algorithms for water constituent retrieval
4 Produce synoptic water quality maps from multispectral satellite data

The achievement of the objectives allows the investigation of the synoptic distribution and temporal variation of cyanobacterial algal blooms, and other water constituents, in Zeekoevlei. A statistical assessment is used to determine the improved accuracy afforded to mean water quality parameter estimates made from synoptic remote sensing maps, as compared to mean estimates made from a small number of *in situ* sample sites. Recommendations concerning future routine processing requirements and research needs in southern Africa are also made.

This introductory chapter is followed by a literature review detailing the problems of eutrophication and cyanobacterial algal blooms in freshwater lakes, and investigating how Zeekoevlei typifies these problems (Chapter 2). Chapter 3 reviews remote sensing instruments; basic remote sensing physics including in-water optical properties; and, the empirical and analytical approaches. It includes a comprehensive review of inland and coastal Case 2 water empirical algorithms, and atmospheric correction procedures. Chapter 4 outlines the project methodology and Chapter 5 presents the main findings. The degree to which the project aims and objectives have been achieved is discussed in Chapter 6, and the final chapter, Chapter 7, presents the conclusions and recommendations concerning future requirements for water remote sensing in southern Africa.

Chapter 2 Eutrophication, Cyanobacterial Algal Blooms and Zeekoevlei Lake

Water is part of all vital processes on the earth and is essential for life. Freshwater resources are in crisis as a consequence of major problems arising from global water scarcity, rising demand from population growth, the degradation of water quality through pollution, and the increasing destruction caused by water related disasters (UNESCO, 2003). Only 2.5% of the total volume of water on the earth is fresh and it is estimated that only 1% of this is suitable for human use, much of which is located far from human populations. Only 0.26% of the earth's freshwater resides in lakes, reservoirs and rivers that are the main water sources for humans (Shiklomanov 1993 cited by Gleick, 2000). Worldwide there are an estimated 304 million natural lakes comprising an area of 4.2 million km^2, at least 500 000 large, engineered impoundments covering 260 000 km^2, and 77 000 km^2 covered by small impoundments (Downing et al., 2006). It is estimated that more than 3% of the earth's continental land surface is covered by surface water in the form of lakes and impoundments. Despite the fact that large volumes of water are stored and withdrawn for human consumption, many people still live in water stressed conditions (Revenga et al., 2000). Furthermore, climate change and global warming is likely to lead to decreased water availability and increasing frequency of water-related natural disasters (IPCC, 2008).

Demand for freshwater resources is expected to severely degrade the condition of aquatic systems worldwide (Postel, 2000). The estimated trillions of US dollars that freshwater ecosystems deliver in goods and services have been grossly undervalued, and consequently, these ecosystems are being intensely modified and degraded by human activities (Revenga et al., 2000, Johnson et al., 2001). Overexploitation, pollution, habitat alteration and destruction, alien species invasion, and global change, are some of the main causes of freshwater species decline and ecosystem degradation (Brönmark & Hansson, 2002, Malmqvist & Rundle, 2002, Dudgeon et al., 2005, Revenga et al., 2005, Sondergaard & Jeppesen, 2007). Furthermore urban sprawl, population growth, and land use change, also have substantial negative effects on water quality (Tong & Chen, 2002, Allan, 2004, Tu et al., 2007). In lakes and ponds of the developing world 'old' threats like eutrophication, acidification, and toxic contamination are likely to become more severe in the near future, while 'new' threats such as global warming, UV radiation, exotic species invasion and endocrine disruptors are also becoming increasingly significant (Brönmark & Hansson, 2002). For example, climate change will not only affect water availability and distribution but will also alter structure, functioning and health of freshwater ecosystems (Meyer et al., 1999, Blenckner, 2007). Consequently, the species that inhabit them are threatened and it is predicted that by 2025 biodiversity in fresh waters will have diminished considerably (Brönmark & Hansson, 2002).

Water quality is a function of the physical, chemical and biological characteristics of water, such as its temperature, its chemical composition and concentration of nutrients, and the living organisms that reside in it (Jian & Sharma, 2005). These and other characteristics determine the suitability and value of water for its intended use (Dallas & Day, 2004). Water quality is therefore a 'human construct' defined as the suitability of water to sustain various uses or processes (Meybeck et al., 1996). Water quality becomes unacceptable when it is unable to sustain the use for which it is intended, be it for human consumption or recreational purposes, or maintenance of eosystems. Natural factors cause variability in the characteristics of water in a lake through landscape features such as geology, topography, and soils and climatic conditions, such as rainfall and atmospheric contributions (U.S. Geological Survey, 2005). This may produce large seasonal variations in water quality according to the seasonal hydrological patterns (Meybeck et al., 1996). However, anthropogenic impacts on water quality have far outweighed these natural variations.

2.1 Eutrophication of Freshwater Resources

One of the foremost problems facing freshwater ecosystems in the 21st century is eutrophication. The term eutrophication means "well-nourished" and comes from the Greek words *eu* meaning "well" and *trophe* meaning "nourishment". The term eutrophication was first used by the German scientist C.A. Weber in 1907 to describe the appearance of peat bogs. Weber developed a simple trophic (literally 'feeding') classification system that Numann (1919) later modified for lakes (Jeffries & Mills, 1990). The term 'cultural eutrophication' was used to refer specifically to nutrient input to aquatic systems from anthropogenic origins such as sewage, detergents, urban run-off and agricultural fertilizers (Hasler, 1947). It was only in the 1960s however, that scientists linked the biological production responses of eutrophication, such as algal blooms and decreased water clarity, to nutrient enrichment by nitrogen and phosphorus (Vollenweider, 1968, Schindler, 2006).

The trophic status of a lake refers to the rate that organic matter is supplied by or to the lake per unit time (Wetzel, 1983). Thus, a lake may be classified as 'oligotrophic', little-nourished, 'mesotrophic', medium-nourished, 'eutrophic', well-nourished, or 'hypertrophic', very well-nourished. The Organisation for Economic Co-operation and Development (OECD) classification system for lakes is based on trophic response indicators such as phytoplankton biomass (Chl *a* concentration), water clarity (Secchi Disk depth) and the concentrations of nitrogen (N) and phosphorus (P) (Janus & Vollenweider, 1981, OECD, 2002). The OECD models are broadly

applicable in the South African context and a similar classification system is used for South African lakes (See Table 2.1) (Walmsley & Thornton, 1984).

Table 2.1 South African trophic classification of lakes based on mean annual water quality variables (DWAF, 2002).

Variable	Unit	Oligotrophic	Mesotrophic	Eutrophic	Hypertrophic
Chl *a*	$\mu g.\ell^{-1}$	0 - 10	10 - 20	20 - 30	> 30
Time Chl *a* > 30 $\mu g.\ell^{-1}$	%	0	0 - 8	8 - 50	> 50
Total P	$mg.\ell^{-1}$	≤ 0.015	0.015 - 0.047	0.047 - 0.130	> 0.130
Cyanobacteria in phytoplankton population	%	0 – 1	1 – 10	10 – 50	> 50

Eutrophication is a consequence of poorly controlled human activity in a water catchment and is virtually inseparable from other problems of water pollution (Davies & Day, 1998). Anthropogenic nutrient input is commonly expressed as originating from point and non-point sources (Carpenter et al., 1998). Point sources are those that can be easily identified and therefore easily regulated and controlled, such as wastewater treatment outflow pipes and storm water outlets. Non-point sources are more difficult to identify because they occur over large areas of land or are derived from the atmosphere. In South Africa, and many parts of the world, point-source pollution is still a substantial source of nutrients (Morrison et al., 2001, Ogunfowokan et al., 2005), such that non-point sources are usually not significant in comparison to point sources (Wiechers & Heynike, 1986). However, the accumulation of phosphorus in soils may lead to increased non-point input from runoff, and in the United States an estimated excess of 80% of all N and P discharges to surface waters are derived from non-point sources (Carpenter et al., 1998, Bennett et al., 2001).

The impacts associated with eutrophication are diverse and destructive (See Table 2.2) (Priyadarshi, 2005, Schindler, 2006, Smith et al., 2006). In broad terms, eutrophication impacts negatively on the ecological, aesthetic, recreational, human health, and economic utilities of an aquatic resource (DWAF, 2002). These impacts pose a significant threat to ecosystems and freshwater supply for human use.

Table 2.2 Adverse effects on lakes, reservoirs, rivers caused by eutrophication (after Carpenter et al., 1998, modified from Smith et al., 2006).
Increased biomass of phytoplankton
Accumulation of organic rich sediment
Changes in biochemical cycling
Loss of biodiversity through shifts in aquatic food webs
Shifts to turbid, phytoplankton dominated water conditions
Shifts in phytoplankton to bloom-forming species that may be toxic or inedible
Increased biomass of benthic and epiphytic algae
Changes in macrophyte species composition and biomass
Decreases in water transparency
Taste, odour and water treatment problems
Oxygen depletion (anoxia)
Increased incidence of fish kills
Loss of desirable fish species
Decreases in perceived aesthetic value of the water body

Eutrophication continues to be a major problem in lakes in developing countries around the world and remains one of the greatest challenges to limnologists and scientists (Brönmark & Hansson, 2002, Schindler, 2006). Moreover global climate change is expected to exacerbate eutrophication in the near future (Carpenter et al., 1992, Blenckner, 2007). Most developed countries including Canada, the countries of the European Union, the USA and Australia, have national programmes to address eutrophication (Banens & Davis, 1998, OECD, 2002, Walmsley, 2003). Previous attempts to control eutrophication in South Africa (Grobler & Toerien, 1986), and the recent implementation of a national eutrophication monitoring programme (DWAF, 2002) have had limited success. Recent surveys have shown that eutrophic conditions exist in approximately one in every five of 75 major impoundments and in at least 18 out of 25 major river catchments (DWAF, 2003, de Villiers & Thiart, 2007). Thus, eutrophication is a significant problem in South Africa's lakes and rivers. Current trends show that conditions are likely to deteriorate further especially given the absence of phosphorus standards in most catchments (Walmsley, 2003).

2.2 Harmful Cyanobacterial Algal Blooms

An increase in phytoplankton biomass and shifts towards species capable of producing toxins are among the worst consequences of eutrophication. Phytoplankton are defined as simple plants without leaves or flowers that are suspended in the water column (van den Hoek et al., 1995). The collection of phytoplankton in a lake, called the phytoplankton assemblage, is usually made up of a large variety of algal species which can be grouped into different divisions and classes based on morphological differences and pigmentation (See Table 2.3).

Table 2.3 Some common algal divisions showing class, common names and pigments (Classification after Lee, 1980).

Division	Class	Common name	Pigments
Chlorophyta	Chlorophyceae	Green algae	Chl *a*, *b*
Chromophyta	Dinophyceae	Dinoflagellates	Chl *a*, *c1*,
	Euglenophyceae	Euglenoids	Chl *a*, *b*
	Cryptophyceae	Cryptophytes	Chl *a*, *c*, phycobiliproteins
	Bacillariophyceae	Diatoms	Chl *a*, *c1*, *c2*, fucoxanthin
Cyanophyta	Cyanophyceae	Cyanobacteria Blue-green algae	Chl *a*, phycobiliproteins
Rhodophyta	Rhodophyceae	Red algae	Chl *a*, *d*, phycobiliproteins

Cyanophyceae, commonly known as cyanobacteria or blue-green algae, are distinct from other phytoplankton in that they have traits in common with prokaryotic bacteria and lack membrane bound organelles. However, they still exhibit oxygen-evolving photosynthesis that is the means of nutrition in all eukaryotic plants and algae. Thus cyanobacteria represent the evolutionary link between bacteria and green plants in that they exhibit both prokaryotic and eukaryotic features (Lee, 1980, Fay, 1983). Cyanobacteria species such as *Microcystis*, exist as slimy colonies of small unicellular cells, while other species have string-like filamentous chains of cells called trichomes that may be straight or spiralled (Fay, 1983).

A recent analysis of 99 well-studied temperate lakes shows that cyanobacteria represent an increasing percentage of the phytoplankton biomass as the supply of total phosphorus increases (Downing et al., 2001). Cyanobacteria exhibit a number of characteristics that give them a competitive advantage over other phytoplankton in turbid eutrophic and alkaline conditions (See Table 2.4). They are able to grow at low light intensities and utilise atmospheric CO_2 and bicarbonate ions (HCO_3^-) as a source of carbon for photosynthesis. Species such as *Microcystis* have a distinct advantage over other algal groups in environments that are low in

Table 2.4 Factors contributing to the dominance of cyanobacterial algal species in eutrophic conditions (Taken from Fay, 1983, Paerl, 1991, Dokulil & Teubner, 2000, Nakano et al., 2003).
Ability to grow at low light intensities
Ability to utilise atmospheric CO_2 and bicarbonate ions as a source of carbon for photosynthesis
Ability to store reserves of nutrients
Some species ability to fix atmospheric nitrogen
Ability to utilise organic substrates as a source of carbon
Ability to regulate their movement up and down in the water column through gas vesicles
Ability to produce toxins that inhibit the growth of other phytoplankton species and prevent grazing by zooplankton

dissolved inorganic carbon (Nakano et al., 2003). Some species, including *Microcystis*, can regulate their position in the water column through gas vesicles in order to maximise their uptake of nutrients and optimise photosynthesis. Cyanobacteria also thrive in nitrogen limited conditions that are rich in dissolved organic matter because some species can fix atmospheric nitrogen and utilize organic substrates as a source of carbon and energy. For example, *Microcystis aeruginosa* is able to assimilate a variety of amino acids (Paerl, 1991). Cyanobacteria also have increased resilience to seasonal fluctuations in nutrient availability due to their ability to store large concentrations of reserve nutrients. Furthermore, toxin production by species such as *Microcystis aeruginosa* inhibits the growth of other phytoplankton and prevents grazing by zooplankton (Singh et al., 2001, Hansson et al., 2007). Thus decreased macroinvertebrate and bacterioplankton species diversity and richness coincide with increasing *Microcystis* toxicity and species abundance (White et al., 2005, Xing et al., 2007).

Cyanobacteria often accumulate in great numbers in eutrophic lakes forming blooms that are manifested as sudden periods of explosive growth resulting in water with a pea-soup green colour and consistency. The ‘over-floating’ of buoyant cyanobacterial cells in calm conditions and reed causes thick green surface ‘scums’ and mats. Cyanobacterial blooms are difficult to predict as bloom initiation may be triggered by many different physical, chemical and biological environmental factors (For more details, see Mur L.R. & Utkilen, 1999, Roelke & Buyukates, 2001, Chu et al., 2007). The release of cyanotoxins into the water through cell lysis, or their ingestion through swallowing, has deleterious effects on animals and humans.

There are two types of cyanotoxins, namely hepatotoxins, and neurotoxins. Hepatotoxins such as *microcystins*, *nodularins* and *cylindrospermopsin*, most commonly encountered by humans and animals, are absorbed by the functional cells of the liver resulting in a range of ill effects such as

weakness, vomiting, heavy breathing and diarrhoea, amongst others (Codd, 2000, Zurawell et al., 2005). *Microcystin* toxins have been found in several planktonic cyanobacterial species including *Microcystis*, *Anabaena*, *Oscillatoria*, *Nostoc*, and *Anabaenopsis* (Sivonen & Jones, 1999). Neurotoxins, such as *anatoxin-a*, *anatoxin-a(s)* and *saxitoxins*, affect the nervous system and result in paralysis and death from respiratory failure and asphyxia (Zurawell et al., 2005). Neurotoxins are present in *Anabaena*, *Oscillatoria*, *Aphanizomenon*, and *Cylindrospermum* species. The potency of toxins, indicated by the lethal dose, shows that some cyanotoxins are more lethal than cobra venom (lethal dose = 20 $\mu g.kg^{-1}$) (See Table 2.5).

Table 2.5 Selected toxin producing cyanobacterial species showing toxins and potency (Data from Oberholster et al., 2005, Zurawell et al., 2005).

Toxins	**Species**	**Lethal Dose ($\mu g.kg^{-1}$)**
Hepatotoxins		
Cylindrospermopsin	*Rhaphidiopsis* *Anabaena*	2100
Microcystins	*Anabaena* *Microcystis aeruginosa* *Anabaenopsis*	50
Nodularia	*Nodularia spumigena*	30
Neurotoxins		
Anatoxin a	*Anabaena*	200
Anatoxin a(s)	*Anabaena*	20
Saxitoxins	*Anabaena*	10

Recreational contact between humans and cyanotoxins has resulted in various symptoms including gastroenteritis, sore throat, blistered mouth, vomiting, pulmonary consolidation, flu-like symptoms, eye and/or ear irritation, rashes, contact dermatitis, and respitory irritation. Ingesting water containing cyanotoxins may lead to gastroenteritis, fevers, abdominal and muscular pains, liver, kidney and intestinal damage and primary liver cancer followed by death (Kuiper-Goodman et al., 1999, Codd, 2000, Falconer, 2001). These symptoms have been documented in many countries around the world, including Australia, Brazil, Sweden, the United States, and Zimbabwe, to name a few (Oberholster et al., 2005). The worst reported cases of human deaths are from Brazil, where cyanotoxins from *Anabaena* and *Microcystis* species have resulted in the deaths of more than 50 people on at least two occasions (Teixeira et al., 1993 cited by Kuiper-Goodman et al., 1999, Codd, 2000). The occurrence of liver cancer in China and most likely Florida in the United States has been linked to *microcystin* toxins (Fleming et al., 2002). In South Africa there are only a few reports of skin irritations and diarrhoea following recreational contact or drinking (Harding & Paxton, 2001). However, there are likely to be many incidences that are falsely diagnosed or are unreported.

Interestingly, animal poisonings by cyanotoxins in South Africa are prolific. There are numerous reports of deaths of livestock, game, dogs and fish, and almost all of these have been associated with *microcystin* toxins from *Microcystis aeruginosa* (Oberholster et al., 2005). In the Western Cape province there are increasing incidences of animal poisonings, with numerous cases of livestock deaths being reported since 1993 (Harding & Paxton, 2001). *Microcystis aeruginosa* is widespread in southern Africa (Scott 1991). In 2004 a survey found *Microcystis* and *Anabaena* species present in more than 35% of 71 major impoundments (Scott, 1991, Van Ginkel, 2004). Further research shows that the occurrence of *microcystin* toxins is strongly correlated with *Microcystis* dominance (Van Ginkel, 2002). Therefore the development of cyanotoxins, particularly *microcystin*, is highly likely in hypertrophic conditions with *Microcystis* dominance, although there are other environmental factors which also control toxin production (For more details see Wicks & Thiel, 1990, Sivonen & Jones, 1999, Jacoby et al., 2000).

2.3 Zeekoevlei Lake

The threat of cyanobacterial blooms is likely to increase in the near future as warmer climates are expected to increase algae counts and cyanobacterial dominance, particularly in shallow lakes (See, for example, Arheimer et al., 2005, Mooij et al., 2007, Johnk et al., 2008). Zeekoevlei is an archetypal shallow lake severely impacted by eutrophication, physical alteration and permanent debilitating cyanobacteria dominance. The lake is dirty, has a bad odour, displeasing water colour and large deposits of silt and organic-rich sludge (Quick & Johansson, 1992). *Microcystis aeruginosa* is the most abundant algal species by far (Harding, 1992) and forms thick green surface scums in sheltered bays and reeds, and congregates on the surface in the middle parts of the lake on calm days. The water colour is bright green and exceptionally turbid as a result of the extremely high phytoplankton biomass and dense clumps of sediment, churned up by fish (Personal observation, April 2008).

Zeekoevlei is the largest of a system of coastal lakes and lies adjacent to the Cape Flats Sewage Works to the south (See Figure 2.1). Zeekoevlei was proclaimed a local nature reserve in 2000 and is an important recreational resource for the City of Cape Town. It forms part of the False Bay Ecology Park, the fifth most important wetland bird area in South Africa and a vital link in the Cape Town biodiversity network (CCT, 2007b). Zeekoevlei's shape can be described as a mirror image of the letter B, due to the arm of land, or peninsula, which extends into the centre of the lake from the west. The lake may be roughly divided into three basins: the Northern Basin, near the mouths of the Great and Little Lotus Rivers; Home Bay, the sheltered corner in the north east; and the Southern Basin, also known as Storm Bay. The lake is about 2.5 km long and approximately 1 km wide with a total surface area of 2.56 ha. Its mean depth is 1.9 m and its maximum depth is 5 m in the Southern Basin (Harding, 1996). The shallowness of the lake is attributed to large deposits of organically rich algal sediment in the northern and southern basins. Zeekoevlei experiences bimodal annual wind patterns: N to NW in winter and S to SE in summer (*ibid.*). Very few windless days are recorded in a year, meaning that the lake is continually mixed or 'hypermictic' (*ibid.*). The main sources of water for the lake are the Great and Little Lotus rivers flowing in from the north. Groundwater also contributes about 15% of total inflow and almost 100% of input during dry summers (Parsons & Harding, 2002).

The Lotus River catchment which drains into Zeekoevlei, has an area of 8.01×10^7 m^2 and an annual estimated runoff volume of 2.01×10^7 m^3 (Grobicki et al., 2001). In 2001 there were an estimated 379 380 people living in the Lotus catchment, of which about 90 000 were living in

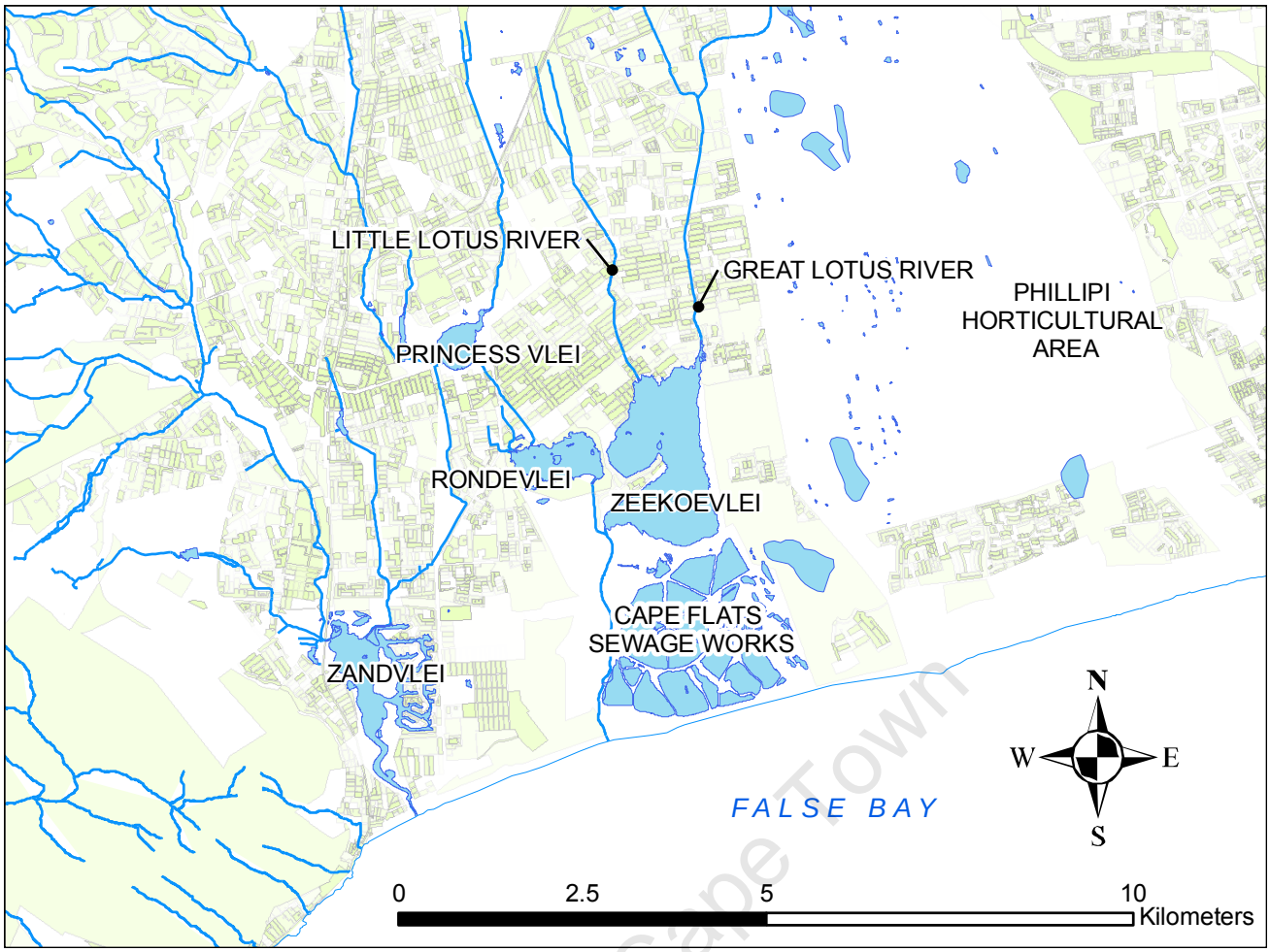

Figure 2.1 Map showing Zeekoevlei and the neighbouring system on lakes on the Cape Flats, south of the City of Cape Town.

informal settlements (*ibid.*). About 6.6% of the total land use constitutes informal settlements, while the majority is serviced residential and agricultural land of the Philippi Horticultural Area (*ibid.*). Therefore, the catchment runoff, flowing into Zeekoevlei via the Great and Little Lotus Rivers, exhibits high counts of faecal coliforms, high concentrations of phosphates (P) and nitrates (N) , and significant amounts of gross litter (*ibid.*).

The water quality of Zeekoevlei has been measured by the City of Cape Town Scientific Services for more than 20 years. Monthly samples taken from four sampling sites around the lake (although not all four sites have always been sampled) provide evidence of nutrient concentrations and other trophic status indicators, such as Chl *a* and Total Suspended Solids (TSS) concentrations, and Secchi Disk depth (SD) (See Table 2.6).

Table 2.6 Selected statistics for water quality parameter data collected from 1981 to 2008 (Data courtesy City of Cape Town Scientific Services).							
Variable	**Unit**	**Mean**	**St. Error**	**St. Dev.**	**Min.**	**Max.**	**N**
Total P	mg.ℓ^{1}	0.819	0.031	0.944	0.005	19.490	906
Total N	mg.ℓ^{1}	3.37	0.11	2.16	0.31	17.84	360
Chl *a*	mg.m^{-3}	235.1	7.7	255.0	2.3	4809.0	1085
TSS	mg.ℓ^{1}	84.1	4.1	117.9	1.0	2240.0	829
SD	cm	27	0.3	11	0	145	1354

Zeekoevlei exhibits very high mean concentrations of dissolved nutrients in the form of total P (0.819±0.031 mg.ℓ^{-1}) and total N (3.37±0.11 mg.ℓ^{-1}). Total P concentrations are much higher than the limit for hypertrophy (0.130 mg.ℓ^{-1}) defined by the South African eutrophication classification system (See Table 2.1). An estimated 34 000 kg of phosphorus enters Zeekoevlei every year, the major contributors being seepage from the adjacent Waste Water Treatment Works (35%), the Great Lotus River (28%), and internal loading derived from organically rich sediment (25%) (Southern Waters Ecological Research and Consulting, 2000). Mean Chl *a* concentration is 235.1±7.7 mg.m^{-3}, mean TSS concentration is 84.1± 4.1 mg.ℓ^{1}, and mean SD depth is a mere 27±0.3 cm.

Zeekoevlei is able to sustain these very high levels of primary production because it is hypermictic, or continually-mixed by persistent prevailing winds. The mixing entrains nutrient rich sediment into the water column and offsets cyanobacteria buoyancy, preventing the formation of surface scums that limit light availability. Thus the lake has been likened to a continuous fermentor or chemostat: a completely mixed reactor system for phytoplankton growth (Harding, 1996 p.177, Harding, 1997 p.100). Significantly, primary production is more dependent on physical environmental conditions (wind and temperature) than nutrients, so that in that sense, the lake is non-nutrient limited (*ibid.*). This hypothesis is supported by correlation analysis performed between the various water quality variables (Table 2.7). The analysis used the Spearman Rank Order correlation coefficient as the variables were non-normally distributed.

Table 2.7 Spearman Rank Order correlation coefficients for selected water quality variables for Zeekoevlei from 1981 to 2008. Correlations in red are significant at the p < 0.05 level.					
	SD	**TSS**	**Total N**	**Total P**	**Chl *a***
SD	1.00	-	-	-	-
TSS	-0.40	1.00	-	-	-
Total N	0.03	0.01	1.00	-	-
Total P	-0.15	0.15	0.20	1.00	-
Chl *a*	-0.27	0.16	-0.00	0.30	1.00

Only weak correlations exist between the variables, the strongest of that are between SD depth and TSS (r = -0.40) and Chl *a* (r = -0.27). The negative correlations are expected since the depth of light penetration decreases with increasing concentrations of suspended matter. Chl *a* is weakly correlated with total P (r = 0.30) showing that biological production is only slightly regulated by nutrient availability.

A time series from the southern basin from 1981 to 2008 shows a trend of increasing total P and Chl *a* concentrations (See Figure 2.2). However, Chl *a* shows a notable decline between 1997 and 1999 as a result of the implementation of an annual water drawdown as a management intervention, for the first time in 1997, to improve water conditions (Harding & Wright, 1999). Although there were an initial sustained decrease in Chl *a* concentrations and an increase in water clarity during 1997 and 1998, these clear-water conditions have not been observed since despite the continued use of the drawdown (Haskins, 15 August 2007). From about 2000 onwards there has been increased variability, with periodic episodes of very high and low total P and Chl *a* concentrations. Therefore the annual drawdown seems only to have temporarily improved water conditions, or limited biological production, but thereafter conditions have deteriorated further than observed at any time previous. Thus the annual water drawdown seems to be more effective as a short-term management strategy than a long-term solution, so long as there continue to be increasing nutrient inputs from the catchment area. The water quality conditions, at least in terms of phytoplankton biomass and total P concentration, appear to have worsened over the last 20 years, a trend that is likely to continue unless the input of nutrients into the lake is reduced.

The phytoplankton assemblage in Zeekoevlei has low species diversity and a unique equilibrium between cyanobacteria and chlorophyta (Harding, 1996). *Microcystis aeruginosa* is by far the most dominant species numerically, with cell counts ranging from 4 000 to 7 000 000 cells.mℓ^{-1}, but in terms of biomass the chlorophyta *Scenedesmus opoliensus* and *Pediastrum boryanum* are co-dominant, with cell counts ranging from 3 000 to 20 000 cells.mℓ^{-1} (*ibid.*). These three species comprise approximately 80% of the freshwater phytoplankton biomass. The lake does not display marked seasonal succession other than increased *Microcystis* numbers during spring following an increase in orthophosphate, and mid-winter maximums of bacilliariophyta (diatoms) (Harding, 1992). Thus *Microcystis* is dominant from August to December and *Scenedesmus opoliensus* and *Pediastrum boryanum* are dominant from January to July (Harding, 1996, Harding & Wright, 1999) (See Table 2.8).

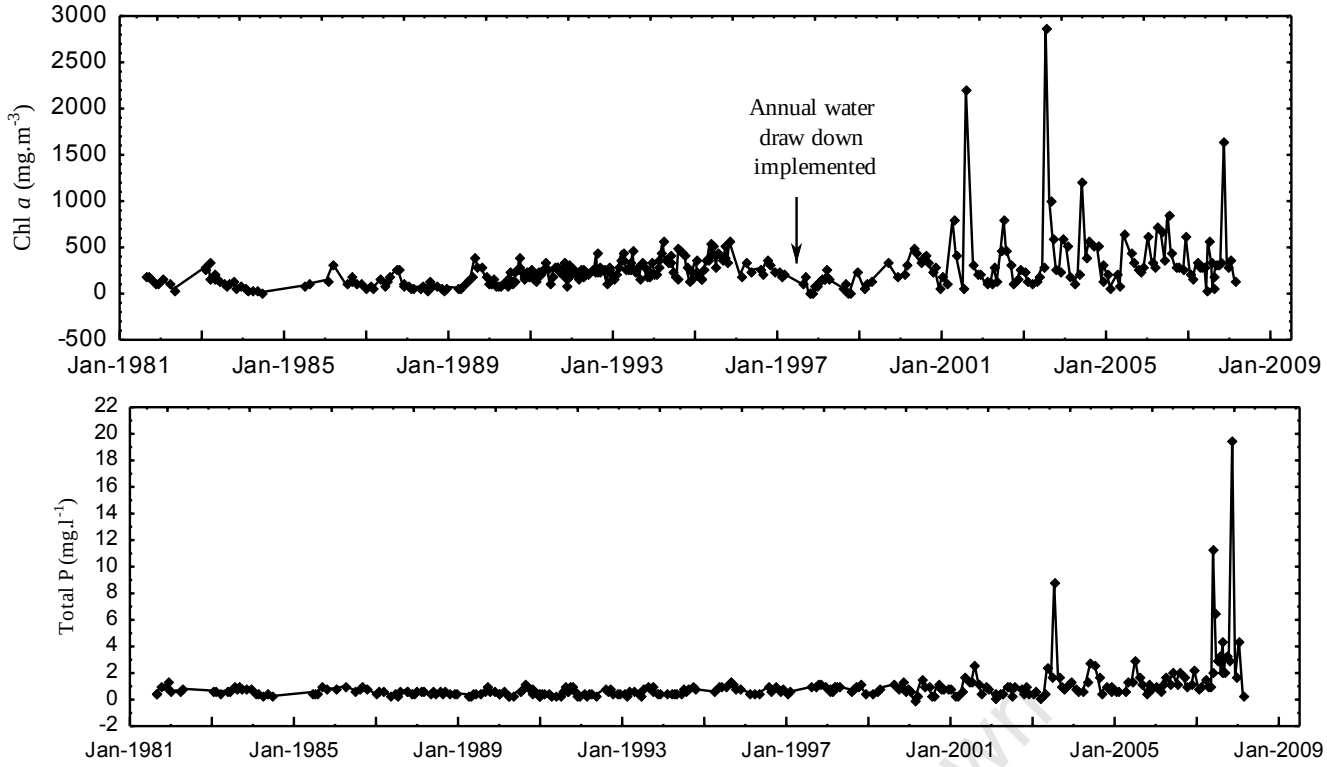

Figure 2.2 Time-series trend of Chl *a* and total P concentrations measured in the southern basin from 1981-2008 by the City of Cape Town Scientific Services. Chl *a* concentrations greater than 3000 mg.m^{-3} are omitted.

Other cyanobacterial species present in Zeekoevlei include the colonial *Merismopedia* and *Chroococcus*, and the filamentous *Anabaena*, *Anabaenopsis*, *Nodularia*, *Spirulina*, and *Pseudoanabaena* and *Rhaphidiopsis*. Other prevalent species are chlorophyta *Tetraedron minimum* and *Golenkiniopsis parvula*, and diatoms *Thalassiosira nana*, *Cyclotella meneghiniana* and *Aulacoseira granulate* (Harding & Wright, 1999). Small numbers of other algal genera such as cryptophytes, euglenoids and dinoflagellates are also present, although the mean number of genera per sampling occasion is only 17 (Harding, 1992). There are no fewer than five cyanobacteria species present in Zeekoevlei capable of producing cyanotoxins, of which *Microcystis* is the most abundant (See Table 2.5). In 1995, a female bull terrier dog was killed by cyanobacterial poisoning at Zeekoevlei attributed to the *nodularin* toxin, which was the first documented case of animal poisoning by *Nodularia spumigena* in a South African lake (Harding et al., 1995). Zeekoevlei has also tested positive for cyanotoxins on other occasions following analysis by the local municipality (Haskins, 15 August 2007). It is reasonable to assume that cyanotoxins continue to threaten the health of animals as well as humans at Zeekoevlei.

The City of Cape Town's Environmental Health section monitors water quality conditions in inland water bodies to establish compliance with respect to health regulations (CCT, 2008). In 2006 water pollution levels were exceptionally high in Cape Town's freshwater rivers and lakes, with about 65% of rivers classified as extensively degraded

Table 2.8 Dominant phytoplankton species in Zeekoevlei showing abundance and seasonality, pigments and absorption maximums (Data from Fay 1983, Harding 1996).

Species	Abundance (cells.mℓ$^{-1}$)	Seasonality	Pigments	Absorption Maximum (nm)
Microcystis aeruginosa	4 000 – 7 000 000	Year-round Spring and summer maximums	Chl a Phycocyanin Carotenes	430, 663 610 – 625 480 – 520
Scenedesmus opoliensis *Pediastrum boryanum* *Golenkiniopsis parvula*	3 000 – 20 000	Year-round	Chl a Chl b Carotenoids	430, 663 ~ 470, 650 480 – 520
Thalassiosira nana	100 – 120 000	Winter	Chl a Chl c1 c2 Fucoxanthin	430, 663 ~450 ~450

(CCT, 2007a). There is a continual need for improved monitoring so as to manage environmental threats to water-resources in Cape Town.

On a national level, monitoring and assessing the overall state of South Africa's water resources is the responsibility of the Department of Water Affairs and Forestry (DWAF, 1997). It is required that national monitoring systems must provide information on the quantity, quality and health of aquatic ecosystems, and to assess compliance with quality objectives and measures taken for rehabilitation (Republic of South Africa, 1998). In order to do so, five major water quality monitoring programmes are currently operating under the Strategic Framework for National Water Resource Quality (Grobler & Ntsaba, 2004). Amongst these is the National Eutrophication Monitoring Programme implemented specifically to monitor the impact of eutrophication. However, in 2003 the programme had not been sufficiently implemented in many regions of the country (Walmsley, 2003). There remains a great need for regular monitoring to determine whether resource quality objectives are being reached, in view of the unsatisfactory progress of some monitoring systems (DWAF, 2004a). New initiatives, from DWAF and the Department of Science and Technology's grand challenge for increased space science and earth observation (DST, 2008), provide opportunities for integrating remote sensing technology into current programmes, so that monitoring of inland freshwater resources may be enhanced (DWAF, 2004b). This leads to the discussion of the next chapter which outlines remote sensing of water quality parameters in inland waters.

Chapter 3 Remote Sensing of Water Quality Parameters in Inland Waters

Inland lakes, coastal oceanic regions and estuaries are often considered Case 2 waters, which are optically complex owing to significant contributions from dissolved organic matter and/or *tripton* as well as phytoplankton (Morel & Prieur, 1977). In contrast to Case 1 waters, that are modelled relatively well as a function of phytoplankton alone (Chl *a* concentration), Case 2 waters are a function of at least three independent variables. Therefore, remote sensing over inland lakes requires more advanced procedures related to sensor requirements, atmospheric correction procedures, and water constituent algorithms (Sathyendranath, 2000). The remainder of this chapter discusses these requirements for inland waters.

3.1 Remote Sensing Instruments and Applications to Freshwater Lakes

Passive remote sensing instruments, whether hand-held or mounted on aircraft or satellites, measuring the light in the visible and near-infrared part of the electromagnetic spectrum (400 to 750 nm) are most often used for water-related applications. This is mostly because water absorbs strongly at wavelengths greater than approximately 700 nm, effectively masking out signals from other water constituents from 750 nm onwards. The spectral, spatial and temporal resolutions and signal-to-noise specifications of the remote sensing instrument determine its overall usefulness for water-related monitoring. The configuration of spectral bands determines the detail with which the water-leaving radiation is resolved such that the detection of certain water constituents, such as Chl *a* and inorganic matter, requires suitably positioned bands (Davis et al., 2000). Generally only sensors with a ground resolution of a few hundred meters, or less, are suitable for monitoring inland water bodies, as the image pixels should be several times smaller than the dimensions of the lake (Lindell et al., 1999 p.87). The sampling frequency of the sensor must also be sufficient to gather regular data, especially when considering that cloud cover may significantly reduce the number of useful images. The selection of a suitable sensor is also determined by the intended application. Certain applications, such as ecosystem analysis, require sensors with sampling frequencies and spatial resolutions high enough to resolve system changes occurring over short time-scales (days/weeks), and higher signal-to-noise ratios for better confidence limits for estimations. Lower resolution change detection applications with larger signals, such as operational HAB detection, do not have as demanding requirements, and sensors with coarse spatial resolutions and lower overpass frequencies are generally more applicable.

Airborne platforms typically carry hyperspectral or multispectral spectrometers that are capable of capturing many spectral bands (>200), forming an almost continuous spectrum of the surface reflectance. Examples of airborne sensors commonly used in studying inland waters are the

Airborne Imaging Spectrometer for Applications (AISA) (Härmä et al., 2001) and the Compact Airborne Spectrographic Imager (CASI) (Ammenberg et al., 2002) (See Appendix 1 for others). The data from these sensors are particularly useful since the spectral widths and positions can normally be adjusted to suit the intended application, or re-sampled to simulate satellite sensors that have broader and fewer bands. The very high spectral resolution presents opportunities for applications that are not feesible with sensors with few and broad bands, such as the detection of specific algal pigments that potentially allows algal species composition determination (Richardson, 1996). The spatial resolution of most airborne sensors is also high, given the low altitude that the images are acquired, with pixels usually representing areas of only a few meters squared on the ground. There are numerous examples where airborne sensors have been used successfully for the detection of water quality parameters in lakes (See, for example, Dierberg & Carriker, 1994, Hakvoort et al., 2002, Koponen et al., 2002). However, the temporal and spatial inconsistency, and high cost, makes this option unviable for most scientists and researchers in the developing world. For example, a hyperspectral campaign recently planned for South Africa intended using the HyVista Corporation HyMap^{TM} sensor, but was cancelled because of the cost. However, a free Airborne Hyperspectral Imager AISA-ES flight over Zeekoevlei was carried out in 2006 to demonstrate the potential for water quality monitoring (Stark et al., 2006).

Satellite platforms offer substantial advantages over airborne platforms mainly because of the temporal and spatial consistency, larger area coverage and reduced data cost (Rees, 2001). There are a wide range of current earth-observation satellites that may be used for water quality monitoring (See Table 3.1). Satellite-based sensors are not usually hyperspectral mainly because of constraints related to instrument design (signal-to-noise ratios) and the large quantities of data that have to be transmitted and stored. The Hyperion Imaging Spectrometer, launched in 2001, was the first experimental hyperspectral sensor to orbit the earth in space and has been used for water-based applications (Brando & Dekker, 2003). Hyperion offers high spectral (220 bands) and spatial resolutions (30 m) with an overpass time equivalent to the Landsat sensors (16 days). However, the instrument is near the end of its life span and so does not acquire images routinely. Similar hyperspectral sensors are likely to be further developed and used more in the future, for example, the South African Multi-Sensor Micro-Satellite Imager (MSMI) (Sunspace) sensor.

Multi-spectral sensors such as IKONOS, LISS 3 and 4, SPOT 4 and 5, Landsat 5 and 7, and ALI, have few, broad bands and high spatial resolutions (4 to 30 m). These sensors are able to view even very small lakes with a large number of pixels, but have poor spectral and often temporal resolutions. Despite this, these sensors have been used successfully in water quality studies,

Table 3.1 Current earth observation satellite sensors showing resolution specifications and full names (Data fromCNES SPOT Image, 2004, European Space Agency, 2006, Indian Space Research Organisation, 2008, U.S. Geological Survey, 2008, GeoEye, 2009, NASA, 2009a, NASA, 2009b).

Satellite	Sensor	Spectral resolution (µm)	Spatial resolution	Temporal resolution
LM900	IKONOS	0.45-0.85 (4 bands)	4 m	3/5 days
IRS-P6	LISS 4	0.52-0.68 (3 bands)	5.8 m	5 days
SPOT 5	HRG	0.48-1.75 (5 bands)	10 m	26 days
Proba-1	CHRIS	0.415-1.050 (19 bands)	18 m	~7 days
SPOT 4	HRVIR	0.50-0.89 (3 bands)	20 m	26 days
IRS-P6	LISS 3	0.52-1.70 (4 bands)	23.5 m	24 days
EO-1	Hyperion	0.4-2.5 (220 bands)	30 m	16 days
EO-1	ALI	0.43-2.35 (9 bands)	30 m	16 days
Landsat 5	TM	0.45-2.35 (6 bands)	30 m	16 days
Landsat 7	ETM+	0.45-2.35 (8 bands)	30 m	16 days
Terra/Aqua	MODIS	0.620-0.876 (2 bands)	250 m	1/2 days
EnviSAT	MERIS	0.412-0.900 (15 bands)	~300 m	2/3 days
IRS-P4	OCM	0.400-0.885 (8 bands)	360 m	2 days
SeaWiFS	WiFS	0.402-0.885 (8 bands)	1 km	2 days

Abbreviation	Full name
IKONOS	Derived from the Greek word for ‘image’
LISS	Linear Imaging Self-Scanning Sensor
HRG	High Resolution Geometric imaging instrument
CHRIS	Compact High Resolution Imaging Spectrometer
HRVIR	High Resolution Visible and Infra Red imaging instrument
ALI	Advanced Land Imager
TM	Thematic Mapper
ETM	Enhanced Thematic Mapper
MODIS	Moderate Resolution Imaging Spectrometer
MERIS	Medium Resolution Imaging Spectrometer
OCM	Ocean Colour Monitor
SeaWiFS	Sea-viewing Wide Field-of-view Sensor

particularly the Landsat 5 TM and 7 ETM+ sensors, and are generally suitable for coarse change detection applications (See Appendix 1, for example, Thiemann & Kaufmann, 2000, Dekker et al., 2001, Vincent et al., 2004, Kutser et al., 2005, Hellweger et al., 2007). However, the lack of suitable bands in the near-infrared in many of these sensors means that they have limited ability to account for atmospheric effects. The experimental CHRIS sensor on board the Proba-1 platform is a multispectral/hyperspectral sensor with 19 bands in ‘water mode’ ideally positioned for water-related studies. The sensor has a high spatial resolution of 18 m however the swath is only approximately 14 km wide. CHRIS is capable of providing an image of a site every seven days, usually for two to three days consecutively, so a total of 8 or more images may be acquired every month, although, because of acquisition plans and priorities, actual data acquisition may be substantially less than this. CHRIS, although only in the experimental stage and facing substantial challenges related to atmospheric correction, offers the advantage of high spectral definition,

fairly regular image acquisition, and high spatial resolution, so that similar sensors are likely to be used increasingly in future (Miksa et al., 2004).

Sensors with lower spatial resolution, such as MODIS, SeaWiFS, OCM and MERIS, have higher acquisition frequencies and better positioned bands for water-related applications and atmospheric correction. MODIS has two broad bands in high resolution mode (250 m) and a high temporal resolution of about one day when using both the Terra and Aqua platforms. MODIS's broad bands are not conducive to Chl *a* detection although there are examples where MODIS data are used for monitoring suspended matter and for water classification in inland lakes and estuaries (Koponen et al., 2004, Chen et al., 2007). SeaWiFS has frequently been used to derive Chl *a* products in the ocean, but its spatial resolution is generally too low (1 km) for all but the largest inland lakes (Vos et al., 2003). The MERIS sensor has the greatest spectral resolution of these sensors with 15 bands in the visible and near-infrared spectrum, specifically positioned for various applications (See Table 3.2 below). Its spatial resolution is 290×260 m with regular image acquisition every 2 or 3 days. MERIS was designed for multiple applications, especially for monitoring biological production in the oceans, but it is also well suited for regular monitoring of inland water bodies. There are several examples where MERIS has been used for deriving water quality products for freshwater lakes (See, for example, Floricioiu et al., 2004, Giardino et al., 2005, Odermatt et al., 2008).

Table 3. 2 MERIS spectral bands and applications (From European Space Agency, 2006).

No.	Band centre (nm)	Band width (nm)	*Applications*
1	412.5	10	Yellow substance and detrital pigments
2	442.5	10	Chlorophyll absorption maximum
3	490	10	Chlorophyll and other pigments
4	510	10	Suspended sediment, red tides
5	560	10	Chlorophyll absorption minimum
6	620	10	Suspended sediment
7	665	10	Chlorophyll absorption & fluorescence reference
8	681.25	7.5	Chlorophyll fluorescence peak
9	708.75	10	Fluorescence reference, atmosphere corrections
10	753.75	7.5	Vegetation, cloud, O_2 absorption band reference
11	760.625	3.75	O_2 R- branch absorption band
12	778.75	15	Atmosphere corrections
13	865	20	Atmosphere corrections
14	885	10	Vegetation, water vapour reference
15	900	10	Water vapour

The selection of a suitable sensor is vital for successful research however, a more often encountered and serious problem is that of acquiring suitable data which may prove difficult and expensive. Data cost is one of the primary hindrances to remote sensing research, certainly at least in the developing world and in South Africa, and only systems providing free data can be

seriously considered for operational monitoring programmes. Data from high resolution sensors such as SPOT, IKONOS and others, are very expensive, even when used for non-commercial purposes, and pre-ordering in advance, as required for field campaigns, is often problematic. Landsat 7 ETM+ data recently became available free of charge over Africa, and although some of the data quality is poor because of instrument failure, it is likely to now be used increasingly (NASA, 2008). Data from sensors such as CHRIS, MERIS, MODIS and others are available free for research, making these sensors a more viable option for scientists and operational monitoring programmes.

Aside from remote sensing instruments mounted on aircraft and satellites, discussed above, the use of portable field spectroradiometers for validation purposes, and for deriving algorithms for water constituents is common (See Appendix 1). Spectroradiometric measurements form an important component in the development of remote sensing systems. Spectroradiometers typically provide detailed water-leaving spectra with hyperspectral (bandwidths less than 5nm) or multispectral resolutions. A number of important studies have been carried out using spectroradiometers describing the relationship between water constituents, such as Chl *a*, and the water-leaving reflectance (See, for example, Gitelson et al., 1993, Schalles et al., 1998, Gons, 1999). The findings of these studies have important implications for remote sensing from airborne and satellite platforms because they form the basis for algorithm development.

There already exists a wide range of applications of remote sensing for inland lakes, reservoirs and rivers. Water quality parameters commonly derived using remotely sensed data include Chl *a* concentration (Kutser, 2004), suspended matter concentration (Dekker et al., 2001), absorption by dissolved organic substances (Kutser et al., 2005), Secchi Disk depth (water clarity) and water temperature (Giardino et al., 2001). Remotely sensed data have also been used to aid in predicting algal blooms (Chang et al., 2004); for detecting potentially toxic cyanobacterial algal blooms (Vincent et al., 2004); for lake classification based on water quality (Koponen et al., 2004); and, trophic status determination (Thiemann & Kaufmann, 2000). Further studies have examined macrophyte monitoring (Nelson et al., 2006); eutrophication monitoring (Vos et al., 2003); sediment and vegetation change detection (Pal & Mohanty, 2002); waste water monitoring (Braude et al., 1995); and, monitoring the impacts of urban runoff on water quality (Ha et al., 2003). Countries where these studies have been carried out are, among others, Australia, China, Finland, India, Italy, Netherlands, Sweden, and the United States (See Appendix 1 for others). In South Africa, however, little research has been done. The only research report found was written in the 1980s and investigated using Landsat to survey lakes for turbidity and Chl *a* (Howman &

Kempster, 1986). However interest is growing, and studies are now starting to appear (For example, Stark et al., 2006, Oberholster et al., 2009).

3.2 Physical Basis of Remote Sensing

It is necessary here to review the physical basis of remote sensing before describing retrieval methods in more detail. Electromagnetic radiation, called light, is emitted from the sun mostly in the visible region of the spectrum, in the wavelengths between 400 and 700 nm. Light photons have energy that varies inversely with their wavelength. Radiant flux, Φ, is the rate of flow of energy (photons), *Q*, per unit time, *t*, and has the units Js^{-1} that is equal to Watts. The radiant intensity, I, is the radiant flux per unit solid angle in a specified direction, ξ. The direction can be described in terms of the zenith angle, θ, (or the nadir angle, θ_n) and the azimuth angle, ϕ, as illustrated below with reference to a beam of light (After Kirk, 1994):

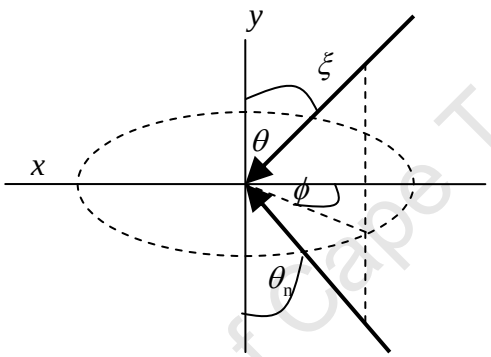

The solid angle, *Ω*, is a three dimensional angle of a small area of a sphere and has the units steradians (sr). Radiance, L, is the radiant intensity per unit area at a right angle to the direction of flow. Thus radiance is the total energy of photons in a given direction per unit time, per unit solid angle, per unit area (Kirk, 1994):

$$L(\theta,\phi) = \frac{dQ}{dt\, dS \cos\theta\, d\Omega} \quad \left(Js^{-1}m^{-2}sr^{-1}\right) \tag{3.1}$$

The cosine operator $dS\cos\theta$ is the projected area perpendicular to the direction of flow. Irradiance, E, is similar to radiance except there is no solid angle (direction). It is defined as the radiant flux per unit area of a surface (Kirk, 1994):

$$E = \frac{dQ}{dt\, dS \cos\theta} \quad \left(Js^{-1}m^{-2}\right) \tag{3.2}$$

The downward irradiance, E_d, and the upward irradiance, E_u, are the integral of radiance, with respect to solid angle, over the whole upper and lower hemispheres respectively. Spectral irradiance, $E(\lambda)$, and radiance, $L(\lambda)$, represent their variation of irradiance and radiance with wavelength, and have units $Wm^{-2}nm^{-1}$ and $Wm^{-2}sr^{-1}nm^{-1}$, respectively. The irradiance reflectance, R, (dimensionless) is the ratio of E_u to E_d and is often used for describing the light field. However, remote sensing reflectance, R_{rs}, defined as the ratio of the water-leaving radiance, L_w, to E_d, just above the surface ($z = 0+$) is most often used in remote sensing measurements. R_{rs} is written as follows (Mobley, 1994):

$$R_{rs}(\theta,\varphi,\lambda,z) = \frac{L_w(\theta,\varphi,\lambda,z)}{E_{\mathrm{d}}(\lambda,z)} \quad \left(\mathrm{sr}^{-1}\right) \tag{3.3}$$

All of the optical properties described above vary approximately exponentially with depth and therefore require an attenuation coefficient, *K*, for calculating their values at various depths in water. The attenuation coefficient for downward irradiance, K_d, may be written as follows (Kirk, 1994):

$$K_d(z) = \frac{-\,\mathrm{d}\ln E_d}{\mathrm{d}z} = -\,\frac{1}{E_d}\frac{\mathrm{d}E_d}{\mathrm{d}z} \tag{3.4}$$

The parameters described above including radiance, irradiance, remote sensing reflectance are called the Apparent Optical Properties (AOPs), although the attenuation coefficients are called 'quasi-inherent' (*ibid.*). The AOPs are effected both by the angular distribution of the light field and by the substances present in the water column (Preisendorfer, 1976).

The schematic diagram above (Figure 3.1) shows the radiances measured by the satellite sensor, that is essentially from three sources: backscattering within the water column, called the water-leaving radiance, L_w; reflection by the water surface, called the reflection radiance, L_r; and the atmosphere, called the atmospheric path radiance, L_p (Robinson & Mitchelson, 1983). Other important radiances contributing to these sources are the upwelling radiance below the water surface, L_u, the light transmitted through the air-water interface, L_t, the light reflected from the lake bottom, L_b, and the radiance reflected from adjacent areas, L_l (Koponen, 2006).

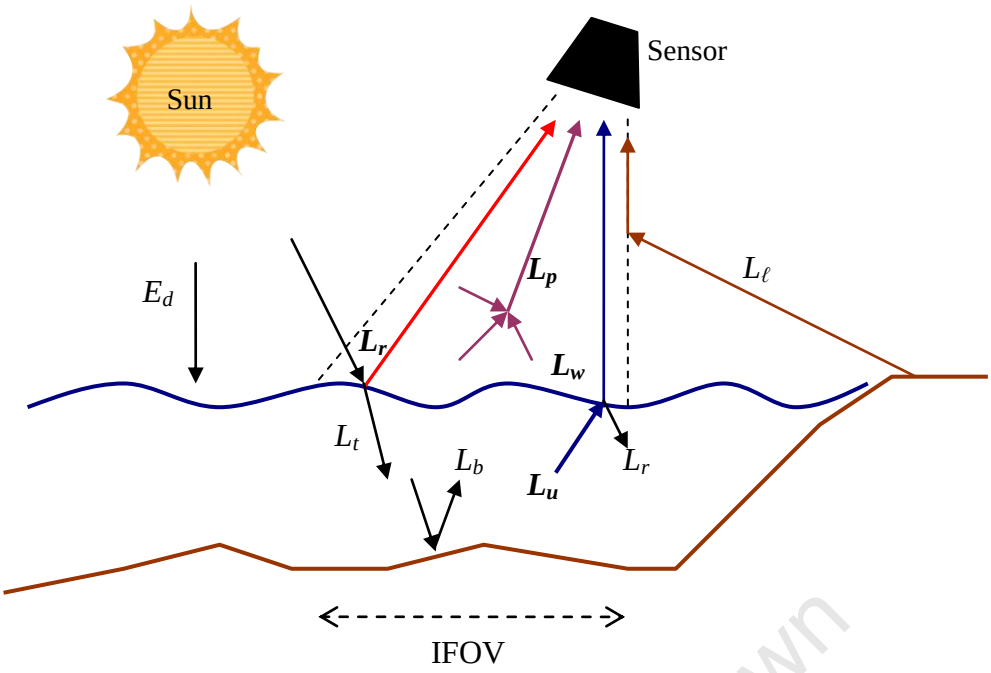

Figure 3.1 Sources of radiance to the satellite sensor. Downwelling irradiance, E_d and the Instantaneous Field Of View (IFOV) of the sensor are also shown (After Koponen, 2006).

The radiance detected by the sensor, L_d, is the sum of the water-leaving, atmospheric and adjacent radiances according to the equation below:

$$L_d = T_{atm}\left(L_w + L_r\right) + L_p + L_l \qquad (Wm^{-2}sr^{-1}) \tag{3.5}$$

where T_{atm} is a coefficient accounting for the transmittance through the atmosphere, as a large amount of scattering and absorption occur while en route to the sensor.

The parameter of most interest for obtaining information on the constituents present in the water column is the upwelling radiance, L_u, which is affected by scattering and absorption in the water column that is dependent on the Optically Active Components (OACs) (Kondratyev et al., 1998). The water-leaving radiance, L_w, the light detected by the sensor after correcting for atmospheric and adjacency effects, is made up of L_u and L_b (in clear water), adjusted for transmission through the air-water interface. It can be seen from Figure 3.1, that in order to obtain L_w, from L_d, several corrections are necessary. L_d must first be corrected for atmospheric effects (L_p) and then, if necessary, for gross surface reflectance caused by sun glint or wave action (L_r), and adjacency effects (L_l). In order to obtain L_u, L_w must then be corrected for the transmission through the air water interface (according to Snell's law) and for bottom reflectance (L_b), if necessary. Fortunately, L_w can be measured *in situ* spectroradiometrically, so that the validity of these

corrections may be assessed. Before discussing these corrections further, the ways that the OACs affect the scattering and absorption of light in water are reviewed.

Inherent Optical Properties (IOPs), in contrast to AOPs, are independent of the light field and depend solely on the water itself and the OACs present in the water column (Kirk, 1994). There are essentially three OACs that influence the IOPs, besides water: phytoplankton or algae (may also include other photosynthetic biota); suspended matter or *tripton*; and, Coloured Dissolved Organic Matter (CDOM), also called gilvin, yellow substances, or gelbstoff (Kirk, 1994). The term *tripton* includes both the organic and the inorganic components of suspended matter that may be separated into organic detritus and inorganic minerals. The attenuation coefficient, *c*, is the sum of the absorption coefficient, *a*, and the scattering coefficient, *b*, that describe the loss of incident flux as a result of absorption and scattering, respectively, by the OACs over a given path length (units m^{-1}). The backward scattering coefficient, b_b, scattering in a backward (upward) direction, is significant because it contributes to the upwelling radiance that reaches the sensor. The way that each of the OACs, including water, contributes towards absorption and scattering are now reviewed briefly.

Optically and chemically pure water scatters mostly in the blue (<450 nm) and absorbs strongly in the red (>600 nm), increasing exponentially in the near infra-red (>700 nm) (See Figure 3.2). Absorption and scattering of water may be considered invariant and the results of Morel and Prieur (1977), Pope and Fry (1997), and others, are commonly used (Pegau et al., 2003).

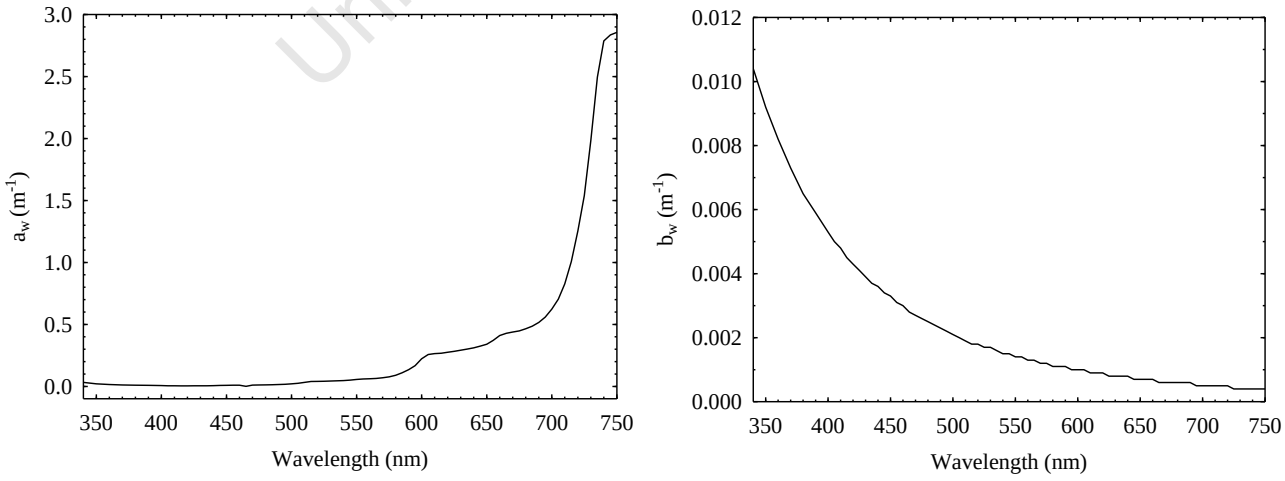

Figure 3.2 Scattering (b_w) and absorption (a_w) coefficients for optically and chemically pure water (Data from Morel & Prieur, 1977).

Phytoplankton absorb primarily through their photosynthetic pigments that include chlorophylls, carotenoids and phycobiliproteins. Chl *a* has absorption peaks at 430 and 663 nm and appears green *in vitro*; carotenoids have absorption maximums between 480 and 520 nm and are yellow, orange or red; and phycobiliproteins are grouped into red phycoerythrins, blue phycocyanin and allophycocyanin, that absorb light between 550 and 570 nm, 610 and 625 nm, and 650 and 670 nm, respectively (Fay, 1983). Approximately 100 algal pigments have been identified that vary according to species, with the exception of Chl *a*, that is present in all phytoplankton (Richardson, 1996). Thus because phytoplankton have different combinations of pigments, some species may be differentiated from others by their absorption properties. The overall absorption spectrum of an alga, come from the combined effects of the pigments present in the cell, modified by the packaging effect, which describes the variation observed between pigments *in vivo*, present in the cell protein complex, and *in vitro*, observed in solution.

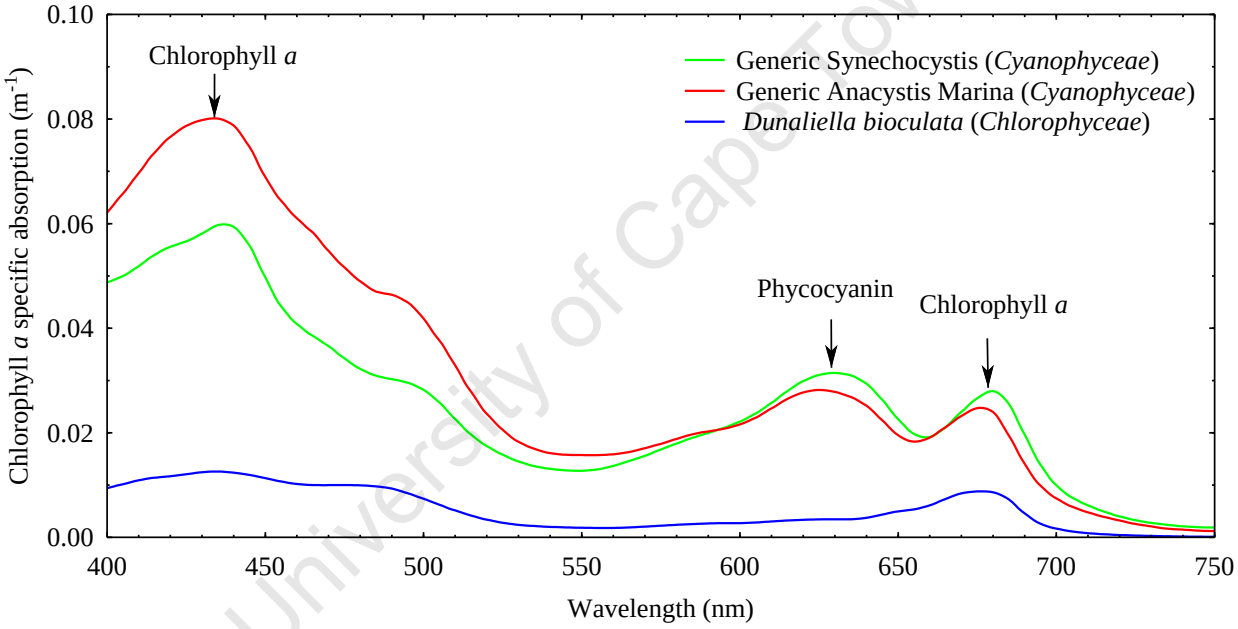

Figure 3.3 Chl *a* specific absorption spectra of two generic marine cyanophyceae and one chlorophyte showing pigment absorption maximums (Data from Ahn et al., 1992 as used by Stramski et al., 2001).

A useful way to represent absorption and scattering by phytoplankton is to normalise the spectra by Chl *a* composition. The Chl *a* specific absorption coefficient, $a_{\phi}^{*}(\lambda)$, units $m^2.mg^{-1}$, is the absorption of the medium, per metre, when the Chl *a* concentration corresponds to 1 $mg.m^{-3}$ (Dekker, 1993) (See Figure 3.3). The values for $a_{\phi}^{*}(\lambda)$ have been found to fall in a broad range because of the complexities associated with phytoplankton populations arising from differences in the species composition of the phytoplankton assemblage, the environmental conditions influencing physiological state, the packaging effect, and cell/colony size and shape (Kirk, 1994, Sathyendranath et al., 2000). Dekker (1993) found values for $a_{\phi}^{*}(\lambda)$ at 676 nm ranging between

0.0055 and 0.0218 $m^2.mg^{-1}$, with an average of 0.0153 $m^2.mg^{-1}$, for lakes in the Netherlands (See also Ganf et al., 1989).

Phytoplankton also contribute significantly to scattering and values of the Chl *a* specific scattering coefficient, $b_\phi^*(\lambda)$, for natural freshwater population vary from 0.8 to 0.22 $m^2.mg^{-1}$ between 400 and 700 nm (Kirk, 1994). On certain occasions, gas vacuoles in *Microcystis* colonies have been estimated to contribute about 80% of the scattered light (Ganf et al., 1989). The shape of the scattering curve is approximately the mirror image of the absorption curve, with peaks around 540 and 710 nm, where absorption by pigments is least (Bricaud et al., 1983). Measurements of the Chl *a* specific backscattering coefficient, $b_{b\phi}^*(\lambda)$, have been shown to be very low (<0.1% of total scattering), and vary notably from one species to another (*ibid.*). Consequently, the observation of the high reflectance observed in bloom conditions from remotely sensed data, has been explained by small organisms, such as bacteria and viruses, which accompany bloom conditions (Sathyendranath et al., 2000). However, recent results suggest that phytoplankton backscattering may be much larger than previously thought (Stramski & Piskozub, 2003).

CDOM, consisting of humic and fulvic acids, contribute greatly towards absorption in the blue region of the electromagnetic spectrum (See Figure 3.4) and negligibly to scattering. The absorption may be approximated by a negative exponential curve, and has often been described with the equation below (Bricaud et al., 1981):

$$a_y(\lambda) = a_y(\lambda_0)\mathrm{e}^{-\mathrm{S}(\lambda-\lambda\mathrm{o})} \qquad (m^{-1}) \tag{3.6}$$

where $a_y(\lambda_0)$ is the reference absorption at wavelength λ_0, and S is the slope of the curve. Using this equation, the absorption can be calculated at the standard reference wavelength of 440 nm if the absorption at another wavelength is known. The value for S reported in the literature is usually between 0.010 and 0.020 nm^{-1} (Dekker, 1993). Values for a_y at 440 nm vary for different inland waters and the values reported by Kirk (1994) range from 0.06 to 14.22 m^{-1}. Interestingly there is no apparent relationship between trophic status and a_y, as it depends more on vegetation in the surrounding catchment, at least in inland waters (*ibid.*).

Absorption by *tripton* is primarily attributed to the detrital (biological) component and scattering to the inorganic component (Pierson et al., 1999). Babin and Stramski (2002) show that absorption by aquatic particles, including phytoplankton detritus, mineral particles and aquatic particles, in inland and coastal waters is negligible in the near infra-red and generally increases with decreasing wavelength. Absorption by detritus closely resembles absorption by yellow substances (the shape of a decreasing exponential function), that is typical of non-pigmented organic substances (Kirk, 1994). For this reason, absorption by detritus is included with yellow substances in many instances (Sathyendranath et al., 2000). However, in turbid water with high concentrations of particulate matter, absorption by *tripton* can be greater than absorption by dissolved yellow substances (Kirk, 1994). Scattering by *tripton* is mainly attributable to inorganic particulate matter, and dominates total scattering in natural waters, such that scattering increases broadly in proportion to the concentration of suspended particulate matter (*ibid.*). The spectral distribution of backscattering by non-pigmented particulate matter shows a gradual increase towards lower wavelengths and may be described by a power law λ^{-n} where n varies between the values 0 and 2 (Bukata et al., 1995).

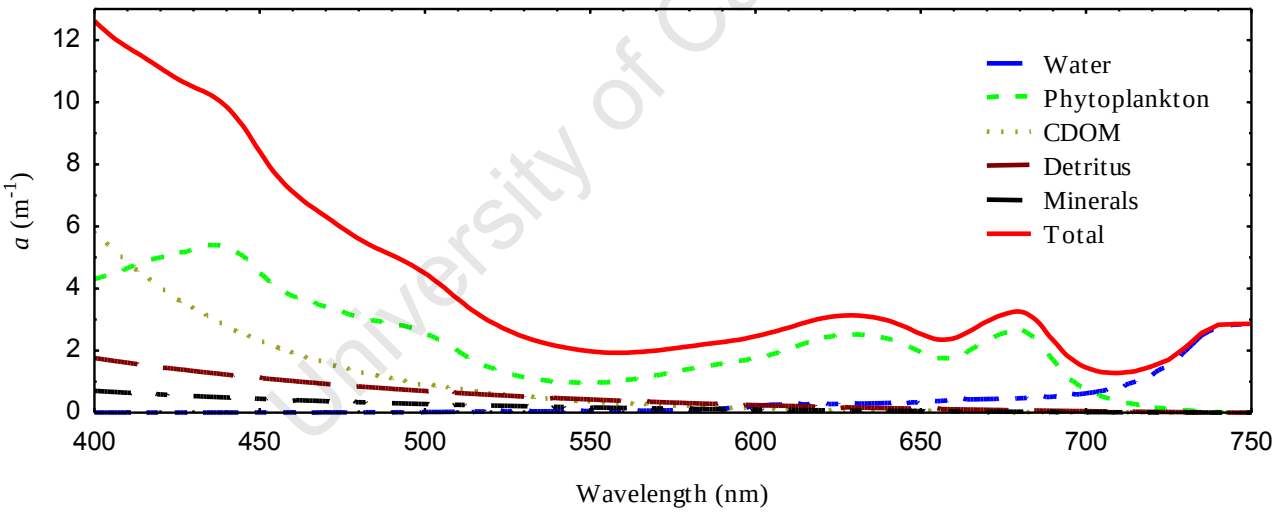

Figure 3.4 Total absorption spectra showing contributions by phytoplankton (Chl *a* = 153.3 mg.m^{-3}), CDOM (*a* 440 nm = 2.78), detritus particles (No. = 6.25E+16) and mineral particles (No. = 2.16E+16) (Data from Pope & Fry, 1997, Stramski et al., 2001, and this study)

The contribution of the OACs to the total IOPs is the sum of the contribution from the individual components or specific absorption/scattering coefficients and may be written as (Sathyendranath et al., 2000):

$$a = a_w + Ca^*_\phi + Ca^*_{CDOM} + Ca^*_s \qquad (m^{-1}) \tag{3.7}$$

$$b_b = b_{bw} + Cb^*_{b\phi} + Cb^*_{bs} \qquad (m^{-1}) \tag{3.8}$$

where subscripts *w*, ϕ, CDOM and *s* stand for water, phytoplankton, Coloured Dissolved Organic Matter, and inorganic suspended matter, respectively, and *C* is the concentration of those components. The sum of the OACs specific absorption/scattering coefficients is called the total absorption/scattering spectrum that influences the upwelling radiance for waters with different concentrations and types of OACs (See Figure 3.4).

The relationships between the OACs and the IOPs can largely be approximated with the empirically derived relationships briefly described above, although not all of these are constant or well-defined. The Radiative Transfer Equation (RTE) describes the relationship between the IOPs and AOPs by relating the variation of radiance of a light beam along a path, passing through a medium, to loss by absorption and scattering, and gain by scattering (Mobley, 1994). The RTE equation is mathematically complex and is beyond the scope of this investigation. Fortunately, the relationship can be approximated much more simply. Kirk (1994) showed that the relationship between remote sensing reflectance and the absorption and backscattering coefficients can be approximated by:

$$R_{rs}(\lambda) = \frac{L_u(\lambda)}{E_d(\lambda)} \approx \frac{f}{Q} \frac{b_b(\lambda)}{\left(a(\lambda) + b_b(\lambda)\right)} \qquad (sr^{-1}) \tag{3.9}$$

where *f/Q* is a constant describing the angular distribution of the light field, with an estimated value in freshwater of approximately 0.083.

Thus, $R_{rs}(\lambda)$ can be estimated at wavelength λ, if the IOPs are known for that wavelength, or alternatively, that the IOPs can be estimated from $R_{rs}(\lambda)$ if either absorption or backscattering are known, or estimated, at that wavelength. Thus, it follows that the concentrations of OACs may be estimated from reflectance data, with an approximation of the radiative transfer in water. Modelling the AOPs from the OACs is called forward bio-optical modelling, whereas inverse modelling gives the OACs from the AOPs (See Figure 3.5). The details of bio-optical modelling, however, are beyond the scope of this investigation (For more details, see Dekker et al., 2001, Stramski et al., 2001).

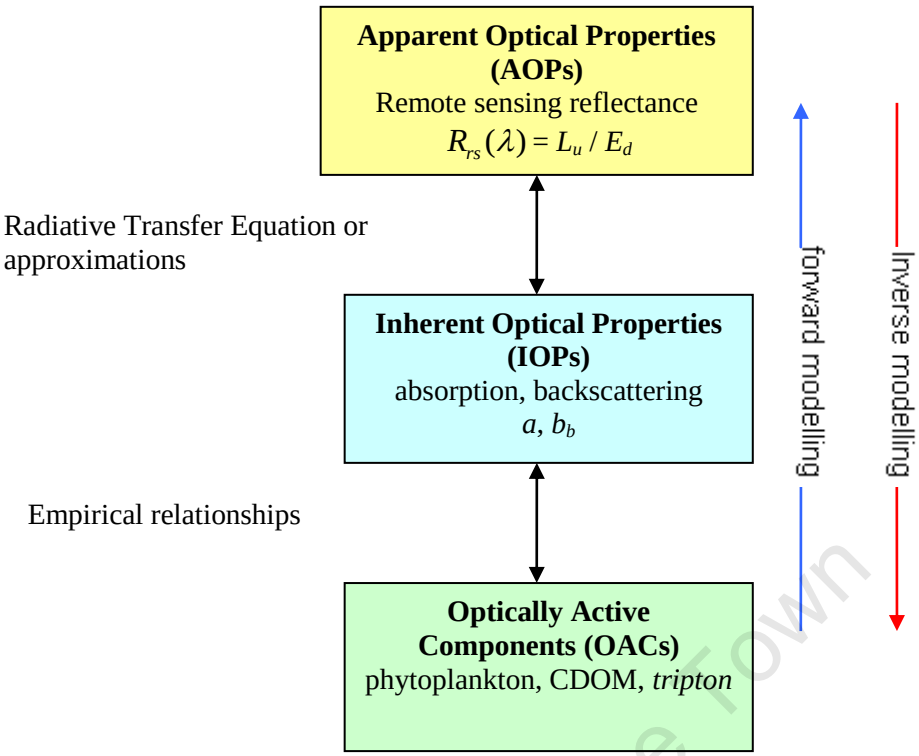

Figure 3.5 Schematic diagram showing forward and inverse bio-optical modelling for estimating the relationships between AOPs, IOPs and OACs.

3.3 Semi-analytical Models

Figure 3.5 shows in essence how water quality parameters are estimated from remote sensing reflectance. Semi-analytical methods estimate the concentrations of OACs using inverse modelling with bio-optical and radiative-transfer models that simulate light propagation through the water and atmosphere respectively (Neumann et al., 2000). Semi-analytical methods (semi-analytical and not purely 'analytical' because all models are dependent on some source of empirical data, and the relationships between the IOPs and OACs must be characterised beforehand for the water body under study) have the advantage of being independent of concurrent *in situ* measurements. A schematic diagram of the process of semi-analytical modelling used by Dekker (2001) is shown in Figure 3.6.

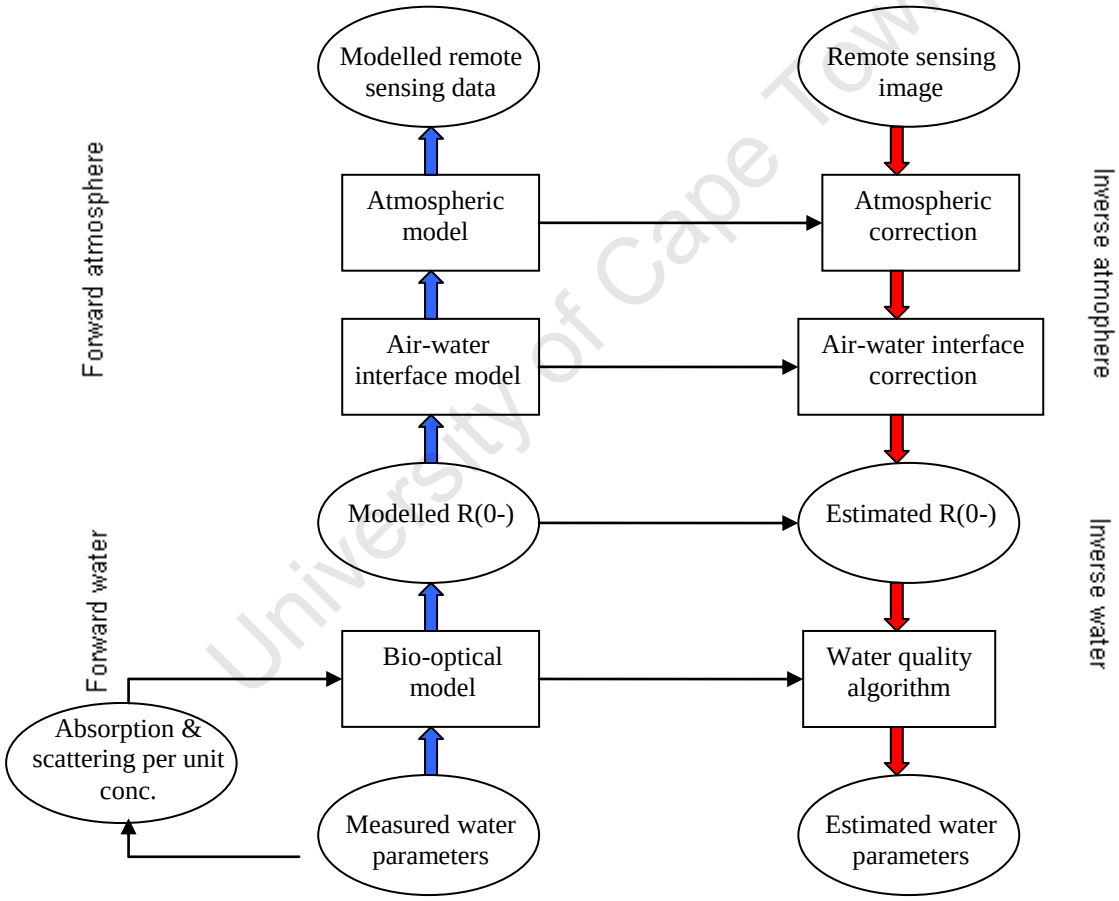

Figure 3.6 Schematic diagram of the semi-analytical model for estimating water quality parameters for remotely sensed data (Redrawn from Dekker et al., 2001).

As shown in the above diagram, semi-analytical methods enable the remotely sensed data at the top of the atmosphere to be forward modelled from measured water quality parameters or alternatively for water quality parameters to be estimated using inverse modelling from remotely sensed data. There are many mathematical techniques that can be employed to solve the inverse

model which include algebraic methods, non-linear optimisation, principal component analysis or the Neural Network (NN) approach (Neumann et al., 2000). Certain techniques require less or more empirical data, and the more sophisticated models allow for the simultaneous retrieval of many unknown quantities, including atmospheric and water quality variables. The correct retrieval of water constituents is highly dependent on the accuracy of the atmospheric correction procedures. If atmospheric corrections are unsatisfactory, the water constituent retrieval from semi-analytical algorithms will always be incorrect. Other problems associated with inverse models are related to the bio-optical model parameterisation, and the training range of concentrations of OACs. Inverse models are more desirable for operational monitoring systems because there is no need for simultaneous *in situ* measurements, and there have been numerous studies that have focussed on their development (See Appendix 1, for example, Dekker et al., 2002, Giardino et al., 2007, Odermatt et al., 2008).

The MERIS level 2 data product uses an inverse model for atmospheric properties and water constituent retrieval. Atmospheric correction is carried out according to a coupled hydrological atmospheric model specifically designed for Case 2 waters (Moore et al., 1999). Water constituents are retrieved by employing an Inverse Radiative Transfer Modelling technique with a Neural Network parameterisation algorithm (IRTM-NN) that iterates to match the measured and modelled spectra for quality estimation (Schiller & Doerffer, 1999, Schiller & Doerffer, 2005). The algorithm uses the atmospherically corrected water-leaving reflectance in 8 bands as input, and retrieves Chl *a* in the range 0.5 to 50 $mg.m^{-3}$, suspended matter in the range 1 to 100 $mg.\ell^{-1}$, and absorption by *gelbstoff* at 440 nm in the range 0.02 to 2 m^{-1}. The bio-optical model is trained using data collected in North European, Mediterranean and North Atlantic coastal waters. There are several validation studies that have shown that the algorithm produces good results in Case 2 waters in European lakes and coastal waters (Cipollini et al., 2001, Schiller & Doerffer, 2005, Reinart & Kutser, 2006). However, the algorithm is limited to conditions with similar IOPs and to concentrations inside the training range, which limits its usefulness in eutrophic/hypertrophic lakes with high suspended matter or a_{CDOM}, as will be demonstrated with Zeekoevlei.

An algorithm specifically trained for eutrophic water was recently developed as a plugin for VISAT BEAM Version 4.2 software toolbox (Brockmann Consult). The Eutrophic Lakes Processor retrieves IOPs and water constituents in eutrophic conditions from full-resolution MERIS level 1 data, using an algorithm similar to the IRTM-NN algorithm used in the Level 2 product (Doerffer & Schiller, 2008a). The algorithm computes total particulate scattering and absorption by Chl *a* and *gelbstoff* at 443 nm, as well as Chl *a* and suspended dry weight

concentrations, the attenuation coefficient for downwelling irradiance at wavelength with maximum transparency (K_{dmin}), and the optical depth from which 90% of the reflected light comes (*z90*). The algorithm is trained using more than 60 000 spectra obtained from bio-optical simulations with the Hydrolight Radiative Transfer Code based on data collected from Spanish lakes, to derive Chl *a* concentrations in the range 0 to 120 $mg.m^{-3}$, total suspended matter in the range 0.42 to 50.9 $mg.\ell^{-1}$ and absorption by *gelbstoff* at 440 nm in the range 0.1 to 3 m^{-1} (Doerffer & Schiller, 2008b). The Eutrophic Lakes Processor is therefore likely to be more applicable to conditions in Zeekoevlei.

3.4 Empirical Approach

In contrast to complex semi-analytical methods, more simple empirical methods rely on concurrent *in situ* data to match the remotely sensed signal with measured water quality parameters using statistical regression techniques (See Figure 3.7).

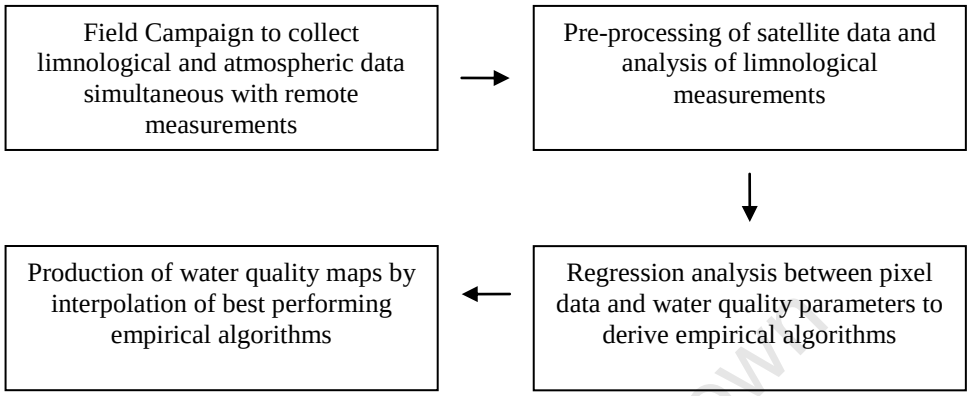

Figure 3.7 Flow diagram illustrating the empirical approach (After Lindell et al., 1999).

The remotely sensed signal is correlated with the water constituent concentrations using linear, multiple-linear, non-linear or other models. The so-called colour ratio is a common empirical algorithm using a ratio of bands formulated according to (Neumann et al., 2000):

$$p = \alpha \frac{R_1}{R_2}^{\beta} + \gamma \qquad (3.10)$$

where p is the estimated water quality parameter, R_i is the reflectance in spectral channel i, and α, β, and γ are coefficients derived from the regression.

There are many other varieties of algorithms that use single bands, band ratios, band arithmetic or multiple bands, sometimes with logarithmic transformations. Empirical algorithms are limited in the sense that they are not applicable across large temporal periods or study areas, and produce reliable results only inside the range of derivation. Furthermore, the covariance that often exists between water constituents, such as between phytoplankton density and suspended matter, means that it may be difficult to separate these sometimes non-unique signals with empirical algorithms. However, as the following discussion shows, empirical algorithms generally produce robust results. Reviews of empirical algorithms have been performed elsewhere (See, for example, Kirk, 1994, Durand et al., 1999, Lindell et al., 1999) however, it was necessary to review the results of more recent studies (See Appendix 1). The results of the review are discussed below with

reference to algorithms for Chl *a*, suspended solids, Secchi Disk depth (SD) and absorption by CDOM (a_{CDOM}) retrieval. The coefficient of determination, r^2, and the Root Mean Square Error, RMSE, in the table in Appendix 1, gives an estimate of the accuracy of the algorithm performance.

3.4.1 Chl *a* Retrieval Algorithms

Chl *a* concentration is one of the most commonly used limnological parameters for trophic status determination of lakes. For this reason it is of interest as it acts as a proxy for algal densities and primary production.

3.4.1.1 R_{700}/R_{670} Algorithms

Appendix 1 shows that in many instances an algorithm including the ratio of reflectance at about 700 and 670 nm, R_{700}/R_{670}, produces good results for estimating Chl *a* concentrations in high-biomass waters. In particular, the studies by Mittenzwey et al. (1992), Gitelson et al. (1993), and Gons (1999) show that the relationship between R_{700}/R_{670} and Chl *a* concentrations is very strong ($r^2 > 0.8$). These studies use spectroradiometric measurements of spectral reflectance from rivers, lakes, estuaries and laboratory measurements in Germany, the Netherlands and other European countries. The combined sample size for these studies is greater than 591 and the concentration of Chl *a* varies in a wide range from 0.1 to 350 $mg.m^{-3}$. Thus the relationship is valid across a wide range of concentrations in different water bodies in different countries.

Other studies using spectroradiometer data or high spectral resolution airborne platforms use the R_{700}/R_{670} ratio or a very similar ratio for Chl *a* concentration retrieval (Dierberg & Carriker, 1994, Jiao et al., 2006, Menken & Brezonik, 2006, Duan et al., 2007). Linear, multiple linear and non-linear regression techniques are used. The r^2 values for these studies range from 0.75 (Duan et al., 2007) to 0.99 (Menken & Brezonik, 2006) showing that the algorithms are very robust. Yacobi et al. (1995) used the ratio R_{max}/R_{670}, where R_{max} is the value of the maximum reflectance near 700 nm, to retrieve Chl *a* with a r^2 value of 0.95 for a wide range of concentrations in Lake Kinneret, Israel. Zimba and Gitelson (2006) used a three band conceptual model for very high biomass hypertrophic waters:

$$\text{Chl } a = \mathrm{R}(\lambda_3)\left(\frac{1}{\mathrm{R}(\lambda_1)} - \frac{1}{\mathrm{R}(\lambda_2)}\right) \qquad (mg.m^{-3}) \qquad (3.11)$$

where $R(\lambda_1)$ is reflectance in wavelength maximally sensitive to Chl *a* absorption (650 nm), $R(\lambda_2)$ is reflectance in wavelength minimally sensitive to absorption by Chl *a* (710 nm), and $R(\lambda_3)$ is reflectance in wavelength minimally effected by absorption that accounts for scattering (740 nm). Using spectroradiometer data in hypertrophic water quality conditions the three band model best described the variation in Chl *a* concentration with a r^2 value of 0.78.

The MERIS sensor has three bands at 665, 681 and 709 nm ideally suited for estimating Chl *a* (Gower et al., 1999). A number of studies in high-biomass marine and inland waters make use of the R_{709}/R_{665} band ratio using MERIS or simulated MERIS data (See Appendix 1, for example, Kallio et al., 2003, Gons et al., 2005, Koponen et al., 2007). For linear and exponential regressions, the r^2 value for these studies varies from 0.84 (Flink et al., 2001) to 0.98 (Kallio et al., 2003) showing that the algorithms are robust across different water conditions and Chl *a* concentrations. Some of these studies improve the strength of the correlation by subtracting a near-infrared band (781 or 754 nm) from the 709 and 665 nm bands (See Härmä et al., 2001, Koponen et al., 2002). This acts as a rough atmospheric correction based on the assumption that the reflectance in the near-infrared over water is mainly due to atmospheric effects.

The algorithm used by Gons et al. (1999, 2002, 2005) is a modified semi-empirical R_{709}/R_{665} algorithm that includes the absorption coefficients for pure water, Chl *a*, and backscattering. The algorithm is presented 'user-ready' for implementation with the MERIS L2 product and is calibrated for well-mixed, high biomass waters. However, the algorithm is limited in that the IOPs of different waters may not match the suggested values and it is based on the assumption that the MERIS L2 product gives accurate water-leaving reflectances.

The peak near 700 nm, sometimes called the 'red-edge', is caused by backscattering from particulate matter which increases towards the infrared and the strong absorption of water that effectively masks out the backscattering signal greater than about 720 nm, causing a sharp peak. At 700 nm absorption by phytoplankton and dissolved organic matter is insignificant allowing backscattering to be increased (Yacobi et al., 1995, Schalles et al., 1998). Thus the height and position of the peak near 700 nm is well correlated with Chl *a* concentrations, with the peak shifting towards greater wavelengths (~715 nm) as Chl *a* increases (Gitelson, 1992). In contrast to the reflectance at 700 nm, the Chl a absorption maximum near 670 nm causes the backscattering signal to be diminished. Thus the reflectance near 670 nm is non-correlated with Chl *a*, being almost constant. Thus, the R_{700}/R_{670} algorithm is effectively a normalisation of the signal from particulate backscattering near 700 nm.

3.4.1.2 FLH and RLH Algorithms

The Fluorescence Line Height (FLH) algorithm (Gower, 1980, cited Gitelson et al., 1994), measures the height of the Chl *a* fluorescence peak at 685 nm from a linear baseline drawn between two points on either side of the peak (Dierberg & Carriker, 1994, Giardino et al., 2005). Importantly, the FLH algorithm is only suitable for low-biomass waters with Chl a concentrations not exceeding about 30 $mg.m^{-3}$, because it is very difficult, or impossible, to differentiate between the signal from particulate backscattering and solar induced fluorescence at high biomass. r^2 values for linear regression FLH algorithms range from 0.73 (Gitelson et al., 1994) to 0.86 (Dierberg & Carriker, 1994) for Chl *a* concentrations not exceeding 79 $mg.m^{-3}$.

Algorithms that are better suited to high-biomass waters are the Reflectance Line Height (RLH) or Scattered Line Height (SLH) algorithm, (Dierberg & Carriker, 1994, Yacobi et al., 1995, Schalles et al., 1998) and the SUM of reflectance (SUM) algorithm (Gitelson et al., 1994, Schalles et al., 1998). The RLH algorithm is a modified FLH algorithm and is written (after Gower et al., 1999):

$$RLH = L_2 - L_1 - \left((L_3 - L_1) \times \frac{(\lambda_2 - \lambda_1)}{(\lambda_3 - \lambda_1)} \right) \qquad (3.12)$$

where L_i is the radiance in band i and λ_i is the centre wavelength of band i. Band $i = 2$ is centred on the reflectance peak close to 700 nm, while bands $i = 1, 3$ on either side determine the baseline (670 and 850 nm). In waters with high Chl *a* concentrations, r^2 values range from 0.85 (Dierberg, Carriker 1994) to 0.96 (Yacobi et al., 1995). Similarly, the SUM algorithm, using the sum of the reflectance above a baseline between 670 and 730 or 850 nm, gave r^2 values greater than 0.84 (Schalles et al., 1998).

3.4.1.3 Algorithms for Landsat

There are many examples of algorithms for estimating Chl *a* from Landsat data (See Appendix 1, for example, Lathrop & Lillesand, 1986, Giardino et al., 2001, Tyler et al., 2006). The statistical techniques used range from simple linear regressions to complex multiple variable regressions and advanced algorithms. The most common algorithms are simple linear and multiple linear regressions of single or log-transformed bands or band ratios. r^2 values range from 0.67 (Duan et al., 2007) to 0.98 (Lathrop & Lillesand, 1986). Multiple variable linear regressions give r^2 values ranging from 0.58 (Alparslan et al. 2007) to 0.99 (Brivio et al., 2001). More advanced algorithms (Sudheer et al., 2006, Chen et al., 2008) do not appear to offer significant enough accuracy

improvements when compared to other studies to justify their mathematical difficulty. Other techniques include classification procedures such as the linear mixture modelling approach (r^2 = 0.95) (Tyler et al., 2006) and chromaticity analysis (Östlund et al., 2001).

3.4.2 TSS Retrieval Algorithms

Total Suspended Solids (TSS) (also called total suspended matter or suspended matter) is the name given to the total mass of suspended particles per litre of water including inorganic and organic components. TSS is important for water quality management since it is related to primary production, the transport of sediments and water clarity (Dekker et al., 2002). Far fewer studies investigate TSS than Chl *a*, and finding algorithms that effectively separate the signals from suspended particulate matter and phytoplankton may be difficult.

Gitelson et al. (1993) used the difference ratio (R560-R520)/(R560+R520) for TSS retrieval from radiometric data. Reflectance at 560 nm is sensitive to changes in TSS because of the phytoplankton absorption minimum here, that allows greater scattering by suspended matter. Conversely, reflectance at 520 nm is relatively insensitive to changes in TSS. Thus the difference ratio acts to normalise the signal at 560 nm for scattering. The r^2 value for 66 samples with suspended matter concentrations ranging from 0.1 to 66 mg.ℓ^{-1} was 0.86, showing that the algorithm performed strongly in these conditions.

TSS retrieval algorithms for MERIS typically use linear regressions with bands at 709, 665 nm and in the near-infrared. The 709 nm band, described above as the 700 nm reflectance peak, is also correlated with TSS because Chl *a* is covariant with TSS, especially when phytoplankton makes up a large component of suspended particulate matter. Backscattering by minerals, the inorganic component of TSS, in the near-infrared means that in some instances bands in this region may also be used in algorithms. Koponen et al. (2007) used the ratio $L_{708}/(L_{560}+L_{665})$, Härmä et al. (2001) used $L_{705}-L_{754}$ and Kallio et al. (2001) used R_{710}. These gave r^2 values of 0.92, 0.81 and 0.85, respectively. The above studies, however, are for relatively low concentrations of TSS, not exceeding 32 mg.ℓ^{-1}.

Research shows that TSS can be successfully estimated in rivers and lakes using Landsat and other broad band sensors. In many instances simple linear regressions of single bands and band ratios produce good correlations ($0.88 \leq r^2 \leq 0.95$) (Östlund et al., 2001, Sváb et al., 2005, Tyler et al., 2006, Onderka & Pekarova, 2008). Multiple linear regressions with single bands gave r^2 values of 0.99 (Alparslan et al., 2007) and 0.52 (Wang et al., 2006), respectively. Lathrop and

Lillesand (1989) used SPOT data and log transformed multiple linear regression to give a r^2 value of 0.93 for Lake Michigan, USA. Miller and McKee (2004) used 250 m MODIS data for TSS retrieval in the Gulf of Mexico using a one band ($L_{620-670}$) algorithm (r^2 = 0.89). Semi-analytical bio-optical modelling with multi-temporal SPOT and Landsat data with found that an exponential power function with (TM2+TM3)/2 can estimate TSS in lakes in the Netherlands with r^2 = 0.99 (Dekker et al., 2002). Sudheer et al. (2006) used an artificial neural network algorithm with TM bands 1 to 4 to retrieve TSS with a r^2 value of 0.98 for a reservoir in Arkansas, USA. Therefore, it appears that using more advanced algorithms, such as the last two examples, may improve TSS retrieval accuracies.

3.4.3 Secchi Disk Depth Retrieval Algorithms

Secchi Disk depth (SD), a proxy for water clarity, measures the depth of penetration of light in the water as perceived by the human eye, and has units m. It is useful for water management because water clarity is often the basis with which water users perceive water quality. SD is negatively correlated with suspended matter concentrations and algal densities, since these decrease water clarity, and approximates gross particulate load that has a large effect on water-leaving reflectance. The SD algorithms show gross changes in particulate load, and to some extent, so do those of other parameters (for example, Chl *a* and TSS).

Studies investigating the retrieval of SD from simulated MERIS data for lakes in Finland, use band difference ratios and simple linear regressions. The ratios $(L_{521}-L_{781})/(L_{700}-L_{781})$ (Koponen et al., 2002), $(L_{490}-L_{754})/(L_{620}-L_{754})$ (Härmä et al., 2001), and $(L_{492}-L_{751})/(L_{622}-L_{751})$ (Kallio et al., 2001), gave r^2 values of 0.93, 0.83 and 0.86, respectively. The subtraction of near-infrared bands from the ratios acts as a rough atmospheric correction procedure. From these studies it appears that the ratio of MERIS band at 490 or 510 nm, to bands at 620 or 709 nm, will most likely produce the best results.

Many studies investigate the retrieval of SD from Landsat. Linear regression with log transformed single bands (Lathrop & Lillesand, 1986, Hellweger et al., 2007), band ratios (Giardino et al., 2001), difference ratios (Härmä et al., 2001) and multiple regressions (Brezonik et al., 2005, Wang et al., 2006, Alparslan et al., 2007) gave r^2 values ranging from 0.59 to 0.99. Wang and Ma (2001) used principal component analysis; however, no estimation of the accuracy was given. Lathrop and Lillesand (1989) retrieved SD from SPOT data with a r^2 value of 0.98, using a linear regression of band 3 for Lake Michigan, USA.

3.4.4 a_{CDOM} Retrieval Algorithms

Absorption by Coloured Dissolved Organic Matter (a_{CDOM}) is a significant contributor to water colour since humic substances absorb strongly in the blue region of the spectrum. In situations where a_{CDOM} is very large, it may influence the retrieval of other water quality parameters.

Gitelson et al. (1993) used a difference ratio algorithm for a_{CDOM} retrieval from radiometric data that includes a correction for absorption by Chl *a*. The algorithm may be written:

$$a\text{CDOM} = \text{a}\left\{\left(\text{R}_{480} - \frac{\text{R}_{700}}{\text{R}_{675}} - \text{R}_{520}\right) \div \left(\text{R}_{480} + \frac{\text{R}_{700}}{\text{R}_{675}} + \text{R}_{520}\right)\right\}^{\text{b}} \qquad (m^{-1}) \qquad (3.13)$$

where a and b are regression coefficients. The 480 nm band is strongly influenced by a_{CDOM} while the 520 nm band is a reference band. The R_{700}/R_{675} ratio is included to correct for Chl *a* absorption in the blue region of the spectrum. The algorithm gave an r^2 value of more than 0.9 for a_{CDOM} at 380 nm in the range 0.1 to 12 m^{-1} in more than 20 inland water bodies (*ibid.*).

a_{CDOM} retrieval from MERIS using linear regressions with band ratios R_{665}/R_{490} (Koponen et al., 2007), R_{665}/R_{550} (Ammenberg et al., 2002) and $(L_{571}\text{-}L_{607})/L_{607}$ (Kallio et al., 2001) gave r^2 values of 0.96, unknown and 0.84, respectively. The results of Kallio et al. (2001) should be treated with some caution as covariance was observed between TSS and a_{CDOM}. The other ratios use the Chl *a* absorption maximum at 665 nm in the numerator, unaffected by CDOM absorption, and the 490 or 550 nm band in the denominator, that is influenced by CDOM absorption. The 665 nm band normalises for the effects of Chl *a* absorption and backscattering by suspended matter and algae. Thus it is expected that a band ratio algorithm using MERIS band 9 (665 nm) in the numerator, and band 5 (560 nm) or 3 (490 nm) in the denominator, will produce the best correlation with a_{CDOM}. However, care should be taken as the blue region of the spectrum is most sensitive to a_{CDOM}, but also to errors in atmospheric correction.

Broad-band sensors can also be used successfully to estimate a_{CDOM} in lakes, although not with the same level of accuracy as for other parameters. Kutser et al. (2005) used a non-linear exponential regression with a band ratio using ALI bands 2 and 3 ($L_{525\text{-}605}/L_{630\text{-}690}$) to give a r^2 value of 0.73 for lakes in the Netherlands. Band 3 acts to normalise the signal, while band 2 is correlated with a_{CDOM}. Using Landsat TM and multiple linear regression, Brezonik et al. (2005) derived a_{CDOM} with a r^2 value of 0.77 for 15 lakes in Minnesota.

3.4.5 Algorithms for Other Water Quality Parameters

Other water quality parameters retrieved using remote sensing and included in the studies in Appendix 1 are turbidity (TURB), Suspended Particulate Inorganic Matter (SPIM) and phycocyanin pigment (PC). TURB is closely related to TSS and SD and is therefore largely redundant where these variables are collected. Suspended Particulate Inorganic Matter (SPIM), the inorganic component of TSS, may be of interest when large amounts of inorganic sediment are entrained in the water column. Ammenberg et al. (2002) found that SPIM could be estimated with an accuracy of $r^2 = 0.83$ from algorithms derived from a bio-optical model based on the R_{705}/R_{664}band ratio.

Phycocyanin (PC), the pigment present in all cyanobacteria, is very useful for predicting the occurrence and development of cyanobacterial blooms. Simis et al. (2007) using simulated MERIS data and a semi-empirical algorithm estimated PC with a r^2 value of 0.90 for turbid cyanobacteria-dominated lakes. Vincent et al. (2004) investigated PC retrieval from Landsat TM and ETM+ and found that multiple linear regressions of band ratios gave r^2 values of 0.63 and 0.78, respectively. Thus, PC estimation from remotely sensed data will likely be used in future to predict cyanobacterial blooms.

3.5 Atmospheric Correction Techniques

Atmospheric correction procedures are intended to remove the effects of radiance reaching the sensor that is absorbed and scattered by aerosols and particles (See Section 3.2). The atmospheric path radiance (L_p) can comprise more than 95% of the signal measured over water targets in instances where the atmosphere is hazy (Bukata et al., 1995). Therefore it is imperative to correct for atmospheric effects if a reliable estimate of the water-leaving reflectance is to be made. This is especially true when considering that the signal from water is usually much smaller than from the surrounding land and is therefore more sensitive to contributions from the atmosphere. Atmospheric corrections over optically complex Case 2 waters are more complicated than for Case 1 waters. The conventional atmospheric corrections for ocean waters (Case 1) utilise the fact that the water leaving signal is negligible in the near infra-red, due to absorption by water, and therefore can be used as an approximation of atmospheric effects (Gordon, 1978). Unfortunately, this assumption breaks down over Case 2 turbid, or so called 'bright-pixel', waters, because suspended particulate matter causes significant backscattering in the near infra-red region (Moore et al., 1999, Vidot & Santer, 2005). Therefore alternative methods of atmospheric correction are required when dealing with Case 2 inland waters. Several methods appear in Appendix 1 for correction for atmospheric contributions, encompassing simple empirical corrections, and more complicated Radiative Transfer Codes (RTCs). These are reviewed briefly.

3.5.1 Dark Object Subtraction (DOS)

Dark Object Subtraction (DOS) is a technique used by a number of the studies reviewed (See, for example, Giardino et al., 2001, Vincent et al., 2004, Alparslan et al., 2007). DOS is an entirely image-based correction, eliminating the need for *in situ* measurements of atmospheric properties, as required by certain radiative transfer models (Chavez, 1996). This is particularly useful in multi-temporal change detection studies from archived satellite data (Song et al., 2001). DOS assumes that atmospheric effects can be estimated from the darkest pixel in the scene in any spectral band, assuming the atmosphere is homogeneous across the entire scene. The equation for correcting at-satellite radiances to surface reflectances is as follows (Moran et al., 1992):

$$\rho(\lambda) = \frac{\pi\left(L_{TOA}(\lambda) - L_{\text{path}}(\lambda)\right)}{T_\lambda \uparrow (kE_0(\lambda)\times\cos\theta_s \times T_\lambda \downarrow + E_{down})} \tag{3.14}$$

where $\rho(\lambda)$ is the atmospherically corrected normalised surface reflectance, L_{TOA} is the Top-Of-Atmosphere spectral radiance, L_{path} is the spectral atmospheric 1path radiance, $T_\lambda\downarrow$ and $T_\lambda\uparrow$ are the downward and upward atmospheric transmittances, respectively, k is the sun-earth distance coefficient that is dependent on the day of the year, E_0 is the top of atmosphere solar spectral irradiance, θ_s is the solar zenith angle and E_{down} is the downwelling spectral irradiance.

The simple DOS model assumes $T_\lambda\downarrow$ and $T_\lambda\uparrow$ are equal to 1 and ignores the effects of downwelling spectral irradiance (E_{down} = 0). The value for $L_{\lambda path}$ is extracted from the darkest object in the scene. Thus, the equation for calculating atmospherically corrected reflectance values using the simple DOS model is (Giardino et al., 2001):

$$\rho(\lambda) = \frac{\pi\,(L_{TOA}(\lambda) - L_{path}(\lambda))}{E_0(\lambda)\cos\theta_s} \tag{3.15}$$

Chavez (1996) proposed an improved cosine or 'COST' method that estimates $T_\lambda\downarrow$ by the cosine of the solar zenith angle, $cos\theta_s$, and $T_\lambda\uparrow$ by the cosine of the viewing zenith angle, $cos\theta_v$. Thus the COST DOS reflectance is calculated according to:

$$\rho(\lambda) = \frac{\pi\,(L_{TOA}(\lambda) - L_{path}(\lambda))}{\cos\theta_v\ E_0(\lambda)\ \cos\theta_s^2} \tag{3.16}$$

where θ_v is the cosine of the viewing angle.

The COST model is a well-tested method for image-based atmospheric correction for Landsat data in water quality studies (See Giardino et al., 2001, Wang et al., 2004, Wang et al., 2006). The atmospheric transmittances could alternatively be measured *in situ*. Other variations of the DOS procedure are proposed (Song et al., 2001), however, no method appears to produce consistently better results than another.

3.5.2 Empirical Line (EL) Method

The Empirical Line (EL) method (See Kutser, 2004, Kutser et al., 2005) requires that the reflectance value of at least one object in the scene be known and that the digital number associated with zero reflectance be estimated (Moran et al., 2001). With this information a regression between the digital numbers and the surface reflectance for the scene is established, and the whole scene can be converted to reflectance based on the prediction equation. The EL

method is limited by the fact that a high-reflectance target is more suited to establishing the regression than a low-reflectance target such as water. If the method is to be reliably utilised, a suitable high-reflectance target appearing consistently across multi-temporal images must be identified, and additional fieldwork carried out in order to measure its reflectance (*ibid.*). This feature of the EL method, however, is its major drawback in situations where there are constraints related to instrumentation or time.

3.5.3 Radiative Transfer Codes (RTCs)

Radiative Transfer Codes (RTCs) are mathematical models that simulate the propagation of light through the atmosphere. There are numerous examples of studies using RTCs to estimate the atmospheric contribution over water targets, and because of their physical accuracy, they are generally preferred over the techniques reviewed above (See Appendix 1, for example, Dor & Ben-Yosef, 1996, Brando & Dekker, 2003, Giardino et al., 2007). Commonly used RTCs are the Second Simulation of the Satellite Signal in the Solar Spectrum code or 6S (Vermote et al., 1997), and MOD/LOWTRAN, the moderate/low resolution atmospheric transmittance code (Kneizys et al., 1988).

The 6S code is used in a number of studies with different data types including MERIS (Floricioiu et al., 2003, Floricioiu et al., 2004, Candiani et al., 2005), Landsat TM (Östlund et al., 2001), and airborne data (Flink et al., 2001, Ammenberg et al., 2002). The code demonstrated good performance in comparison to *in situ* measurements over inland lake waters, and performed better than the MERIS L2 product atmospheric correction (See below) (Flink et al., 2001, Floricioiu & Rott, 2003, Floricioiu & Rott, 2005). The code requires various inputs including: geometrical conditions (month, day, longitude and latitude); an atmospheric model; target and sensor altitude; spectral conditions (satellite bands); and ground reflectance. The code also requires the aerosol optical depth at 550 nm, which can be measured *in situ* with a sun photometer, or alternatively estimated through the Dark Dense Vegetation (DDV) technique (See Floricioiu & Rott, 2005). A user friendly interface that creates input files for inexperienced users is available at http://modis-sr.ltdri.org/6S_code/index.html, along with a copy of V1.1 of the code and user manuals.

The MOD/LOWTRAN code has been applied to a variety of data types, notably SPOT and Landsat (Dor & Ben-Yosef, 1996, Dekker et al., 2002), the hyperspectral Hyperion sensor (Brando & Dekker, 2003, Kutser, 2004, Giardino et al., 2007), in addition to various airborne hyperspectral sensors (Kallio et al., 2001, Hakvoort et al., 2002). Giardino et al. (2007) show that the accuracy of MODTRAN for correcting Hyperion hyperspectral data over Lake Garda, Italy, is

good in the visible spectrum (RMSE of 14%), but inferior in the near-infrared (RMSE of 77%), as a result of adjacency effects from vegetation on the shores of the lake. Adjacency effects are a significant source of error in near-infrared bands, especially in inland and coastal waters (Santer & Schmechtig, 2000). Brando and Dekker (2003) included a correction for adjacency effects to gain better agreement with *in situ* measurements in the near-infrared, for the coastal esturine waters of Moreton Bay, Australia. Adjacency effects over Zeekoevlei, because of its small surface area, are likely to contribute significantly to radiance measured at the sensor in near-infrared bands. Correction of adjacency effects for MERIS TOA data may be achieved using the Improve Contrast between Ocean and Land (ICOL) processor (Santer & Zagolski, 2008).

3.5.4 MERIS L2 Atmospheric Correction Procedure

The MERIS Level 2 (L2) product gives water-leaving reflectances for Case 2 waters using a coupled hydrological atmospheric model that solves the water-leaving radiance and atmospheric path radiance in the near-infrared (Antoine & Morel, 1999, Moore et al., 1999). Studies assessing the validity of the atmospheric correction procedure, in lake and coastal Case 2 waters (Moore et al., 1999, Ruddick et al., 2003, Gege & Plattner, 2004), found that there is generally good agreement between *in situ* spectra and atmospherically corrected spectra derived from the airborne/satellite data. However, all the studies showed divergence in the blue (400 to 500 nm) part of the spectrum, signifying either overestimation or underestimation of the atmospheric effects (See also Reinart & Kutser, 2006). Furthermore, correction efficiency is variable across the spectrum and typicall best in the near-infrared. Therefore caution should be exercised when using the MERIS L2 product, and comparisons should be made with *in situ* measurements, where possible, to assess the validity of the results.

3.5.5 No Atmospheric Correction

Appendix 1 shows that in some cases atmospheric correction has been ignored. Giardino et al. (2005) successfully used uncorrected TOA MERIS data to derive Chl *a* for Lake Guarda, Italy. Similarly, Onderka and Pekárová (2008) derived TSS concentrations from uncorrected Landsat 7 ETM+ data for the Danube River, Slovakia, with a r^2 coefficient of 0.93. These two examples, and others, show that atmospheric correction is not always necessary when using empirical algorithms for gross change detection applications (See also Kallio et al., 2003, Hellweger et al., 2007). This is because with a single-date image, empirical or image-based atmospheric correction procedures amount only to relative changes in the pixel values that do not affect classification or correlation analysis (Song et al., 2001, Chen et al., 2008). Therefore, when using certain empirical algorithms, atmospheric correction is in some cases unnecessary. However, in multi-temporal studies comparing images of different dates, or when using semi-analytical algorithms,

which are highly dependent on the derivation of accurate water-leaving reflectances, atmospheric correction remains indispensable.

Chapter 4 Methodology

The simultaneous acquisition of remotely sensed and *in situ* experimental data is paramount for developing water quality parameter algorithms using the empirical approach. Thus field measurements formed an important component of this study, and empirical algorithms for MERIS are derived directly from simultaneous water quality parameter measurements. *In situ* hyperspectral radiometric measurements of the upwelling radiance allow for the main in-water optical features of Zeekoevlei to be identified and for the influence of the water constituents on the water-leaving reflectance to be assessed. Algorithms from the radiometric data form the basis for algorithm development from MERIS. Radiometric reflectance measurements are also useful for assessing the validity of atmospheric correction procedures. Empirical algorithms for Landsat 7 are based on simultaneous simulated radiometric reflectance and limnological data. This chapter contains four sections: Section 4.1 deals with the fieldwork and laboratory methods; Section 4.2 deals with the field spectroradiometry; Section 4.3 describes the method used for the estimation of water quality parameters from MERIS; and Section 4.4 outlines the method for the estimation of water quality parameters from Landsat 7 ETM+.

4.1 Limnological Methods

Field measurements coinciding with satellite data acquisitions were conducted at four sample sites during the month of April 2008 (See Figure 4.1). April was chosen because it preceeds the winter rainy season when cloud cover could severely impact on the number of cloud-free acquisitions. Sample sites were selected to coincide with historical sampling sites used by Harding (1991, 1996) and by the City of Cape Town Scientific Services water quality monitoring programme. The sample sites were located so as to represent each of the four main basins in Zeekoevlei. A handheld Garmin GPS 60 Navigator was used to locate the co-ordinates of the four sites (Table 4.1). Sites 1 to 4 where sampled on days coinciding with possible acquisitions of CHRIS, while only sites 2 and 3 were measured on days exclusively with MERIS overpasses (See Section 4.3.1). No sampling took place on completely overcast days.

Table 4.1 GPS co-ordinates of the four sampling sites

ZEV 1	18º 30.532' E	34º 03.686' S
ZEV 2	18º 30.837' E	34º 03.370' S
ZEV 3	18º 30.919' E	34º 04.040' S
ZEV 4	18º 30. 549' E	34º 04.137' S

4.1.1 Physical measurements

Water samples were collected between 9 and 12 am on clear or partially cloudy days coinciding with satellite overpasses, normally within an hour of the overpass. Samples were

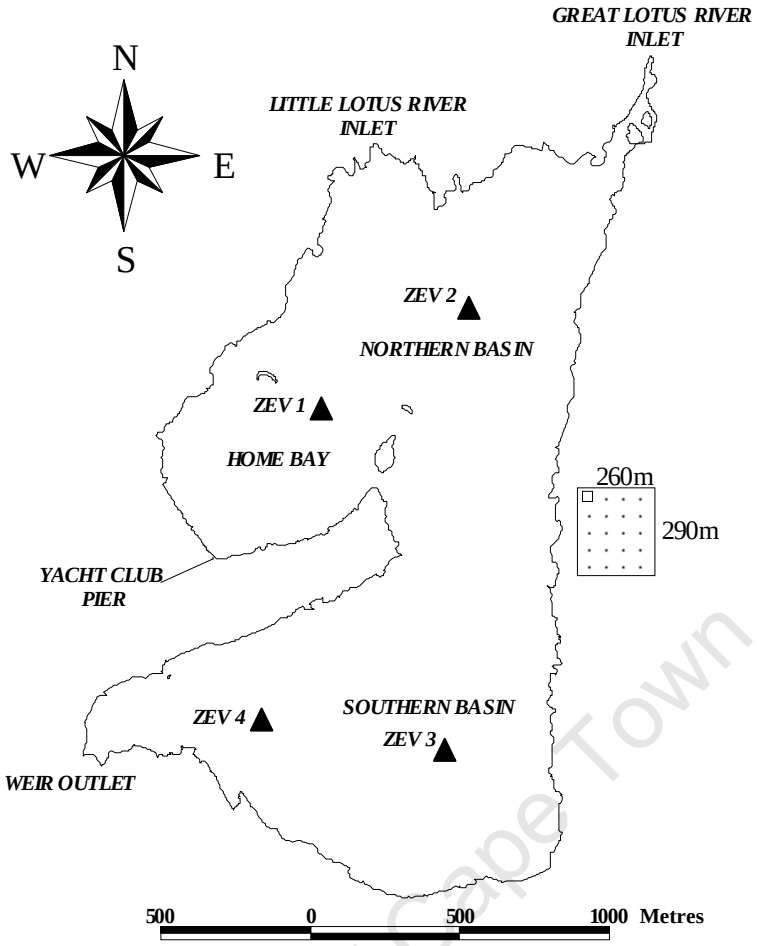

Figure 4.1 Location of the four sampling sites around Zeekoevlei Lake (solid triangles), showing the approximate ground resolutions of MERIS (large rectangle), and Landsat (small rectangle) pixels.

collected using 1 litre clear plastic screw-lid bottles. Each bottle was thoroughly rinsed with lake water before scooping a sample from the surface of the lake. The bottles were kept cool under a damp black cloth during sampling and transportation. The Aerosol Optical Thickness (AOT) was measured using a handheld Microtops II Sun Photometer Version 5.5 manufactured by Solarlight Co. (2003). The sun photometer measures the AOT at five wavelengths in the visible and infrared spectrum (λ = 440, 500, 675, 870 and 900 nm). The AOT scan with the lowest value after four separate scans was taken to be the true AOT value. Measurements were made within 30 minutes of the satellite overpass. Secchi disk depth was measured using a matt white disk of 15 cm diameter using the mean of the depths at which the disk disappeared when lowered into the water, and reappeared when brought to the surface, on the sunny side of the boat (Golterman, 1978). Temperature and pH were measured using a Martini pH 55 Pocket Size Meter calibrated with pH 4 and pH 7 solutions. Wind speed was measured at each sample site using a hand held Sims Model DIC anemometer, and wave height was measured using a ruler. Water colour and sky conditions were recorded by capturing a digital photograph.

4.1.2 Laboratory Methods

Water samples were analysed for phytoplankton pigment (Chl *a*) and Total Suspended Solids (TSS) concentrations, and absorption by Coloured Dissolved Organic Matter (a_{CDOM}) at 440 nm, within three to four hours after the time of collection. Analysis of Chl *a* and TSS was carried out in triplicate for all sample sites using the mean of the three results as the final value.

4.1.2.1 Chl *a* by Fluorometric Analysis

Chl *a* concentration was measured by fluorometric analysis using a Turner Designs 10-AU Fluorometer according to the JGOFS Protocols (1994) and Holm-Hansen et al. (1965). A known amount of sample (normally 20 mℓ) was filtered through a Whatmann GF/F 25 mm Glass Fibre Filter using a syringe. The filter paper was folded and submerged in 9 mℓ of acetone (90%) solution in 10 mℓ plastic acetone resistant test tubes and ground with a glass rod for 1 minute. The test tubes were capped and stored in the dark in a freezer for 24 hours to allow for pigment extraction. Thereafter the test tubes were centrifuged at 2500 rpm for 5 minutes to reduce turbidity, and the supernatant transferred to 13 × 100 mm disposable culture glass tubes that were read in the fluorometer. The supernatant was normally diluted seven times with 90% acetone solution so that the reading was within the linear range of the fluorometer. The fluorometer was zeroed using 90% acetone prior to taking readings. The supernatant was acidified to correct for pheophytin pigments with 0.15 mℓ 0.2N HCL solution using a Pasteur pipette and allowed to stand for 1 ½ minutes before being re-read in the fluorometer. The corrected Chl *a* concentration was calculated using the following formulae:

$$Chl\ a = a \times (R_b - R_a) \times \left(\frac{extraction\ \ vol.}{sample\ vol.} \right) \times DF \qquad (mg.m^{-3}) \qquad (4.1)$$

where a is the calibration coefficient (= 310.37), R_b is the fluorometer reading before acidification, R_a is the fluorometer reading after acidification, and DF is the Dilution Factor.

4.1.2.2 Chl *a* by Spectrophotometric Analysis

During the laboratory analysis, it appeared that the Chl *a* measurements from fluorometric analysis in 90% acetone were conspicuously lower than historical measurements for Zeekoevlei. Previous measurements of Chl *a* in Zeekoevlei by the Cape Metropolitan Council's Scientific Services were made spectrophotometrically in 95% ethanol extraction solution. It appeared that the unusually low Chl *a* concentrations were the result of poor extraction efficiency of acetone with cyanobacterial algal species, as noted by several authors (Robarts & Zohary, 1984, Sartory

& Grobbelaar, 1984, Pápista et al., 2002). Since the algal population in Zeekoevlei is dominated by the cyanophyte *Microcystis*, it was decided to use ethanol instead of acetone as the extracting agent. In order to correct the data already collected and to maintain consistency with the Scientific Services data archives, fluorometric analysis in 90% acetone was conducted simultaneously with spectrophotometric analysis in 95% ethanol for water samples collected on five days.

Spectrophotometric Chl *a* analysis in 95% ethanol was carried out according to the method described in Sartory and Grobbelaar (1984), as used by the Scientific Services water quality monitoring programme. A known amount of sample (usually 20 mℓ) was filtered through a Whatmann GF/F 25 mm Glass Fibre Filter using a syringe. The filter paper was folded and submerged in 9 mℓ of 95% ethanol solution in 10 mℓ plastic test tubes and ground with a glass rod for 1 minute. The test tubes were capped and heated in an oven set to 80° C for 5 minutes before being placed in a freezer for 24 hours for Chl *a* extraction. The supernatant was centrifuged at 2500 rpm for 5 minutes after being removed from the freezer to reduce turbidity. The absorbance was read using a Shimadzu UV-2501 spectrophotometer with matching 1 cm quartz cuvettes. Thereafter 3 mℓ of supernatant was transferred to the first cuvette with 95% ethanol used as a reference in the second curvette. The absorbance was read at 750 and 665 nm. The sample was then acidified with 100 µl of 0.3 M HCL to correct for absorption by pheophytin pigments and allowed to stand for 1 ½ minutes before being re-read at the same wavelengths. Final Chl *a* concentrations were calculated using the formula below:

$$Chl\ a = K \times \left[\left(a(665) - a(750) \right) - \left(a^{a}(665) - a^{a}(750) \right) \right] \times \left(\frac{extraction\ vol.}{sample\ vol.} \right) \qquad (mg.m^{-3}) \qquad (4.2)$$

where K is the absorption co-efficient of Chl a (= 28.66), $a(\lambda)$ is the absorbance value before acidification, and $a^{a}(\lambda)$ is the absorbance value after acidification.

Chl *a* concentrations extracted using the fluorometer in 90% acetone were underestimated by an average of at least 60% compared to those extracted using the spectrophotometer in 95% ethanol (See Table 4.2). The Chl *a* measurements made fluorometrically on all days, were multiplied by the average correction factor (= 1.64) to correct for the poor pigment extraction, assuming that the differential extraction efficiency and phytoplankton species assemblage remained constant. The corrected fluorometric Chl *a* values were used for the remainder of the study (final column Table 4.2).

Table 4.2. Comparison of Chl a concentrations measured fluorometrically in 90% acetone and spectrophotometrically in 95% ethanol. Units are in mg.m^{-3}. Sample key is sample point, day, month. For example 21404 is sample point 2 on the 14th April 2008.

Sample	Fluorometric	Spectrophotometric	Correction factor	Fluorometric (corrected)
21404	107.2	186	1.74	176.2
31404	106.9	163	1.52	175.7
21704	76.3	120	1.57	125.4
31704	74.6	124	1.66	122.6
22004	104.3	181	1.74	171.5
32004	118.4	206	1.74	194.6
12304	74.6	134	1.79	122.6
12404	86.2	139	1.61	141.7
22404	93.5	134	1.43	153.7
Average	93.6	154	1.64	148.6

4.1.2.4 Suspended Solids

Total Suspended Solids (TSS) were measured according to the US Environmental Protection Agency method as used previously in Zeekoevlei (EPA, 1983). Whatmann GF/F 47 mm glass fibre filter papers were ashed overnight in porcelain dishes in a muffle furnace at 500° F, and stored in a dessicator. The filter papers were weighed using a digital scale, before a known volume of sample (usually 100 mℓ) was filtered using a suction flask and filtration apparatus. The filter paper was dried in an oven at 105° C for at least 2 hours (usually overnight), and cooled in a dessicator before being re-weighed to constant weight. TSS concentration was calculated as the difference between mass before and after filtration, per volume of sample. The inorganic components of TSS were estimated by burning off the organic component of non-filterable residue in a muffle furnace at 500° F overnight and then re-weighing the burnt filter paper. The mass of Inorganic Suspended Solids (ISS) was estimated by the difference in mass before and after burning. Organic Suspended Solids (OSS) was estimated by the difference between TSS and ISS.

4.1.2.5 Absorption by CDOM

a_{CDOM} was measured using a Shimadzu UV-2501 spectrophotometer fitted with a 10 mm quartz curvette. Samples were filtered through a Whatmann GF/F glass fibre filter before the absorbance was measured between 250 and 700 nm. Reference absorbance spectra for Milli-Q water were measured in the same range and subtracted from the sample spectra. Data were converted to absorption coefficients using the following equation (Green & Blough, 1994):

$$a(\lambda) = \frac{2.303A(\lambda)}{I} \qquad (m^{-1}) \qquad (4.3)$$

where $a(\lambda)$ is the absorption coefficient (m^{-1}), $A(\lambda)$ is the absorbance, and I is the pathlength (m). A null-point correction was performed at 750 nm. The curves were fitted to the negative exponential function (Equation 3.6) using least-squares, casewise nonlinear estimation.

4.1.3 Correlation Analysis between Variables

The relationships between the water quality and environmental variables were tested using Pearson product moment regression analysis. The correlation coefficient, r, was used to test the significance of the correlations. The variables were tested for normality using the Shapiro-Wilk test (Shapiro et al., 1968).

4.1.4 Statistical Parameters for *In Situ* Data

The standard error of estimation of the mean, for each of the above parameters, was calculated according to (Shaw & Wheeler, 1994):

$$SE_{\bar{X}} = \frac{s}{\sqrt{n}} = \sqrt{\frac{\sum_{i=1}^{n}(X_i - \bar{X})^2}{n-1}} \times \frac{1}{\sqrt{n}} \qquad (4.4)$$

where s is sample standard deviation, n sample size, X_i is ith value of X and $\bar{X}$ is the mean. The confidence interval for the mean was calculated according to (Shaw & Wheeler, 1994):

$$\bar{X} \pm SE_{\bar{X}} \times t \qquad (4.5)$$

where t is the critical statistic at the 95% confidence interval for the *t*-distribution with $n-1$ degrees of freedom.

4.2 Field Spectroradiometry

The upwelling spectral radiance at a depth of 0.66 m, $L_u(0.66)$, and the downwelling irradiance above the surface, $E_d(0+)$, were measured using a Hyperspectral Tethered Surface Radiometer Buoy (HyperTSRB S/N 018) manufactured by Satlantic Inc. (Halifax, Canada). The TSRB measures the light in the spectral range 400 to 800 nm with a resolution of 3.3 nm and an accuracy of 0.3 nm. The TSRB was deployed away from the boat and measurements were recorded on a laptop computer using the SatView Software Version 2.8 (Satlantic Inc.). The median value for the sampling period (usually 3 minutes) was taken to obtain a single spectrum for $L_u(0.66)$ and $E_d(0+)$. The spectra were re-sampled to a spectral resolution of 1 nm. TSRB measurements were made at sample sites 2 and 3 only, simultaneous to other limnological measurements.

4.2.1 Data Processing

$L_u(0.66)$ and $E_d(0+)$ spectra were corrected for errors and processed into normalised water-leaving surface reflectance, ρ_w, values, as shown below. The upward vertical attenuation coefficient, K_u, that is required for converting $L_u(0.66)$ to $L_u(0+)$, was estimated using an approximate bio-optical model.

4.2.1.1 Correction of $L_u(0.66)$

The most significant source of error associated with TSRB measurements, in this instance, is from instrument self-shading. The absence of large waves in Zeekoevlei meant that errors associated with tilt and roll could be ignored. Self-shading errors increase in turbid waters, and can cause remote sensing reflectance derived from $L_u(0.66)$ to be underestimated. The self-shading error causes water constituent retrieval algorithms to operate less accurately, because the error is wavelength dependent. The magnitude of the error depends on the total absorption coefficient of the water and the position of the sun (Leathers et al., 2001). The total self-shading error was calculated according to (Leathers et al., 2001):

$$\varepsilon(\lambda) = \frac{\varepsilon_{sun} + \varepsilon_{sky} f}{1 + f} \tag{4.6}$$

where $\varepsilon(\lambda)$ is the total self-shading error, ε_{sun} is the error from direct sunlight, ε_{sky} is the error from diffuse skylight, and f is the ratio of skylight to direct sunlight.

The self-shading error corresponding to the appropriate absorption values and solar zenith angle were calculated by extrapolating Table 1 in Leathers et al. (2001). The values in Table 1 are for optically deep water (as in Zeekoevlei), and it is sufficient to assume that these represent the minimum approximation for Zeekoevlei. The total absorption and scattering coefficients were estimated using a bio-optical model in a 400 to 750 nm range (See below for details on the model). The ratio of skylight to direct sunlight was taken from published values for clear sky summer conditions for the Cape west coast of South Africa (Walters et al., 1985). Only spectra measured in clear-sky conditions and corresponding to simultaneous MERIS acquisitions were corrected, due to the lack of *in situ* measurements of the ratio of skylight to direct sunlight. Corrected $L_u(0.66)$ were calculated according to (Leathers et al., 2001):

$$L_u^{true}(\lambda) = \frac{L_u^{measured}(\lambda)}{1-\varepsilon(\lambda)} \qquad (Wm^{-2}sr^{-1}nm^{-1}) \tag{4.7}$$

where $L_u^{true}(\lambda)$ is the true radiance spectrum, and $L_u^{measured}(\lambda)$ is the measured radiance spectrum.

4.2.1.2 Calculation of ρ_w and Derivation of K_u

$L_u(0.66)$ and $E_d(0+)$ were processed to derive the above normalised water-leaving surface reflectance, ρ_w, using the equation below:

$$\rho_w = \frac{\pi \times L_u(z) \times e^{K_u z} \times \frac{0.98}{1.33}}{E_d} \tag{4.8}$$

where z is depth in meters, K_u is the vertical attenuation coefficient for upward radiance, and (0.98/1.33) is the water-air interface correction according to Snell's law. The upward vertical attenuation coefficient for radiance, K_u, can be approximated by (Albert & Mobley, 2003):

$$K_u(\lambda) = (a(\lambda) + b_b(\lambda)) \times \left(1 + \left(\frac{b_b(\lambda)}{a(\lambda) + b_b(\lambda)}\right)\right)^{3.5421} \times \left(1 + \left(\frac{-0.2786}{\cos\theta_s}\right)\right) \tag{4.9}$$

where $a(\lambda)$ is the total absorption coefficient, $b_b(\lambda)$ is the total backscattering coefficient, and θ_s is the subsurface solar zenith angle.

Simulations using a bio-optical model based on the model developed by Stramski et al. (2001) were used in order to calculate $a(\lambda)$ and $b_b(\lambda)$. $a(\lambda)$ was calculated according to the equation below:

$$a(\lambda) = a_w(\lambda) + Ca_\phi^*(\lambda) + a_{CDOM}(\lambda) + Na_d^*(\lambda) + Na_m^*(\lambda) \qquad (m^{-1}) \qquad (4.10)$$

where a_d^* is the particle specific absorption coefficient for detritus, a_m^* is the particle specific absorption coefficient for minerals, and N is the number of particles (See Equation 3.7). $b_b(\lambda)$ was modelled using the following equation:

$$b_b(\lambda) = b_{bw}(\lambda) + Cb_{b\phi}^*(\lambda) + Nb_{bd}^*(\lambda) + Nb_{bm}^*(\lambda) \qquad (m^{-1}) \qquad (4.11)$$

where b_{bd}^* is the particle specific backscattering coefficient for detritus, b_{bm}^* is the particle specific backscattering coefficient for minerals, and N is the number of particles (See Equation 3.8).

The absorption and scattering coefficients for pure water were taken from Pope and Fry (1997) and Buiteveld et al. (1994), respectively (Pegau et al., 2003). The backscattering coefficient for water was estimated as half the value of the scattering coefficient. Measurements of the various IOPs are not available for Zeekoevlei. Therefore, the absorption and backscattering coefficients for phytoplankton were taken from Ahn et al. (1992) as used in Stramski et al. (2001). Two marine phytoplankton species were used in the model: *Synechocystis*, a generic phycocyanin rich cyanobacterial picophytoplankton; and *Dunaliella Bioculata*, a chlorophyte. These were weighted equally in their contributions to Chl *a* in order to simulate the co-dominance of cyanobacterial and chlorophyte phytoplankton species in Zeekoevlei (See Section 3.3).

Absorption and backscattering by detritus and minerals was taken from generic particle specific cross sections obtained from Mie-scattering calculations for homogeneous spheres (See Table 4.3). It is important to realise that the values in Table 4.3 are only estimates for background contributions of detritus and minerals, and should be used with some care, however, they are likely to be satisfactory as first order approximations.

Table 4.3 Spectra absorption and backscattering cross-sections for generic components of detritus and minerals. Cross-sections are in units μm² and wavelength is in nanometers (From Stramski et al. 2001).		
Component	**Absorption**	**Backscattering**
Detritus	$\sigma_{a,det} = 8.791\times10^{-4}\times\exp(-0.00847\lambda)$	$\sigma_{bb,det} = 5.881\times10^{-4}\lambda^{-0.8997}$
Minerals	$\sigma_{a,min} = 1.013\times10^{-3}\times\exp(-0.00846\lambda)$	$\sigma_{bb,min} = 1.790\times10^{-2}\lambda^{-0.9140}$

It was decided to keep the number of particles constant in the simulations, despite the fact that *in situ* data indicated that suspended matter is variable. This was because the measured concentrations of suspended matter cannot be expressed in number of particles, and to avoid unnecessary complexities by introducing another source of variability into the model. The number of particles were determined by their contributions to absorption by particulate matter at 440nm, $a_p(440)$, as in Stramski et al. (2001). The contribution to $a_p(440)$ by detritus was about 17% and about 7% by minerals when using the average *in situ* measured values for Chl *a* concentration and a_{CDOM} as input into the model. This gave $N = 6.25\times10^{16}$ for detritus and $N = 2.16\times10^{16}$ for minerals. The relative contributions of phytoplankton, CDOM and non-algal particles to particulate and soluble absorption at 440 nm were approximately equal to 54%, 28% and 17%, respectively. These are comparable to the values measured by Babin et al. (2003) in coastal European waters, since there is a lack of similar data for inland waters. Figure 4.2 and 4.3 show examples of the absorption and scattering components simulated by the model. Figure 4.4 shows the spectral variation of K_u calculated using Equation (4.9) in the range 400 to 750 nm.

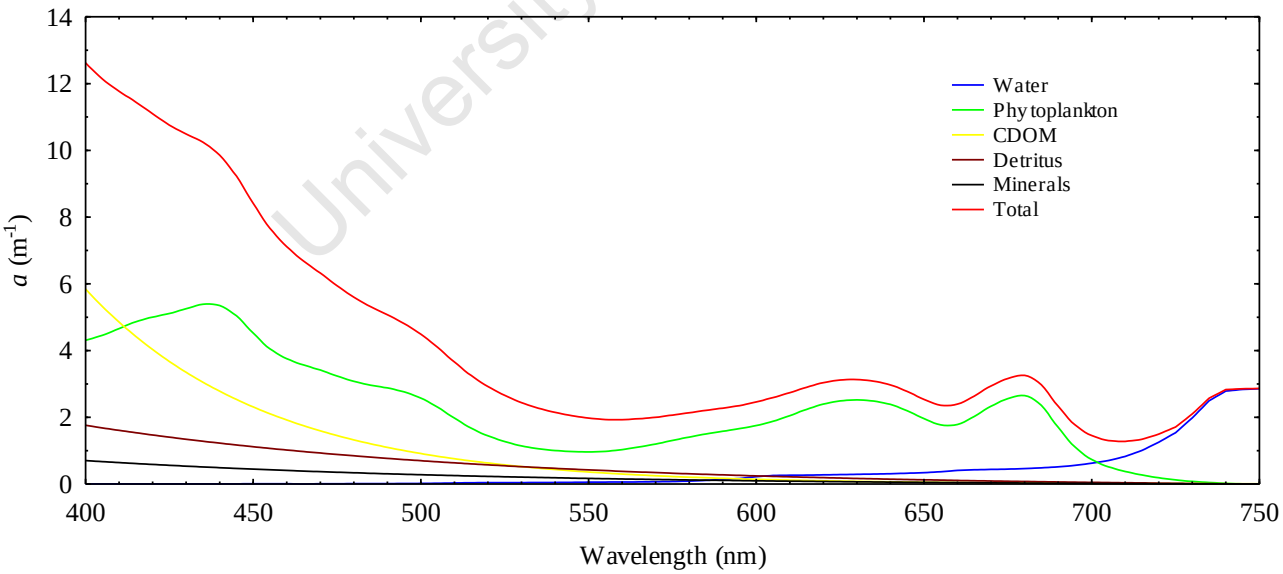

Figure 4.2 Components of the total absorption coefficient used for bio-optical simulations for K_u derivation. Chl *a* = 153.3 mg.m^{-3}; $a_{CDOM}(440) = 2.78$ m^{-1}; detritus $N = 6.25\times10^{16}$; minerals $N = 2.16\times10^{16}$.

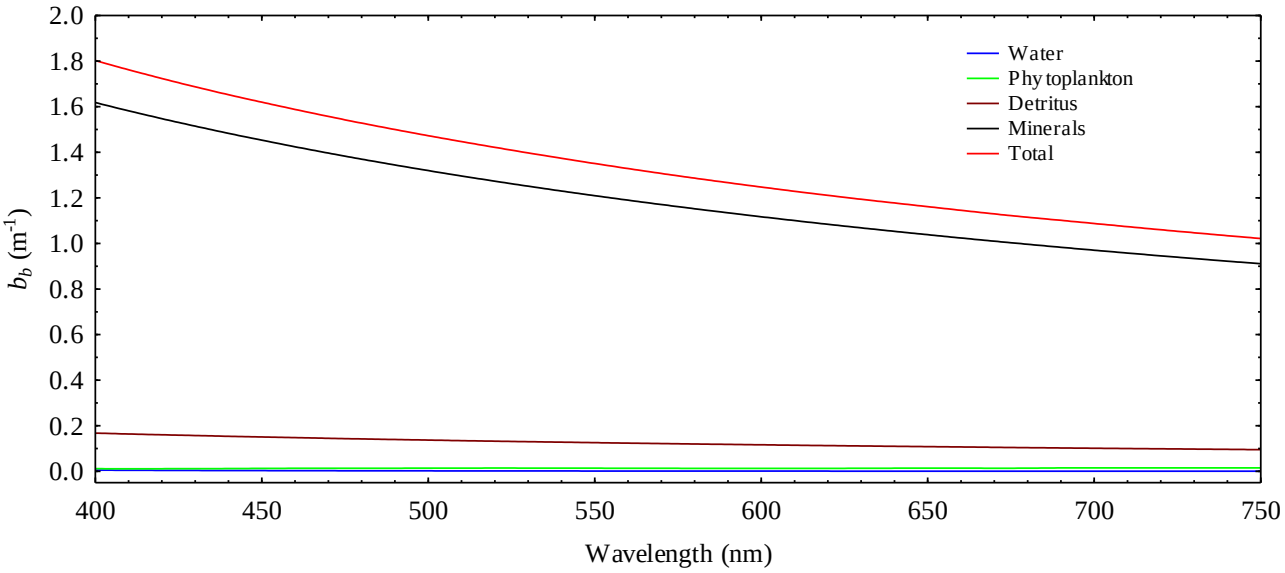

Figure 4.3 Components of the total scattering coefficient used in bio-optical simulations for K_u derivation Chl a = 153.3 mg.m^{-3}; $a_{CDOM}(440)$ = 2.78 m^{-1}; detritus $N = 6.25\times10^{16}$; minerals $N = 2.16\times10^{16}$.

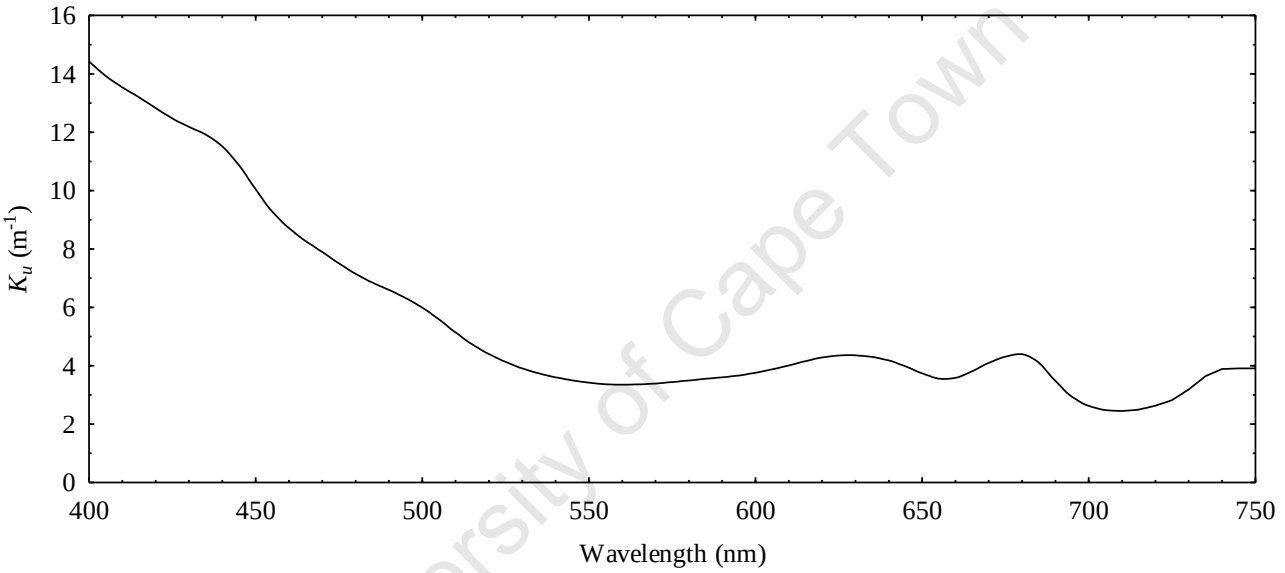

Figure 4.4 K_u calculated using the total absorption and backscattering coefficients in Figure 4.2 and 4.3. θ_s = 0.547 rad.

In order to assess the magnitude of the error introduced to ρ_w through using K_u estimations from the bio-optical simulations, a simple test was performed. The value of K_u was varied (between 5% and 50% in the positive and negative direction) while observing the change to ρ_w. The total error for ρ_w was then calculated using the RMS formula according to:

$$RMS\ error\,(\%) = \sqrt{a^2 + b^2} \tag{4.12}$$

where a and b are estimated errors from instrument self-shading and K_u estimation, in percentage, respectively.

In order to avoid the error associated with calculating ρ_w from K_u estimates, the in-water remote sensing reflectance, $R_{rs}(0.66)$, was also calculated according to the equation:

$$R_{rs}(0.66) = \frac{L_u(0.66)}{E_d(0+)} \tag{4.13}$$

Importantly, $R_{rs}(0.66)$ was calculated only because of how the TSRB made measurements, and the error in $R_{rs}(0.66)$ is assumed to be smaller than the error in ρ_w, although this is not conclusive.

4.2.2 Correlations Analysis with Water Quality Parameters

$R_{rs}(0.66)$ was used for correlation analysis rather than ρ_w in order to avoid the error introduced through estimating K_u, and for assessing $L_u(0.66)$ variance. The correlation between simultaneous $R_{rs}(0.66)$ and water quality parameter measurements was tested using Pearson product moment linear regression analysis. The square of the Pearson product moment correlation coefficient, r^2, was used to ascertain the significance of the correlations. Algorithms were derived from the literature (See Section 3.4) (Table 4.4). The water quality parameters were used as normal and log-transformed. The relationship between the height (magnitude) and position (wavelength) of the reflectance peak near 700 nm with Chl *a* concentration was also tested after normalising $R_{rs}(0.66)$ at 640 nm to account for background scattering.

Table 4.4 Single band, band ratio and band arithmetic algorithms extracted from the literature, used to test the correlation between water quality parameters and TSRB $R_{rs}(0.66)$ (See Section 3.4). Numbers represent wavelengths of $R_{rs}(0.66)$ bands.

	Chl *a*	**TSS, ISS, OSS**	**SD**	**a_{CDOM}**
Algorithm independent variables	700	700	700	*Gitelson et al.*[1]
	(700/670)	(700/670)	(700/670)	(677/480)
	Max~700	Max~700	Max~700	453
	RLH[2]	RLH[2]	RLH[2]	-
	700/(560+670)	700/(560+670)	700/(560+670)	-
	(560-520)/(560+520)	(560-520)/(560+520)	(560-520)/(560+520)	-
	560	560	560	-
	Average500→600	Average500→600	Average500→600	-
	Max~700/677	Max~700/677	(520/700)	-
	(700/677)	Max~560	(490/620)	-
	740((1/670)-(1/710))	750	650	-
	FLH[3]	-	640	-
	670	-	(640/677)	-
	677	-	(650/677)	-
	628	-	(560/677)	-
	Ln(700/670)	-	-	-

[1]see Equation 3.13: (453-(700/670)-520)/(453+(700/670)+520)
[2]see Equation 3.12: L700-L670-((L750-L670)×(700-670)/(750-670))
[3]see Equation 3.12: L685-L670-((L730-L670)×(685-670)/(730-670))

4.3 Water Quality Estimation from MERIS

4.3.1 Data acquisition

MERIS Full Resolution (FR) Geo-located and Calibrated Top-of-Atmosphere (TOA) Radiance (MER_FR_1P) and Full Resolution Geophysical Ocean, Land and Atmosphere (MER_FR_2P) data was pre-ordered from ESA under project AOE470 using the Earthnet OnLine Interactive (Eoli-sa) client version 6.0.1. Thumbnails were inspected in Eoli-sa to ensure that images were cloud free and that Zeekoevlei was visible in the scene. CHRIS data, in water Mode 2, was also pre-ordered from ESA for April 2008. The schedule for data acquisition for the MERIS and CHRIS sensors for April 2008 for Zeekoevlei is presented in Table 4.5.

Table 4.5 Satellite data acquisition schedule for Zeekoevlei for April 2008.

Image Number	Date	Satellite sensor(s)	Pass-over Times (am)
1, 2	1/4/08	MERIS, CHRIS	10:21; 10:27
3	2/4/08	CHRIS	10:42
4	4/4/08	MERIS	10:27
5	7/4/08	MERIS	10:33
6	8/4/08	MERIS	09:43
7, 8	10/4/08	MERIS, CHRIS	10:34; 10:38
9, 10	11/4/08	MERIS, CHRIS	10:07; 10:44
11	13/4/08	MERIS	10:44
12	14/4/08	MERIS	10:13
13	17/4/08	MERIS	10:19
14	18/4/08	CHRIS	10:25
15	19/4/08	CHRIS	10:36
16, 17	20/4/08	MERIS, CHRIS	10:24; 10:47
18	23/4/08	MERIS	10:30
19	24/4/08	MERIS	09:43
20	26/4/08	MERIS	10:36
21, 22	27/4/08	MERIS, CHRIS	10:04; 10:27
23	28/4/08	CHRIS	10:38

4.3.2 Data processing

The MERIS Level 1P product was processed using VISAT BEAM Version 4.2 software toolbox (Brockmann Consult) available freely from ESA online at http://www.brockmann-consult.de/beam/downloads.html. MERIS images were visually inspected in BEAM for cloud cover and data errors using the bitmask overlay tool. The Smile Correction Processor (V.1.1.2) plug-in was used to correct for the 'smile effect' that causes small variations in the spectral wavelength of each pixel along the track. The data were converted to normalised Top-Of-

Atmosphere (TOA) apparent reflectance using the Radiance-To-Reflectance Processor (V1.3.100) according to the following equation:

$$\rho_{TOA}(\lambda) = \frac{\pi L_{TOA}(\lambda)}{E_0(\lambda)\cos\theta_s} \tag{4.14}$$

where ρ_{TOA} is normalised TOA apparent reflectance, L_{TOA} is the TOA radiance, E_0 is solar spectral irradiance, that includes a correction for the earth-sun distance, and θ_s is the solar zenith angle.

Unfortunately the water bitmask overlay in the 1P product often failed to classify Zeekoevlei as water pixels. Therefore water pixels were identified by low reflectance values in the near-infrared band 13 (864 nm) using the spectrum viewer tool. These water pixels were extracted using the Region Of Interest (ROI) Manager by including pixels by condition inside a rectangular area around the lake. The data were extracted and used as 'raw' TOA radiance, 'smile corrected' TOA radiance, and TOA 'apparent reflectance'.

The MER_FR_2P atmospherically corrected normalised surface reflectance, ρ_w, in 13 bands, and water constituents including Chl *a* and TSS concentrations, and a_{CDOM} at 440nm, computed by the MERIS Case 2 NN algorithm, were extracted for Zeekoevlei. The Eutrophic Lakes Processor plug-in was also implemented in BEAM 4.2 to derive ρ_w and water constituents (See Section 3.3 for details on the MERIS Level 2 and Eutrophic Lakes Processor products).

4.3.3 Correction for Atmospheric Contributions

The MERIS_FR_1P data were corrected for atmospheric contributions to derive ρw in 14 spectral bands, using the DOS model (Equation 3.15), and the COST model (Equation 3.16). The atmospheric path radiance, L_{path}, in each spectral band, was estimated by extracting a low reflectance, ocean-water pixel in each scene. The values for E_0, θ_v, and θ_s, were taken from the MERIS product. Spectra corresponding to *in situ* radiometric measurements were also corrected using the 6S radiative transfer code V1.1, in the Linux operating system (Vermote et al., 1997). The input parameters used with the code are shown in Table 4.6 below. A correction for adjacency effects for Zeekoevlei was attempted using the ICOL processor in BEAM 4.2. However, Zeekoevlei was overlaid by the 1P land mask, so the ICOL processor failed to identify and correct the water pixels. Nonetheless, to guage the magnitude of the adjacency effect, north-south and east-west transects of TOA radiance in the near-infrared bands were plotted.

Table 4.6 Input parameters used with the 6S radiative transfer code.	
Geometrical conditions	Month, day, solar zenith and azimuthal angle, viewing zenith and azimuthal angle
Atmospheric model	Mid-latitude summer
Aerosol model	Urban
Aerosol optical thickness (550 nm)	*In situ* measurements
Target type	Lake water
Ground reflectance	Homogeneous surface, no directional effects
Target elevation	5 m
Atmospheric correction	Lambertian assumption

4.3.4 Derivation of Empirical Algorithms

Empirical algorithms were derived using regression analysis with pixels from MERIS scenes corresponding to sample sites from simultaneously acquired water quality parameter measurements. The pixel radiance/reflectance values were utilised as the independent variables in the regression while the water quality parameters were used as the dependent variables. The independent variables used in the algorithms for Chl *a*, TSS, ISS, OSS, Secchi Disk depth (SD) and a_{CDOM}, were extracted from the literature (Section 3.4, Table 4.7). The r^2 coefficient of determination was calculated to determine the significance of the correlation, and the p-value of significance was 0.05. No outliers were removed from the regressions due to the small sample size. Neither the water quality parameters nor the pixel values were log transformed. The data types used in the regression were 'raw' uncorrected TOA radiance, 'smile corrected' TOA radiance, TOA 'apparent reflectance', 'DOS' reflectance, 'COST' reflectance and '6S' corrected reflectance. Some algorithms that account for atmospheric effects are not applied to the atmospherically corrected data types.

Table 4.7 Single band, band ratio and band arithmetic algorithms extracted from the literature used to derive empirical algorithms for MERIS (See Section 3.4). Numbers represent radiance/reflectance in MERIS wavebands.

	Chl *a*	**TSS, ISS, OSS**	**SD**	**a_{CDOM}**
Algorithm independent variables	708	708	708	412
	(708/664)	(708/664)	(708/664)	442
	RLH[1]	RLH[1]	RLH[1]	(559-619)/619
	753((1/664)-(1/708))	708/(559+664)	(509/708)	((559-778) - (619-778))/ (619-778)
	FLH[2]	(559-509)/(559+509)	(509-864)/(708-864)	(664/489)
	559	559-619	(489/619)	(664-778)/(489-778)
	(559/664)	(708-864)	(489-778)/(619-778)	(664/559)
	708/680	619 + 664		(664-778)/(559-778)
	(708-864)/(664-864)	864		*Gitelson et al.*[3]
	(708-778)/(664-778)	559		

[1] see Equation 3.12: L708-L664-((L864-L664)×(708-664)/(864-664))
[2] see Equation 3.12: L680-L664-((L753-L664)×(680-664)/(753-664))
[3] see Equation 3.13: (442-(708/664)-509)/(442+(708/664)+509)

Pearson linear regression analysis was formulated according to the model:

$$y = a + bx \tag{4.15}$$

where y is the dependent water quality parameter, x is the independent variable (band combination/difference/ratio) and a and b are regression coefficients.

Non-linear least squares regression was applied according to the model:

$$y = ax^b \tag{4.16}$$

Multiple linear regression analysis was formulated according to the model:

$$y = a + bx_1 + cx_2 \tag{4.17}$$

where x_1 and x_2 are independent variables, and a, b and c are regression coefficients.

The analysis was performed in Statistica 8.0 (StatSoft, Inc). The F-value and the t-statistic were further determined to establish the significance of the regression results. The F-value was calculated according to (Shaw & Wheeler 1994):

$$F = \frac{s_{\hat{y}}^2}{s_e^2} = \frac{\sum_{i=1}^{N}(\hat{Y}_i - \bar{Y}_i)^2}{k} \Bigg/ \frac{\sum_{i=1}^{N}(\hat{Y}_i - Y_i)^2}{N-k-1} \tag{4.18}$$

where N is the number of observations, $\hat{Y}$ is the estimated value of the water quality parameter, $\bar{Y}$ is the mean of observed water quality parameter, Y is the observed value the water quality parameter and k is the number of predictors. Since F is the ratio of 'explained variance' to 'unexplained variance' a large F-value indicates that the independent variable, X, may be used to reliably estimate dependent variable, Y, which in this case is the water quality parameter. The F-values were compared to critical F-values at the 0.05 significance level.

The standard error of the residuals, also called the Root of the Mean Square of the Error *(RMSE),* was calculated to determine the error associated with the estimations using the formula (Shaw & Wheeler, 1994):

$$s_e(RMSE) = \sqrt{\frac{\sum_{i=1}^{N}(\hat{Y}_i - Y_i)^2}{N-k-1}} \tag{4.19}$$

where N is the number of observations, $\hat{Y}$ is the estimated value of the water quality parameter, Y is the observed value the water quality parameter (i.e. measured *in situ*) and k is the number of predictors.

The 95% confidence limits for the water quality parameter estimates (displayed on graphs) were determined as follows (Shaw & Wheeler, 1994):

$$\hat{Y}_i \pm SE_{\hat{Y}_i} \times t \tag{4.20}$$

where t is the critical statistic at the 95% confidence interval for the *t*-distribution with $n-1$ degrees of freedom.

4.3.5 Mapping of Water Quality Parameters

Maps of the water quality parameters were produced for Zeekoevlei by applying the empirical algorithms to the MERIS pixels for each simultaneously acquired scene. The maps were made in Matlab V.7.3.0 (The MathWorks, Inc) using the 'pcolor' function that produces pseudocolour checkerboard plots. Each cell in the plot represents a single 260 × 290 m MERIS pixel, and a colour bar indicates the unique values of the water quality parameters for each pixel. Statistics derived from the maps included the number of pixels, the area, the mean, median, minimum and maximum water quality parameter values, the standard deviation, the standard error, and the observed error of *in situ* data (Kallio et al., 2003). This was in order to determine the improved accuracy delivered by coupling *in situ* measurements with remotely sensed MERIS measurements. The standard error of the mean for remotely sensed estimates was calculated using the formula below (Shaw & Wheeler, 1994):

$$SE_{\bar{\hat{Y}}} = s_e \sqrt{\frac{1}{n} + \frac{(X_k - \bar{X})^2}{\sum_{i=1}^{N}(X_i - \bar{X})^2}} \tag{4.21}$$

where s_e is the standard error of residuals (Equation 4.19), n is number of observations, X_k is the mean value of the independent variable x (band combination/difference/ratio) for all estimations, $\bar{X}$ is the mean of independent variable x for observed values, and X_i is the observed value of independent variable x. Accordingly the 95% confidence limits for the mean were calculated according to Equation 4.20. The observed error of the *in situ* data were calculated using the equation below (Kallio et al., 2003):

$$E = \bar{X}_{insitu} - \bar{X}_{remotelysensed} \tag{4.22}$$

where $\bar{X}_{insitu}$ is the mean of *in situ* and $\bar{X}_{remotelysensed}$ the mean of remotely sensed water quality parameter estimates.

4.4 Water Quality Estimation from Landsat 7 ETM +

4.4.1 Data acquisition

As of the 31st March 2008 Landsat 7 ETM+ data were made available free of charge over Africa by the United States Geological Survey (USGS) and NASA. SLC-off mode (the Scan Line Corrector failed on May 31, 2003) Landsat 7 scenes were downloaded from the online Landsat Archive database using EarthExplorer (online at http://edcsns17.cr.usgs.gov/EarthExplorer/). The data were delivered in Digital Numbers (DNs) and projected in Universal Transverse Mercator (UTM) Zone 34, with the World Geodetic System (WGS) 1984 spheroid.

4.4.2 Data Processing

Landsat 7 ETM+ data were processed in ERDAS Imagine 9.1 (Leica Geosystems Geospatial Imaging). The data were not corrected for the SLC failure. The DNs were converted into at-sensor radiance, L_d, using the ERDAS Imagine Model Maker and the following equation (NASA, 2008):

$$L_d(\lambda) = \left(\frac{L_{\max\lambda} - L_{\min\lambda}}{Q_{cal\max} - Q_{cal\min}} \right) \times (Q_{cal} - Q_{cal\min}) + L_{\min\lambda} \qquad (Wm^{-2}sr^{-1}\mu m^{-1}) \qquad (4.23)$$

where Q_{cal} is the pixel value in DN, $L_{max\lambda}$ is spectral radiance scaled to Q_{calmax} ($Wm^{-2}sr^{-1}\mu m^{-1}$), $L_{min\lambda}$ is spectral radiance scaled to Q_{calmin} ($Wm^{-2}sr^{-1}\mu m^{-1}$), Q_{calmax} is the maximum quantized calibrated pixel value in DN, equal to 255, and Q_{calmin} is the minimum quantized calibrated pixel value in DN, equal to 1. The values used to compute the at-sensor spectral radiance for each band are shown in Table 4.8 below.

Table 4.8 Values used to compute at-sensor radiance from Landsat 7 ETM+ DNs (from NASA, 2008).

Band No.	$L_{max\lambda}$ ($Wm^{-2}sr^{-1}\mu m^{-1}$)	$L_{min\lambda}$ ($Wm^{-2}sr^{-1}\mu m^{-1}$)
1	191.6	-6.2
2	196.5	-6.4
3	152.9	-5.0

At-sensor radiance was converted to normalised TOA apparent reflectance using the equation (NASA, 2008):

$$\rho_{TOA}(\lambda) = \left(\frac{\pi \times L_{TOA} \times d^2}{E_0 \times \cos\theta_s} \right) \qquad (4.20)$$

where d is earth-sun distance in astronomical units (AU) (See Equation 4.14). The values for d, $E_{0,}$ and θ_s, were taken from the Landsat 7 User Handbook and the Landsat product (NASA, 2008).

4.4.3 Atmospheric Correction

ρ_w was calculated using the DOS model according to Equation 3.15. L_{path} for each spectral band were estimated from an in-scene dark pixel, taken from a shadow in the mountainous region, north-east of Cape Town.

4.4.4 Empirical Algorithms

Empirical algorithms were derived from TSRB ρ_w data, re-sampled to simulate the first three bands of the Landsat 7 ETM+ sensor (band 1: 435 - 520 nm; band 2: 500 - 624 nm; band 3: 588 - 678 nm). The mean of the re-sampled TSRB ρ_w over the Landsat bandwidth, after multiplying by the spectral response curve of the Landsat band (NASA, 2008), was used as the value for the band. The empirical water quality parameter algorithms were derived using Pearson Product Moment linear regression analysis (Equation 4.15) with the independent variables listed in Table 4.9, and normal and log transformed *in situ* water quality parameter measurements. Statistical analysis of the algorithms was carried out as in Section 4.3.4.

Table 4.9 Independent variables used to formulate empirical algorithms from simulated Landsat ETM+ data.

b1	b3/b1	Ln b3	Ln(b2)/Ln(b3)
b2	b3/b2	Ln(b2/b1)	Ln(b3)/Ln(b1)
b3	b2-b1	Ln(b2/b3)	Ln(b3)/Ln(b2)
b1/b2	b2-b3	Ln(b3/b1)	Ln(b2-b1)
b1/b3	b3-b1	Ln(b1)/Ln(b2)	Ln(b2-b3)
b2/b1	Ln b1	Ln(b1)/Ln(b3)	Ln(b3-b1)
b2/b3	Ln b2	Ln(b2)/Ln(b1)	

4.4.5 Mapping Water Quality Parameters

Pixels from the atmospherically corrected Landsat 7 ETM+ scene for Zeekoevlei were extracted in ERDAS Imagine using the Area Of Interest (AOI) and the region growing tools. The empirical algorithms were applied to the Landsat pixels over Zeekoevlei in ERDAS Model Maker. Maps were drawn using ArcMap, and displayed in 5 colour classes using natural breaks divisions. Statistical analysis of the maps included the calculation of the number of pixels and the area; and the mean, median, minimum, maximum, standard deviation, and standard error of the mean, for water quality parameters, according to Section 4.3.5.

Chapter 5 Results

This chapter follows the layout of the previous chapter, giving the results of the field and laboratory work (5.1); the field spectroradiometry (5.2); water quality parameter estimation from MERIS (5.3); and water quality parameter estimation from Landsat 7 ETM+ (5.4).

5.1 Water Quality and Environmental Conditions

5.1.1 Overall Water Quality and Environmental Conditions

A total of 31 measurements of water quality and environmental parameters, from the four sampling sites, was made between April 1st and April 24th. The overall descriptive statistics for the parameters are shown in Table 5.1.

Table 5.1 Descriptive statistics for water quality and environmental parameters for Zeekoevlei for April 2008. OSS is expressed as a percentage of TSS.

Parameter	Unit	Mean	Med.	Min.	Max.	Range	St. Dev.	S_e (mean)	N
Chl *a*	$mg.m^{-3}$	148.6	161.8	61.0	247.4	186.4	45.4	8.1	31
TSS	$mg.l^{-1}$	49.1	50.7	26.3	65.3	39.0	11.2	2.0	31
ISS	$mg.l^{-1}$	12.0	12.7	1.3	24.0	22.7	5.7	1.0	31
OSS	%	76.9	75.3	60.5	95.7	35.2	7.6	1.4	31
SD	cm	27.9	26.0	23.0	38.0	15.0	4.4	0.8	31
a_{CDOM} 440nm	m^{-1}	2.69	2.72	1.83	3.73	1.90	0.47	0.08	31
S	-	0.0188	0.0186	0.0169	0.0212	0.0043	0.0010	0.0002	31
Wave height	cm	5	3	0	15	15	4	1	31
Wind speed	$m.s^{-1}$	11.9	11.0	0.0	30.0	30.0	9.9	1.8	31
Water temp.	°C	19.4	18.8	18.2	22.7	4.5	1.4	0.2	31
pH	-	9.8	9.8	9.6	10.1	0.5	0.1	0.02	31

The concentration of Chl *a* varied between 61.0 and 247.4 $mg.m^{-3}$ during April, with a mean of 148.6±8.1 $mg.m^{-3}$, which is within the range previously measured for Zeekoevlei (See Section 2.3). Very high Chl *a* concentrations confirms that primary production levels are typical of hypertrophy. The concentration of TSS has a mean value of 49.1±2.0 $mg.\ell^{-1}$ and a range of 39.0 $mg.\ell^{-1}$, which is also within the range of concentrations previously measured for Zeekoevlei. ISS has a mean value of 12.0±1.0 $mg.\ell^{-1}$ with a maximum of 24.0 $mg.\ell^{-1}$ and a minimum of 1.3 $mg.\ell^{-1}$, showing that the concentration of the inorganic particulate matter is variable. The contribution of OSS to TSS is on average 76.9±1.4% with a minimum of 60.5% and a maximum of 95.7%. Thus it is apparent that organic matter (presumably from phytoplankton and detritus) makes up the overwhelming majority of suspended matter in Zeekoevlei. Using a conversion factor of 1 $mg.m^{-3}$ Chl *a* ≈ 0.07 - 0.09 $mg.\ell^{-1}$ dry weight (Dekker, 1993), the total contribution of phytoplankton to organic suspended matter was estimated to be between 28 and 35%. The remainder of the organic matter is probably detrital material mixed into the water column from the organically rich sediment accumulations on the lake floor (Harding, 1996).

The mean Secchi Disk depth is 27.9±0.8 cm and varies within a small range of 15 cm, with a maximum of only 38 cm. Thus, the depth of light penetration in Zeekoevlei is very small, as a result of turbidity from high concentrations of algae and suspended particulate matter. Therefore the assumption can be made that the signals detected by the satellite sensors during April/May were not affected by reflectance from the lake bottom, i.e. Zeekoevlei is optically deep. a_{CDOM} has a mean value of 2.69±0.08 m^{-1} at 440 nm, and ranges between a minimum of 1.83 m^{-1} and a maximum of 3.73 m^{-1} (Figure 5.1). These high values are within the typical range measured in other inland waters (Kirk, 1994). The values of the slope, S, after fitting the curves to Equation 3.6, varied between 0.0169 and 0.0212, with a mean of 0.0188 ± 0.0002. This is similar to the ranges measured in New Zealand and Australian inland waters (Kirk, 1994). The close agreement between the magnitude and shapes of the spectra in Figure 5.1 indicate that a_{CDOM} is relatively spatially and temporally constant in Zeekoevlei.

The mean wind speed for April was 11.9±1.8 $m.s^{-1}$, with a minimum of 0 $m.s^{-1}$ and a maximum of 30 $m.s^{-1}$. Wave height had a mean of 5±1 cm, with a minimum of 0 cm and a maximum of 15 cm. Therefore, a number of the days during April were very calm with no wind or wave action. This is rare given the persistent wind climate usually observed at Zeekoevlei (Harding 1996). Water temperature varied between 18.2° C and 22.7° C showing that the lake was warm, and pH values were alkaline varying within a small range between 9.6 and 10.1.

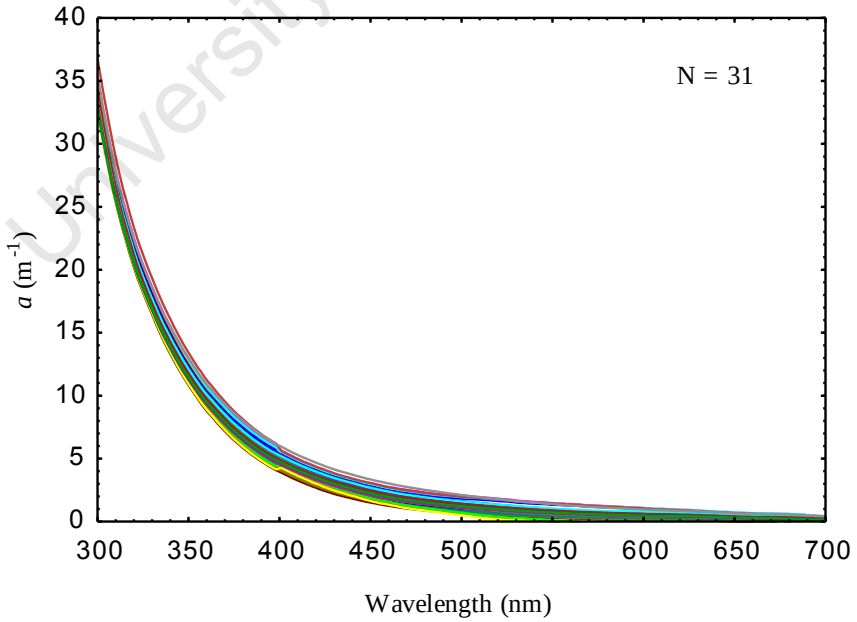

Figure 5.1 Absorption by CDOM between 300 and 700 nm for Zeekoevlei, measured during April 2008.

5.1.2 Spatial Variability of Water Quality and Environmental Parameters

The variation in the water quality and environmental variables between the four sampling sites is small, showing that water quality conditions are relatively uniform across the lake (Table 5.2).

The average Chl *a* concentration is greater in the Southern basin (ZEV3 = 160.5 mg.m^{-3}, ZEV4 = 171.4 mg.m^{-3}) compared to the Northern basin (ZEV1 = 134.0 mg.m^{-3}; ZEV2 = 134.0 mg.m^{-3}) showing increased algal bloom activity in the southern basin. The most probable explanation for this is the underground seepage of N and P nutrients from the WWTW adjacent to the Southern basin, which encourages biological production. The variation of TSS is small, with the concentration slightly higher at ZEV2 (50.6 mg.ℓ^{-1}) and slightly lower at ZEV1 (45.8 mg.ℓ^{-1}). Mean ISS concentration is greatest at ZEV2 (13.5 mg.ℓ^{-1}) and lowest at ZEV1 (10.0 mg.ℓ^{-1}). TSS is composed of a slightly greater percentage of organic matter at ZEV1 (78.1%) than the other sample sites, the lowest being 73.4% for ZEV2. Average Secchi Disk depth is greatest at ZEV2 (28.8 cm), and smallest at ZEV1 (26.7 cm), although the difference between these is very small (2.1 cm). a_{CDOM} at 440 nm appears to be uniform between the sample sites.

Table 5.2 Mean water quality and environmental variables for the four sampling sites collected during April 2008. OSS is expressed as a percentage of TSS.

Variable	Unit	ZEV1	ZEV2	ZEV3	ZEV4
Chl *a*	mg.m^{-3}	134.0	134.0	160.5	171.4
TSS	mg.ℓ^{-1}	45.8	50.6	49.7	49.1
ISS	mg.ℓ^{-1}	10.0	13.5	11.8	11.5
OSS	%	78.1	73.4	76.2	76.5
SD	cm	26.7	28.8	27.8	28.0
a_{CDOM} (440nm)	m^{-1}	2.69	2.61	2.83	2.55
Wave height	cm	2	7	5	3
Wind speed	m.s^{-1}	9.3	12.3	13.4	11.4
Temperature	°C	19.3	19.5	19.5	19.0
pH		9.8	9.9	9.8	9.7
N		6	10	10	5

The variation of wind speed and wave height is more pronounced between the sample sites. Average wind speed is greater at ZEV3 (13.4 m.s^{-1}) and ZEV2 (12.3 m.s^{-1}), than at ZEV4 (11.4 m.s^{-1}) and ZEV1 (9.3 m.s^{-1}). Accordingly, average wave height is greatest at ZEV2, due to the large fetch afforded to the predominantly southerly wind, and smallest at ZEV1, which is located in the more sheltered Home Bay. Therefore, the highest average concentrations of TSS and ISS at ZEV2 may be explained by wind and wave action which cause mixing and entrainment of bottom sediments into the water column. Accordingly, the lowest concentrations of TSS and ISS are observed at ZEV1, where entrainment of bottom sediments by wind and wave action is decreased. The sheltered conditions at ZEV1 are also conducive to the flotation and collection at the surface of buoyant cyanobacterial algae, such as the dominant *Microcystis*, and may explain the shallow SD depths and increased contribution of organic matter to TSS observed there. This may explain how ZEV1 can simultaneously display the lowest average concentrations of TSS and

ISS, the highest contribution of organic matter to TSS, and the lowest average SD depths. In contrast, it is evident that the greater mixing at ZEV2 prevents buoyant cyanobacteria collecting at the surface, and results in increased depths of light penetration and lower contributions of organic matter to TSS, despite the fact that more bottom sediments are entrained into the water column by wind and waves. The variation of water temperature and pH across the four sample sites is small and is unlikely to be significant.

5.1.3 Correlation between Water Quality and Environmental Parameters

The correlations between water quality parameters during April 2008 were substantially more significant than those of the long-term data (Table 2.7). Thus, it appears that the short-term temporal trends in the water constituents differ from variations occuring over longer time scales. Chl *a* is significantly positively correlated with TSS (r = 0.76) and OSS (r = 0.79) (See Table 5.3). This means that organic matter, which makes up a large percentage of the suspended matter (on average 76.7%), is dependent upon phytoplankton containing Chl *a*. Chl *a* is strongly negatively correlated with Secchi Disk depth (r = -0.79) which is also significantly negatively correlated with TSS (r = -0.76). While Secchi Disk depth failed the test for normality (p = 0.0005), these significant negative correlations are reasonable, as higher densities of algae and suspended matter leads to decreased depths of light penetration. TSS is very significantly correlated with ISS (r = 0.91) and OSS (r = 0.93), as expected, and strongly with wave height (r = 0.78) and wind speed (r = 0.72). ISS and OSS are also significantly correlated with wind speed and wave height. This confirms the suggestion that inorganic and organic sediment is entrained into the water column by wave action in windy conditions.

Table 5.3 The correlation coefficient, r, between water quality and environmental variables for Zeekoevlei for April 2008. Significant correlations (p < 0.05) are in red. Bold italics indicates parameters that failed the Shapiro-Wilk test for normality.

	Chl a	**TSS**	**ISS**	**OSS**	**SD**	**a_{CDOM}**	**Wave height**	**Wind speed**	**Water temp.**
Chl a	1.00								
TSS	0.76	1.00							
ISS	0.59	0.91	1.00						
OSS	0.79	0.93	0.68	1.00					
SD	***-0.79***	***-0.76***	***-0.69***	***-0.70***	1.00				
a_{CDOM}	0.59	0.61	0.50	0.61	*-0.60*	1.00			
Wave height	***0.52***	***0.78***	***0.77***	***0.68***	***-0.57***	***0.61***	1.00		
Wind speed	***0.47***	***0.72***	***0.72***	***0.61***	***-0.51***	***0.71***	***0.75***	1.00	
Water temp.	***-0.81***	***-0.86***	***-0.78***	***-0.80***	***0.81***	***-0.49***	***-0.61***	***-0.52***	***1.00***

Absorption by CDOM is positively correlated with Chl *a* (r = 0.59), TSS (r = 0.61) and OSS (r = 0.61) revealing a weak relationship between humic matter and organic solids. The suggestion by Kirk (1994), that humic matter may be generated by the decomposition of plant matter in very

productive conditions, may be the cause of this correlation. As expected, a_{CDOM} is negatively correlated with Secchi Disk depth (r = -0.60), since greater concentrations of CDOM increase the attenuation of light in water, especially in the blue region of the spectrum. The strong correlations of some of the variables with water temperature is difficult to explain causally and is likely to be an artifact of the data since water temperature failed the test for normality (p = 0.00003). Figure 5.2 below shows scatter plots of some of the variables with the square of the correlation coefficient and the p-value of significance.

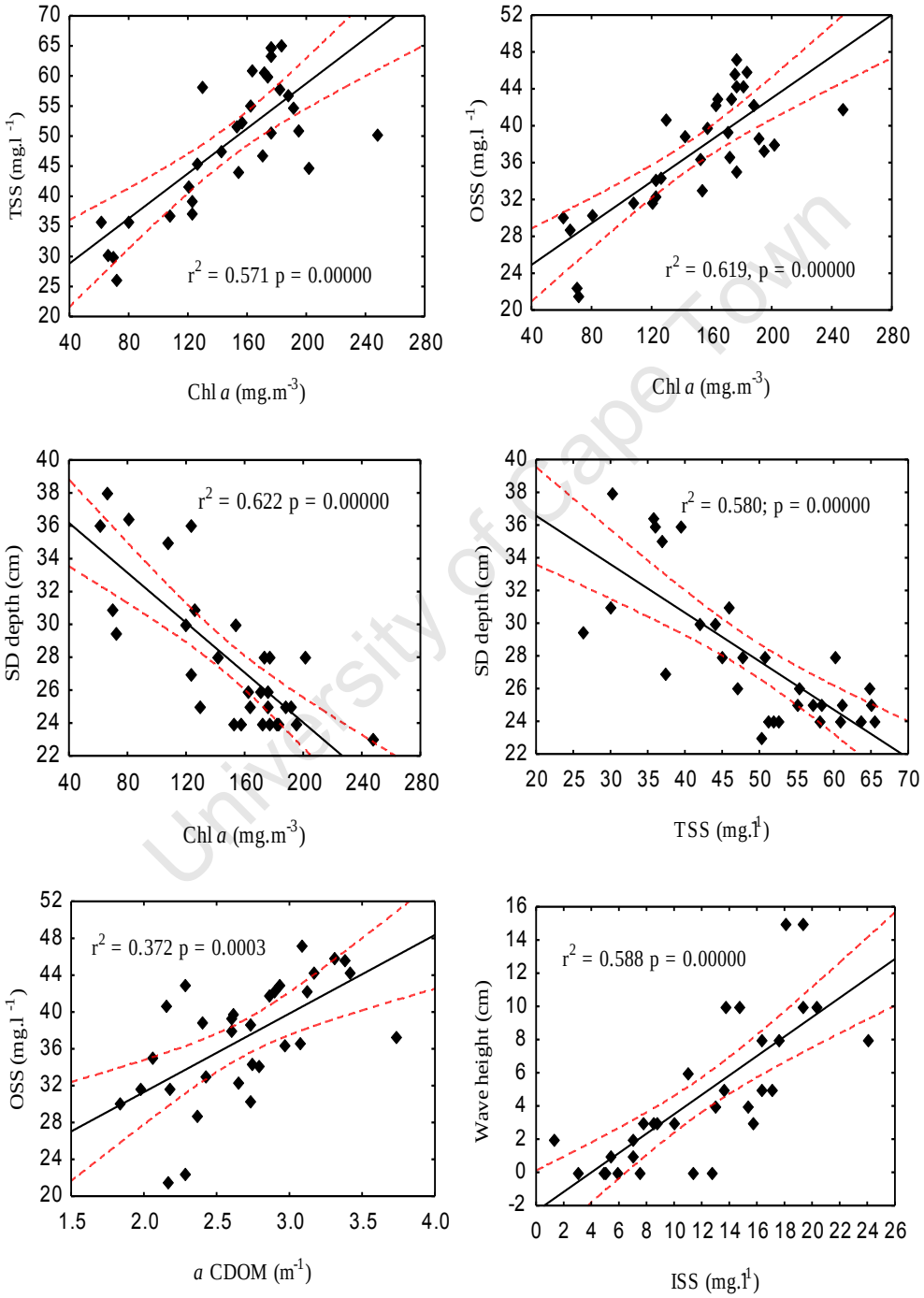

Figure 5.2 Selected scatterplots of water quality and environmental parameters showing the square of the Pearson correlation coefficient, r^2, and the p-value of significance. The dotted red lines represent the 95% confidence intervals for the regression lines.

5.2 Field Spectroradiometry

Overall 18 measurements of the upwelling spectral radiance, $L_u(0.66)$, and the downwelling irradiance, $E_d(0+)$, were made with the TSRB simultaneous to *in situ* water quality parameter measurements. Two of the spectra were excluded from the data set as the $L_u(0.66)$ values were anomalously small.

5.2.1 $L_u(0.66)$ and $E_d(0+)$ Spectra

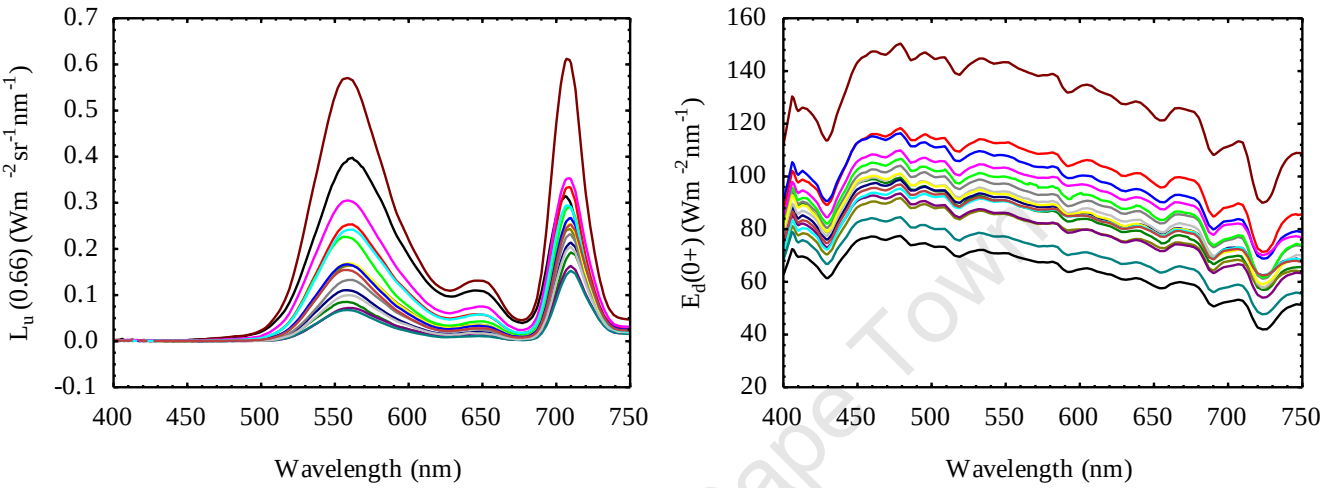

Figure 5.3 $L_u(0.66)$ and $E_d(0+)$ spectra measured using the TSRB on 10 days in April 2008 (N = 16).

The $L_u(0.66)$ spectra show two distinct peaks at about 560 and 710 nm (Figure 5.3). These indicate strong scattering by suspended particulate matter. There is very little upwelling light in the blue region of the spectrum (< 500 nm) owing to the strong absorption by CDOM and Chl *a* (430 nm). Two clear phytoplankton absorption maxima are present at about 630 and 680 nm, which are the absorption maxima of the pigments phycocyanin and Chl *a*, respectively, which is characteristic of the dominant cyanobacterial algal species in Zeekoevlei. The upwelling radiance spectra all display very similar shapes showing that the $L_u(0.66)$ is spectrally relatively invariant. The $E_d(0+)$ spectra display the characteristic absorption bands by ozone, oxygen and water vapour. The variation in magnitude of the spectra is partly due to the effects of cloud cover, as measurements were made under different sky conditions at different times of the day (between 9am and 12am).

5.2.2 Correction of $L_u(0.66)$ for Instrument Self-Shading

The total self shading error, $\varepsilon(\lambda)$, calculated according to Equation 4.6, and the ratio of skylight to direct sunlight, $f(\lambda)$, are presented alongside the measured and corrected spectra for clear-sky conditions, calculated using Equation 4.7, in Figure 5.4 below. $\varepsilon(\lambda)$ has a minimum value of 18% and varies considerably across the spectrum, growing exponentially at wavelengths less than

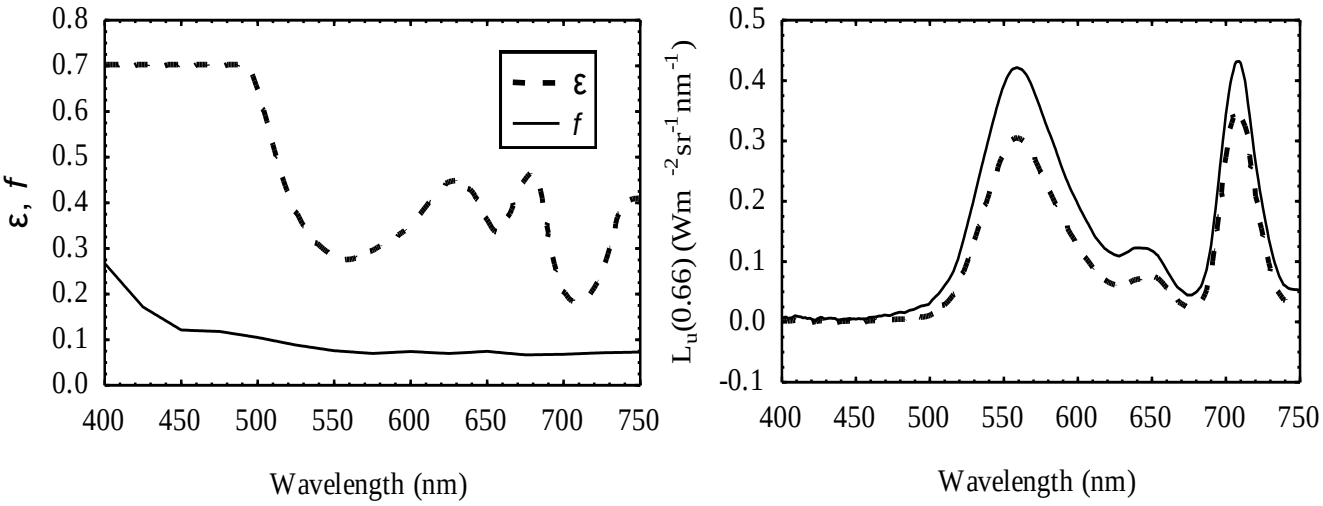

Figure 5.4 Correction of $L_u(0.66)$ for instrument self-shading. The left hand plot shows the total self shading error, ε, and the ratio of skylight to direct sunlight, *f*. The right hand plot shows a measured (dotted line), and corrected (solid line), L_u(0.66) spectrum for 23 April 2008.

500 nm. The large error in the blue is a consequence of the large absorption and scattering values generated by the bio-optical simulation (See Figures 4.2 and 4.3). Because errors larger than 100% were predicted in this region of the spectrum, $\varepsilon(\lambda)$ was made constant for wavelengths less than 500 nm, at its value at 500 nm. The magnitude of $L_u(0.66)$ increased when corrected for the effects of instrument self-shading (Figure 5.4).

5.2.3 Calculation of Water-Leaving Reflectance using K_u

Figure 5.5 shows 16 K_u, spectra, calculated using the bio-optical simulation and Equation 4.9, and the corresponding ρ_w, calculated using Equation 4.8.

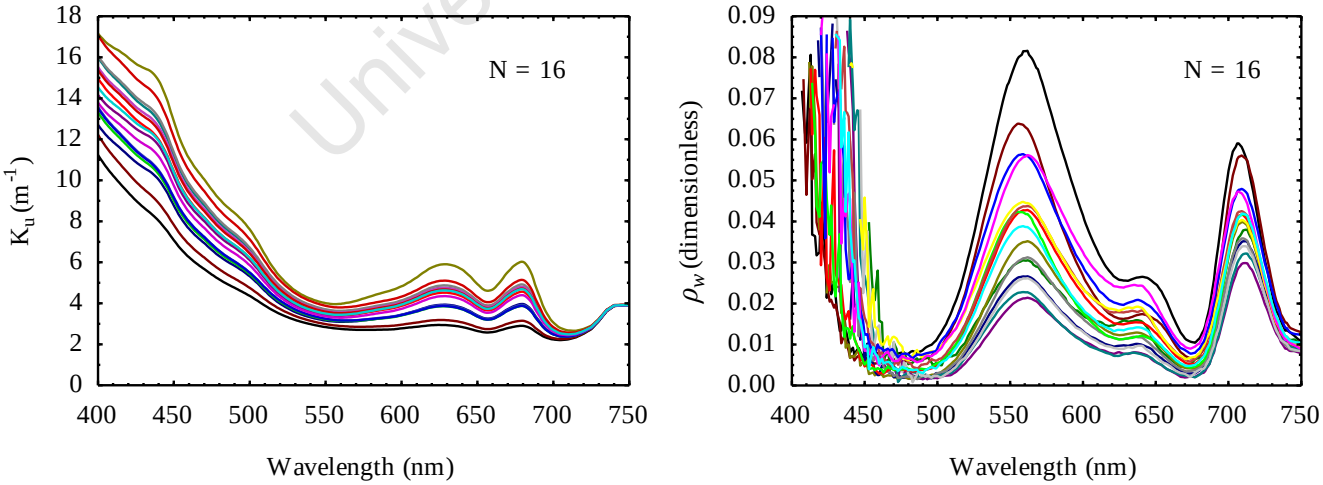

Figure 5.5 K_u (left hand side) derived from the bio-optical model and the corresponding ρ_w (right hand side).

The reflectance in the blue region, 400 to 480 nm, shows very large and erratic values, uncharacteristic of the high absorption in this region, and of the shapes of L_u(0.66) (Figure 5.3).

The very high values observed for K_u was caused by the inability of the bio-optical simulation to account for the offset to absorption by scattering from suspended matter, in this region. In order to alleviate this error, the value of K_u below 500nm was made constant equal to its value at 500 nm. While the K_u values are somewhat synthetic, $L_u(0.66)$ values at wavelengths less than 500 nm are close to 0, and the correction is a simple way of reducing processing errors for very small signals. The corresponding values of reflectance appear more normal when this rough correction is applied (See Figure 5.6).

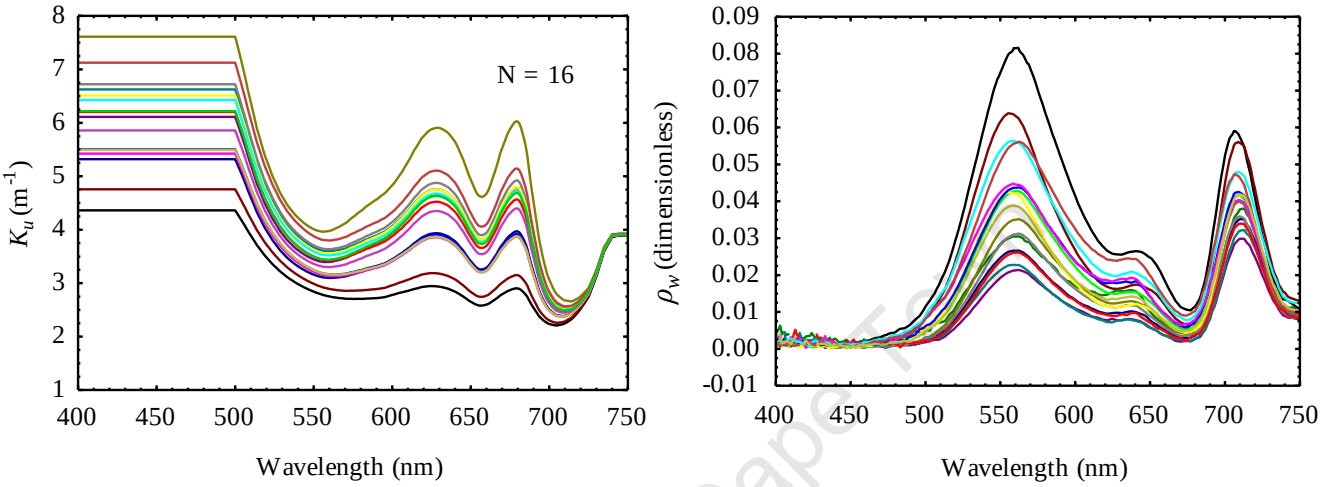

Figure 5.6 Modified K_u values (left hand side) and corresponding ρ_w (right hand side).

The reflectance values shown in Figure 5.6 are comparable with values measured in other eutrophic waters (See Dekker, 1993, Schalles et al., 1998). The difference in magnitude of the spectra indicates the variability of backscattering owing to changes in the concentration of suspended particulates, which is spectrally relatively invariant. $R_{rs}(0.66)$, calculated using Equation 4.13, are presented in Figure 5.7 below. The spectra show very low values in the blue (>500 nm) in agreement with the corrected ρ_w spectra in Figure 5.5.

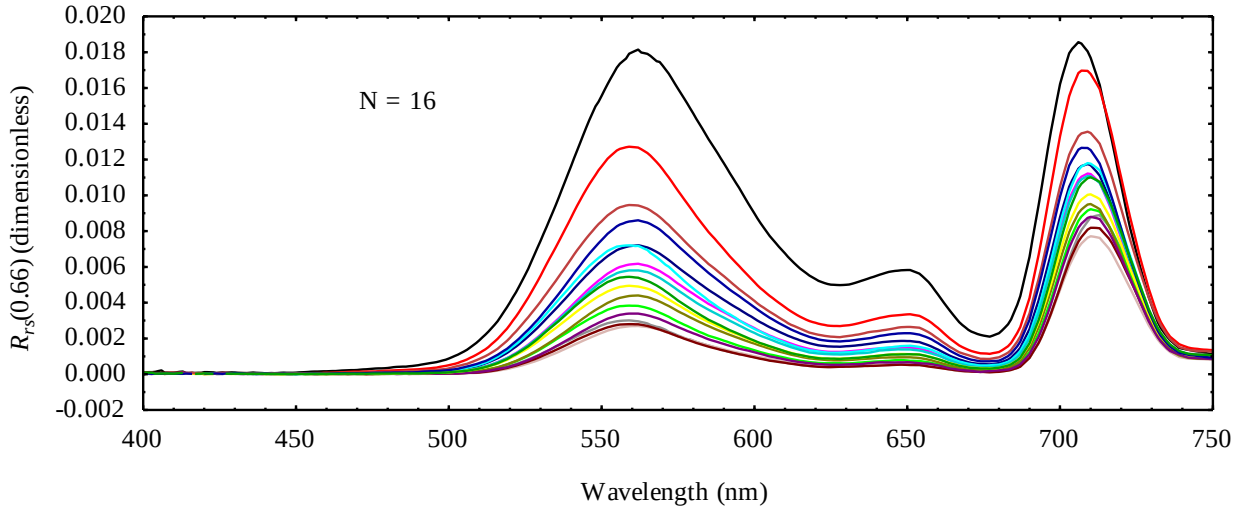

Figure 5.7 $R_{rs}(0.66)$ for Zeekoevlei for April 2008.

The estimates of the error introduced to ρ_w through K_u, where the change to ρ_w is the average percentage change over the wavelengths 400 to 700 nm, shows that a change in K_u leads to a change in the value of ρ_w usually at least twice as large as that to K_u (Table 5.4).

Table 5.4 Estimation of errors to ρ_w associated with K_u.

% change to K_u	**average % change to ρ_w**	
	-	+
5%	10%	12%
10%	20%	25%
20%	35%	58%
50%	65%	229%

Assuming that K_u is accurate to within 10% of its value, the associated average errors for ρ_w over the visible spectrum are 20% negative and 25% positive, respectively. The total RMS error estimated for self-shading (assuming clear-sky conditions) and K_u, assuming estimates are accurate to within 10%, calculated using Equation 4.12, is shown in Figure 5.8 below.

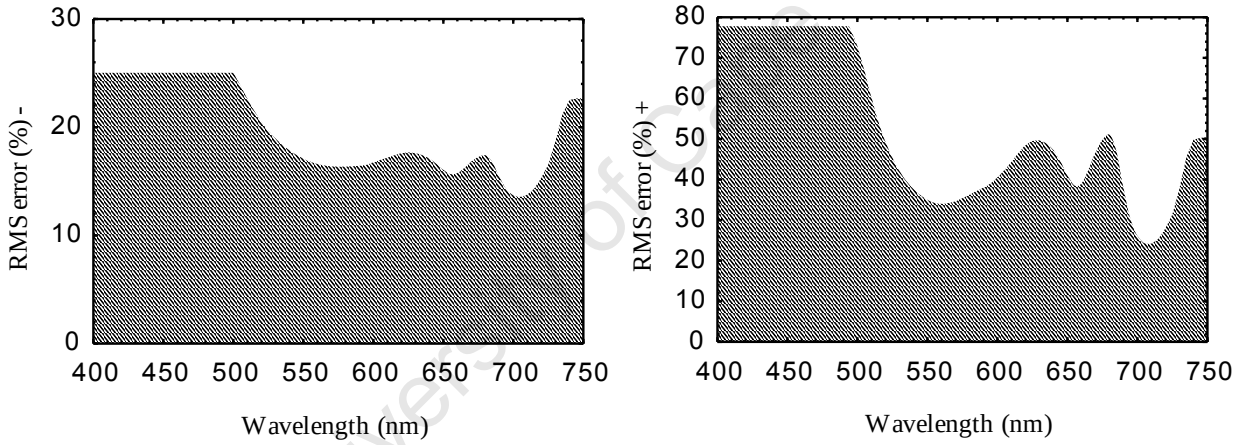

Figure 5.8 Estimated negative (left hand side) and positive (right hand side) RMS error (%) for ρ_w spectra measured in clear-sky conditions and assuming a 10% error for K_u.

The change is greater in the positive direction, because the instrument self-shading error is only in the positive direction. Although the errors appear very large at less than 500 nm, the relative change to the ρ_w is small, because the values in this region are very small (See Figure 5.6).

5.2.4 Correlation of R_{rs}(0.66) with Water Quality Parameters

The correlation between R_{rs}(0.66) and the water quality parameters was tested for all wavelengths at a 1nm resolution (Figure 5.9). The correlation coefficients reach their highest values, for most variables, at about 540 and 710 nm, which correspond to the peaks of ρ_w (Figure 5.6). Thus it can be inferred that the water constituents contribute towards the reflectance peaks, to different extents, and that the height of these peaks corresponds well to the concentrations of the water constituents. The r^2 value for Chl *a* is higher than for the other parameters, reaching a maximum

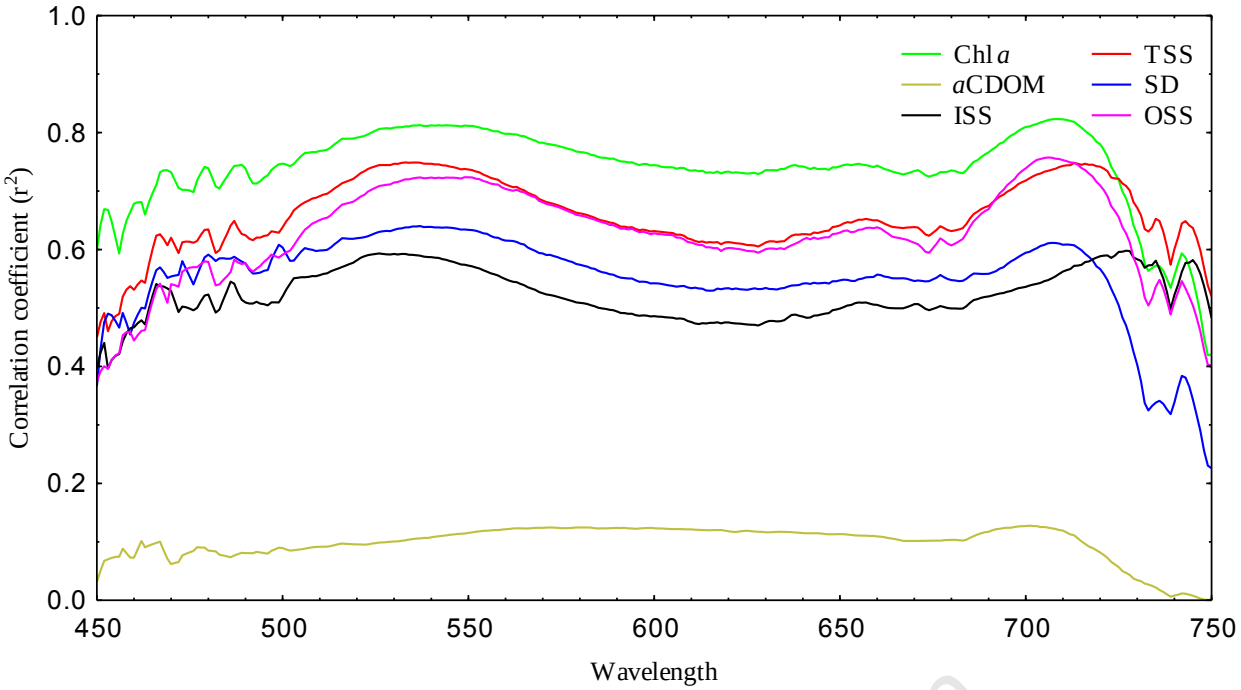

Figure 5.9 r^2 correlation coefficients for water quality parameters and hyperspectral radiometric reflectance (0.66 m). Data < 450 nm was removed due to noise.

near 710 nm. The shape of the correlation curve for Chl *a* is very similar to those for TSS, OSS and SD depth. The ISS curve deviates slightly from this shape, with the highest correlation coefficient value near 730 nm. This is most likely because inorganic minerals contribute towards increased scattering in the near infrared part of the spectrum. The correlation coefficient for a_{CDOM} is low over all wavelengths and is not significant. It can be deduced that the gross particle load of suspended particulates has the dominant influence on $R_{rs}(0.66)$. Further correlation analysis with the algorithms in Table 4.4, reveals that the majority of the water quality parameters can be estimated well (Table 5.5).

Table 5.5 r^2 correlation coefficients for independent $R_{rs}(0.66)$ variables with water quality parameters. Significant correlations (p < 0.05) are in red. Strongest correlations are in bold. N = 16.

Algorithm	Chl *a*	LnChl *a*	TSS	LnTSS	ISS	LnISS	OSS	LnOSS	SD	LnSD
RLH	**0.771**	**0.856**	0.709	0.763	0.470	0.640	0.774	0.809	0.669	0.661
700	0.762	0.854	0.713	0.770	0.481	0.661	0.766	0.802	0.666	0.656
Max~700	0.729	0.833	0.751	0.802	0.525	0.676	0.782	0.816	0.672	0.659
(700/670)	0.627	0.600	0.661	0.654	0.358	0.409	0.849	0.839	0.478	0.491
(560-520)/(560+520)	0.516	0.566	**0.874**	**0.870**	**0.620**	0.650	**0.897**	0.895	0.566	0.566
700/(560+670)	0.671	0.680	0.773	0.776	0.477	0.542	**0.897**	**0.898**	0.601	0.610
560	0.737	0.852	0.713	0.780	0.505	**0.715**	0.733	0.775	0.681	0.666
Average(500-600)	0.730	0.848	0.707	0.776	0.504	0.723	0.721	0.763	0.673	0.657
FLH	0.667	0.767	-	-	-	-	-	-	-	-
740((1/670)-(1/710))	0.657	0.578	-	-	-	-	-	-	-	-
(520/700)	-	-	-	-	-	-	-	-	**0.684**	**0.679**
(490/620)	-	-	-	-	-	-	-	-	0.531	0.500

The RLH algorithm performed best with Chl *a*, and the r^2 value (0.856) is higher than that derived by Schalles et al. (0.83) (1998), although not as high as that derived by Yacobi et al.

(0.98) (1995) (Figure 5.10). The 740((1/670)-(1/710)) algorithm, used by Zimba and Gitelson (2006) in hypereutrophic water, did not perform very strongly (r^2 = 0.657). The highest correlation with TSS, given with the reflectance difference ratio (560-520)/(560+520), was higher (r^2 = 0.874) than that derived by Gitelson et al. (r^2 = 0.86) (1993). ISS and OSS also produced the strongest correlations with the difference ratio (r^2 = 0.620 and 0.897, respectively).

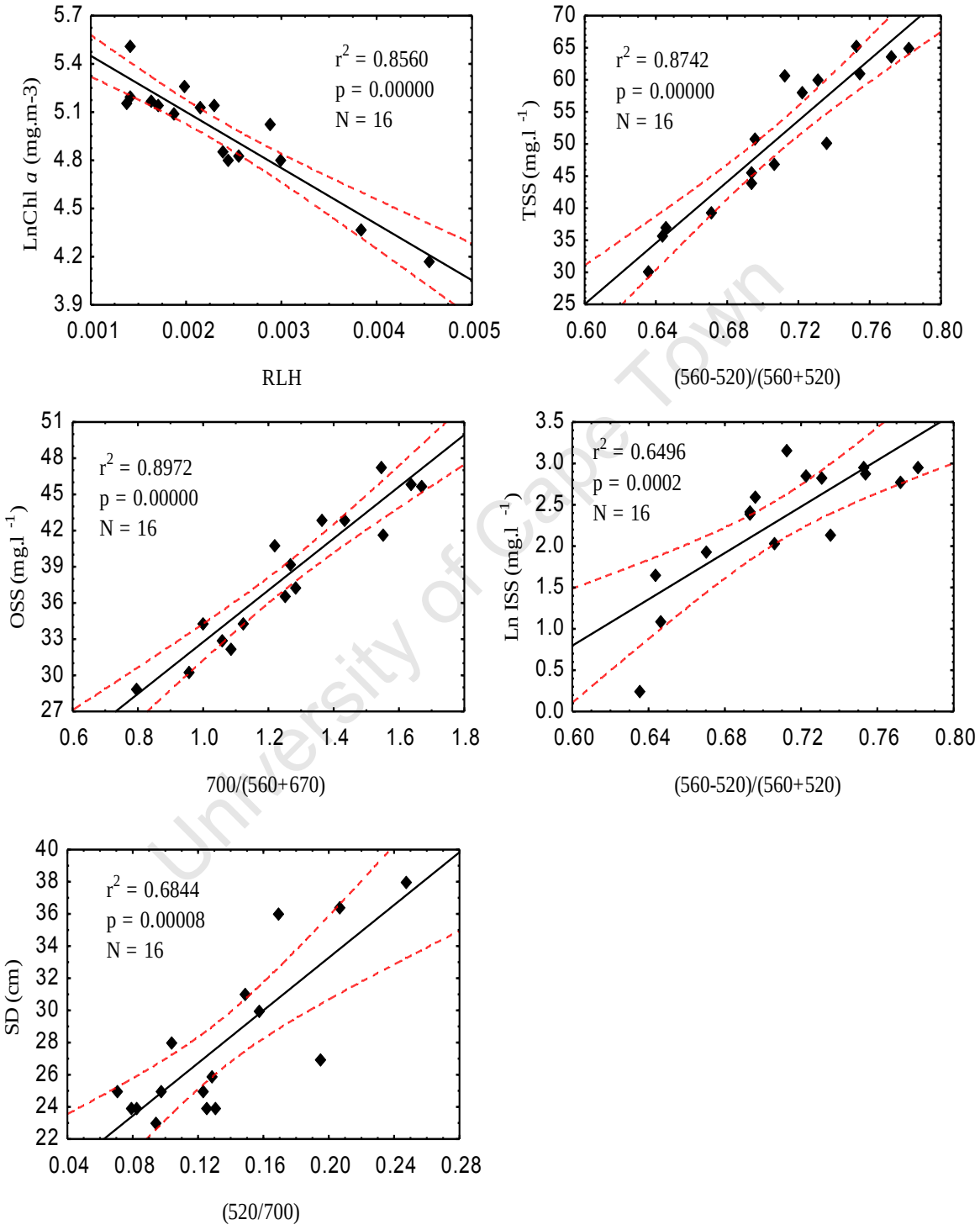

Figure 5.10 Scatterplots of empirical algorithms for estimating water quality parameters from R_{rs}(0.66). Dotted red lines show the 95% confidence limits

For OSS the 700/(560+670) band ratio algorithm (Koponen et al. 2007) also gave very significant results (r^2 = 0.897). The most significant correlation for SD was given with the algorithm using the band ratio (520/700) (r^2 = 0.684), as used by Koponen et al. (2002). The strong performance of many algorithms across different water quality parameters shows that it is difficult to separate signals from the different parameters using empirical algorithms.

There are significant correlations between the magnitude (r^2 = 0.698) and position (r^2 = 0.771) of the reflectance peak near 700 nm normalised at 640 nm with Chl *a* concentration, in agreement with other workers (See Gitelson, 1992, Schalles et al., 1998) (See Figure 5.11).

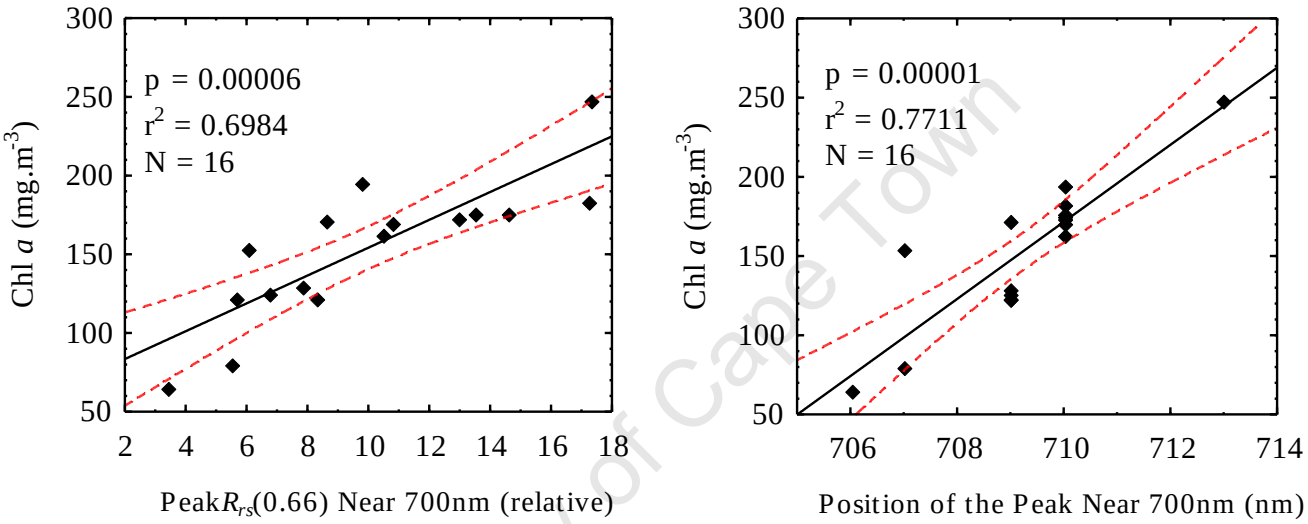

Figure 5.11 The height (left) and position (right) of the peak near 700 nm versus Chl *a* concentration for R_{rs}(0.66) normalized at 640 nm. Dotted red lines show the 95% confidence limits.

This indicates that phytoplankton backscattering is the dominant causal IOP of the peak. The wavelength shift with greater Chl *a* concentrations is caused by increasing backscattering relative to absorption by water at the 'red edge'. Although the position of the peak near 700 nm was found to be non-normally distributed (Shapiro-Wilk p = 0.021), the nonparametric Spearman Rank Order statistic gave a coefficient of determination, R, equal to 0.86 ($p < 0.05$). Figure 5.12 shows six normalised R_{rs}(0.66) spectra with the corresponding *in situ* simultaneously measured Chl *a* concentrations. The spectra clearly show that the magnitude of the reflectance peaks at 560 nm and 710 nm increase as Chl *a* concentrations increase.

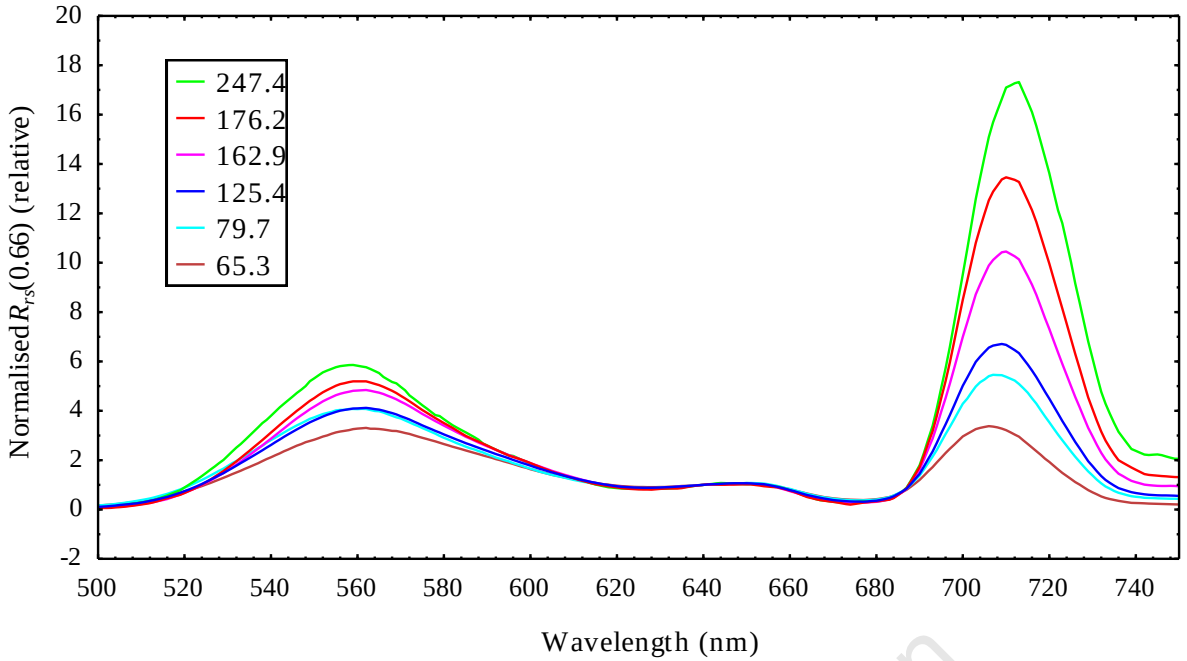

Figure 5.12 Normalised R_{rs}(0.66) at 640 nm showing corresponding simultaneously measured Chl *a* concentrations (units are in mg.m^{-3}).

5.3 Water Quality Estimation from MERIS

5.3.1 Data acquisition

MERIS data was successfully acquired on fourteen of the eighteen days of the fieldwork. Table 5.6 shows the types of data collected on the sampling days and the success of the collection.

Table 5.6 Results of MERIS and in situ data acquisition for April 2008.

Date	Was data successfully acquired?			Comments	Simultaneous MERIS acquisition?
	Water quality	TSRB	MERIS		
1/4/08	YES	NO	YES	TSRB failure, otherwise good	YES
2/4/08	NO	NO	NO	Fieldwork cancelled due to overcast conditions	NO
4/4/08	YES	YES	YES	Zeekoevlei not visible in MERIS scene due to overcast conditions	NO
7/4/08	YES	YES	YES	Good	YES
8/4/08	YES	YES	YES	Zeekoevlei outside of MERIS scene	NO
10/4/08	YES	YES	YES	Zeekoevlei not visible in MERIS scene due to overcast conditions	NO
11/4/08	YES	YES	YES	Zeekoevlei outside of MERIS scene	NO
13/4/08	NO	NO	YES	Fieldwork cancelled for rest	NO
14/4/08	YES	YES	YES	Zeekoevlei outside of MERIS scene	NO
17/4/08	YES	YES	YES	Zeekoevlei outside of MERIS scene	NO
18/4/08	NO	NO	NO	Fieldwork cancelled due to overcast conditions	NO
19/4/08	NO	NO	NO	Fieldwork cancelled due to overcast conditions	NO
20/4/08	YES	YES	YES	Good	YES
23/4/08	YES	YES	YES	Good	YES
24/4/08	YES	YES	YES	Zeekoevlei outside of MERIS scene	NO
26/4/08	NO	NO	YES	Zeekoevlei not visible in MERIS scene due to overcast conditions	NO
27/4/08	NO	NO	YES	Zeekoevlei not visible in MERIS scene due to overcast conditions	NO
28/4/08	NO	NO	NO	Fieldwork cancelled	NO

In only five of the fourteen MERIS scenes collected were Zeekoevlei visible without cloud cover. The remainder of the MERIS scenes were not used due to cloud cover, or Zeekoevlei being outside of the scene. Simultaneous *in situ* water quality and MERIS data were available on four days during April (See pie chart, Figure 5.13). Hence 25% of MERIS images where acquired successfully, simultaneous with water quality and environmental measurements. These scenes were used for validating the MERIS L2 products, and for deriving empirical algorithms and mapping water constituents from the L1 product. Nine pixels, corresponding to *in situ* sample sites were extracted from the scenes for this purpose.

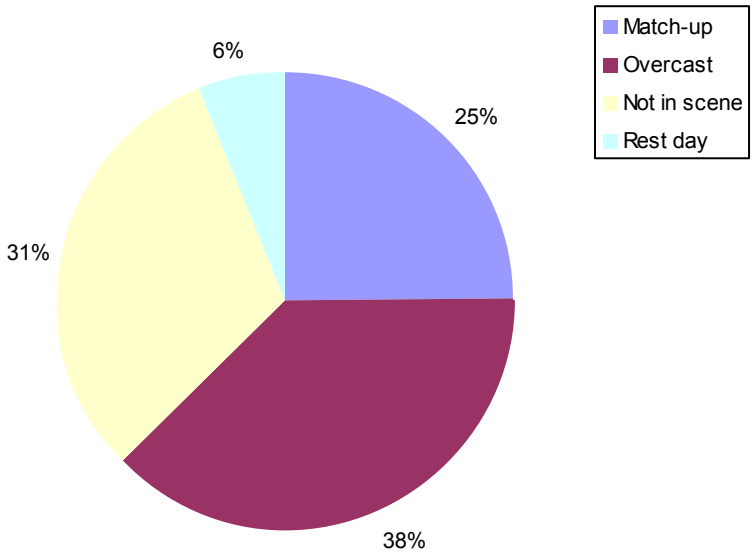

Figure 5.13 Outcome of MERIS data acquisition during April 2008.

5.3.2 Validation of MERIS Products

5.3.2.1 MERIS L 1P

The spectra for TOA radiance (smile corrected) and apparent reflectance from nine pixels corresponding to *in situ* measurements are presented in Figure 5.14. The systematic error estimated for radiance measurements is less than 4% (European Space Agency, 2006). The oxygen absorption band at 761 nm was excluded.

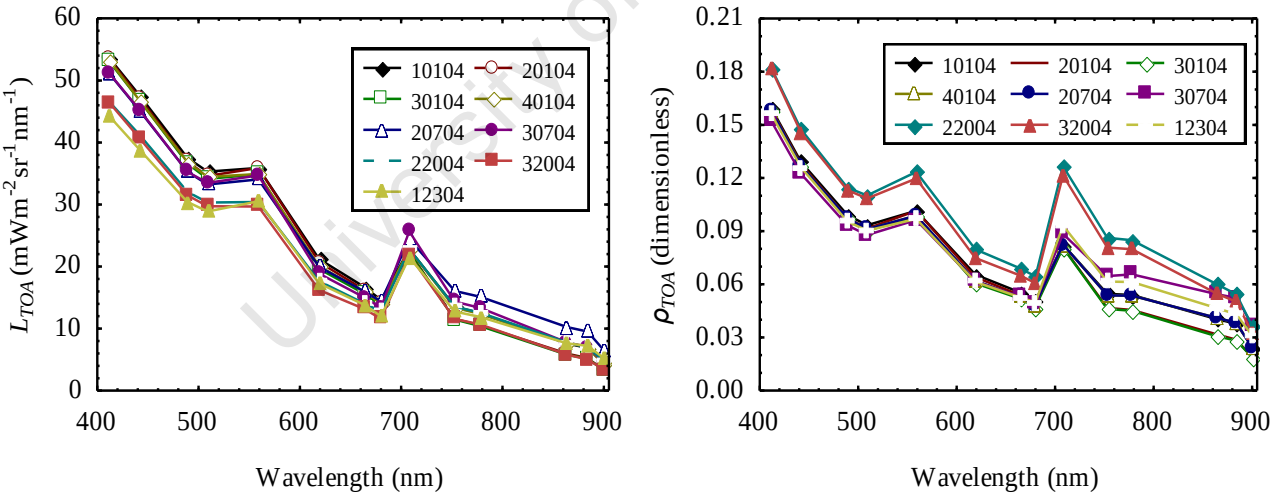

Figure 5.14 MERIS smile corrected L_{TOA} (left hand side) and ρ_{TOA} (right hand side). Legend key is sample point number followed by day and month. For example, 10104 is sample point 1, on the 1st of April, 2008.

The TOA spectra display spectral shapes similar to those measured *in situ* (Figure 5.6), although obvious discrepancies are visible in the blue region of the spectrum (<500 nm). This is caused by atmospheric scattering that contributes greatly to the signal measured at the satellite in the blue. Distinctive peaks are visible in the 559 and 708 nm bands which correspond to the peaks measured *in situ*. The bands at 664 and 680 nm show the characteristic absorption maxima of Chl *a* pigments. The near-infrared bands show low values that correspond to absorption by water in

this region. Despite not being corrected for atmospheric effects, the MERIS L 1P spectra show the distinctive characteristics of the light field over Zeekoevlei without any obvious errors.

5.3.2.2 MERIS L 2P

The MERIS L 2 Case 2 processor product gave between 6 and 14 pixels covering Zeekoevlei for the four simultaneous acquisitions. The reflectance was invariably flagged as 'invalid' turbid, Case 2, sediment-dominated water. Invalid flags were also raised for water constituent retrieval and occasionally for aerosol retrieval. The normalised water-leaving reflectance spectra corresponding to *in situ* measurements are presented in Figure 5.15 below. The error of reflectance retrieval has previously been estimated at less than 5% by validation studies in European coastal Case 2 waters (Aiken & Moore, 2000), but is obviously much larger in this instance.

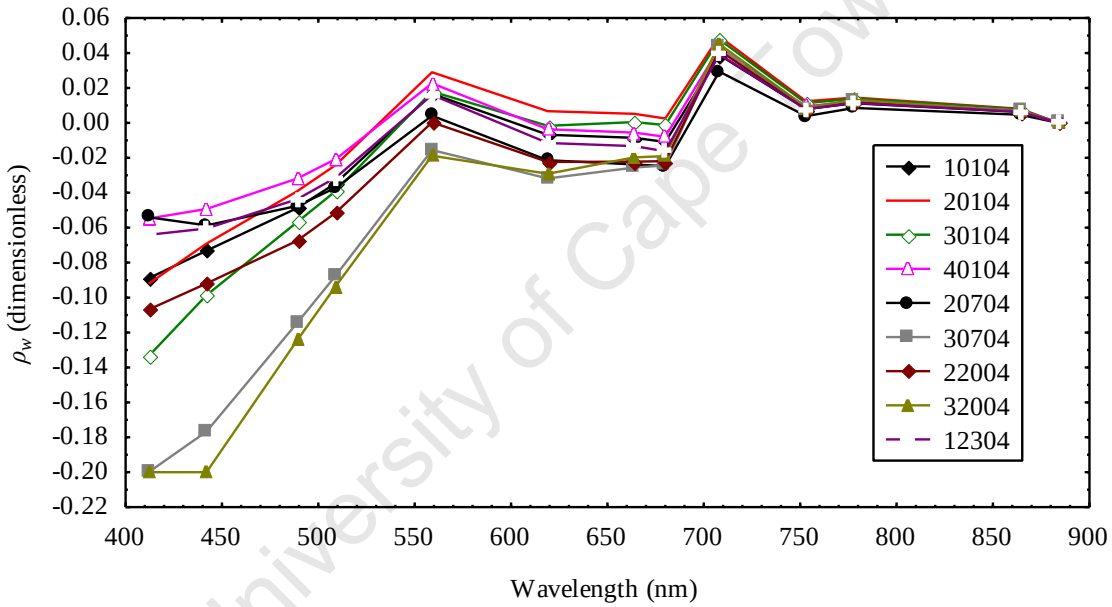

Figure 5.15 MERIS L 2 ρ_w for nine pixels corresponding to *in situ* sample sites. The legend key is the same as in Figure 5.14.

The negative reflectance values in the blue region of the spectra indicate a failure in the atmospheric correction procedure, possibly as a result of the very high sediment concentrations and type of sediment in Zeekoevlei, or the presence of anomalous atmospheric conditions (Aiken & Moore, 2000). A comparison of the Aerosol Optical Thickness (AOT) estimated by the MERIS L 2 product, and *in situ* sun photometer measurements, indicate the failure of the retrieval of the AOT at 443 nm (negative values) (See Table 5.8). The results of the MERIS Case 2 water constituent retrieval algorithm are presented beside *in situ* measurements for comparison (Table 5.8). Not suprisingly, the retrieval of Chl *a* and TSS is severely underestimated by the L 2 product while a_{CDOM} is overestimated, due to the invalid water-leaving reflectance used as input for the algorithm, as a result of the atmospheric correction failure, and because the water

conditions in Zeekoevlei are well outside the NN training range. Other possible reason for the failure is the differences between the IOPs of the water constituents in Zeekoevlei, and those used to parameterise the NN algorithm.

Table 5.8 Comparison of the results of the MERIS L2 product and in situ measurements. The sample number key follows Figure 5.14.

	MERIS L2				*In situ*			
Sample No.	**Chl *a***	**TSS**	**a_{CDOM}**	**AOT443**	**Chl *a***	**TSS**	**a_{CDOM}**	**AOT440**
10104	7.9	8.2	3.24	-0.006	69.2	30.0	2.27	0.251
20104	27.1	19.6	4.17	-0.006	61.0	36.0	1.83	0.251
30104	7.9	8.2	3.34	-0.006	71.3	26.3	2.16	0.251
40104	8.2	9.5	3.13	-0.006	107.5	36.8	1.97	0.251
20704	9.5	3.8	4.04	-0.006	119.5	41.8	2.17	0.104
30704	10.6	4.8	3.91	-0.006	247.4	50.3	2.85	0.104
22004	10.6	4.8	3.91	-0.006	171.5	60.7	3.07	0.13
32004	10.2	5.1	3.79	-0.006	194.6	51.0	3.73	0.13
12304	7.9	7.6	3.24	-0.006	122.6	37.3	2.78	0.081

5.3.2.3 MERIS Eutrophic Lakes Processor

The Eutrophic Lakes Processor gave between 6 and 17 pixels covering Zeekoevlei. The nine ρ_w spectra corresponding to *in situ* measurements are presented in Figure 5.16.

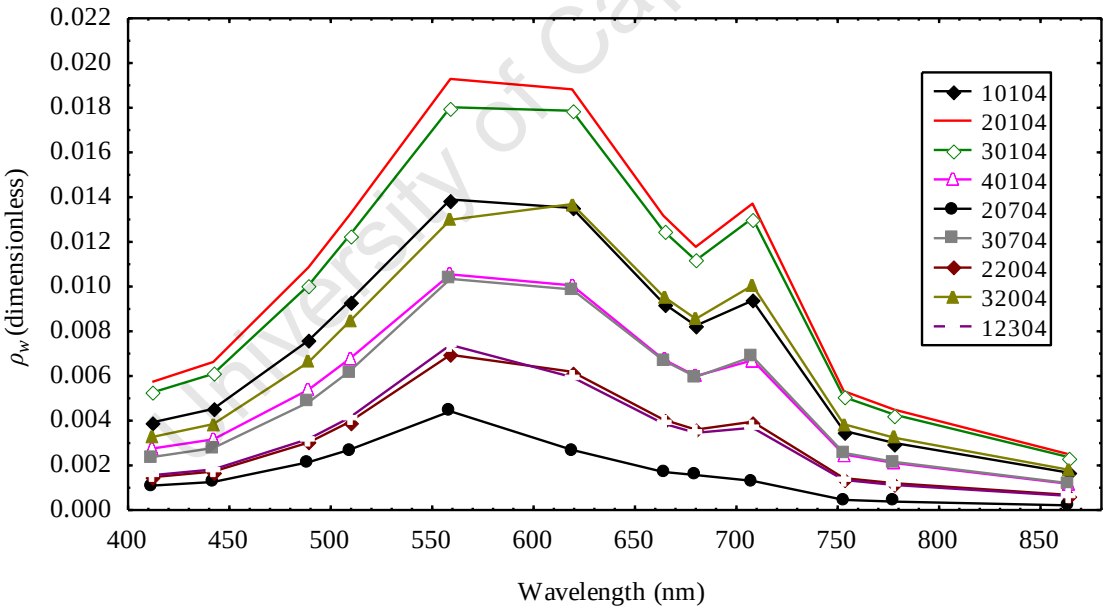

Figure 5.16 ρ_w derived from the Eutrophic Lakes Processor for nine pixels corresponding to *in situ* sample sites. The legend key is the same as in Figure 5.14.

The results indicate that the atmospheric correction procedure used by the Eutrophic Lakes Processor is more robust than the L 2 product since there are no negative reflectance values. The spectra clearly show the peaks at 560 and 708 nm, in accordance with *in situ* observations. Uncharacteristically however, the shape is inflected at 619 nm, the absorption maxima of phycocyanin, and greatly enlarged in the 509 nm and other blue spectrum bands. This is most likely a result of differences between the IOPs in Zeekoevlei, especially concerning the

cyanobacteria dominated phytoplankton assemblage and high CDOM levels, and those used to parameterise the bio-optical model used by the Eutrophic Lakes NN algorithm. Furthermore, the magnitudes of the spectra are on average a good deal smaller than those measured with the TSRB (compare with Figure 5.5). The poor overall agreement between the spectra is a result of the poor performance of the NN algorithm. Discrepancies between the IOPs used in the bio-optical model and those of Zeekoevlei result in errors in the atmospheric correction, because the NN algorithm is dependent on the bio-optical water model (Doerffer & Schiller, 2008a). The large differences between the water constituents measured *in situ* and those retrieved by the Eutrophic Lakes processor, indicate that the training range is also well below that required for Zeekoevlei, particularly for Chl *a* and a_{CDOM} (Table 5.9).

Table 5.9 Comparison of the results of the MERIS Eutrophic Lakes Processor and in situ measurements. Sample number key is the same as in Figure 5.14.

	MERIS				***In situ***			
Sample No.	**Chl *a***	**TSS**	**a_{CDOM}**	**AOT550**	**Chl *a***	**TSS**	**a_{CDOM}**	**AOT500**
10104	19.7	29.6	1.28	0.268	69.2	30.0	2.27	0.210
20104	20.9	40.8	1.16	0.243	61.0	36.0	1.83	0.210
30104	21.0	39.6	1.23	0.241	71.3	26.3	2.16	0.210
40104	19.2	21.7	1.20	0.265	107.5	36.8	1.97	0.210
20704	10.9	3.7	0.53	0.074	119.5	41.8	2.17	0.102
30704	20.2	18.5	1.04	0.213	247.4	50.3	2.85	0.102
22004	18.9	12.1	0.94	0.254	171.5	60.7	3.07	0.125
32004	20.6	29.7	1.51	0.250	194.6	51.0	3.73	0.125
12304	18.1	10.1	0.68	0.092	122.6	37.3	2.78	0.073

Chl *a*, TSS and a_{CDOM} are generally underestimated (besides for TSS concentrations for the first four samples), as a result of the poor atmospheric correction, differences between the IOPs, and the narrow range of the NN algorithm. Overall the Eutrophic Lakes Processor performs poorly in terms of atmospheric correction and water constituent retrieval over Zeekoevlei, although the results are better than the standard MERIS L 2 product.

5.3.3 Atmospheric Correction of MERIS L 1P

5.3.3.1 Dark Object Subtraction

The viewing zenith angle, θ_v, and the solar zenith angle, θ_s, were used to estimate $T_\lambda\downarrow$ and $T_\lambda\uparrow$ using the COST model, for four MERIS spectra corresponding to a simultaneous TSRB ρ_w measurements (Table 5.10). The atmospheric path radiance, L_{path}, estimated from dark ocean water pixels, and the solar spectral irradiance, E_0, were determined for each of the four MERIS scenes (Table 5.11).

Table 5.10 The viewing zenith angle (θ_v) and the solar zenith angle (θ_s) used to estimate $T_\lambda\downarrow$ and $T_\lambda\uparrow$ for spectra corresponding to sample sites. Sample no. key same as in Figure 5.14.				
Spectrum	θ_v	θ_s	$T\uparrow$	$T\downarrow$
30704	0.349912	0.905801	0.939403	0.617055
22004	0.087453	0.985536	0.996178	0.552417
32004	0.087817	0.985749	0.996147	0.552239
12304	0.264956	0.985435	0.965104	0.5525

Table 5.11 L_{path} and E_0 in each spectral band for four MERIS scenes in April 2008.								
	L_{path} (mWm^{2}nm^{-1}sr^{-1})				E_0 (mWm^{2}nm^{-1})			
Band (nm)	**1-Apr**	**7-Apr**	**20-Apr**	**23-Apr**	**1-Apr**	**7-Apr**	**20-Apr**	**23-Apr**
412	51.85106	48.79732	47.00468	44.12812	1718.421	1712.449	1700.2	1697.423
442	46.07211	41.8498	41.09166	37.81412	1882.896	1876.353	1862.931	1859.888
489	35.18277	30.08567	30.09841	27.06563	1932.446	1925.73	1911.956	1908.832
509	29.73503	26.01373	25.14229	23.11677	1933.046	1926.329	1912.55	1909.425
559	19.5599	17.25088	15.69102	14.60322	1806.918	1800.639	1787.759	1784.839
619	12.54666	9.808554	9.205089	8.358437	1654.291	1648.542	1636.75	1634.077
664	10.36525	7.299363	6.930252	6.22216	1534.89	1529.556	1518.615	1516.134
680	9.570238	6.746483	6.21226	5.639877	1475.305	1470.178	1459.662	1457.277
708	8.050249	5.371459	5.142443	4.524795	1410.943	1406.039	1395.982	1393.702
753	6.59552	3.955406	3.764784	3.21198	1268.741	1264.331	1255.288	1253.237
761	2.342459	1.766604	1.678762	1.542119	1257.254	1252.885	1243.923	1241.891
778	5.873936	3.252642	3.120778	2.665248	1179.768	1175.668	1167.258	1165.352
864	4.046618	1.9197	1.857143	1.509173	960.4273	957.0895	950.2435	948.6913
884	3.686034	1.752377	1.718807	1.201822	931.8192	928.581	921.9388	920.4329
900	2.532813	1.391852	1.284327	0.997594	897.3676	894.249	887.8525	886.4022

The atmospherically corrected MERIS L 1P reflectance spectra, using the DOS and COST image-based methods, show close comparisons between simultaneously acquired TSRB ρ_w measurements (Figure 5.17). The TSRB spectra are presented using the middle wavelengths of the first 10 MERIS bands to ease comparison. The agreement between the spectral shapes and magnitudes of the atmospherically corrected MERIS and *in situ* TSRB spectra is excellent, especially in the bands centred at 489, 509, 559 and 619 nm. The negative reflectances in some MERIS spectra at 412nm and 442nm signify that these spectra were overcorrected as a result of the value of the dark object (oceanic water in this instance) being too large at these wavelengths. At wavelengths greater than 619 nm the atmospheric correction models overestimate the water-leaving reflectance, particularly in the infrared part of the spectrum (>700 nm). The DOS and COST spectra are very similar in shape, however the magnitudes of the COST model spectra are larger. It is difficult to tell which model produces the best results as the TSRB measurements usually lies between the two models up to the 619 nm band. However, in the remainder of the spectrum (619 to 753 nm), the simpler DOS model produces values closer to

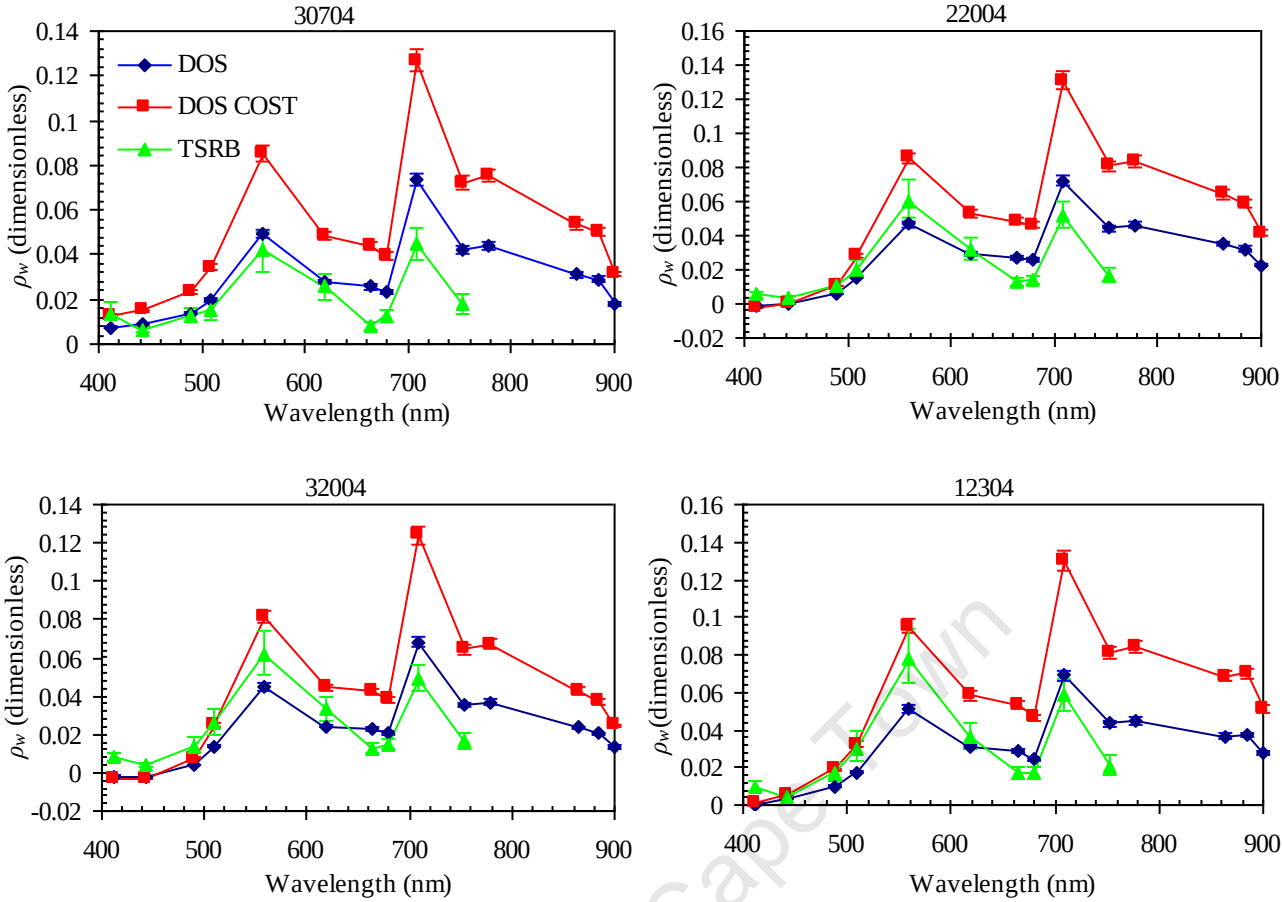

Figure 5.17 Comparison of DOS and COST model atmospherically corrected MERIS L 1 and *in situ* TSRB ρ_w (corrected for self-shading effects). Error bars represent systematic error for MERIS (5%), and the error associated with K_u estimation (TSRB).

those measured *in situ*, and therefore appears to be the more accurate of the two models in this instance.

4.3.3.2 6S Radiative Transfer Code

A comparison between MERIS L 1P spectra corrected using the 6S radiative transfer code and ρ_w TSRB spectra show excellent agreement between the spectral shapes (Figure 5.18). The 6S spectra clearly demonstrate the reflectance peaks at 560 and 708 nm, as well as the Chl *a* absorption maxima. In the near infrared and blue regions of the spectrum the code seems to perform well with no negative reflectance values, although the values are larger than those measured with the TSRB. Thus it would appear that the code under-corrects for atmospheric effects in the blue and near-infrared parts of the spectrum. Small adjacency effects from radiance from the surrounding land are visible as increased reflectance in the band at 900 nm. The 6S water-leaving reflectances appear to show less spectral bias than the DOS and COST spectra in Figure 5.17. Therefore, the 6S code produces reflectances that are more physically robust than the DOS and COST image-based techniques, although the spectral shapes are very similar.

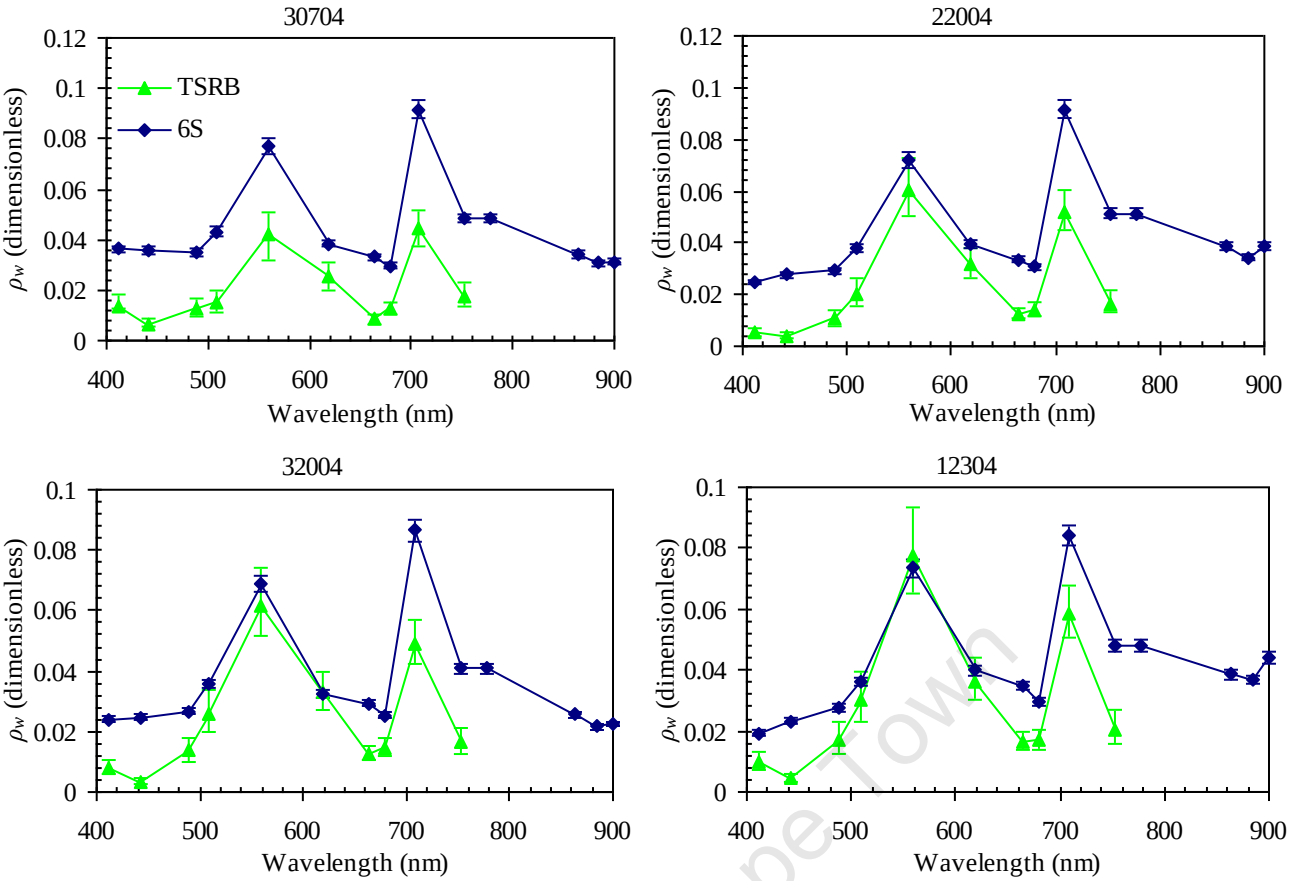

Figure 5.18 Comparison of MERIS 6S atmospherically corrected and *in situ* TSRB ρ_w spectra (corrected for self-shading effects). Error bars represent systematic error for MERIS (5%), and the error associated with K_u estimation (TSRB).

5.3.3.3 Investigation of Adjacency Effects

Figure 5.19 shows the water pixel transects in west-east and north south directions for near-infrared bands plotted to investigate the adjacency effect.

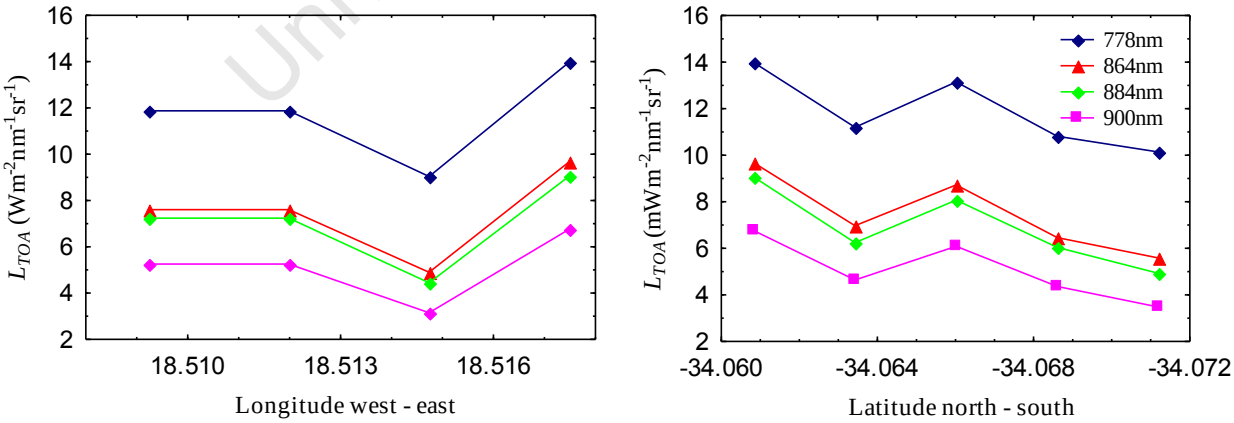

Figure 5.19 West-east (left hand side) and north-south (right hand side) transects for Zeekoevlei for near infrared bands for 23 April 2008.

The west-east transect shows the increased radiance from the adjacency effect towards the edges of Zeekoevlei while the north-south transect clearly shows the increased radiance associated with the arm of land (peninsula) that extends into Zeekoevlei from the east. The lowest radiance value

is located in the centre of the northern basin, the furthest distance from land. Therefore, adjacency effects increase towards the edges of Zeekoevlei, so care was taken to avoid selecting pixels too near the shore of the lake for water constituent retrieval and mapping.

5.3.4 Empirical Algorithms for Water Quality Parameters

Linear regression analysis was first used to test the correction of water quality parameters with MERIS single bands. The correlation between 11 single MERIS TOA radiance bands and water quality parameters show that at wavelengths less than 680 nm, the correlation with a_{CDOM} is unusually significant ($r^2 > 0.5$). SD is also significantly correlated with the bands centred at 619 and 664 nm. The other water quality parameters however, are poorly correlated with single bands.

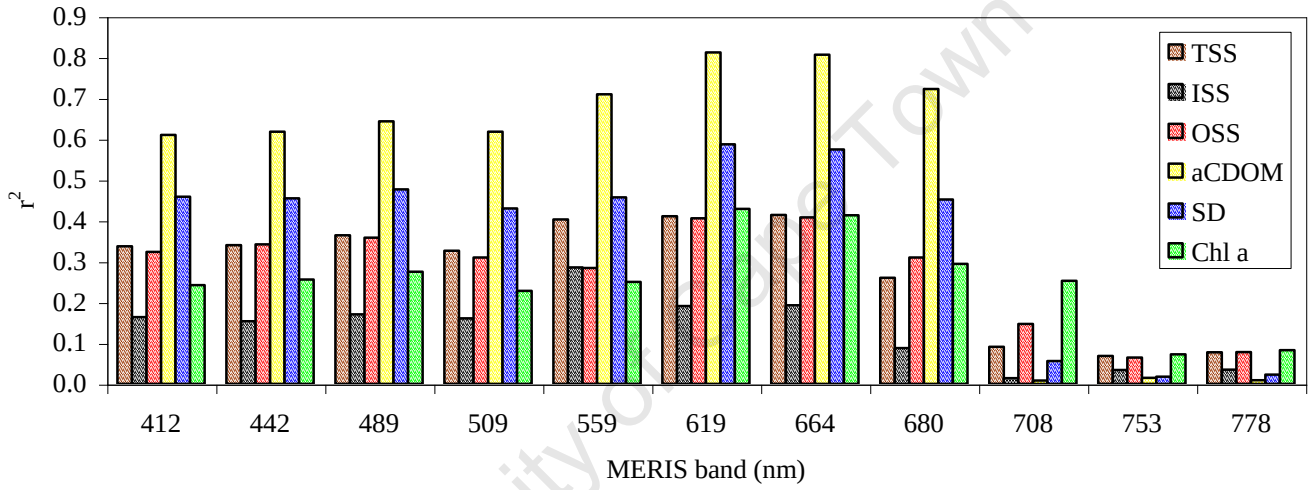

Figure 5.20 r^2 correlation coefficients between single TOA radiance MERIS bands and water quality parameters.

In order to improve the correlations, further algorithms (Table 4.7) were tested for each water quality parameter. Only algorithms which gave strong correlations are included in the tables below.

5.3.4.1 Chl *a* Algorithms

Table 5.12 r^2 correlation coefficients for best performing algorithms for Chl a. Significant correlations (p<0.05) are in red. N = 9.

Algorithms	Data type					
	Raw	Smile corrected	Apparent reflectance	DOS	COST	6S
(708/664)	**0.925**	**0.925**	**0.925**	0.093	0.093	0.784
RLH	0.910	0.910	0.887	0.918	0.812	0.865
753((1/664)-(1/708))	0.809	0.808	0.782	0.712	0.712	0.772
708	0.246	0.252	0.252	0.702	0.626	0.800

The strongest correlation with Chl *a* was derived using the 708/664 band ratio algorithm with uncorrected TOA MERIS data (boldened Table 5.12). Interestingly the 708/664 ratio performed poorly with image-based DOS and COST atmospherically corrected data, due to the spectral bias introduced through these procedures. The Reflectance Line Height (RLH) algorithm is very robust and produced consistently good results across the different data types. The 753((1/664)-(1/708)) algorithm (Zimba & Gitelson, 2006) also produced consistently good results but was less accurate than the RLH algorithm. The 708 nm single band algorithm appeared to produce poor correlations for TOA data but good correlations with atmospherically corrected data. 6S corrected data were the only data type that produced good correlations for all the variables, showing that the atmospheric correction is physically sound. In order to improve the correlation, nonlinear estimation and multiple regression analysis was performed. It is reasonable to assume that a non-linear relationship exists with Chl *a* in Zeekoevlei owing to complex causal effects. Multiple regression analysis with variables (708/664) and $(708/664)^2$ after Mittenzwey et al. (1992) improved the r^2 (adjusted) value to 0.957. However, the best performance was given using nonlinear estimation which gave $r^2 = 0.965$ (Table 5.13).

Table 5.13 Results of non-linear and multiple regression analysis for Chl a with MERIS TOA apparent reflectance. N = 9.

Form	X_1	X_2	a	b	c	r^2	p
$y = aX^b$	(708/664)	-	5.931	5.935	-	0.965	0.00000
$y = a + bX_1 + cX_2$	(708/664)	$(708/664)^2$	2093.230	-6.144	7.109	0.957	0.00003

5.3.4.2 Suspended Solids Algorithms

An algorithm using the 708 nm band with 6S corrected data produces the best correlation ($r^2 = 0.810$) with TSS (Table 5.14).

Table 5.14 r^2 correlation coefficients for best performing algorithms for suspended solids. Significant correlations (p<0.05) are in red. N = 9.

	Data type					
Algorithms	**Raw**	**Smile corrected**	**Apparent reflectance**	**DOS**	**COST**	**6S**
TSS						
(708/664)	0.690	0.691	0.691	0.013	0.013	0.634
708/(559+664)	0.763	0.763	0.760	0.753	0.753	0.792
RLH	0.540	0.542	0.501	0.718	0.712	0.741
708	0.086	0.091	0.091	0.655	0.625	**0.810**
ISS						
(559-509)/(559+509)	0.428	0.437	0.437	0.044	0.044	0.114
708/(559+664)	0.377	0.378	0.372	0.433	0.433	**0.483**
708	0.013	0.014	0.014	0.283	0.274	0.455
OSS						
(708/664)	**0.764**	0.763	0.763	0.012	0.012	0.566
708/(559+664)	0.722	0.721	0.725	0.638	0.638	0.639
RLH	0.666	0.666	0.626	0.745	0.724	0.647
708	0.142	0.147	0.147	0.678	0.641	0.697

However, over all data types the 708/(560+664) ratio algorithm appears to be the most robust. Only weak correlations exist with ISS, with the 708/(559+664) ratio algorithm also producing the best overall results (r^2 = 0.483). OSS was best estimated using MERIS TOA data with the 708/664 algorithm (r^2 = 0.764). The 708/(559+664) and RLH algorithms also produced significant correlations with OSS across different data types, while the 708 band algorithm gave significant correlations only with atmospherically corrected data.

5.3.4.3 Secchi Disk Depth Algorithms

The best correlation with SD depth, a proxy for gross particle load, is given with the RLH algorithm and COST model atmospherically corrected reflectance (r^2 = 0.822) (Table 5.15).

Table 5.15 r^2 correlation coefficients for best performing algorithms for Secchi Disk depth. Significant correlations (p<0.05) are in red. N = 9.

Variables	Data type					
	Raw	**Smile corrected**	**Apparent reflectance**	**DOS**	**COST**	**6S**
RLH	0.624	0.624	0.600	0.805	**0.822**	0.756
(708/664)	0.801	0.801	0.801	0.025	0.025	0.685
(509/708)	0.686	0.687	0.687	0.052	0.052	0.556
(509-864)/(708-864)	0.782	0.783	0.681	-	-	-
708	0.053	0.056	0.056	0.690	0.693	0.697

The RLH variable performed strongly over all data types and appears to be the most robust SD estimator. The 708/664 algorithm gave the next most significant correlation with TOA data (r^2 = 0.801). The 509/708 ratio algorithm also gave good correlations (besides for DOS and COST reflectance), and through subtracting the 864 nm band from TOA data, a rough atmospheric correction, the correlation was further improved. The 708 nm single band algorithm also gave significant correlations with atmospherically corrected data types.

5.3.4.4 a_{CDOM} Algorithms

The very small signal from Zeekoevlei in the blue, together with the small variability in a_{CDOM}, means that there is less expectation for a_{CDOM} algorithms to perform well, as confirmed by the results (Table 5.16).

Table 5.16 r^2 correlation coefficients for best performing algorithms for a_{CDOM}. Significant correlations (p<0.05) are in red. N = 9.

Variables	Data type					
	Raw	**Smile corrected**	**Apparent reflectance**	**DOS**	**COST**	**6S**
(559-619)/619	0.363	0.372	0.372	0.033	0.033	0.204
Gitelson et al.*	0.336	0.398	**0.751**	0.144	0.134	0.630
412	0.614	0.610	0.610	0.466	0.442	0.249
442	0.611	0.618	0.618	0.140	0.129	0.289
*(442-(708/664)-509)/(442+(708/664)+509)						

The best correlations for a_{CDOM} are produced with Gitelson et al.'s (1993) band ratio algorithm. a_{CDOM} is also strongly correlated with TOA bands at 412 and 442 nm despite the large influence by atmospheric scattering at these wavelengths (See Figure 5.20). The 412 nm band algorithm gives the best overall performance between all data types.

5.3.5 Mapping Water Quality Parameters using Empirical Algorithms

Empirical algorithms were used to make water quality maps from the four cloud-free MERIS acquisitions. The shapes of the maps differ because the number of pixels varies between 15 and 20, and some duplicated pixels were removed. The longitude and latitude of the pixels were not geo-corrected and were taken from the MERIS scenes. The area of the maps is between 1.1 ha and 1.5 ha at the 260×290 m MERIS pixel resolution, well below the 2.6 ha total surface area of the lake. Thus the pixels used in mapping are from the central 'core' area of the lake, reducing the chance of erroneous 'land' pixels being included in the maps, and decreasing the magnitude of the adjacency effects, which is greatest for pixels directly in contact with the shoreline. The final empirical algorithms made use of the TOA 'apparent reflectance' data type (Table 5.17, Figure 5.21).

Table 5.17 Empirical algorithms used for mapping water quality parameters from MERIS TOA apparent reflectance.

Y	X	r^2	t	p	F	RMSE	Regression Equation	N
Chl *a*	(708/664)	0.964	-	0.0000	563.3	9.8%	$Y = 5.931X^{5.934}$	9
TSS	708/(559+664)	0.760	4.7	0.0022	22.2	14.1%	$Y = -84.428 + 218.329X$	9
ISS	(559-509)/(559+509)	0.437	-2.3	0.0524	5.4	56.9%	$Y = 30.600 - 479.079X$	9
OSS	(708/664)	0.763	4.7	0.0021	22.5	10.9%	$Y = -37.411 + 41.934X$	9
SD	(708/664)	0.801	-5.3	0.0011	28.2	8.0%	$Y = 79.469 - 30.596X$	9
a_{CDOM}	Gitelson et al.*	0.751	-4.6	0.0025	21.1	13%	$Y = -25.137 - 31.806X$	9
*(442-(708/664)-509)/(442+(708/664)+509)								

The r^2 values indicate that for all variables, except ISS, more than 75% of the variation in the water quality parameters can be explained. The RMSE is less than 15% for all variables except ISS. The critical value of the t-statistic and the F-values (Equation 4.18) at a 95% confidence limit is exceeded by all variables (except ISS), indicating again that the variance is well explained. Therefore it can be concluded the algorithms with independent variables X, can be used to reliably estimate all the water quality parameters, Y, except for ISS. The environmental conditions recorded during the MERIS acquisition are used to explain the distribution and concentrations of the water constituents (Table 5.18), and statistical analysis gives an estimation of the accuracy of the maps.

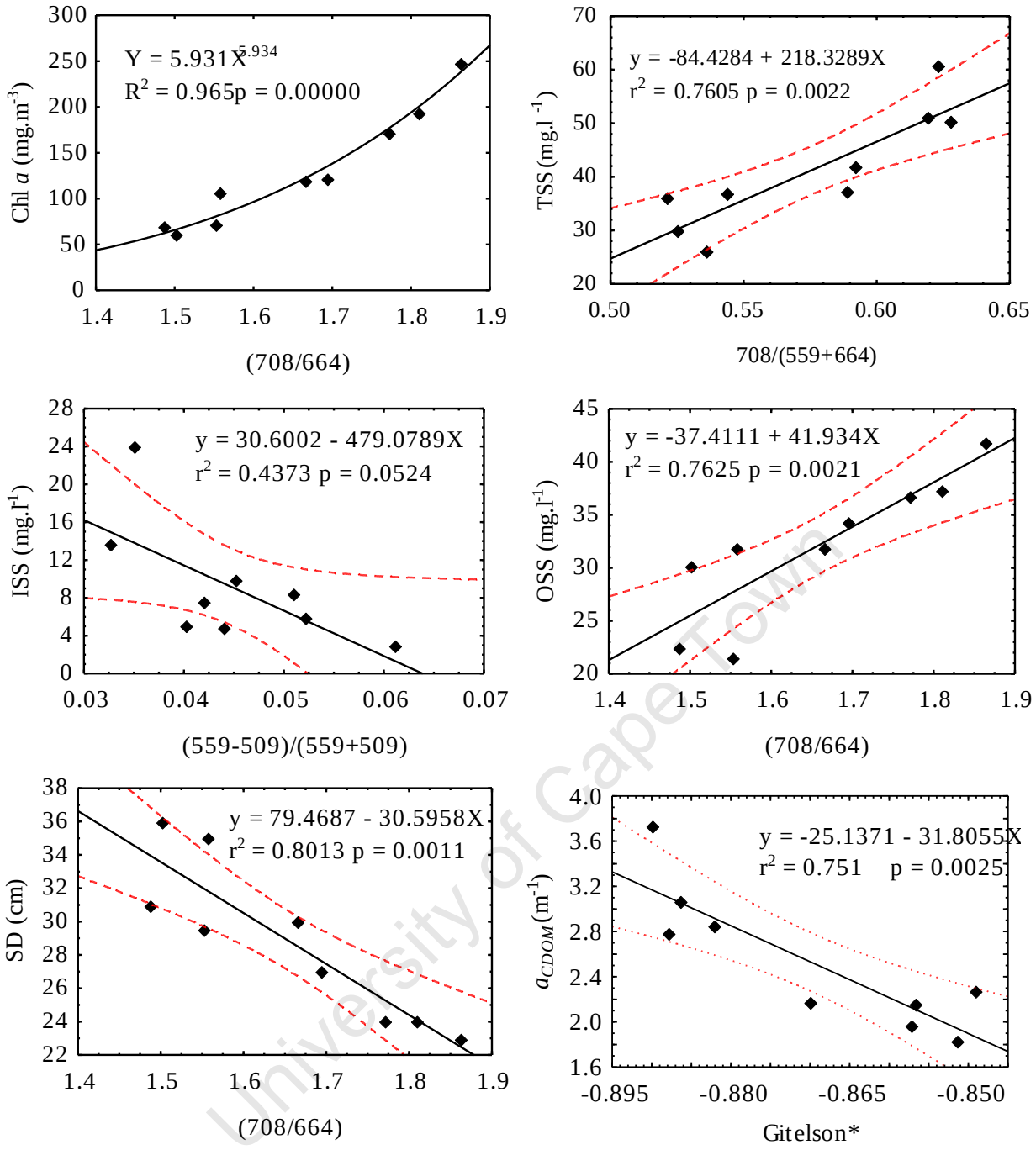

Figure 5.21 Scatterplots of empirical algorithms used for estimating water quality parameters from TAO MERIS apparent reflectance. The 95% confidence intervals are shown by the dotted red lines.

Table 5.18 Average environmental conditions for Zeekoevlei on four days in April 2008.

Date	Sample Sites	Sky conditions	Wind speed/ direction		Wave height	Water Temp.	Water conditions
1st	1 – 4	Clear.	0 m.s^{-1}	-	0 cm	21.5° C	Bright green with surface bloom.
7th	2 – 3	Partly cloudy.	7 m.s^{-1}	S	3 cm	19.8° C	Medium green.
20th	2 – 3	Clear. High cirrus.	19 m.s^{-1}	SE	9 cm	18.6° C	Dark green.
23rd	Pier	Clear.	5 m.s^{-1}	SW	0 cm	20.1° C	Bright green with surface bloom.

5.3.5.1 Chl *a* Maps

There is appreciable variation in both the magnitude and the spatial distribution of Chl *a* in Zeekoevlei across the four days in April (Figure 5.22).

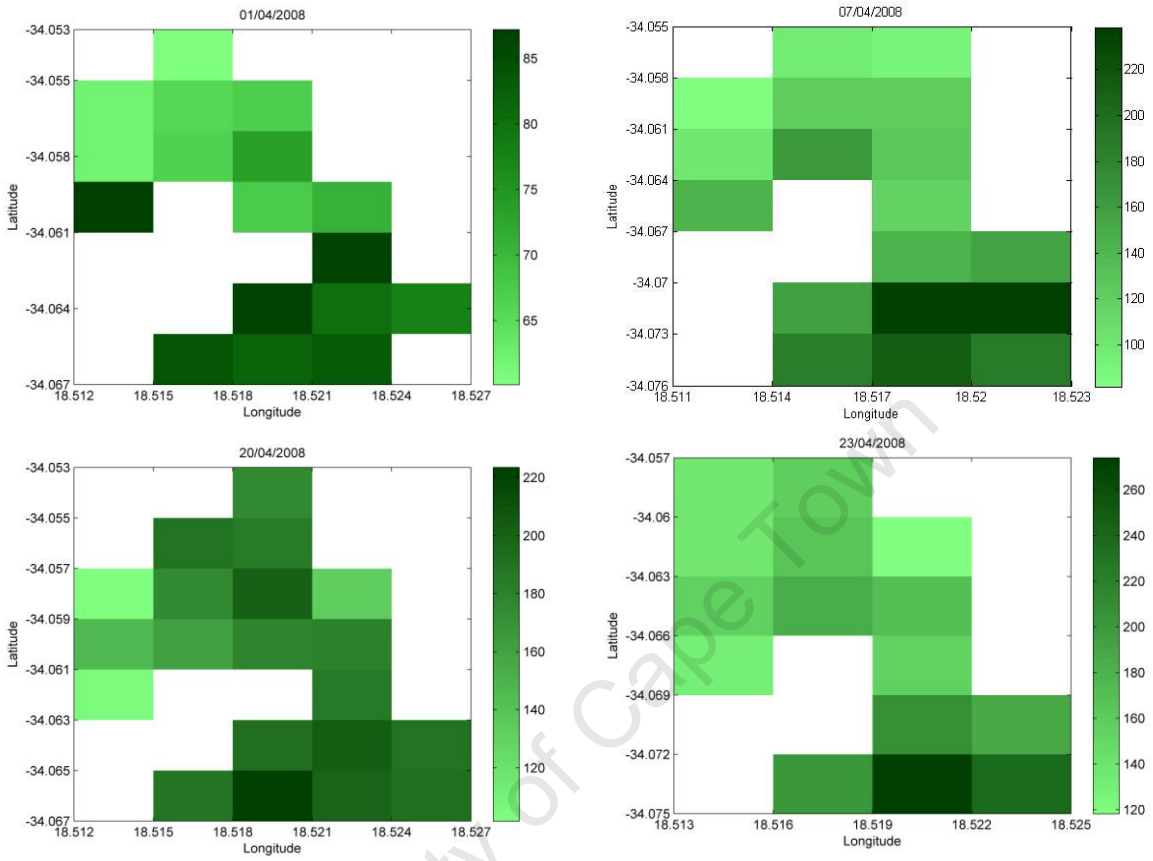

Figure 5.22 Chl *a* distribution maps for Zeekoevlei on four dates in April generated using empirical algorithm with MERIS. Units are in mg.m^{-3}. Note differences in colour bar scales.

The highest concentrations of Chl *a* appear in the southern basin on all days, which is in agreement with *in situ* measurements (See Section 5.1.2). As previously explained, this may be attributed to nutrient input from the adjacent WWTW that maintains the high levels of phytoplankton production. Chl *a* concentration in the northern basin and in Home Bay appears to show greater variation, revealing an alternating pattern of higher/lower concentrations over the four days. The unusually very calm conditions experienced on the morning of April 1st, coincided with Chl *a* concentrations that were notably lower than observed on the other days (maximum of only 87.2 mg.m^{-3}) (See Table 5.19). It appears that the windless and waveless conditions caused decreased mixing of nutrient-rich bottom sediments and phytoplankton cells into the euphotic zone, leading to less turbid conditions and reduced overall phytoplankton density in the surface water layer, despite the fact that some cyanobacteria were observed collecting on the water surface (Table 5.18). Conversely, the highest concentrations in the northern basin, and for the lake as a whole (mean = 175.5 mg.m^{-3}), appeared on April 20th (bottom left map in Figure 5.22),

the day on which there was a strong southerly wind (Table 5.18). The windier conditions seem to have elevated the Chl *a* concentrations owing to increased water column overturn. Therefore, it appears that that the algal biomass in the northern basin is more responsive to environmental conditions, such as wind and waves, than that in the southern basin.

Table 5.19 Statistics for MERIS Chl a maps.

		Image date			
	Units	**1-Apr**	**7-Apr**	**20-Apr**	**23-Apr**
No. pixels		17	18	20	15
Area	m^2	1281800	1357200	1508000	1131000
Min.	$mg.m^{-3}$	60.1	81.8	101.6	118.2
Max.	$mg.m^{-3}$	87.2	238.4	223.5	274.0
Range	$mg.m^{-3}$	27.2	156.6	122.0	155.8
St. Dev.	$mg.m^{-3}$	9.6	47.8	31.7	42.5
Median	$mg.m^{-3}$	73.4	144.8	185.3	165.4
Mean (MERIS)	$mg.m^{-3}$	74.3	149.5	175.5	175.2
SE mean (MERIS)	$mg.m^{-3}$	5.1 (6.9%)	3.5 (2.3%)	4.6 (2.6%)	4.8 (2.7%)
CI (95%) -	$mg.m^{-3}$	63.5	142.1	165.9	164.9
CI (95%) +	$mg.m^{-3}$	85.1	156.9	185.1	185.5
Mean (Obs.)	$mg.m^{-3}$	77.3	183.5	183.1	122.6
SE mean (Obs.)	$mg.m^{-3}$	14.6 (19.7%)	76.0 (50.8%)	13.7 (7.8%)	-
CI (95%) -	$mg.m^{-3}$	30.9	-782.5	9.4	-
CI (95%) +	$mg.m^{-3}$	123.7	1149.5	357.6	-
Observed error	$mg.m^{-3}$	3.0 (4.0%)	33.9 (22.7%)	7.6 (4.3%)	-52.6 (-30%)

The standard error of the mean remote sensing estimates, calculated using Equation 4.21, ranged between 2.3% and 6.9%, which is smaller than the standard error for *in situ* measurements, calculated using Equation 4.19 (Table 5.19). Therefore mean estimates of the Chl *a* concentration made from MERIS maps have improved confidence limits than mean estimates made from a small number of sample sites. The observed error between remotely sensed and *in situ* measurements is as large as negative 30%. Therefore, assuming that the true mean for Zeekoevlei is the MERIS estimate, estimates of the mean Chl *a* concentration using *in situ* measurements alone may be anywhere between 4% and 30% wrong. However, the accuracy of *in situ* measurements may be improved by using multiple sample sites (compare April 1st, four *in situ* measurements, with April 23rd, only one).

5.3.5.2 Suspended Solids Maps

The maps for TSS are similar to those for Chl *a*, although there are clear differences in the concentration distributions (positions and shading of pixels) (Figure 5.23).TSS concentration is generally higher in the southern basin, and the lowest concentrations are near the inlet of the Great Lotus River in the northern basin. This is expected as TSS is largely composed of organic matter (mean of 76.9%) and the Chl *a* maps also display this feature. The divergence between the

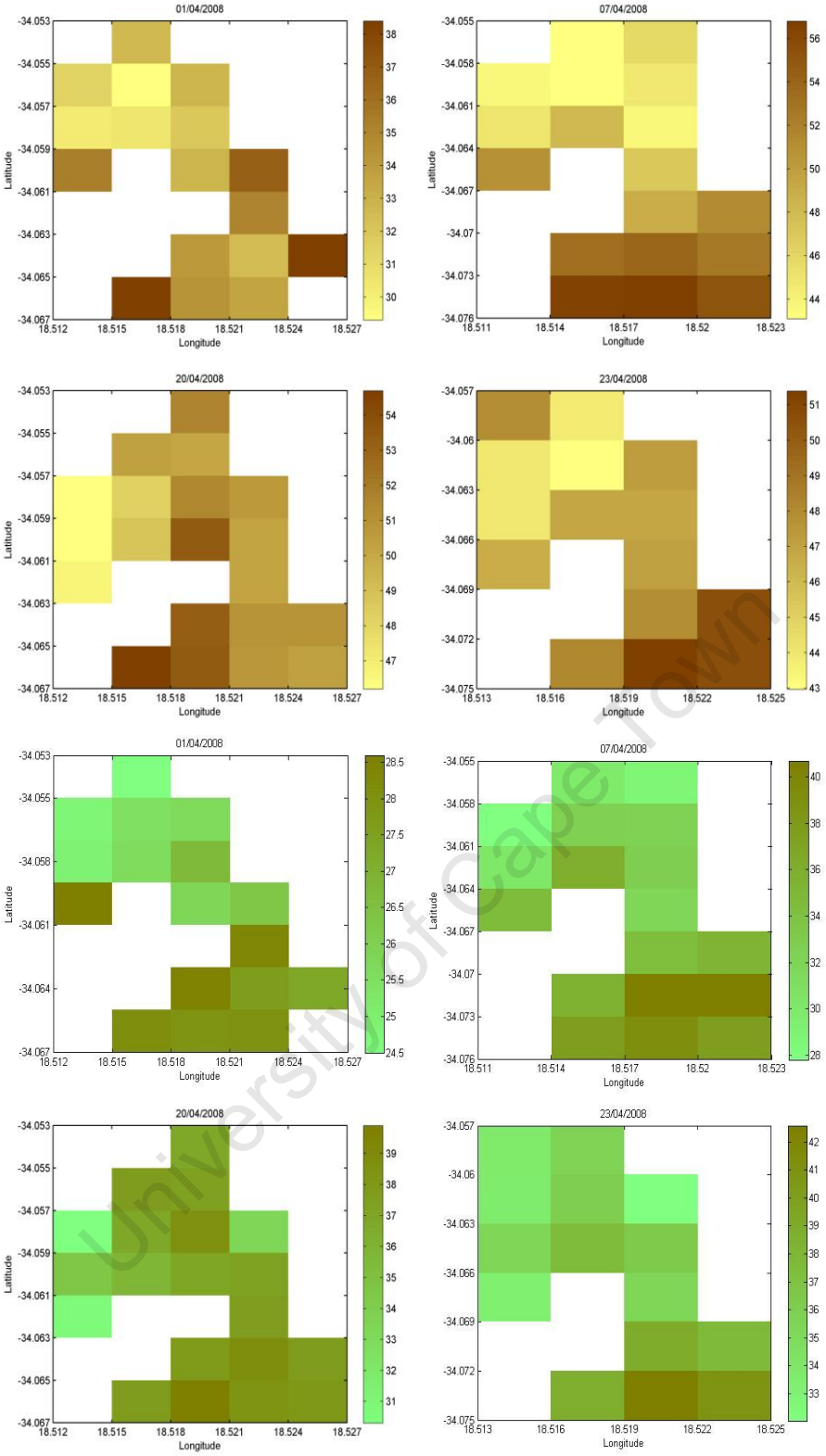

Figure 5.23 Total Suspended Solids (top) and Organic Suspended Solids (bottom) distribution maps for Zeekoevlei on four dates in April generated using empirical algorithms with MERIS. Units are in mg.l^{-1}. Note differences in colour bar scales.

Chl *a* and TSS maps may be explained by the inorganic component (ISS maps were not plotted because correlations were not significant). OSS maps are nearly identical to those for Chl *a*, with the position and shading of pixels corresponding almost exactly. Since both algorithms make use of the 708/664 ratio they vary proportionately with one another. However, the similarity is not

unexpected, since *in situ* measurements of organic matter were well correlated with Chl *a* (r = 0.79). In agreement with the Chl *a* maps, the suspended solids concentrations were lower on April 1st than on the other days.

The inference that there is decreased re-suspension of bottom sediments because of an absence of wind is confirmed by the suppressed TSS concentrations (maximum of 38.4 mg.ℓ^{-1}). The higher concentrations of OSS and TSS observed on the other days, show that even a gentle breeze is sufficient to begin mixing the water column, leading to increased concentrations of suspended solids. The proposal that an absence of mixing leads to decreased overall phytoplankton density at the surface, is also supported by the observation of lower OSS concentrations on April 1st. In calm conditions, non-buoyant algal cells sink down in the water column, leading to decreased Chl *a* and OSS concentrations. As organic solids, composed of detritus and Chl *a* containing phytoplankton cells, are mixed into the water column, the concentration of Chl *a* increases.

Table 5.20 Statistics for MERIS Total Suspended Solids (TSS) and Organic Suspended Solids (OSS) maps.

	TSS (mg.l^{-1})				OSS (mg.l^{-1})			
	1-Apr	**7-Apr**	**20-Apr**	**23-Apr**	**1-Apr**	**7-Apr**	**20-Apr**	**23-Apr**
Mean (MERIS)	33.5 ± 2.2	49.1 ± 2.2	50.4 ± 2.4	47.1 ± 2.0	26.7 ± 1.4	34.3 ± 1.0	36.6 ± 1.3	36.5 ± 1.3
SE (MERIS) (%)	6.4	4.4	4.7	4.2	5.3	2.8	3.4	3.6
St. Dev.	2.6	4.8	2.3	2.6	1.4	3.9	2.5	2.9
Min.	29.3	43.1	46.2	43.0	24.5	27.8	30.3	32.0
Max.	38.4	56.8	54.7	51.4	28.6	40.7	39.9	42.6
Mean (Obs.)	32.3 ± 1.8	46.1 ± 5.1	55.9 ± 5.8	37.3	26.5 ± 2.2	36.8 ± 2.9	37 ± 0.2	34.3
SE (Obs.) (%)	5.4	10.4	11.5	-	8.2	8.4	0.5	-
Observed error (%)	-3.7	-6.2	10.7	-20.8	-0.8	7.2	1.1	-6.1

The SE of the mean TSS and OSS estimate is improved for MERIS measurements (Table 5.20). The observed error shows that mean TSS estimates based on one *in situ* sample point may be up to 20% incorrect. For OSS there is only a small improvement in the accuracy of mean estimates through using MERIS.

5.3.5.3 Secchi Disk Depth and a_{CDOM} Maps

Secchi Disk depth (SD) (Figure 5.24) displays a spatial variability identical to that of Chl *a* and OSS, as might be expected since the SD algorithm uses the 708/664 ratio. The shading is the reverse of the Chl *a* and OSS maps, where dark blue represents greater depths of light penetration. Thus, the general pattern of SD shows that the depth of light penetration is greater in the northern basin than in the southern basin. This is mainly due to greater algal density in the

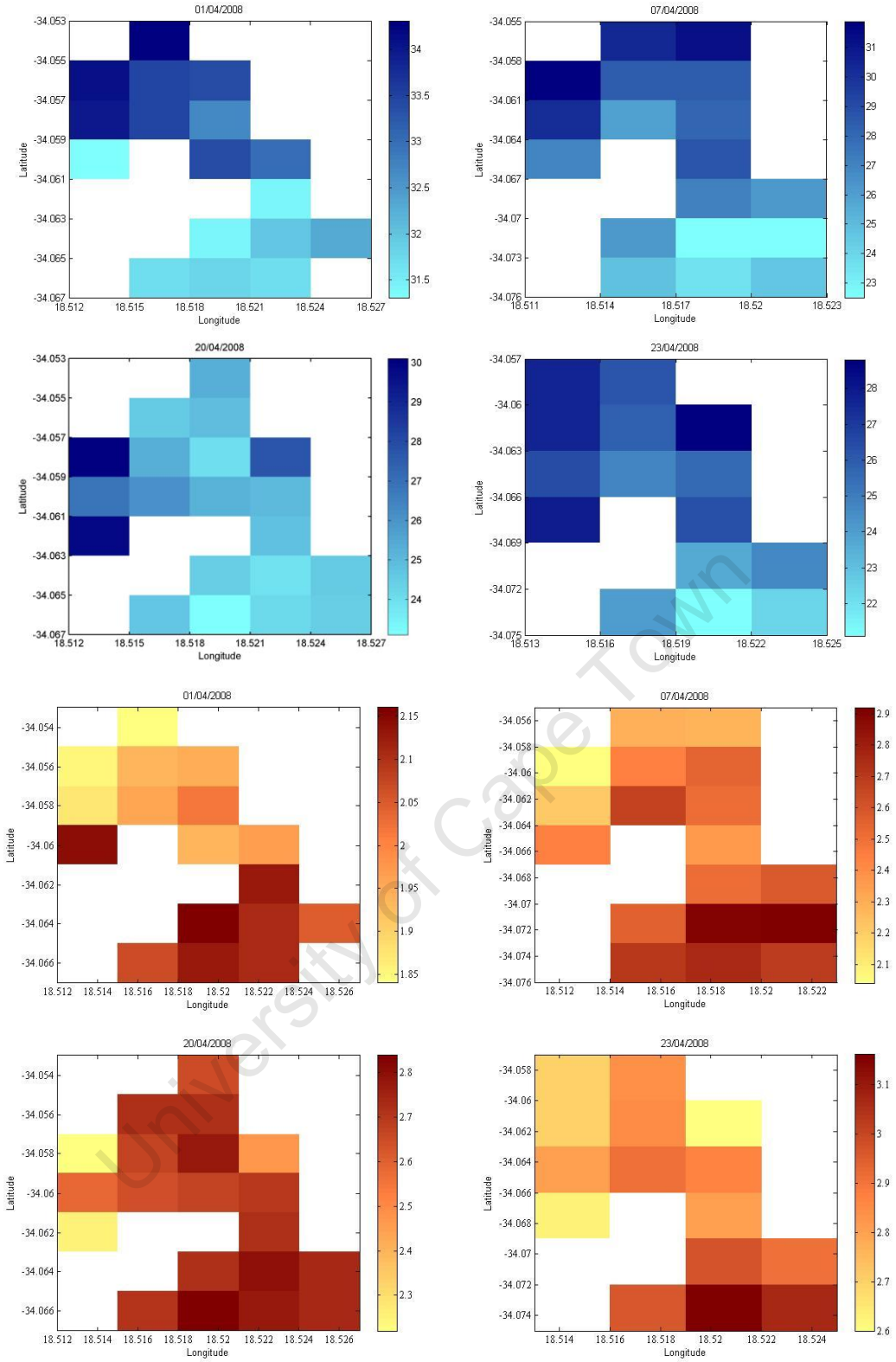

Figure 5.24 Secchi Disk depth (top) and a_{CDOM} (bottom) distribution maps for Zeekoevlei on four dates in April generated using empirical algorithms with MERIS. Units are in cm and m^{-1}, respectively. Note differences in colour bar scales.

southern basin, as shown in the Chl *a* and OSS maps. Secchi disk depth was greatest on April 1st (mean of 32.7±0.9 cm) in agreement with lower concentrations of Chl *a* and suspended solids. The a_{CDOM} maps show spatial patterns practically identical to OSS and Chl *a*, probably because of the inclusion of the 708/664 ratio in Gitelson et al.'s algorithm (Figure 5.20). a_{CDOM} tends to

have the highest concentration in the southern basin, which is in accord with the other parameters (See also Table 5.2) and an irregular spatial distribution in the northern basin. The covariance between *a*CDOM and many of the other parameters makes it very difficult to separate the signals from one another.

The SE of mean Secchi Disk depth estimates is typically smaller for MERIS than that for *in situ* measurements alone (Table 5.21). However, the observed error is small, showing that remotely sensed observations do not result in great improvements in SD estimates for Zeekoevlei. This is because the the variation in SD is small, within a range of less than 10cm. The accuracy of mean a_{CDOM} retrieval improves slightly with MERIS estimations, except on April 20th. The maximum MERIS a_{CDOM} estimate is below the mean observed value on April 20th, showing that the ability of the algorithm for estimating higher a_{CDOM} values may be limited.

Table 5.21 Statistics for MERIS SD depth and a_{CDOM} maps

	Secchi Disk depth (cm)				**a_{CDOM} (m^{-1})**			
	1-Apr	**7-Apr**	**20-Apr**	**23-Apr**	**1-Apr**	**7-Apr**	**20-Apr**	**23-Apr**
Mean (RS)	32.7 ± 0.9	27.1 ± 0.6	25.5 ± 0.8	25.5 ± 0.9	2.02 ± 0.14	2.52 ± 0.09	2.66 ± 0.11	2.85 ± 0.16
SE (RS) (%)	2.8	2.3	3.2	3.4	7.06	3.47	4.00	5.56
St. Dev.	1.0	2.8	1.9	2.1	0.11	0.23	0.16	0.16
Min.	31.3	22.5	23.9	21.1	1.84	2.04	2.22	2.60
Max.	34.3	31.9	30.1	28.8	2.16	2.92	2.84	3.16
Mean (Obs)	32.9 ± 1.5	26.5 ± 4.2	24 ± 0.0	27.0	2.06 ± 0.13	2.51 ± 0.13	3.4 ± 0.40	2.78
SE (Obs.) (%)	4.6	15.5	0.0	-	6.45	6.45	16.06	-
Observed error (%)	0.6	-2.3	-5.7	5.8	2.07	-0.46	28.06	-2.44

5.4 Water Quality Estimation from Landsat 7 ETM+

5.4.1 Data Acquisition

A cloud-free Landsat 7 ETM+ SLC-off scene was acquired just a few days after the fieldwork, on May 2nd 2008. Zeekoevlei is present in the centre of the scene and is not apparently affected by the SLC failure, visible as red stripes on the left hand side of the image (Figure 5.25).

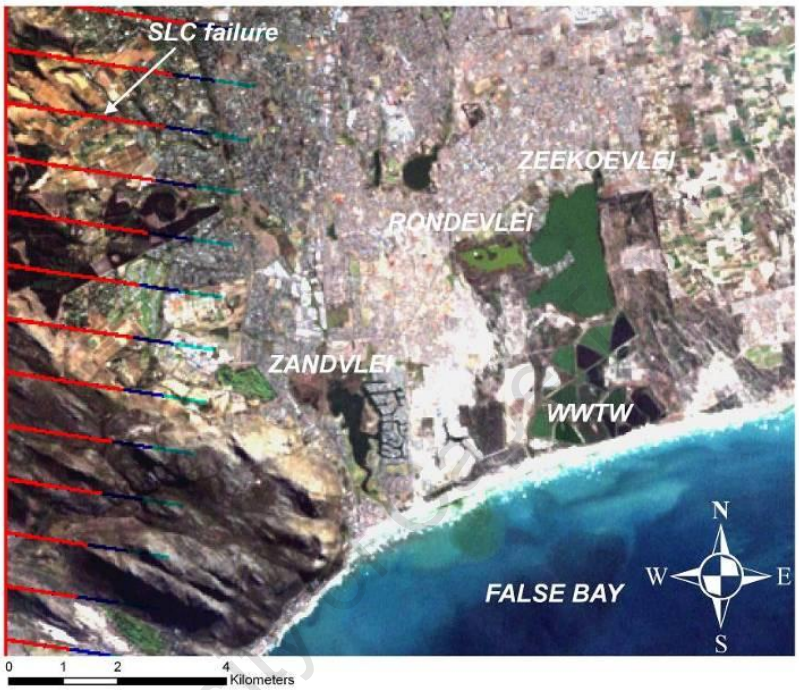

Figure 5.25 RGB composite of the first three Landsat 7 ETM+ bands for May 2nd 2008 showing Zeekoevlei, adjacent Lakes and Waste Water Treatment Works (WWTW).

5.4.2 Landsat 7 Simulation

TSRB ρ_w data were re-sampled to the first 3 spectral bands of the Landsat 7 ETM+ sensor (Figure 5.26).

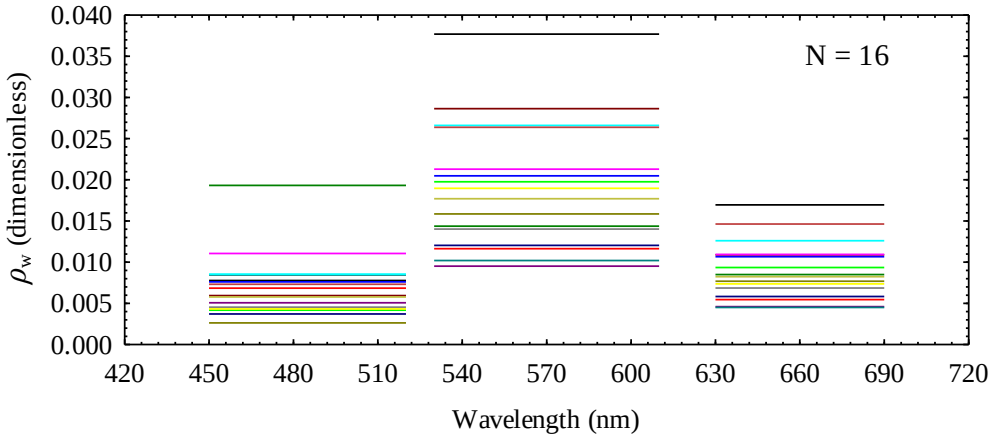

Figure 5.26 TSRB ρ_w re-sampled to the bandwidths of the first three Landsat 7 ETM+ sensor bands.

There is an appreciable variation in magnitude of the spectra and between the three Landsat bands. Band 2 shows the greatest magnitude as it corresponds to the reflectance peak near 560 nm (See Figure 5.5). The small reflectance values in bands 1 and 3 correspond to absorption by CDOM and Chl *a*, respectively.

5.4.3 Atmospheric Correction

The shadow pixel from the mountainous region north-east of Cape Town used to estimate L_{path} in each spectral band and the values for E_0, d, and θ_s, used in Equation 4.25, are shown in Table 5.22 (NASA, 2008).

Table 5.22 Input parameters used in the Landsat 7 DOS atmospheric correction.

	Units	**Band 1**	**Band 2**	**Band 3**
$L_{\lambda path}$	($Wm^2\mu m^{-1}sr^{-1}$)	28.065	15.967	9.92
E_o	($Wm^2\mu m^{-1}$)	1969	1840	1551
d	AU	1.008	1.008	1.008
θ_s	(Radians)	0.5249	0.5249	0.5249

The mean, minimum and maximum reflectance values for DOS corrected pixels over Zeekoevlei were compared to the simulated reflectance values measured *in situ* with the TSRB (Table 5.23).

Table 5.23 Comparison between real and simulated Landsat ETM+ ρ_w.

Data	Landsat 7ETM+			Simulated TSRB		
Band	Band 1	Band 2	Band 3	Band 1	Band 2	Band 3
Mean	0.013	0.023	0.013	0.007	0.019	0.009
Minimum	0.007	0.018	0.007	0.003	0.010	0.005
Maximum	0.019	0.029	0.019	0.019	0.038	0.017

The real Landsat water-leaving reflectance spectra, derived using the DOS atmospheric correction, are within the range of the simulated spectra. Therefore it appears that the DOS correction procedure produces acceptable reflectance values.

5.4.4 Regression Analysis with Water Quality Parameters

The regression analysis with simulated Landsat 7 ETM+ bands produced strong correlations with water quality parameters (Table 5.24). Chl *a* is best estimated using the b2-b1 variable (r^2 = 0.826), while TSS and ISS is best estimated with the b2-b3 variable (r^2 = 0.840 and 0.704, respectively). OSS was estimated most accurately with the logarithm of the b2-b3 variable (r^2 = 0.911). Secchi Disk depth was strongly correlated with the Ln(b3)/Ln(b2) variable (r^2 = 0.727). The best results for a_{CDOM} was achieved with the b3/b1 variable (r^2 = 0.569). Thus, the water quality parameters can be estimated well using simple linear regression equations and simulated Landsat 7 reflectance. However, the substantial covariance between the parameters, and the

existence of non-unique signals, means that in most instances the algorithms detect changes in the gross particulate loading, such that the algorithms ability to distinguish between the different parameters is somewhat limited.

Table 5.24 r^2 correlation coefficients for water quality parameters from regressions with simulated Landsat reflectance. Significant correlations ($p<0.05$) are in red. Strongest correlations are in bold. N=16.

Variable	Chl *a*	Ln TSS	Ln ISS	Ln OSS	SD	Ln a_{CDOM}
b3/b1	0.531	0.176	0.072	0.314	0.287	**0.569**
b2-b1	**0.826**	0.601	0.437	0.750	0.619	0.218
b2-b3	0.679	**0.840**	**0.704**	0.859	0.656	0.106
Ln(b2-b3)	0.633	0.818	0.601	**0.911**	0.590	0.112
Ln(b3)/Ln(b2)	0.770	0.562	0.432	0.544	**0.727**	0.060

5.4.5 Mapping Water Quality Parameters using Empirical Algorithms

The most statistically significant empirical algorithms from the regressions were used for mapping water quality parameters (Table 5.25). All algorithms passed the test for significance using the p and F-values at the 95% confidence interval. The greatest RMSE was 19.1% for ISS and was smaller than 12.6% for all other parameters.

Table 5.25 Empirical algorithms for estimating water quality parameters using simulated Landsat 7 ETM+ reflectance.

Y	X	r^2	p	F	RMSE	N	Regression Equation
Chl a	b2-b1	0.826	0.00000	66.3	12.6%	16	$Y = 211.02 - 4809.35X$
Ln TSS	b2-b3	0.840	0.00000	73.3	2.6%	16	$Y = 4.399 - 49.434X$
Ln ISS	b2-b3	0.704	0.00005	33.3	19.1%	16	$Y = 3.786 - 146.840X$
Ln OSS	Ln(b2-b3)	0.911	0.00000	143.7	1.3%	16	$Y = 1.987 - 0.352X$
Ln a_{CDOM}	b3/b1	0.569	0.00073	18.5	9.9%	16	$Y = 1.279 - 0.171X$
SD	Ln(b3)/Ln(b2)	0.727	0.00003	37.2	9.6%	16	$Y = -106.181 + 113.050X$

The empirical algorithms were applied to the atmospherically corrected Landsat 7 ETM+ scene. The maps produced realistic values for all of the water quality parameters owing to the robustness of the empirical algorithms, although no simultaneous *in situ* data were available for validation (See Figure 5.27). The 30×30 m resolution gave a total of 2662 pixels covering the lake (2.4 ha), thus the higher resolution affords that the spatial distribution of the water constituents are visible in much greater detail when compared to the MERIS maps (Section 5.3.5). The distribution of Chl *a* is patchy, with a mean concentration of 163.0±1.8 $mg.m^{-3}$ (Table 5.26). The map does not reveal well however the higher Chl *a* concentrations in the southern basin visible from MERIS. The standard error of the mean estimate is only 1.1%, showing that the large number of Landsat pixels leads to better confidence intervals (compare Table 5.19). The noticeable elevation of Chl *a*

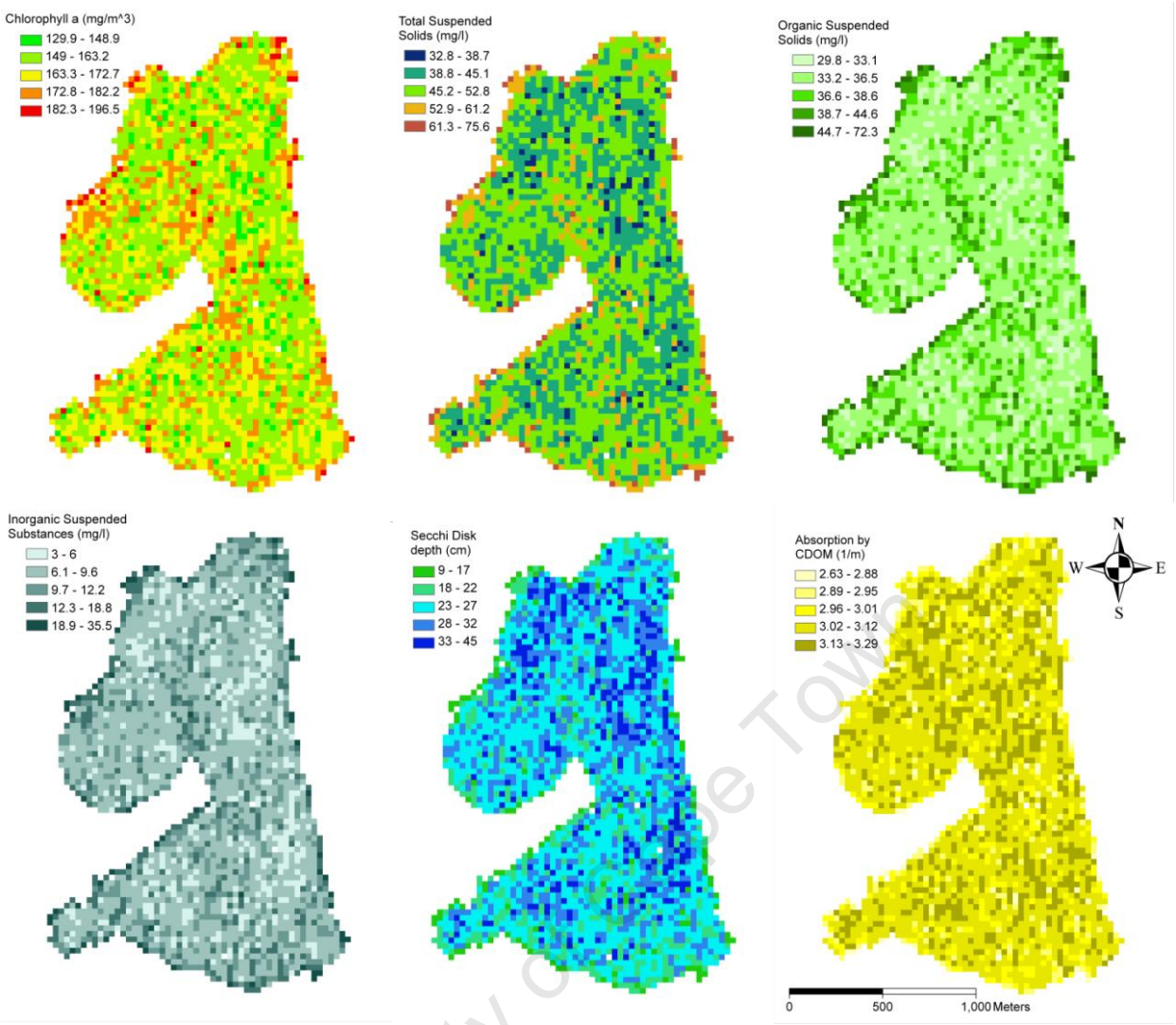

Figure 5.27 Water quality parameter maps generated using simulated empirical algorithms for a Landsat 7 ETM+ scene on the 2nd May 2008

concentration (red pixels) in a patch just north of the peninsula and in the north of Home Bay, correspond to small islands (See Figure 4.1), and to reeds. In the central and north eastern regions of the southern basin there are also patchy areas of higher concentrations which may indicate areas of increased algal bloom activity occurring on this day. Many pixels adjacent to the shoreline also display high values (also clearly visible in the maps for other water quality

Table 5.26 Statistics for water quality parameter maps derived from Landsat ETM+

	Chl *a*	**TSS**	**ISS**	**OSS**	**SD**	**a_{CDOM}**
Units	$mg.m^{-3}$	$mg.l^{-1}$	$mg.l^{-1}$	$mg.l^{-1}$	cm	m^{-1}
N	2662	2662	2662	2662	2662	2662
Area (m^2)	2395800	2395800	2395800	2395800	2395800	2395800
Min.	129.9	32.8	3.0	29.8	9.2	2.63
Max.	196.2	75.5	35.4	72.2	45.2	3.29
Mean	163.0 ± 1.8	54.2 ± 1.0	19.2 ± 1.0	51.0 ± 1.0	25.7 ± 0.4	2.96 ± 1.02
SE Mean (%)	1.1	1.9	5.3	2.0	1.4	34.5
St. Dev.	19.3	12.4	9.4	12.3	4.9	0.19

parameters), which are most likely the result of the adjacency effect where water pixels have become contaminated by land pixels and/or reeds, leading to higher reflectance values. Therefore pixels adjacent to the shoreline were treated with special caution and excluded from further analysis.

The maps for TSS, OSS and ISS show a spatial variability similar to the Chl *a* map. The middle and southern parts of the southern basin clearly display patches of increased TSS concentrations. The a_{CDOM} map shows a spatial pattern uncorrelated with other parameters, in that there appears to be an almost even distribution of high and low absorption across the lake. The adjacency effect appears in the map as low values (light yellow) in pixels adjacent to the shoreline. The large error associated with the mean a_{CDOM} estimate (34.5%), is the result of the empirical algorithm that has a r^2 value of only 0.569. The Secchi Disk depth map reveals a clear pattern of increased depths of light penetration (dark blue) in large parts of the northern basin and in small areas the north-eastern and western regions of the southern basin. The SD map is a useful tool which functions as an overall index of the gross particle load. Areas of decreased light penetration (green) agree with the areas identified in the other maps, but is pronounced along the southern shoreline, adjacent to the WWTW. It can be determined on the basis of the SD map that the northern basin showed slightly improved water quality conditions on May 2nd than Home Bay and the southern basin, in agreement with the MERIS maps for April. The standard errors of the means from Landsat are smaller than those for MERIS, because of the large number of pixels (See Tables in Section 5.3.5).

5.4.6 Variability of the Distribution of Water Quality Parameters

In order to better quantify the spatial variation in the water quality parameters, the maps were divided into the 3 regions: Home Bay; the northern basin; and the southern basin (See Figure 4.1). Pixels adjacent to the shoreline were removed in order to avoid the adjacency effect. The mean, minimum, maximum, and standard deviation of the parameters were determined for each region in order to compare the water quality conditions (Table 5.27).

Mean concentrations of Chl *a*, TSS, OSS and ISS are greater in Home Bay and in the southern basin than in the northern basin. Water clarity is better in the northern basin in agreement with the dark areas visible on the SD map and the MERIS maps. a_{CDOM} is almost invariable between the 3 regions. Therefore, although the 3 regions display very similar water quality characteristics, on this occasion the northern basin may be said to show slightly improved water quality conditions.

Table 5.27 Spatial variability of water quality parameters between 3 regions for Zeekoevlei from Landsat 7ETM+ maps.						
	Chl *a*	**TSS**	**ISS**	**OSS**	**SD**	**a_{CDOM}**
Units	$mg.m^{-3}$	$mg.\ell^{-1}$	$mg.\ell^{-1}$	$mg.\ell^{-1}$	cm	m^{-1}
Home Bay						
No.	399	399	399	399	399	399
Mean	162.9	47.7	9.2	36.1	26.2	3.06
Min.	136.2	32.8	3.0	29.8	16.1	2.81
Max.	188.8	60.8	18.5	44.4	42.6	3.27
St. Dev.	9.3	4.4	2.6	2.3	4.0	0.08
Northern basin						
No.	805	805	805	805	805	805
Mean	160.6	46.7	8.7	35.6	27.4	3.06
Min.	129.9	35.3	3.7	30.7	14.7	2.63
Max.	188.8	65.8	23.4	49.6	42.6	3.29
St. Dev.	9.8	4.6	2.6	2.4	4.5	0.09
Southern basin						
No.	925	925	925	925	925	925
Mean	161.8	47.3	9.1	35.9	25.9	3.06
Min.	136.2	33.0	3.0	29.9	13.8	2.77
Max.	188.1	64.6	22.2	48.2	45.2	3.26
St. Dev.	9.1	4.7	2.8	2.5	4.2	0.08

A north-south and east-west transect of Chl *a* reveals more clearly the patchy distribution of the phytoplankton biomass (Figure 5.28)

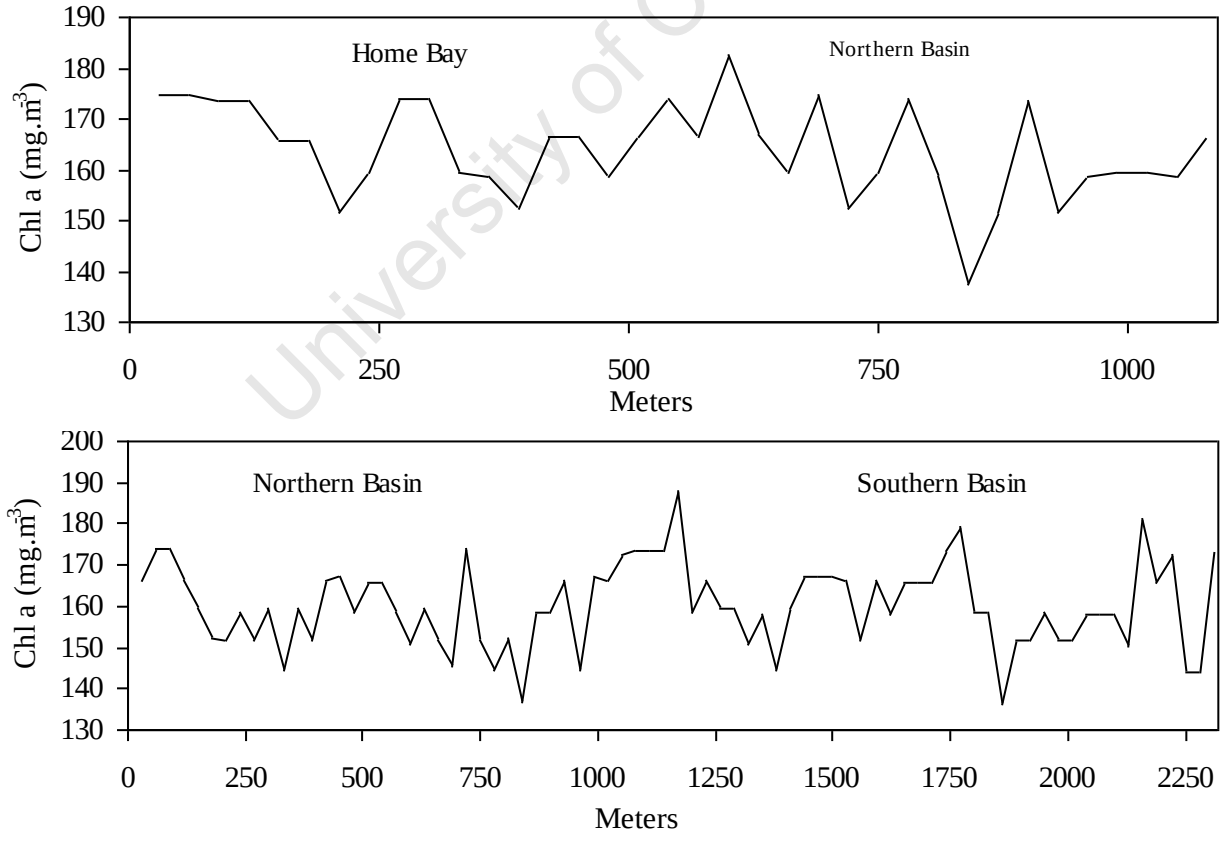

Figure 5.28 North-south (top) and east-west (bottom) transects of Chl *a* maps derived from Landsat.

The transects run north-south down the length of the lake (>2000 m) through the northern and southern basin, and east-west through Home Bay and the northern basin (~1000 m). The irregular spatial distribution of the phytoplankton biomass across the lake is emphasised, with the Chl *a* concentration varying inside a moderate range of 50 $mg.m^{-3}$. Some caution is required when interpreting the shapes of the transects as the data appears quite noisy. However, it can be determined that the algal blooms in Zeekoevlei tend to exist as patches distributed irregularly across the lake surface. The obvious peak in the middle of the east-west transect corresponds to pixels near the island just north of the peninsula. The northern basin appears to have peaks that are smaller than those for the southern basin and Home Bay. The far right and far left of the east-west transect shows clearly that Home Bay has elevated concentrations compared to the northern basin.

Chapter 6 Discussion

The previous chapter's results demonstrate that empirical procedures can successfully be used for estimating water quality parameters from remotely sensed data, with a good degree of accuracy given the constraints of the data set, in the turbid cyanobacteria-dominant water in Zeekoevlei. Thus, the projects aims and objectives, set forth in Chapter 1, have largely been achieved, and are discussed in the remainder of this chapter.

6.1 The Suitability of Multispectral Satellite Sensors for Monitoring in Zeekoevlei

The multispectral MERIS and Landsat 7 ETM+ images, used in this study, were selected due to constraints imposed by the cost and availability of data. Unsuccessful acquisition of CHRIS data owing to conflicting priorities and cloud cover; the excessive cost of SPOT 4 and 5 data; and the unavailability or cancellation of hyperspectral airborne campaigns, meant that data options were limited. MERIS data became available free of charge through a scientific research grant, while the Landsat 7 data over Africa also became available in the middle of 2008, at no cost.

The MERIS and Landsat sensors differ considerably in terms of their spectral, temporal and spatial characteristics providing an interesting contrast between two dissimilar sensors used for the same application. During April 2008 numerous scenes were collected by MERIS, so that eventually four scenes simultaneous to *in situ* fieldwork measurements were acquired. Conversely, over this same period, in the absence of the option to pre-order in advance there were no Landsat 7 acquisitions, at least none that became freely available. The scene acquired on the 2nd May was thus a stroke of good fortune, and only through simulation of hyperspectral radiometric reflectance was it possible to produce the Landsat water quality parameter maps. Thus the suitability of the Landsat sensor is severely hampered by the insufficient availability of data. The free and frequent availability of MERIS data gives it a substantial advantage over Landsat and other similar remote sensing systems for regular or real-time monitoring applications observing change occurring over short time scales.

Zeekoevlei was detected by MERIS by between 15 and 20 pixels, whereas with Landsat, the number of pixels was more than 2000. Therefore, Landsat provided substantially finer detail than MERIS such that the patchy spatial distribution of algal blooms in different regions of the lake is clearly visible in pixel transects. However, this is not to suggest that the maps from MERIS were in any way homogeneous. They also showed the concentrations of water quality parameters varying in a broad range despite the small number of pixels. In fact, it was often easier to distinguish areas of high/low concentrations of water quality parameters from the MERIS maps

because of the sharp contrast between adjacent pixels. While Landsat presented finer detail, the coarse resolution of MERIS was no less, if not more effective, in showing the spatial variability of the water quality parameters between different regions of the lake.

The MERIS spectral band arrangement designed for water-related applications, allowed for close comparisons with *in situ* hyperspectral radiometric reflectance and for the application of a number of different empirical algorithms. The TOA and atmospherically corrected MERIS spectra showed the main spectral characteristics of the water-leaving reflectance, including the peaks near 560 and 700 nm, and the Chl *a* absorption maximums near 665 and 430 nm. In contrast, the simulated three bands of the Landsat sensor, while showing appreciable variation in magnitude, failed to identify these main spectral features. Therefore, the spectral definition of the MERIS sensors is far better suited for identifying the main characteristics of the water-leaving reflectance, for validation of the atmospheric correction procedures, and for algorithm application. MERIS's higher signal-to-noise ratio and radiometric resolution also gives substantially better accuracy over low-reflectance water targets than the Landsat sensor.

In summary, MERIS's frequent acquisition schedule and free data availability make it well-suited for frequent or real-time monitoring applications, whereas systems such as Landsat, and others, are thoroughly unsuited for this purpose. The higher spatial resolution of the Landsat sensor does not seem to present substantial advantages over the lower resolution MERIS sensor in its ability to detect spatial variability and ranges of concentrations of water quality parameters, despite the very small surface area of Zeekoevlei. Lastly, the spectral definition and higher signal-to-noise ratio of MERIS presents better opportunities for characterising the main features of the water-leaving reflectance than does the Landsat sensor.

6.2 Water Constituents and Influence on the Water-Leaving Reflectance

Water quality conditions for Zeekoevlei during April 2008 were not dissimilar to those previously observed by Harding (1991, 1996) and the City of Cape Town Scientific Services. The lake displayed the characteristic symptoms of hypertrophy: very high phytoplankton biomass with surface accumulations of buoyant cyanobacterial algal cells, turning the water bright-green; large accumulations of organic-rich sludge causing high levels of turbidity; and very low water transparency. These observations were substantiated by measurements of very high concentrations of Chl *a* and suspended matter, up to 247.4 $mg.m^{-3}$, and 65.3 $mg.\ell^{-1}$, respectively; by the overwhelming contribution of organic matter (detritus and phytoplankton) to suspended particulates; and by SD depths that were very small. Absorption by CDOM, not previously

measured for Zeekoevlei, was also found to contribute significantly to light attenuation in the blue region of the spectrum. The lake showed low overall spatial variability in water quality conditions, apart from somewhat increased bloom activity in the southern basin, and slightly clearer conditions near the inflow of the Great and Little Lotus Rivers in the northern basin. The variability was attributed to the proximity of the southern basin to nutrient seepage from the Waste Water Treatment Works, and to wind-induced mixing in the northern basin. The strong covariance found between many of the water quality parameters during April 2008 has important implications for the widespread applicability of the algorithms derived here, seen as this was uncharacteristic of the long-term trends in Zeekoevlei.

The OACs, described above, have a substantial influence on the upwelling radiance and in-water remote sensing reflectance, as measured by the hyperspectral radiometer, in Zeekoevlei. The spectral shape appears to be dominated by the effects of absorption from cyanobacterial phytoplankton species, evident by Chl *a* (664 nm), and phycocyanin (620 nm) absorption maxima; scattering from processes of suspended particulates, shown by the large peaks at 560 and 710 nm; and by a_{CDOM} which strongly diminishes the signal less than 500 nm. A large proportion of the variance of the in-water reflectance peaks near 560 and 710 nm may be explained by Chl *a* (>85%) and organic suspended matter (composed of detritus and phytoplankton cells) (>73%), and to a lesser degree, by inorganic particulates (>48%). Empirical algorithms extracted from the literature enabled water quality parameters, besides a_{CDOM}, to be estimated with a considerable degree of certainty from the in-water reflectance. The RLH algorithm estimated 85% of the variability of Chl *a*, and a difference ratio algorithm (Gitelson et al., 1993) estimated 87% and 90% of the variability in TSS and OSS, respectively. The covariance between the parameters means that the algorithms are good estimators of changes in the gross particulate load, more than of the individual parameters. Furthermore, the height and position of the normalised reflectance peak near 710 nm was found to be strongly correlated with Chl *a* concentration, revealing that backscattering from phytoplankton is the dominant causal IOP. Therefore, there are significant correlations between the optically active water constituents and the in-water reflectance which are in agreement with the relationships found in other similar eutrophic lakes.

In summary, water quality conditions in Zeekoevlei were characteristic of the hypertrophic, cyanobacteria dominant conditions previously observed, and the inwater reflectance was significantly influenced by the presence of optically active suspended particulate and dissolved

organic matter. A large proportion of the variance observed in the in-water reflectance can be attributed to the OACs, with backscattering from phytoplankton being the dominant causal IOP.

6.3 Empirical and Semi-analytical Algorithms for Estimating Water Quality Parameters

Multi-temporal empirical algorithms for estimating water quality parameters in Zeekoevlei were successfully derived using simultaneous fieldwork and remotely sensed MERIS and simulated Landsat data. Many of the same algorithms used with the hyperspectral radiometry also worked well with MERIS owing to the spectral arrangement of the bands.

The 708/664 algorithm using TOA MERIS data performed better than for radiometric data, explaining more than 69% of the variability of the parameters Chl *a*, TSS, OSS and SD depth (93% for Chl *a*). The correlation with Chl *a* was improved by using nonlinear regression such that 97% of the variability could be explained. The outcome that a nonlinear algorithm using the ratio 708/664 is a particularly robust estimator of Chl *a* in Zeekoevlei is in agreement with findings in other high biomass waters (See Gitelson et al., 1993, Bernard et al., 2006, Jiao et al., 2006, Menken & Brezonik, 2006). As with the radiometric data, a single band algorithm at the reflectance peak at 708 nm was able to explain a large amount of the variance in these same parameters (>70%). However, this algorithm only performed well after MERIS TOA data had been corrected for atmospheric effects. The RLH algorithm, which measures the height of the reflectance peak near 700 nm, was also found to be a robust estimator of these parameters, performing well with MERIS TOA data and atmospherically corrected data. An algorithm based on Zimba and Gitelson's (2006) three band conceptual model designed for estimating Chl *a* in hypertrophic waters also gave good results using MERIS data, although these were not as significant as the results of the RLH and 708/664 algorithms. It has been suggested that the algorithm's performance could be improved by tuning the model to the optical properties of the water body (Dall'Olmo & Gitelson, 2005), which indeed could improve the correlation achieved with radiometric data in this study; however, tuning is obviously not feasible with the fixed band positions of MERIS. Nevertheless, it appears that even an untuned model is well-suited for estimating Chl *a* in Zeekoevlei's hypertrophic conditions from both TOA and atmospherically corrected MERIS data.

The retrieval of ISS was not significant enough for mapping from TOA data, however significant correlations were attained using Gitelson et al.'s (1993) difference ratio and Koponen et al.'s (2007) ratio algorithms from atmospherically corrected reflectance, although less than 50% of the

variability was explained. These algorithms were effective because ISS was found to be correlated with the 708 and 560 nm peaks measured radiometrically. a_{CDOM} was estimated best by Gitelson et al.'s difference ratio algorithm from TOA reflectance, although the single bands at 412 and 442 nm also performed well. The correlation of a_{CDOM} with single bands up to 680 nm is difficult to explain since the signal from a_{CDOM} is significant only in the blue. The covariance between a_{CDOM} and some of the other parameters may be the explanation for this observation.

Therefore, it appears that algorithms used to estimate water quality parameters in other high biomass Case 2 waters also work well in Zeekoevlei. The water quality parameters which measure the gross changes in particulate matter were best estimated with algorithms incorporating the 708 nm reflectance peak. Therefore, the very strong signal in the red is suitable at least as a first order indicator of water quality conditions typical of hypertrophy. The substantial covariance observed between many of the parameters in Zeekoevlei meant that many algorithms performed, or at least appeared to perform, equally well across a number of the parameters. Furthermore, the existance of non-unique signals, for example, from phytoplankton (Chl *a*) and TSS largely composed of organic matter, meant that the algorithms have limited ability to separate between the parameters. Therefore, it may be assumed that many of the algorithms show changes in covariant gross particulates, rather than signals from the individual or independent OACs.

Atmospheric correction improved the performance of algorithms that were sensitive to atmospheric contributions, such as the single band 708 nm algorithm, but had limited impact on algorithms which are more robust, such as the RLH and 708/664 algorithms. The image-based atmospheric corrections introduced a spectral bias which caused some of the algorithms to operate poorly. The 6S RTC atmospheric correction operated consistently well, often improving the performance of the algorithms. Therefore the 6S RTC atmospheric correction is preferable over image-based techniques because it introduces fewer errors so that water quality algorithms operate more acurately. However the finding that, for many algorithms, water quality parameters can be satisfactorily estimated from TOA MERIS data indicates that atmospheric correction is not a precondition to water quality parameter retrieval from MERIS. Furthermore, a comparison between the accuracy with which the parameters were estimated using radiometric reflectance, and MERIS, reveals that there is only a slight advantage in using a hyperspectral resolution sensor over the multispectral MERIS channels. Thus the arrangement of MERIS's spectral bands allows for a large range of empirical algorithms to be applied and is therefore adequate for monitoring the different water quality parameters over Zeekoevlei.

Using simulated Landsat 7 ETM+ reflectance more than 83% of the variability of Chl *a*, and 84% of the variability of TSS and OSS was explained using the b2-b1 and b2-b3 linear algorithms, respectively. More than 70% of the variability of ISS and SD was explained using the b2-b3 and b3/b2 linear algorithms, respectively. a_{CDOM} was also estimated with a certainty of 57% with the linear band ratio algorithm b3/b1. The significance of these results are equal to, or better, than those of other similar studies (See, for example, Hellweger et al. 2004, Han & Jordan 2005, Tyler et al., 2006). Therefore, despite the broad widths of the Landsat's spectral bands, it appears to be capable of resolving the main water constituents in Zeekoevlei, although as already explained, there are problems from non-unique signals as many of the parameters are covariant. Importantly, the MERIS and simulated Landsat empirical algorithms are only accurate inside the range of water and atmospheric conditions used for their derivation. Thus they are not applicable cross-spatially in other water bodies and have limited multi-temporal applicability in Zeekoevlei.

Atmospheric and water products from the MERIS standard L 2 Case 2 algorithm and Eutrophic Lakes Processor showed invalid and erroneous results, respectively. Negative reflectances from the L 2 product caused the NN algorithm to fail to produce realistic concentrations of water constituents, while for the Eutrophic Lakes Processor, the water-leaving reflectance and the water constituents were grossly underestimated. The obvious explanations for the failure of these algorithms gives insight into some of the negative aspects associated with semi-analytical techniques. Firstly, atmospheric correction procedures that are sensitive to higher than normal reflectances in the near-infrared caused by high sediment concentrations, or are dependent on a bio-optical model which is not correctly parameterised for the study area, produce erroneous reflectance values that causes semi-analytical algorithms to fail. Therefore, semi-analytical algorithms are highly dependent on the ability of atmospheric correction procedures to accurately define the water-leaving reflectance, and break down where atmospheric correction fails. Secondly, a failure to correctly account for the optical properties and concentration ranges of the OACs in Zeekoevlei meant that the bio-optical simulations forming the basis of the algorithms were unable to realistically model the water constituents. Semi-analytical methods which are dependent on the bio-optical characterisation of the water body operate poorly where the optical properties and concentration ranges of water constituents deviate from those used to train the algorithm. Unfortunately, the development and in-depth investigation of semi-analytical algorithms was outside of the scope of this study as a result of time constraints. However, they are the only feasible way of effectively separating water constituents and so much attention should be given to their development in future.

In summary, empirical algorithms were able to estimate water quality parameters for Zeekoevlei from MERIS with a high degree of certainty within the constraints of the data set and atmospheric correction was not a precondition to good algorithm performance. The covariance between water quality parameters meant that in some instances non-unique signals led to the same algorithms operating well for a number of the different water quality parameters. Therefore the algorithms mostly show changes of covariant gross particulates rather than of individual parameters. Hyperspectral instruments do not have a great advantage over the MERIS spectral arrangement, and even the broad widths of the simulated Landsat 7 bands are not unsuitable for algorithm development. The MERIS Case 2 semi-empirical algorithms produced erroneous results owing to a departure in the concentration ranges and IOPs used to train the algorithms and those of Zeekoevlei, and the failure of atmospheric corrections over bright-pixel waters.

6.4 Water Quality Maps and the Implications for Management

Maps from four MERIS scenes and one Landsat scene allowed the spatial and temporal variability of the water constituents in Zeekoevlei to be observed with a synoptic coverage unrivalled by conventional monitoring methods. As already explained in Section 6.1, the lower spatial resolution of the MERIS maps relative to Landsat did not reduce the range or diminish the spatial variability with which the water constituents were observed. On the contrary, the four MERIS maps gave considerable insights into the temporal and spatial fluctuations of the water constituents and their relationships with environmental variables such as wind and wave height during April 2008. The southern basin was characterised by persistently higher phytoplankton biomass and suspended matter concentrations, resulting in lower depths of light penetration. This might be explained by increased nutrient input to the southern basin by underground seepage from the adjacent WWTW. In contrast, the northern basin exhibited slightly improved water quality conditions with lower concentrations of suspended particulates and higher Secchi Disk depths. The only day on which the northern basin showed water quality conditions matching the southern basin, was on April 20th, when there was a strong southerly wind. Wave action caused the entrainment of bottom sediments into the water column, and the transport of phytoplankton into the northern basin from the southern basin, leading to the observation of increased suspended matter and Chl *a* concentrations. Therefore, it may be inferred that water quality in the northern basin was more dependent on wind, and more variable, than in the southern basin during April.

The higher spatial definition of the Landsat maps on May 2nd confirmed the observation of slightly clearer conditions in the northern basin, and further revealed the patchy distribution of

cyanobacterial algal blooms and suspended matter across the lake. The greater number of data points from Landsat meant that the standard errors of the spatial means for water quality parameters were smaller than for MERIS, although this does not imply that they were more accurate The RMSE of mean estimates from Landsat was less than 2% for Chl *a*, TSS, OSS and SD depth, and less than 6.9% from MERIS. The RMSE for mean *in situ* measurements was usually much larger than this. The observed error, the difference between remotely sensed and observed means, was as large as 30% for Chl *a*, 21% for TSS, 7% for OSS, 6% for SD depth, and 28% for a_{CDOM}. Therefore, assuming that the remotely sensed mean is correct, estimates of the mean from a small number of *in situ* sample sites may be incorrect by up to the same percentages. Therefore, remote sensing from MERIS leads to improved spatial mean water quality estimates in Zeekoevlei, especially for Chl *a* and TSS.

In summary, maps produced from MERIS and Landsat give significant insight into the synoptic and temporal variability of water constituents, and provide better understanding on the relationships between water conditions and environmental variables, such as wind, in Zeekoevlei. Water quality conditions were slightly better in the northern basin than in the southern basin and Home Bay during April 2008. Estimates of the mean water quality parameters may be improved and the error reduced by combining a small number of *in situ* sample sites with remotely sensed data.

Chapter 7 Conclusion and Recommendations

Zeekoevlei has proved to be an ideal study area for developing and assessing remote sensing techniques for inland and coastal Case 2 waters experiencing severe problems related to hypertrophy and cyanobacterial algal blooms, despite the challenges related to its small size. The findings of this investigation presents substantial opportunities for improving monitoring in other lakes and coastal waters with similar water quality problems, following the application techniques similar to the ones used in this study. The research question, set forth in Chapter 1, has therefore been answered conclusively: Current operational earth observation satellites (MERIS in particular) are able to monitor water quality parameters, hyper-eutrophication and cyanobacterial blooms in a small inland lake with a significant degree of confidence. The aim of the research to provide remote sensing products which enhance the understanding and monitoring of eutrophication and cyanobacterial algal blooms, has been successfully achieved. The following conclusions may be made concerning the four project objectives:

1. MERIS is well-suited for monitoring eutrophication and cyanobacterial algal blooms even in very small lakes such as Zeekoevlei. MERIS's spectral arrangement and signal-to-noise ratio is sufficient to estimate most water constituents. Therefore, MERIS is the optimal current sensor, over Landsat and other similar sensors, for frequent or real-time environmental change detection applications in inland waters.

2. The high concentrations of OACs in Zeekoevlei have a significant influence on the upwelling radiance, and backscattering from cyanobacterial algal species appears to be the dominant causal IOP. The light field in Zeekoevlei displays properties similar to those observed in other eutrophic/hypertrophic cyanobacteria-dominated waters.

3. Empirical algorithms were able to estimate a large amount of the variability of the water quality parameters in Zeekoevlei. Algorithms incorporating the MERIS 708 nm band are ideally suited for Chl *a* and suspended particulate matter estimations, although there may be difficulties with separating signals from covariant parameters. Atmospheric correction is not always a precondition to good algorithm performance. The MERIS Case 2 semi-analytical NN algorithms failed owing to departures between the concentration ranges and IOPs of constituents, and poor atmospheric correction.

4. Synoptic maps of water quality parameters provide valuable information for management and understanding of the spatial and temporal patterns of cyanobacterial algal blooms and water quality, in Zeekoevlei. Remote sensing yields better spatial mean water quality

estimates than conventional water quality monitoring programmes which are dependent on a few sampling points.

The recommendations for future work from this study are as follows:

- Future sensors for real-time or frequent environmental change applications such as HAB detection in inland waters should have specifications similar to MERIS, although a slightly higher spatial resolution would be advantageous for smaller lakes. The Indian Space Agency's OCM 2 300 m resolution sensor should also be considered alongside MERIS for this purpose.

- Further characterisation of the IOPs in southern Africa's inland waters should be undertaken so that bio-optical models for semi-analytical algorithms can be developed. Phycocyanin pigment concentrations should be be measured along with Chl *a* to derive cyanobacterial algal bloom specific algorithms.

- Future work should be dedicated to the development and investigation of various semi-analytical methods rather than empirical methods, because of their multitemporal applicability, independence from simultaneous experimental data, and their ability to separate signals from different constituents. Regional semi-analytical algorithms should be trained with novel bio-optical simulations using the concentration ranges and IOPs specific to hypertrophic/eutrophic southern African waters. Atmospheric correction, a crucial requirement for semi-analytical algorithms, should be improved by the establishment of remote Aerosol Robotic Network (AERONET) retrieval sites and the tailoring of atmospheric models.

- Remote sensing should be integrated into inland water quality monitoring programmes in southern Africa, in order to better determine the regional status and trends of environmental threats from eutrophication and cyanobacterial algal blooms. In order to achieve this attention should be given to the development of operational platform-independent, real-time remote monitoring systems. The operational requirements are: investment in infrastructure and human resources for routinely acquiring and processing high volumes of full-resolution data; the development of integrated *in situ* and remote systems including the deployment of buoys fitted with optical instruments at key sites allowing calibration and validation, and continuous surveillance of water quality; and the establishment of AERONET sites for atmospheric correction. Multi-site, multi-scale pilot

projects should be initiated at key sites across southern African, including water-supply reservoirs, for the development and validation of semi-analytical algorithms. The development of an operational inland water quality monitoring system based on remote sensing that enables the early warning of and rapid response to environmental threats would have immense benefits for southern Africa.

References

AHN, Y.H., BRICAUD, A. and MOREL, A., 1992. Light backscattering efficiency and related properties of some phytoplankters. *Deep-Sea Research,* **39**, 1835-1835.

AIKEN, J. and MOORE, G., 2000. *Algorithm theoretical basis document: case 2 (S) bright pixel atmospheric correction.* PO-TN-MEL-GS-0005. Plymouth Marine Laboratory: Centre for Coastal & Marine Sciences.

ALBERT, A. and MOBLEY, C., 2003. An analytical model for subsurface irradiance and remote sensing reflectance in deep and shallow case-2 waters. *Optics Express,* **11**(22), 2873-2890.

ALLAN, J.D., 2004. Landscapes and riverscapes: The influence of land use on stream ecosystems. *Annual Review of Ecology, Evolution and Systematics,* **35**, 257-284.

ALPARSLAN, E., AYDONER, C., TUFEKCI, V. and TUFEKCI, H., 2007. Water quality assessment at Omerli Dam using remote sensing techniques. *Environmental monitoring and assessment,* **135**(1-3), 391-398.

AMMENBERG, P., FLINK, P., LINDELL, T., PIERSON, D. and STROMBECK, N., 2002. Bio-optical modelling combined with remote sensing to assess water quality. *International Journal of Remote Sensing,* **23**(8), 1621-1638.

ANDERSON, D.M., GLIBERT, P.M. and BURKHOLDER, J.M., 2002. Harmful algal blooms and eutrophication: nutrient sources, composition, and consequences. *Estuaries,* **25**(4B), 704-726.

ANTOINE, D. and MOREL, A., 1999. A multiple scattering algorithm for atmospheric correction of remotely sensed ocean colour (MERIS instrument): principle and implementation for atmospheres carrying various aerosols including absorbing ones. *International Journal of Remote Sensing,* **20**(9), 1875-1916.

ARHEIMER, B., ANDREASSON, J., FOGELBERG, S., JOHNSSON, H., PERS, C.B. and PERSSON, K., 2005. Climate change impact on water quality: model results from southern Sweden. *Ambio,* **34**(7), 559-566.

BABIN, M. and STRAMSKI, D., 2002. Light absorption by aquatic particles in the near-infrared spectral region. *Limnol.Oceanogr,* **47**(3), 911-915.

BABIN, M., STRAMSKI, D., FERRARI, G.M., CLAUSTRE, H., BRICAUD, A., OBOLENSKY, G. and HOEPFFNER, N., 2003. Variations in the light absorption coefficients of phytoplankton, nonalgal particles, and dissolved organic matter in coastal waters around Europe. *J.Geophys.Res,* **108**(C7), 3211–3230.

BANENS, R.J. and DAVIS, J.R., 1998. Comprehensive approaches to eutrophication management: the Australian example. *Water Science and Technology,* **37**(3), 217-225.

BARTRAM, J., CARMICHAEL, W.W., CHORUS, I., JONES, G. and SKULBERG, O.M., 1999. Introduction. In: I. CHORUS and J. BARTRAM, eds, *Toxic cyanobacteria in water: a guide to their public health consequences, monitoring and management.* 1st edn. London: E & FN Spon, pp. 12-24.

BENNETT, E.M., CARPENTER, S.R. and CARACO, N.F., 2001. Human impact on erodable phosphorus and eutrophication: a global perspective. *Bioscience,* **51**(3), 227-234.

BERNARD, S., BALT, C., PITCHER, G., PROBYN, T., FAWCETT, A. and DU RANDT, A., 2006. The use of MERIS for harmful algal bloom monitoring in the southern Benguela. Journal article edn. Cape Town: University of Cape Town.

BLENCKNER, T., 2007. Climate-related effects on water quality. In: J.L. LOZAN, H. GRASSL, P. HUPFER, L. MENZEL and C. SCHONWIESE, eds, *Global change: Enough water for all?* 2nd edn. Hamburg: Wissenschaftliche Auswertungen/GEO, pp. 231-234.

BRANDO, V.E. and DEKKER, A.G., 2003. Satellite hyperspectral remote sensing for estimating estuarine and coastal water quality. *IEEE Transactions on Geoscience and Remote Sensing,* **41**(6), 1378-1387.

BRAUDE, C., YOSEF, N.B. and DAR, I., 1995. Satellite remote sensing of waste water reservoirs. *International Journal of Remote Sensing,* **16**(16), 3087-3114.

BREZONIK, P., MENKEN, K.D. and BAUER, M., 2005. Landsat-based remote sensing of lake water quality characteristics, including chlorophyll and Colored Dissolved Organic Matter(CDOM). *Lake and Reservoir Management,* **21**(4), 373-382.

BRICAUD, A., MOREL, A. and PRIEUR, L., 1981. Absorption by dissolved organic matter of the sea (yellow substance) in the UV and visible domains. *Limnol.Oceanogr,* **26**(1), 43-53.

BRICAUD, A., MOREL, A. and PRIEUR, L., 1983. Optical efficiency factors of some phytoplankters. *Limnol.Oceanogr,* **28**(5), 816-832.

BRIVIO, P.A., GIARDINO, C. and ZILIOLI, E., 2001. Determination of chlorophyll concentration changes in Lake Garda using an image-based radiative transfer code for Landsat TM images. *International Journal of Remote Sensing,* **22**(2), 487-502.

BRÖNMARK, C. and HANSSON, L.A., 2002. Environmental issues in lakes and ponds: current state and perspectives. *Environmental Conservation,* **29**(03), 290-307.

BUITEVELD, H., HAKVOORT, J.H.M. and DONZE, M., 1994. Optical properties of pure water, *Proceedings of SPIE,* 1994, SPIE pp174.

BUKATA, R.P., JEROME, J.H., KONDRATYEV, K.Y. and POZDNYAKOV, D.V., 1995. Optical properties and remote sensing of inland and coastal waters. Boca Raton, Florida: CRC Press.

CANDIANI, G., FLORICIOIU, D., GIARDINO, C. and ROTT, H., 2005. Monitoring water quality of the perialpine Ilalian Lake Guarda through multi-temporal MERIS data, H. LACOSTE, ed. In: *Proceedings of the MERIS (A)ATSR Workshop, Frascati, Italy 26 - 30 Spetember 2005,* 2005, ESA pp1.

CARPENTER, S.R., FISHER, S.G., GRIMM, N.B. and KITCHELL, J.F., 1992. Global change and freshwater ecosystems. *Annual Review of Ecology and Systematics,* **23**, 119-139.

CARPENTER, S.R., CARACO, N.F., CORRELL, D.L., HOWARTH, R.W., SHARPLEY, A.N. and SMITH, V.H., 1998. Nonpoint pollution of surface waters with phosphorus and nitrogen. *Ecological Applications*, **8**(3), 559-568.

CCT, 2007a. *City of Cape Town Sustainability Report 2006.* Cape Town: Environmental Resource Management Department.

CCT, 2007b. *False Bay Ecology Park information poster.* Cape Town: Eco-logic, City of Cape Town Environmental Resource Management Department.

CCT, 2008-last update, environmental health [Homepage of City of Cape Town], [Online]. Available: http://www.capetown.gov.za/EN/CITYHEALTH/ENVIROHEALTH/Pages/EnvironmentalHealth.aspx [February 22, 2009].

CHANG, K.W., SHEN, Y. and CHEN, P.C., 2004. Predicting algal bloom in the Techi reservoir using Landsat TM data. *International Journal of Remote Sensing*, **25**(17), 3411-3422.

CHAVEZ, P.S., 1996. Image-based atmospheric corrections - revisited and improved. *Photogrammetric Engineering & Remote Sensing*, **62**(9), 1025-1036.

CHEN, L., TAN, C.H., KAO, S.J. and WANG, T.S., 2008. Improvement of remote monitoring on water quality in a subtropical reservoir by incorporating grammatical evolution with parallel genetic algorithms into satellite imagery. *Water research*, **42**(1-2), 296-306.

CHEN, Z.Q., HU, C.M. and MULLER-KARGER, F., 2007. Monitoring turbidity in Tampa Bay using MODIS. *Remote Sensing of Environment*, **109**(2), 207-220.

CHU, Z.S., JIN, X.C., IWAMI, N. and INAMORI, Y.H., 2007. The effect of temperature on growth characteristics and competitions of Microcystis aeruginosa and Oscillatoria mougeotii in a shallow, eutrophic lake simulator system. *Hydrobiologia*, **581**, 217-223.

CIPOLLINI, P., CORSINI, G., DIANI, M. and GRASSO, R., 2001. Retrieval of sea water optically active parameters from hyperspectral data by means of generalized radial basis function neural networks. *IEEE Transactions on Geoscience and Remote Sensing*, **39**(7), 1508-1524.

CNES SPOT IMAGE, 2004, 2004-last update, SPOT technical information [Homepage of Spot Image], [Online]. Available: http://www.spotimage.fr/html/_167_.php [3 June, 2007].

CODD, G.A., 2000. Cyanobacterial toxins, the perception of water quality, and the prioritisation of eutrophication control. *Ecological Engineering*, **16**(1), 51-60.

DALLAS, H.F. and DAY, J.A., 2004. *The effect of water quality variables on aquatic ecosystems: a review.* TT 224/04. Rondebosch, Cape Town: Freshwater Research Unit, University of Cape Town.

DALL'OLMO, G. and GITELSON, A.A., 2005. Effect of bio-optical parameter variability on the remote estimation of chlorophyll-a concentration in turbid productive waters: experimental results. *Applied Optics*, **44**(3), 412-422.

DAVIES, B.R. and DAY, J.A., 1998. Vanishing waters. Cape Town: UCT Press.

DAVIS, C.O., KIRK, J.T.O., PARSLOW, J.S. and SATHYENDRANATH, S., 2000. Measurement requirements for case 2 waters. In: S. SATHYENDRANATH, ed, *Remote sensing of ocean colour in coastal, and other optically-complex waters.* Dartmouth, Canada: Report No. 3 of the International Ocean-Colour Coordinating Group, pp. 77-91.

DE VILLIERS, S. and THIART, C., 2007. The nutrient status of South African rivers: concentrations, trends and fluxes from the 1970s to 2005. *South African Journal of Science,* **103**(7-8), 343-349.

DEKKER, A., 1993. *Detection of optical water quality parameters for eutrophic waters by high resolution remote sensing,* Free University.

DEKKER, A.G., VOS, R.J. and PETERS, S.W.M., 2001. Comparison of remote sensing data, model results and in situ data for total suspended matter (TSM) in the southern Frisian lakes. *Science of the Total Environment,* **268**(1-3), 197-214.

DEKKER, A.G., VOS, R.J. and PETERS, S.W.M., 2002. Analytical algorithms for lake water TSM estimation for retrospective analyses of TM and SPOT sensor data. *International Journal of Remote Sensing,* **23**(1), 15-35.

DIERBERG, F.E. and CARRIKER, N.E., 1994. Field testing two instruments for remotely sensing water quality in the Tennessee Valley. *Environmental science & technology,* **28**(1), 16-25.

DOERFFER, R. and SCHILLER, H., 2008a. *MERIS regional coastal and lake case 2 water project - atmospheric correction Algorithm Theoretical Basis Document (ATBD).* 1.0. Geesthacht: GKSS Research Centre.

DOERFFER, R. and SCHILLER, H., 2008b. *MERIS lake water algorithm for BEAM Algorithm Theoretical Basis Document (ATBD).* 1.0. Geesthacht: GKSS Forschungszentrum.

DOKULIL, M.T. and TEUBNER, K., 2000. Cyanobacterial dominance in lakes. *Hydrobiologia,* **438**(1), 1-12.

DOR, I. and BEN-YOSEF, N., 1996. Monitoring effluent quality in hypertrophic wastewater reservoirs using remote sensing. *Water Science and Technology,* **33**(8), 23-29.

DOWNING, J.A., PRAIRIE, Y.T., COLE, J.J., DUARTE, C.M., TRANVIK, L.J., STRIEGL, R.G., MCDOWELL, W.H., KORTELAINEN, P., CARACO, N.F. and MELACK, J.M., 2006. The global abundance and size distribution of lakes, ponds, and impoundments. *Limnology and Oceanography,* **51**(5), 2388-2397.

DOWNING, J.A., WATSON, S.B. and MCCAULEY, E., 2001. Predicting Cyanobacteria dominance in lakes. *Canadian Journal of Fisheries and Aquatic Sciences,* **58**(10), 1905-1908.

DST, 2008. *Ten-year innovation plan.* Pretoria: South African Department of Science and Technology.

DU PLESSIS, H.M. and VAN VEELEN, M., 1991. Water quality, salinization and eutrophication time-series and trends in South Africa. *South African Journal of Science,* **87**(1-2), 11-16.

DUAN, H.T., ZHANG, Y.Z., ZHAN, B., SONG, K.S. and WANG, Z.M., 2007. Assessment of chlorophyll-a concentration and trophic state for Lake Chagan using Landsat TM and field spectral data. *Environmental monitoring and assessment,* **129**(1-3), 295-308.

DUDGEON, D., ARTHINGTON, A.H., GESSNER, M.O., KAWABATA, Z.I., KNOWLER, D.J., LÉVÊQUE, C., NAIMAN, R.J., PRIEUR-RICHARD, A.H., SOTO, D. and STIASSNY, M.L.J., 2005. Freshwater biodiversity: importance, threats, status and conservation challenges. *Biological Reviews,* **81**(2), 163-182.

DURAND, D., POZDNYAKOV, D.V., SANDVEN, S., CAUNEAU, F., WALD, L., JACOB, A., KLOSTER, K. and MILES, M., 1999. *Characterisation of inland and coastal waters with space sensors: final report.* Technical report No. 164. Norway: Nansen Environmental and Remote Sensing Centre (NERSC).

DWAF, 1997. White paper on a national water policy for South Africa. White paper edn. Pretoria: South African Department of Water Affairs and Forestry.

DWAF, 2002. *National eutrophication monitoring programme: implementation manual.* Pretoria: South African Department of Water Affairs and Forestry.

DWAF, 2003. *Trophic status report: trophic status of impoundments.* Pretoria: South African Department of Water Affairs and Forestry.

DWAF, 2004a. *National Water Resources Strategy.* Pretoria: South African Department of Water Affairs and Forestry.

DWAF, 2004b. *A 5-year water resource quality monitoring plan: internal report.* Pretoria: Directorate: Information Programmes, South African Department of Water Affairs and Forestry.

EPA, 1983. Residue, non filterable method 160.2 (gravimetric, dried at 103-105°C). In: US ENVIRONMENTAL PROTECTION AGENCY, ed, *Methods for chemical analysis of water and waste.* 3rd edn. Cincinnati, Ohio: Environmental Monitoring and Support Laboratory Office of Research and Development, pp. 160 2.1-160 2.3.

EUROPEAN SPACE AGENCY, 2006. *MERIS product handbook.* 2.1.

FALCONER, I.R., 2001. Toxic cyanobacterial bloom problems in Australian waters: risks and impacts on human health. *Phycologia,* **40**(3), 228-233.

FAY, P., 1983. The blue-greens: Cyanophyta-Cyanobacteria. London: Edward Arnold.

FLEMING, L.E., RIVERO, C., BURNS, J., WILLIAMS, C., BEAN, J.A., SHEA, K.A. and STINN, J., 2002. Blue green algal (cyanobacterial) toxins, surface drinking water, and liver cancer in Florida. *Harmful Algae,* **1**(2), 157-168.

FLINK, P., LINDELL, T. and ÖSTLUND, C., 2001. Statistical analysis of hyperspectral data from two Swedish lakes. *The Science of the total environment,* **268**(1-3), 155-169.

FLORICIOIU, D., RIEDL, C., ROTT, H. and ROTT, E., 2003. Envisat MERIS capabilities for monitoring the water quality of perialpine lakes, *Proceedings of IEEE Geoscience and Remote Sensing Symposium, 21-25 July 2003, Toulouse, France,* 2003, IEEE IGARSS 2003 pp2134-2136.

FLORICIOIU, D. and ROTT, H., 2003. Aerosol retrieval and atmospheric correction for MERIS data over lakes, H. LACOSTE, ed. In: *Proceedings of MERIS user workshop (ESA SP-549), 10 - 13 November 2003, Friscati, Italy*, 2003, ESRIN ESA pp18.1-9092.

FLORICIOIU, D., ROTT, H., ROTT, E., DOKULIL, M. and DEFRANCESCO, C., 2004. Retrieval of limnological parameters of perialpine lakes by means of MERIS data, H. LACOSTE and L. OUWEHAND, eds. In: *Proceedings of the 2004 Envisat & ERS Symposium (ESA SP-572), 6 - 10 September, Salzberg, Austria*, 2004, ESRIN-ESA pp1-5.

FLORICIOIU, D. and ROTT, H., 2005. Atmospheric correction of MERIS data over perialpine regions, H. LACOSTE, ed. In: *Proceedings of the MERIS/(A)ATSR Workshop (ESA SP-597), 26 - 30 Spetember 2005m Frascati, Italy*, 2005, ESRIN ESA pp45.1.

FRASER, R.N., 1998. Hyperspectral remote sensing of turbidity and chlorophyll a among Nebraska Sand Hills lakes. *International Journal of Remote Sensing*, **19**(8), 1579-1589.

GANF, G.G., OLIVER, R.L. and WALSBY, A.E., 1989. Optical properties of gas-vacuolate cells and colonies of Microcystis in relation to light attenuation in a turbid, stratified reservoir (Mount Bold Reservoir, South Australia). *Australian Journal of Marine and Freshwater Research*, **40**(6), 595-611.

GEGE, P. and PLATTNER, S., 2004. Meris validation activities at Lake Constance in 2003, *Proceedings of MERIS User Workshop (ESA SP-549)*, 10-13 November 2003 2004, ESA-ESRIN pp9.1.

GEO, 2007. *Group on Earth Observations inland and nearshore coastal water quality remote sensing workshop, 27 - 29 March.* Geneva, Switzerland: GEO.

GEOEYE, unknown, 2009-last update, products: imagery sources [Homepage of GeoEye], [Online]. Available: http://www.geoeye.com/CorpSite/products/imagery-sources/Default.aspx#ikonos [January 23, 2009].

GIARDINO, C., PEPE, M., BRIVIO, P., GHEZZI, P. and ZILIOLI, E., 2001. Detecting chlorophyll, Secchi disk depth and surface temperature in a sub-alpine lake using Landsat imagery. *The Science of The Total Environment*, **268**(1-3), 19-29.

GIARDINO, C., CANDIANI, G. and ZILIOLI, E., 2005. Detecting chlorophyll-a in Lake Guarda using TOA MERIS radiances. *Photogrammetric Engineering & Remote Sensing*, **71**(9), 1045-1051.

GIARDINO, C., BRANDO, V.E., DEKKER, A.G., STRÖMBECK, N. and CANDIANI, G., 2007. Assessment of water quality in Lake Garda (Italy) using Hyperion. *Remote Sensing of Environment*, **109**(2), 183-195.

GITELSON, A., 1992. The peak near 700 nm on radiance spectra of algae and water: relationships of its magnitude and position with chlorophyll concentration. *International Journal of Remote Sensing*, **13**(17), 3367-3373.

GITELSON, A., GARBUZOV, G., SZILAGYI, F., MITTENZWEY, K., KARNIELI, A. and KAISER, A., 1993. Quantitative remote sensing methods for real-time monitoring of inland waters quality. *International Journal of Remote Sensing*, **14**(7), 1269-1295.

GITELSON, A., MAYO, M., YACOBI, Y.Z., PARPAROV, A. and BERMAN, T., 1994. The use of high-spectral-resolution radiometer data for detection of low chlorophyll concentrations in Lake Kinneret. *Journal of Plankton Research,* **16**(8), 993-1002.

GITELSON, A.A., YACOBI, Y.Z., KARNIELI, A. and KRESS, N., 1996. Reflectance spectra of polluted marine waters in Haifa Bay, Southeastern Mediterranean: features and application for remote estimation of chlorophyll concentration. *Israel Journal of Earth Science,* **45**, 127-136.

GLASGOW, H.B., BURKHOLDER, J.M., REED, R.E., LEWITUS, A.J. and KLEINMAN, J.E., 2004. Real-time remote monitoring of water quality: a review of current applications, and advancements in sensor, telemetry, and computing technologies. *Journal of experimental marine biology and ecology,* **300**(1-2), 409-448.

GLEICK, P.H., 2000. The world's water 2000-2001: The biennial report on freshwater resources. Island Press.

GOLTERMAN, H.L., 1978. Methods for physical and chemical analysis of fresh waters. 2nd edn. Oxford: Blackwell.

GONS, H.J., 1999. Optical teledetection of chlorophyll *a* in turbid inland waters. *Environmental science & technology,* **33**(7), 1127-1132.

GONS, H.J., RIJKEBOER, M. and RUDDICK, K.G., 2002. A chlorophyll-retrieval algorithm for satellite imagery (Medium Resolution Imaging Spectrometer) of inland and coastal waters. *Journal of Plankton Research,* **24**(9), 947-951.

GONS, H.J., RIJKEBOER, M. and RUDDICK, K.G., 2005. Effect of a waveband shift on chlorophyll retrieval from MERIS imagery of inland and coastal waters. *Journal of Plankton Research,* **27**(1), 125-127.

GORDON, H.R., 1978. Removal of atmospheric effects from satellite imagery of the oceans. *Applied Optics,* **17**(10), 1631-1636.

GOWER, J.F.R., DOERFFER, R. and BORSTAD, G.A., 1999. Interpretation of the 685nm peak in water-leaving radiance spectra in terms of fluorescence, absorption and scattering, and its observation by MERIS. *International Journal of Remote Sensing,* **20**(9), 1771-1786.

GREEN, S.A. and BLOUGH, N.V., 1994. Optical absorption and fluorescence properties of chromophoric dissolved organic matter in natural waters. *Limnology and Oceanography,* **39**(8), 1903-1916.

GROBICKI, A., MALES, R., MARTINEZ, I., MATIKA, S. and ARCHIBALD, S., 2001. *Integrated catchment management in an urban context: the Great and Little Lotus Rivers, Cape Town.* 864/1/01. Pretoria: Water Research Commission.

GROBLER, D.C. and TOERIEN, D.F., 1986. New Developments in the Control of Eutrophication. *South African Journal of Science,* **82**(6), 288-288.

GROBLER, D.C. and NTSABA, M., 2004. *Strategic Framework for National Water Resource Quality Monitoring Programmes.* N/0000/REQ0204. Pretoria: Department of Water Affairs and Forestry.

HA, S.R., PARK, S.Y. and PARK, D.H., 2003. Estimation of urban runoff and water quality using remote sensing and artificial intelligence. *Water Science and Technology,* **47**(7-8), 319-325.

HAKVOORT, H., DE HAAN, J., JORDANS, R., VOS, R., PETERS, S. and RIJKEBOER, M., 2002. Towards airborne remote sensing of water quality in The Netherlands—validation and error analysis. *ISPRS Journal of Photogrammetry and Remote Sensing,* **57**(3), 171-183.

HAN, L. and JORDAN, K., 2005. Estimating and mapping chlorophyll a concentration in Pensacola Bay, Florida using Landsat ETM data. *International Journal of Remote Sensing,* **26**(23), 5245-5254.

HANSSON, L.A., GUSTAFSSON, S., RENGEFORS, K. and BOMARK, L., 2007. Cyanobacterial chemical warfare affects zooplankton community composition. *Freshwater Biology,* **52**(7), 1290-1301.

HARDING, W.R., 1991. *The ecology of some urban-impacted coastal vleis on the Cape Flats near Cape Town, with special reference to phytoplankton periodicity*, University of Cape Town.

HARDING, W.R., 1992. Zeekoevlei - water chemistry and phytoplankton periodicity. *Water Sa,* **18**(4), 237-246.

HARDING, W.R., ROWE, N., WESSELS, J.C., BEATTIE, K.A. and CODD, G.A., 1995. Suspected toxicosis of a dog attributed to the cyanobacterial (blue-green algal) hepatotoxin nodularin in South Africa. *Journal of the South African Veterinary Association,* **66**(4), 256-259.

HARDING, W.R., 1996. *The phytoplankton ecology of a hypertrophic, shallow lake, with particular reference to primary production, periodicity and diversity*, University of Cape Town.

HARDING, W.R., 1997. Phytoplankton primary production in a shallow, well-mixed, hypertrophic South African lake. *Hydrobiologia,* **344**, 87-102.

HARDING, W.R. and WRIGHT, S., 1999. Initial findings regarding changes in phyto- and zooplankton composition and abundance following the temporary drawdown and refilling of a shallow, hypertrophic South African coastal lake. *Lake and Reservoir Management,* **15**(1), 47-53.

HARDING, W.R. and PAXTON, B.R., 2001. *Cyanobacteria in South Africa: a review (TT 153/01).* Pretoria: Water Research Commission.

HÄRMÄ, P., VEPSALAINEN, J., HANNONEN, T., PYHALAHTI, T., KAMARI, J., KALLIO, K., ELOHEIMO, K. and KOPONEN, S., 2001. Detection of water quality using simulated satellite data and semi-empirical algorithms in Finland. *The Science of the total environment,* **268**(1-3), 107-121.

HASKINS, C., 15 August 2007. Personal communication. Athlone: City of Cape Town Scientific Services Department.

HASLER, A.D., 1947. Eutrophication of lakes by domestic drainage. *Ecology,* **28**(4), 383-395.

HELLWEGER, F.L., MILLER, W. and OSHODI, K.S., 2007. Mapping turbidity in the Charles River, Boston using a high-resolution satellite. *Environmental monitoring and assessment,* **132**(1-3), 311-320.

HOLM-HANSEN, O., LORENZEN, C.J., HOLMES, R.W. and STRICKLAND, J.D.H., 1965. Fluorometric Determination of Chlorophyll. *Journal du Conseil,* **30**(1), 3.

HOWMAN, A.M. and KEMPSTER, P.L., 1986. *Landsat water quality surveillance - development of the model CALMCAT.* TR 128. South African Department of Water Affairs: Hydrological Research Institute.

INDIAN SPACE RESEARCH ORGANISATION, unknown, 2008-last update, indian space research organisation: programmes [Homepage of Department of Space], [Online]. Available: http://www.isro.org/programmes.htm [January 23, 2008].

IPCC, 2008. *Climate change 2007: synthesis report. Contribution of working groups I, II and III to the fourth assessment report of the intergovernmental panel on climate change.* Geneva, Switzerland: Intergovernmental Panel on Climate Change.

JACOBY, J.M., COLLIER, D.C., WELCH, E.B., HARDY, F.J. and CRAYTON, M., 2000. Environmental factors associated with a toxic bloom of Microcystis aeruginosa. *Canadian Journal of Fisheries and Aquatic Sciences,* **57**(1), 231-240.

JANUS, L.L. and VOLLENWEIDER, R.A., 1981. *Summary report: The OECD co-operative programme on eutrophication: Canadian contribution (C&EE18).* Burlington: Canada Centre for Inland Waters.

JEFFRIES, M. and MILLS, D., 1990. Freshwater ecology: principles and applications. London: Belhaven Press.

JGOFS PROTOCOLS, 1994. *Chapter 14: Measurement of chlorophyll a and pheopigments by fluorometric analysis.* 19. UNESCO.

JIAN, C.K. and SHARMA, K.D., 2005. Water quality management. In: J. LEHR and J. KEELEY, eds, *Water encyclopedia: Water quality and resource development.* New Jersey: John Wiley & Sons, pp. 316.

JIAO, H.B., ZHA, Y., GAO, J., LI, Y.M., WEI, Y.C. and HUANG, J.Z., 2006. Estimation of chlorophyll a concentration in Lake Tai, China using in situ hyperspectral data. *International Journal of Remote Sensing,* **27**(19), 4267-4276.

JOHNK, K.D., HUISMAN, J., SHARPLES, J., SOMMEIJER, B., VISSER, P.M. and STROOM, J.M., 2008. Summer heatwaves promote blooms of harmful cyanobacteria. *Global Change Biology,* **14**(3), 495-512.

JOHNSON, N., REVENGA, C. and ECHEVERRIA, J., 2001. Ecology: managing water for people and nature. *Science (New York, N.Y.),* **292**(5519), 1071-1072.

KALLIO, K., KUTSER, T., HANNONEN, T., KOPONEN, S., PULLIAINEN, J., VEPSALAINEN, J. and PYHALAHTI, T., 2001. Retrieval of water quality from airborne imaging spectrometry of various lake types in different seasons. *The Science of the total environment,* **268**(1-3), 59-77.

KALLIO, K., KOPONEN, S. and PULLIAINEN, J., 2003. Feasibility of airborne imaging spectrometry for lake monitoring—a case study of spatial chlorophyll a distribution in two meso-eutrophic lakes. *International Journal of Remote Sensing,* **24**(19), 3771-3790.

KIRK, J.T.O., 1994. Light and photosynthesis in aquatic ecosystems. 2nd edn. Bristol: J.W. Arrowsmith.

KNEIZYS, F.X., SHETTLE, E.P., ABREU, L.W., CHETWYND, J.H., ANDERSON, G.P., GALLERY, W.O., SELBY, J.E.A. and CLOUGH, S.A., 1988. *Users guide to LOWTRAN 7: environmental research report ERP No. 1010.* Hanscom AFB, MA: Air Force Geophysics Lab.

KONDRATYEV, K.Y., POZDNYAKOV, D.V. and PETTERSSON, L.H., 1998. Water quality remote sensing in the visible spectrum. *International Journal of Remote Sensing,* **19**(5), 957-979.

KOPONEN, S., PULLIAINEN, J., KALLIO, K. and HALLIKAINEN, M., 2002. Lake water quality classification with airborne hyperspectral spectrometer and simulated MERIS data. *Remote Sensing of Environment,* **79**(1), 51-59.

KOPONEN, S., KALLIO, K., PULLIAINEN, J., VEPSALAINEN, J., PYHALAHTI, T. and HALLIKAINEN, M., 2004. Water quality classification of lakes using 250-m MODIS data. *Geoscience and Remote Sensing Letters, IEEE,* **1**(4), 287-291.

KOPONEN, S., 2006. *Remote sensing of water quality for Finnish lakes and coastal areas*, Helsinki University of Technology.

KOPONEN, S., ATTILA, J., PULLIAINEN, J., KALLIO, K., PYHÄLAHTI, T., LINDFORS, A., RASMUS, K. and HALLIKAINEN, M., 2007. A case study of airborne and satellite remote sensing of a spring bloom event in the Gulf of Finland. *Continental Shelf Research*, **27**(2), 228-244.

KUIPER-GOODMAN, T., FALCONER, I. and FITZGERALD, J., 1999. Human health aspects. In: I. CHORUS and J. BARTRAM, eds, *Toxic cyanobaqcteria in water: a guide to their public health consequences, monitoring and management.* 1st edn. London: E & FN Spon, pp. 125-160.

KUTSER, T., 2004. Quantitative detection of chlorophyll in cyanobacterial blooms by satellite remote sensing. *Limnology and Oceanography*, **49**(6), 2179-2189.

KUTSER, T., PIERSON, D.C., KALLIO, K.Y., REINART, A. and SOBEK, S., 2005. Mapping lake CDOM by satellite remote sensing. *Remote Sensing of Environment,* **94**(4), 535-540.

LATHROP, R.G. and LILLESAND, T.M., 1989. Monitoring water quality and river plume transport in Green Bay, Lake Michigan with SPOT-1 imagery. *Photogrammetric Engineering and Remote Sensing*, **55**(3), 349-354.

LATHROP, R.G. and LILLESAND, T.M., 1986. Use of thematic mapper data to assess water quality in Green Bay and Central Lake Michigan. *Photogrammetric Engineering and Remote Sensing,* **52**(5), 671-680.

LEATHERS, R., DOWNES, T.V. and MOBLEY, C., 2001. Self-shading correction for upwelling sea-surface radiance measurements made with buoyed instruments. *Optics Express,* **8**(10), 561-570.

LEE, R.E., 1980. Phycology. Cambridge: Cambridge University Press.

LINDELL, T., BRIVIO, P.A., FERRO, G., FLINK, P., GIARDINO, C., GHEZZI, P., HALLIKAINEN, M., HANNONEN, T., HÄRMÄ, P., KALLIO, K., ÖSTLUND, C., PEPE, M.,

PULLIAINEN, J., PYHALAHTI, T. and ZILIOLI, E., 1999. Remote sensing of lakes. In: T. LINDELL, D. PIERSON, G. PREMAZZI and E. ZILIOLI, eds, *Manual for monitoring european lakes using remote sensing techniques.* 1st edn. Luxembourg: Office for Official Publications of the European Communities, pp. 45.

LOZAN, J.L., MEYER, S. and KARBE, L., 2007. Water as the basis of life. In: J.L. LOZAN, H. GRASSL, P. HUPFER, L. MENZEL and C. SCHONWIESE, eds, *Global change: enough water for all?* 2nd edn. Hamburg: Wissenschaftliche Auswertungen/GEO, pp. 19-25.

MALMQVIST, B. and RUNDLE, S., 2002. Threats to the running water ecosystems of the world. *Environmental Conservation,* **29**(02), 134-153.

MENKEN, K.D. and BREZONIK, P.L., 2006. Influence of chlorophyll and colored dissolved organic matter (CDOM) on lake reflectance spectra: Implications for measuring lake properties by remote sensing. *Lake and Reservoir Management,* **22**(3), 179-190.

MERTES, L.A.K., 2002. Remote sensing of riverine landscapes. *Freshwater Biology,* **47**(4), 799-816.

MEYBECK, M., KUUSISTO, E., MAKELA, A. and MALKKI, E., 1996. Water Quality. In: J. BARTRAM and R. BALLANCE, eds, *Water quality monitoring: a practical guide to the design and implementation of freshwater quality studies and monitoring programmes.* London: E & F Spoon, pp. 9.

MEYER, J.L., SALE, M.J., MULHOLLAND, P.J. and POFF, N.L., 1999. Impacts of Climate Change on Aquatic Ecosystem Functioning and Health. *Journal of the American Water Resources Association,* **35**(6), 1373-1386.

MIKSA, S., GEGE, P. and HEEGE, T., 2004. Investigations on the capability of CHRIS-Proba for monitoring of water constituents in Lake constance compared to MERIS, *Proceedings of the 2nd CHRIS-PROBA workshop (SP-578),* 28-30 April 2004 2004, ESA pp38-30.

MILLER, R.L. and MCKEE, B.A., 2004. Using MODIS Terra 250 m imagery to map concentrations of total suspended matter in coastal waters. *Remote Sensing of Environment,* **93**(1-2), 259-266.

MITTENZWEY, K., GITELSON, A., ULLRICH, S. and KONDRATIEV, K., 1992. Determination of chlorophyll a of inland waters on the basis of spectral reflectance. *Limnology and Oceanography,* **37**(1), 147-149.

MOBLEY, C., 1994. Light and Water: radiative transfer in natural waters. 1st edn. San Diego: Academic Press.

MOOIJ, W.M., JANSE, J.H., DE SENERPONT DOMIS, L.N., HÜLSMANN, S. and IBELINGS, B.W., 2007. Predicting the effect of climate change on temperate shallow lakes with the ecosystem model PCLake. *Hydrobiologia,* **584**(1), 443-454.

MOORE, G.F., AIKEN, J. and LAVENDER, S.J., 1999. The atmospheric correction of water colour and the quantitative retrieval of suspended particulate matter in Case II waters: application to MERIS. *International Journal of Remote Sensing,* **20**(9), 1713-1733.

MORAN, M.S., JACKSON, R.D., SLATER, P.N. and TEILLET, P.M., 1992. Evaluation of simplified procedures for retrieval of land surface reflectance factors from satellite sensor output. *Remote Sensing of Environment,* **41**(2), 169-184.

MORAN, M., BRYANT, R., THOME, K., NOUVELLON, W., GONZALES-DUGO, M., QI, J. and CLARKE, T., 2001. A refined empirical line approach for reflectance factor retrieval from Landsat-5 TM and Landsat-7 ETM. *Remote Sensing Environ,* **78**, 71-82.

MOREL, A. and PRIEUR, L., 1977. Analysis of variations in ocean color. *Limnol.Oceanogr.,* **22**(4), 709-722.

MORRISON, G., FATOKI, O.S., PERSSON, L. and EKBERG, A., 2001. Assessment of the impact of point source pollution from the Keiskammahoek Sewage Treatment Plant on the Keiskamma River-pH, electrical conductivity, oxygen-demanding substance (COD) and nutrients. *Water SA,* **27**(4), 475-480.

MUR L.R., S., O.M. and UTKILEN, H., 1999. Cyanobacteria in the environment. In: I. CHORUS and J. BARTRAM, eds, *Toxic cyanobacteria in water: a guide to their public heath consequences, monitoring and management.* 1st edn. London: E & FN Spon, pp. 25-54.

NAKANO, S., MURABE, A., TSUJIMURA, S., HAYAKAWA, K., NAKAJIMA, T., KUMAGAI, M., JIAO, C. and KAWABATA, Z., 2003. Dominance of microcystis with special reference to carbon availability in lake water. *Microbes and Environments,* **18**(1), 38-42.

NASA, 16 July 2008, 2008-last update, landsat 7 science data users handbook [Homepage of Landsat Project Science Office], [Online]. Available: http://landsathandbook.gsfc.nasa.gov/handbook/handbook_toc.html [4 November 2008, 2008].

NASA, 22 January, 2009a-last update, the landat programme [Homepage of National Aeronautica and Space Administration], [Online]. Available: http://landsat.gsfc.nasa.gov/ [January 23, 2009].

NASA, 15 January, 2009b-last update, ocean color web [Homepage of NASA], [Online]. Available: http://oceancolor.gsfc.nasa.gov/ [January 23, 2009].

NAVALGUND, R.R., JAYARAMAN, V. and ROY, P.S., 2007. Remote sensing applications: an overview. *Current science,* **93**(12), 1747-1766.

NELSON, S.A.C., CHERUVELIL, K.S. and SORANNO, P.A., 2006. Satellite remote sensing of freshwater macrophytes and the influence of water clarity. *Aquatic Botany,* **85**(4), 291-300.

NEUMANN, A., DOERFFER, R., KRAWCZYK, H., DOWELL, M.D., ARNONE, R., DAVIS, C.O., KISHINO, M., TANAKA, A., HU, C., BUKATA, R.P., GORDON, H.R., CAMPBELL, J. and SATHYENDRANATH, S., 2000. Algorithms for case 2 waters. In: S. SATHYENDRANATH, ed, *Remote sensing of ocean colour in coastal, and other optically-complex, waters.* Dartmouth, Canada: International Ocean-Colour Coordinating Group, pp. 47.

OBERHOLSTER, P.J., BOTHA, A.M. and CLOETE, T.E., 2005. An overview of toxic freshwater cyanobacteria in South Africa with special reference to risk, impact and detection by molecular marker tools. *Biokemistri,* **17**(2), 57-71.

OBERHOLSTER, P.J., CLOETE, T.E., VAN GINKEL, C.E., BOTHA, A.M. and ASHTON, P.J., 2009. The use of remote sensing and molecular markers as early-warning indicators of the development of cyanobacterial hyperscum crust and microcystin-producing genotypes in the hypertrophic Lake Hartebeespoort, South Africa. Report edn. Pretoria: CSIR Natural Resources and the Environment.

ODERMATT, D., HEEGE, T., NIEKE, J., KNEUBÜHLER, M. and ITTEN, K., 2008. Water quality monitoring for Lake Constance with a physically based algorithm for MERIS data. *Sensors*, **8**, 4582-4599.

OECD, 10 May, 2002-last update, eutrophication of waters: monitoring, assessment and control [Homepage of Soil & Water Conservation Society of Metro Halifax], [Online]. Available: http://www.chebucto.ns.ca/ccn/info/Science/SWCS/TPMODELS/OECD/oecd.html [27 May, 2008].

OGUNFOWOKAN, A.O., OKOH, E.K., ADENUGA, A.A. and ASUBIOJO, O.I., 2005. An assessment of the impact of point source pollution from a university sewage treatment oxidation pond on a receiving stream - a preliminary study. *Journal of Applied Sciences*, **5**(1), 36-43.

ONDERKA, M. and PEKAROVA, P., 2008. Retrieval of suspended particulate matter concentrations in the Danube River from Landsat ETM data. *Science of the Total Environment*, **397**(1-3), 238-243.

ÖSTLUND, C., FLINK, P., STROMBECK, N., PIERSON, D. and LINDELL, T., 2001. Mapping of the water quality of Lake Erken, Sweden, from imaging spectrometry and Landsat Thematic Mapper. *The Science of the total environment*, **268**(1-3), 139-154.

PAERL, H.W., 1991. Growth and reproductive strategies of freshwater blue-green algae (cyanobacteria). In: C.D. SANDGREN, ed, *Growth and reproductive strategies of frewshwater phytoplankton.* 1st edn. Cambridge: Cambridge University Press, pp. 261-315.

PAL, S.R. and MOHANTY, P.K., 2002. Use of IRS-1B data for change detection in water quality and vegetation of Chilka lagoon, east coast of India. *International Journal of Remote Sensing*, **23**(6), 1027-1042.

PÁPISTA, É., ÁCS, É. and BÖDDI, B., 2002. Chlorophyll-a determination with ethanol–a critical test. *Hydrobiologia*, **485**(1), 191-198.

PARSONS, R. and HARDING, B., 2002. The role of groundwater in determining the quantity and quality on inflows to a hypertrophic wetland system, 2002, DH Environmental Consulting.

PEGAU, S., ZANEVELD, J.R.V., MITCHELL, B.G., MUELLER, J.L., KAHRU, M., WIELAND, J. and STRAMSKA, M., 2003. Inherent optical properties: instruments, characterizations, field measurements and data analysis protocols. In: J.L. MUELLER, G.S. FARGION and C.R. MCCLAIN, eds, *Ocean Optics Protocols For Satellite Ocean Color Sensor Validation, Revision 4, Volume IV*. Goddard Space Flight Space Center, Greenbelt, Maryland: National Aeronautical and Space Administration, pp. 39-65.

PIERSON, D., ALBEROTANZA, L., FERRO, G., KUTSER, T., PROFETI, G., RAMASCO, C. and STROMBECK, N., 1999. Optical analysis of water. In: T. LINDELL, D. PIERSON, G. PREMAZZI and E. ZILIOLI, eds, *Manual for monitoring European lakes using remote sensing techniques.* 1st edn. Luxembourg: European communities, pp. 29.

POPE, R.M. and FRY, E.S., 1997. Absorption spectrum (380-700 nm) of pure water. II. Integrating cavity measurements. *Applied Optics,* **36**(33), 8710-8723.

POSTEL, S.L., 2000. Entering and era of water scarcity: the challanges ahead. *Ecological Applications,* **10**(4), 941-948.

PREISENDORFER, R.W., 1976. Hydrologic Optics. 1st edn. Honolulu: U.S. Dept of Commerce, NOAA, ERL, Pacific Marine Environmental Laboratory.

PRIYADARSHI, N., 2005. Cultural eutrophication. In: J. LEHR and J. KEELEY, eds, *Water Encyclopedia: Surface and agricultural water.* New Jersey: John Wiley & Sons, pp. 114.

QUICK, A.J.R. and JOHANSSON, A.R., 1992. User assessment survey of a shallow fresh-water lake, Zeekoevlei, Cape-Town, with particular emphasis on water-quality. *Water Sa,* **18**(4), 247-254.

REES, G., 2001. Physical principles of remote sensing. 2nd edn. Cambridge: Cambridge University Press.

REINART, A. and KUTSER, T., 2006. Comparison of different satellite sensors in detecting cyanobacterial bloom events in the Baltic Sea. *Remote Sensing of Environment,* **102**(1-2), 74-85.

REPUBLIC OF SOUTH AFRICA, 1998. National Water Act. 1st edn. Cape Town: Republic of South Africa.

REVENGA, C., BRUNNER, J., HENNINGER, N., PAYNE, R. and KASSEM, K., 2000. *Pilot analysis of global ecosystems: freshwater systems.* Washington, DC: World Resources Institute.

REVENGA, C., CAMPBELL, I., ABELL, R., DE VILLIERS, P. and BRYER, M., 2005. Prospects for monitoring freshwater ecosystems towards the 2010 targets. *Philosophical Transactions of the Royal Society B-Biological Sciences,* **360**(1454), 397-413.

RICHARDSON, L.L., 1996. Remote Sensing of Algal Bloom Dynamics. *Bioscience,* **46**(7), 492-501.

ROBARTS, R.D. and ZOHARY, T., 1984. Microcystis aeruginosa and underwater light attenuation in a hypertrophic lake (Hartbeespoort Dam, South Africa). *Journal of Ecology,* **72**(3), 1001-1017.

ROBINSON, I.S. and MITCHELSON, E.G., 1983. Satellite observations of ocean colour [and discussion]. *Philosophical Transactions of the Royal Society of London. Series A, Mathematical and Physical Sciences (1934-1990),* **309**(1508), 415-432.

ROELKE, D. and BUYUKATES, Y., 2001. The diversity of harmful algal bloom-triggering mechanisms and the complexity of bloom initiation. *Human and Ecological Risk Assessment,* **7**(5), 1347-1362.

RUDDICK, K., DE CAUWER, V., PARK, Y., BECU, G., DE BLAUWE, J.P., DE VREKER, E., DESCHAMPS, P.Y., KNOCKAERT, M., NECHAD, B. and POLLENTIER, A., 2003. Preliminary validation of MERIS water products for Belgian coastal waters, ANONYMOUS, ed. In: *Proceedings of Envisat Validation Workshop (ESA SP-531), 9 - 13 December 2002 ESRIN, Frascati, Italy,* 2003, ESA pp1-15.

SANTER, R. and SCHMECHTIG, C., 2000. Adjacency effects on water surfaces: primary scattering approximation and sensitivity study. *Applied Optics,* **39**(3), 361-375.

SANTER, R. and ZAGOLSKI, F., 2008. *Improve Contrast between Ocean and Land (ICOL): Algorithm Theoretical Basis Document (ATBD): The MERIS Level-1C.* France: Université du Littoral Côte d'Opale, ADRINORD.

SARTORY, D.P. and GROBBELAAR, J.U., 1984. Extraction of chlorophyll a from freshwater phytoplankton for spectrophotometric analysis. *Hydrobiologia,* **114**(3), 177-187.

SATHYENDRANATH, S., 2000. General introduction. In: S. SATHYENDRANATH, ed, *Remote sensing of ocean colour in coastal, and other optically complex, waters.* Dartmouth, Canada: Reports of the International Ocean-Colour Coordinating Group, IOCCG, No. 3, pp. 1.

SATHYENDRANATH, S., BUKATA, R.P., ARNONE, R., DOWELL, M.D., DAVIS, C.O., BABIN, M., BERTHON, J.F., KOPELEVICH, O.V. and CAMPBELL, J.W., 2000. Colour of case 2 waters. In: S. SATHYENDRANATH, ed, *Remote sensing of ocean colour in coastal, and other optically-complex, waters.* Dartmouth, Canada: Reports of the International Ocean-Colour Coordinating Group, No. 3, IOCCG, pp. 23.

SCHALLES, J.F., GITELSON, A.A., YACOBI, Y.Z. and KROENKE, A.E., 1998. Estimation of chlorophyll a from time series measurements of high spectral resolution reflectance in an eutrophic lake. *Journal of Phycology,* **34**(2), 383-390.

SCHILLER, H. and DOERFFER, R., 1999. Neural network for emulation of an inverse model operational derivation of Case II water properties from MERIS data. *International Journal of Remote Sensing,* **20**(9), 1735-1746.

SCHILLER, H. and DOERFFER, R., 2005. Improved determination of coastal water constituent concentrations from MERIS data. *IEEE Transactions on Geoscience and Remote Sensing,* **43**(7), 1585-1591.

SCHINDLER, D.W., 2006. Recent advances in the understanding and management of eutrophication. *Limnology and Oceanography,* **51**(1), 356-363.

SCOTT, W.E., 1991. Occurrence and significance of toxic cyanobacteria in southern Africa. *Water Science and Technology,* **23**(1-3), 175-180.

SHAPIRO, S.S., WILK, M.B. and CHEN, H.J., 1968. A comparative study of various tests for normality. *Journal of the American Statistical Association,* **63**(324), 1343-1372.

SHAW, G. and WHEELER, D., 1994. Statistical techniques in geographical analysis. 2nd edn. London: David Fulton.

SIMIS, S.G.H., RUIZ-VERDU, A., DOMINGUEZ-GOMEZ, J.A., PENA-MARTINEZ, R., PETERS, S.W.M. and GONS, H.J., 2007. Influence of phytoplankton pigment composition on remote sensing of cyanobacterial biomass. *Remote Sensing of Environment,* **106**(4), 414-427.

SINGH, D.P., TYAGI, M.B., KUMAR, A., THAKUR, J.K. and KUMAR, A., 2001. Antialgal activity of a hepatotoxin-producing cyanobacterium, Microcystis aeruginosa. *World Journal of Microbiology & Biotechnology,* **17**(1), 15-22.

SIVONEN, K. and JONES, G., 1999. Cyanobacterial toxins. In: I. CHORUS and J. BARTRAM, eds, *Toxic cyanobacteria in water: a guide to their public health consequences, monitoring and management.* 1st edn. London: E & FN Spon, pp. 55-124.

SMITH, V.H., JOYE, S.B. and HOWARTH, R.W., 2006. Eutrophication of freshwater and marine ecosystems. *Limnology and Oceanography,* **51**(1), 351-355.

SONDERGAARD, M. and JEPPESEN, E., 2007. Anthropogenic impacts on lake and stream ecosystems, and approaches to restoration. *Journal of Applied Ecology*, **44**(6), 1089-1094.

SONG, C., WOODCOCK, C., SETO, K.C., LENNEY, M.P. and MACOMBER, S.A., 2001. Classification and change detection using Landsat TM Data- When and how to correct atmospheric effects? *Remote Sensing of Environment,* **75**(2), 230-244.

SOUTHERN WATERS ECOLOGICAL RESEARCH AND CONSULTING, 2000. Zeekoevlei/Rondevlei rehabilitation study: final report. Cape Town: DH Environmental Consulting.

STARK, R., PILLAY, G., HASKINS, C., BRAUN, O., MARGALIT, N. and MOSES, G., 2006. The use of airborne hyper-spectral remote sensing for environmental related topics in the vacinity of the greater Cape Town area, South Africa. unpublished edn. Haifa, Israel: Remote sensing applications for a sustainable future.

STRAMSKI, D., BRICAUD, A. and MOREL, A., 2001. Modeling the inherent optical properties of the ocean based on the detailed composition of the planktonic community. *Applied Optics,* **40**(18), 2929–2945.

STRAMSKI, D. and PISKOZUB, J., 2003. Estimation of scattering error in spectrophotometric measurements of light absorption by aquatic particles from three-dimensional radiative transfer simulations. *Applied Optics,* **42**(18), 3634-3646.

STRÖMBECK, N., CANDIANI, G., GIARDINO, C. and ZILIOLI, E., 2004. Water quality monitoring of Lake Garda using multi-temporal MERIS data, H. LACOSTE, ed. In: *Proceedings of MERIS User Workshop (ESA SP-549) 10-13 November 2003, Frascati, Italy,* 2004, ESA-ESRIN ppp. 17.1.

SUDHEER, K.P., CHAUBEY, I. and GARG, V., 2006. Lake water quality assessment from Landsat thematic mapper data using neural network: An approach to optimal band combination selection. *Journal of the American Water Resources Association,* **42**(6), 1683-1695.

SVÁB, E., TYLER, A.N., PRESTON, T., PRÉSING, M. and BALOGH, K.V., 2005. Characterizing the spectral reflectance of algae in lake waters with high suspended sediment concentrations. *International Journal of Remote Sensing,* **26**(5), 919-928.

THIEMANN, S. and KAUFMANN, H., 2000. Determination of chlorophyll content and trophic state of lakes using field spectrometer and IRS-1C satellite data in the Mecklenburg lake district, Germany. *Remote Sensing of Environment,* **73**(2), 227-235.

TONG, S.T.Y. and CHEN, W.L., 2002. Modeling the relationship between land use and surface water quality. *Journal of environmental management,* **66**(4), 377-393.

TU, J., XIA, Z.G., CLARKE, K.C. and FREI, A., 2007. Impact of urban sprawl on water quality in eastern Massachusetts, USA. *Environmental management,* **40**(2), 183-200.

TYLER, A.N., SVAB, E., PRESTON, T., PRÉSING, M. and KOVÁCS, W.A., 2006. Remote sensing of the water quality of shallow lakes: A mixture modelling approach to quantifying phytoplankton in water characterized by high-suspended sediment. *International Journal of Remote Sensing,* **27**(8), 1521-1537.

U.S. GEOLOGICAL SURVEY, 2005. Water Quality. In: J. LEHR and J. KEELEY, eds, *Water encyclopedia.* New Jersey: John Wiley & Sons, pp. 316.

U.S. GEOLOGICAL SURVEY, 23 June 2008, 2008-last update, earth observing 1 (EO 1) sensors [Homepage of U.S. Geological Survey], [Online]. Available: http://eo1.usgs.gov/sensors.php [January 23, 2009].

UNESCO, 2003. *Water for people, water for life: The United Nations world water development report.* Barcelona: United Nations Educational, Scientific and Cultural OrganiZation (UNESCO) and Berghahn Books.

VAN DEN HOEK, C., MANN, D.G. and JAHNS, H.M., 1995. Algae : an introduction to phycology. Cambridge: Cambridge University Press.

VAN GINKEL, C.E., 2002. *Trophic status assessment: executive summary.* Pretoria: South African Department of Water Affairs and Forestry.

VAN GINKEL, C.E., 2004. *A national survey of the incidence of cyanobacterial blooms and toxin production in major impoundments.* N/0000/00/DEQ/0503. Pretoria: South African Department of Water Affairs and Forestry.

VERMOTE, E.F., TANRE, D., DEUZE, J.L., HERMAN, M. and MORCETTE, J.J., 1997. Second Simulation of the Satellite Signal in the Solar Spectrum, 6S: an overview. *Geoscience and Remote Sensing, IEEE Transactions on,* **35**(3), 675-686.

VIDOT, J. and SANTER, R., 2005. Atmospheric correction for inland waters-application to SeaWiFS. *International Journal of Remote Sensing,* **26**(17), 3663-3682.

VINCENT, R.K., QIN, X.M., MCKAY, R.M.L., MINER, J., CZAJKOWSKI, K., SAVINO, J. and BRIDGEMAN, T., 2004. Phycocyanin detection from LANDSAT TM data for mapping cyanobacterial blooms in Lake Erie. *Remote Sensing of Environment,* **89**(3), 381-392.

VISSER, P.M., IBELINGS, B.W., MUR, L.R. and WALSBY, A.E., 2005. The ecophysiology of the harmful cyanobacterium *microcystis*. In: J. HUISMAN, H.C.P. MATTHIJS and P.M. VISSER, eds, *Harmful cyanobacteria.* Netherlands: Springer, pp. 109-142.

VOLLENWEIDER, R.A., 1968. *Scientific fundementals of the eutrophication of lakes and flowing waters, with particular reference to nitrogen and phosphorusas factors in eutrophication.* DAS/CSI/68.27. Paris: Organisation for Economic Co-operation and Development.

VOS, R.J., HAKVOORT, J.H.M., JORDANS, R.W.J. and IBELINGS, B.W., 2003. Multiplatform optical monitoring of eutrophication in temporally and spatially variable lakes. *The Science of The Total Environment,* **312**(1-3), 221-243.

WALMSLEY, R.D. and THORNTON, J.A., 1984. Evaluation of Oecd-Type Phosphorus Eutrophication Models for Predicting the Trophic Status of Southern African Man-made Lakes. *South African Journal of Science,* **80**(6), 257-259.

WALMSLEY, R.D., 2003. *Project report: phase 1: development of a strategy to control eutrophication in South Africa.* Pretoria: Mzuri Consultants.

WALTERS, N.M., KOK, C.J. and CLAASE, C., 1985. Optical properties of the South African marine environment. In: L.V. SHANNON, ed, *South African ocean colour and upwelling experiment.* Cape Town, South Africa: Sea Fisheries Research Institute, pp. 157.

WANG, F., HAN, L., KUNG, H.T. and VAN ARSDALE, R.B., 2006. Applications of Landsat-5 TM imagery in assessing and mapping water quality in Reelfoot Lake, Tennessee. *International journal of remote sensing,* **27**(23-24), 5269-5283.

WANG, X.J. and MA, T., 2001. Application of remote sensing techniques in monitoring and assessing the water quality of Taihu Lake. *Bulletin of environmental contamination and toxicology,* **67**(6), 863-870.

WANG, Y., XIA, H., FU, J. and SHENG, G., 2004. Water quality change in reservoirs of Shenzhen, China: detection using LANDSAT/TM data. *The Science of the total environment,* **328**(1-3), 195-206.

WETZEL, R.G., 1983. Limnology. 2nd edn. Fort Worth: Saunders College Publishing.

WHITE, S.H., DUIVENVOORDEN, L.J. and FABBRO, L.D., 2005. Impacts of a toxic Microcystis bloom on the macroinvertebrate fauna of Lake Elphinstone, Central Queensland, Australia. *Hydrobiologia,* **548**, 117-126.

WICKS, R.J. and THIEL, P.G., 1990. Environmental factors affecting the production of peptide toxins in floating scums of the cyanobacterium Microcystis aeruginosa in a hypertrophic African reservoir. *Environmental science & technology,* **24**(9), 1413-1418.

WIECHERS, H.N.S. and HEYNIKE, J.J.C., 1986. Sources of phosphorus which give rise to eutrophication in South-African waters. *Water Sa,* **12**(2), 99-102.

XING, P., KONG, F.X., CAO, H.S., ZHANG, M. and TAN, X., 2007. Variations of bacterioplankton community composition during Microcystis spp. blooms in a shallow eutrophic lake. *Journal of Freshwater Ecology,* **22**(1), 61-67.

YACOBI, Y.Z., GITELSON, A. and MAYO, M., 1995. Remote sensing of chlorophyll in Lake Kinneret using highspectral-resolution radiometer and Landsat TM: spectral features of reflectance and algorithm development. *Journal of Plankton Research,* **17**(11), 2155-2173.

ZIMBA, P.V. and GITELSON, A., 2006. Remote estimation of chlorophyll concentration in hyper-eutrophic aquatic systems: Model tuning and accuracy optimization. *Aquaculture,* **256**(1-4), 272-286.

ZURAWELL, R.W., CHEN, H.R., BURKE, J.M. and PREPAS, E.E., 2005. Hepatotoxic cyanobacteria: A review of the biological importance of microcystins in freshwater environments. *Journal of Toxicology and Environmental Health-Part B-Critical Reviews,* **8**(1), 1-37.

Appendix 1

Review of Remote Sensing Studies for Deriving Water Quality Parameters in Inland and Coastal Case 2 Waters

Year	*Country*	*Study area*	*Data type*[1]	*Atmospheric correction*	*WQPs*[2]	*Data range*[3]	*Statistical technique*	*Bands/algorithm*[4]	r^2	*RMSE*[5] *(%)*	*N*	*Reference*
Studies using MERIS or simulated MERIS bands												
2008	Germany	Lake Constance	MERIS	MIP	Chl *a*	0 - 20	Analytical	MIP	0.79	-	8	Odermatt et al., 2008
					TSS	0 - 10	Analytical	MIP	-	-	-	
					a_{CDOM}	0 - 0.3	Analytical	MIP	-	-	-	
2007	Netherlands; Spain	59 Lakes	Sl. Spec.	Empirical	PC	~0 - 1100	Semi-analytical	R709/R620	0.90	-	223	Simis et al., 2007
2006	South Africa	Southern Benguela	Sl. Spec.	None	Chl *a*	1 - 300	NLR	L665/L709	0.87	-	65	Bernard et al., 2006
2006	Gulf of Finland	Baltic Sea	MERIS	None	Chl *a*	22 - 95	LR	L709/L665	0.87	22	51	Koponen et al., 2007
					TSS	2.9 - 12	LR	L709/(L560+L665)	0.92	16	51	
					a_{CDOM}	1.29 - 2.15	LR	L665/L490	0.96	5	51	
2006	Finland	Baltic Sea	MERIS	MERIS Level 2	Chl *a*	2.8 - 16.0	Analytical	algal_2 Neural Network algorithm	-	-	-	Reinart & Kutser, 2006
2005	Italy	Lake Guarda	Sl. MIVIS	None	Chl *a*	3.5 - 8.9	LR	(L440-L780)/ (L480-L700)	0.69	9	22	Giardino et al., 2005
			MERIS	None	Chl *a*	0.2 - 2.5	LR	L489	0.83	26	31	
2005	Italy	Lake Guarda	MERIS	6S, DDV	Chl *a*	~2 - 11	LR	L560/L665	0.49	1.20mg.m^{-3}	7	Candiani et al., 2005
2004	Italy	Lake Garda	MERIS	Empirical	Chl *a*	0.7-2.5	Polynomial	L620/L709	0.76	0.27mg.m^{-3}	12	(Strömbeck et al., 2004)
2004	Austria; Italy	4 Austrian Lakes; Lake Guarda	MERIS	6S	Chl *a*	1.0 - 5.6	LR	L665/L560	0.75	0.66mg.m^{-3}	29	Floricioiu et al., 2004
2003	Austria	3 Austrian Lakes	Sl. ROSIS	6S	Chl *a*	1.42 - 5.17	LR	L620/L490 + L560/L510	0.93	1.0mg.m^{-3}	13	Floricioiu et al., 2003
2003	Finland	Lake Hiidenvesi	Sl. AISA	None	Chl *a*	6 - 44	LR	L705/L662	0.98	11.1	12	Kallio et al., 2003
2002	Netherlands	Ijssel Lagoon	Sl. Spec.	None	Chl *a*	3 - 185	LR	L708/L664	0.96	8.3mg.m^{-3}	114	Gons et al., 2002, 2005
2002	Finland	Finnish Lakes	Sl. AISA	None	Chl *a*	1.3 - 100	LR	(L700-L781)/ (L662-L781)	0.94	-	80	Koponen et al., 2002
					SD	0.4 - 7.0	LR	(L521-L781)/ (L700-L781)	0.93	-	102	
					TURB	0.4 - 26 FNU	LR	L714	0.85	-	99	
2002	Sweden	Lake Märalen	Sl. CASI	6S	Chl *a*	2.5 - 18.9	Semi-analytical	R705/R664	0.88	-	570	Ammenberg et al., 2002
					SPIM	0.5 - 2.3	Semi-analytical	R705/R664	0.83	0.34mg.m^{-3}	570	
					a_{CDOM}	1.13 - 2.07	Semi-analytical	R664/R550	-	-	2	
2001	Sweden	Lakes Erken and Märalen	Sl. CASI	6S	Chl *a*	2.9 - 50.6	LR	R550	0.94	-	13	Flink et al., 2001

Year	*Country*	*Study area*	*Data type*[1]	*Atmospheric correction*	*WQPs*[2]	*Data range*[3]	*Statistical technique*	*Bands/algorithm*[4]	r^2	*RMSE*[5] *(%)*	*N*	*Reference*
					Chl *a*	2.9 - 50.7	LR	R708/R678	0.84	-	13	
					Chl *a*	2.9 - 50.8	MLR	R708/R678 + R643/R628	0.87	-	13	
					Chl *a*	2.9 - 50.9	PCA; MLR	PC1 + PC2 + PC3 + PC4	0.96	-	13	
2001	Finland	Lakes	Sl. AISA	None	Chl *a*	1.3 - 100	LR	(L705-L754)/ (L665-L754)	0.9	37	85	Härmä et al., 2001
					TSS	0.7 - 23	LR	L705-L754	0.81	34	67	
					SD	0.4 - 7.0	LR	(L490-L754)/ (L620-L754)	0.83	35	85	
2001	Finland	11 Lakes	Sl. AISA	MODTRAN	Chl *a*	1 - 100	LR	L702/L674	0.91	29	88	Kallio et al., 2001
					TSS	0.7 - 32	LR	R710	0.85	32	74	
					SD	0.4 - 7	LR	(L492-L751)/ (L622-L751)	0.86	30	103	
					a_{CDOM}	1.2 - 14	LR	(L571-L607)/L607	0.84	20	47	
					TURB	0.4 - 26 FNU	LR	R710	0.93	23	105	
Studies using Landsat and SPOT												
2008	Slovakia	Danube River	LS 7 ETM+	None	TSS	19.5 - 57.5	LR	etm4	0.93	1.79mg.l^{-1}	10	Onderka & Pekárová, 2008
2008	Taiwan	Feitsui Reservoir	LS 7 ETM+	None	Chl *a*	0.48 - 4.02	MLR	etm1; etm2; etm3; etm4; etm5; etm7	0.68	0.37mg.m^{-3}	24	Chen et al., 2008
					Chl *a*	0.48 - 4.03	GEGA	etm1; etm4; etm5; etm7	0.79	0.30mg.m^{-3}	24	
2007	Turkey	Ömerli Dam	LS 7 ETM+	DOS	Chl *a*	1.2 - 2.5	MLR	etm1 + etm2 + etm3 + etm4	0.58	49	6	Alparslan et al., 2007
					TSS	0.4 - 2.9	MLR	etm1 + etm2 + etm3 + etm5	0.99	1	6	
					SD	2.5 - 3.4	MLR	etm1 + etm2 + etm3 + etm6	0.99	2	6	
2007	China	Lake Chagan	LS TM	None	Chl *a*	6.3 - 58.2	LR	tm4/tm3	0.67	2.06mg.m^{-3}	20	Duan et al., 2007
			Spec.	None	Chl *a*	6.3 - 58.2	LT-LR	Ln(R700/R670)	0.75	-	54	
2006	US	Reelfoot Lake	LS 5 TM	Radiometric	Chl *a*	66 - 189	MLR	tm2; tm3	0.71	-	18	Wang et al., 2006
					TSS	11.5 - 33.5	MLR	tm2; tm3; tm4	0.52	-	18	
					SD	16 - 33	MLR	tm2; tm3	0.59	-	18	
					TURB	20.0 - 4.1	MLR	tm2; tm3	0.54	-	18	
2006	Central Europe	Lake Balaton	LS TM; ETM+	DOS	Chl *a*	~ 5 - 115	LMM	tm1; tm2; tm3 OR etm1; etm2; etm3	0.95	-	11	Tyler et al., 2006

Year	*Country*	*Study area*	*Data type*[1]	*Atmospheric correction*	*WQPs*[2]	*Data range*[3]	*Statistical technique*	*Bands/algorithm*[4]	r^2	*RMSE*[5] *(%)*	*N*	*Reference*
					TSS	~ 5 - 50	LR	tm3	0.89	-	11	
2006	US	Beaver Reservoir	LS TM	None	Chl *a*	~1.7 - 10	ANN; LR	tm1; tm2	0.54	12.34mg.m^{-3}	~25	Sudheer et al., 2006
					TSS	~0 - 11.5	ANN; LR	tm1; tm2; tm3; tm4	0.98	2.02mg.m^{-3}	~25	
2005	Central Europe	Lake Balaton	Sl. Spec.	None	TSS	2 - 40.5	LR	tm2/tm3	0.88	-	10	Svab et al., 2005
2005	US	Pensacola Bay	LS 7 ETM+	Radiometric	Chl *a*	1.1 - 23.2	LT-LR	Log etm1/log etm3	0.67	19	16	(Han & Jordan, 2005)
2005	US	15 Minnesota Lakes	LS TM	None	Chl *a*	2.1 - 279	LT-MLR	tm1 + tm1/tm3	0.88	-	15	Brezonik et al., 2005
					TURB	0.3 - 155	LT-MLR	tm3	0.84	-	15	
					SD	0.15 - 4.4	LT-MLR	tm1 + tm1/tm3	0.91	-	39	
					a_{CDOM}	0.6 - 19.4	LT-MLR	tm1 + tm1/tm4	0.77	-	15	
2004	China	Shenzhen Reservoirs	LS TM	DOS	TOC	~ 3.0 - 5.3	MLR	tm1; tm2; tm3; tm4	0.83	25	40	Wang et al., 2004
					COD	~ 2.5 - 3.7	MLR	tm1; tm2; tm3;	0.63	30	42	
					BOD	~ 3.3 - 4.7	MLR	tm1; tm2; tm3;	0.71	24	42	
2004	Taiwan	Techi Reservoir	LS TM	DOS	Cell density	~ 50 - 2400	LT-MLSR	tm1; tm2; tm3; tm4	0.73	-	120	Chang et al., 2004
2004	US	Lake Erie	LS 5 TM	DOS	PC	~ 7.5 - 19	MLR	tm1; tm2; tm3; tm4; tm5	0.63	-	20	Vincent et al., 2004
			LS 7 ETM+	DOS	PC	~ 0.9 - 4.9	MLR	etm1; etm2; etm3; etm4; etm5	0.78	15	30	
					TURB	~ 14.2 - 1.3	MLR	etm3/etm2	0.85	9	30	
2004	US	New York Harbour	LSTM	Radiometric	SD	~ 0.45 - 2	LT-LR	Log tm3	0.85	-	21	Hellweger et al., 2004
					Chl *a*	~ 5 - 50	LT-LR	Log(tm2/tm3)	0.78	-	16	
2002	Netherlands	Southern Frisian Lakes	SPOT HRV; LS 5 TM	MODTRAN-3	TSS	3 - 411	Analytical	(tm2 + tm3)/2 OR (XS1 + XS2)/2	0.99	-	-	Dekker et al., 2002
2001	Southern Finland	Lakes	Sl. AISA	None	TSS	0.7 - 23	LT-LR	(tm1-tm4)/ (tm3-tm4)	0.73	52	67	Härmä et al., 2001
					SD	0.4 - 7.0	LR	(tm1-tm4)/ (tm3-tm4)	0.81	34	85	
2001	Sweden	Lake Erken	LS TM	6S	Chl *a*	2.1 - 27.4	CHROM	tm1/tm1+tm2+tm3	0.93	-	19	Östlund et al., 2001
					Chl *a*	2.1 - 27.4	LT-LR	Log(tm1/tm2)	0.88	-	19	
					TSS	1.45 - 5.25	LR	tm1	0.95	-	19	
2001	Italy	Lake Iseo	LS TM	DOS	Chl *a*	5.5 - 7.7	LR	tm1; tm2	0.99	5.4	4	Giardino et al., 2001
					SD	4.6 - 6.8	LR	tm1/tm2	0.85	45	4	

Year	*Country*	*Study area*	*Data type*[1]	*Atmospheric correction*	*WQPs*[2]	*Data range*[3]	*Statistical technique*	*Bands/algorithm*[4]	r^2	*RMSE*[5] *(%)*	*N*	*Reference*
2001	Italy	Lake Guarda	LS TM	RTC - DOS	Chl *a*	3.0 - 6.0	LR	(tm1 - tm3)/tm2	0.82	37	5	Brivio et al., 2001
					Chl *a*	1.9 - 3.2	LT-MLR	Ln tm1 - Ln tm2	0.68	49	5	
2001	China	Lake Taihu	LS TM	None	TSS	10 - 107	LT-MLR	Ln(tm3 + tm4)/ (tm1 + tm2)	-	-	15	Wang & Ma, 2001
					SD	0.2 - 0.5	PCA	Lntm1; Lntm2; Lntm3; Lntm5; Lntm7	-	-	15	
1996	Israel	Haifa Bay	Sl. Spec.	None	Chl *a*	2 - 70	LT-LR	Log(tm3/tm1)	0.74	-	18	(Gitelson et al., 1996)
1996	Israel	4 wastewater reservoirs	SPOT	LOWTRAN 7	Chl *a*	1.3 - 1600	BOM;PCA	XS1; XS2; XS3	-	-	4	Dor & Ben-Yosef, 1996
					TSS	2 - 195	BOM;PCA	XS1; XS2; XS3	-	-	4	
1995	Israel	Lake Kinneret	Spec.	None	Chl *a*	5.1 - 185	LR	Rmax./R670	0.95	3.4	41	Yacobi et al., 1995
					Chl *a*	5.1 - 186	LR	$RLH_{660-850}$	0.96	3.2	41	
			LS TM	RTC	Chl *a*	5.1 - 187	LR	tm4/tm3	0.79	4	40	
1989	US	Lake Michigan	SPOT HRV	Radiometric	SD	0.6 - 2.0	LT-LR	XS3	0.83	20	11	Lanthrop & Lillesand, 1989
					TURB	11.9 - 1.2	LT-LR	(XS2/XS1) + XS3	0.88	29	11	
					TSS	4.6 - 28.9	LT-LR	(XS2/XS1) + XS3	0.93	19	11	
1986	US	Lake Michigan	LS TM	None	Chl *a*	1.0 - 50.3	LT-LR	Ln tm2	0.98	1.04mg.m^{-3}	13	Lanthrop & Lillesand, 1986
					SD	0.5 - 9	LT-LR	Ln tm2	0.98	1.05m	9	
					TURB	12 - 0.54	LT-LR	Ln tm3	0.99	1.04NTU	13	
Studies using radiometric and other satellite and airborne sensors												
2007	US	Charles River	IKONOS	None	TURB	1.9 - 7.3	LR	$DN_{632-698}$	0.7	-	3084	Hellweger et al., 2007
2007	Italy	Lake Guarda	Hyperion	MODTRAN	Chl *a*	1.30 - 2.16	Analytical	Matrix inversion algorithm	0.59	20	8	Giardino et al., 2007
					TURB	0.95 - 2.13	Analytical	Matrix inversion algorithm	0.57	31	7	
2007	US	Tampa Bay	MODIS	RTC	TURB	0.9 - 8.0	LR	R645	0.73	-	43	Chen et al., 2007
2006	US	Aquaculture ponds	Spec.	None	Chl *a*	107 - 3078	LR	(R740/R710)-(R740/R650)	0.78	319mg.l^{-3}	~64	Zimba & Gitelson, 2006
2006	China	Lake Tai	Spec.	Empirical	Chl *a*	20 - 190	NLR	R719/R667	0.87	-	28	Jiao et al., 2006
2006	US	15 Minnesota Lakes	Spec.	None	Chl *a*	1.8 - 397	NLR	R700/R670	0.99	-	15	Menken & Brezonik, 2006
2005	Finland; Sweden	Many Lakes	ALI	ELM	a_{CDOM}	0.68 - 11.13	NLR	$L_{525-605}/L_{630-690}$	0.73	-	30	Kutser et al., 2005

Year	*Country*	*Study area*	*Data type*[1]	*Atmospheric correction*	*WQPs*[2]	*Data range*[3]	*Statistical technique*	*Bands/algorithm*[4]	r^2	*RMSE*[5] *(%)*	*N*	*Reference*
2004	Germany	Lake Constance	CHRIS	RTM	Chl *a*	1.4 - 4.4	Analytical	MIP	-	-	17	Miksa et al., 2004
					TSS	1.1 - 2.6	Analytical	MIP	-	-	17	
					a_{CDOM}	0.13 - 0.30	Analytical	MIP	-	-	17	
2004	Finland	Gulf of Finland	Hyperion; ALI	MODTRAN 4; ELM	Chl *a*	1 - 1024	SAM; BOM	-	-	-	-	Kutser, 2004
2004	Finland	Finnish Lakes	MODIS	None	Classes	1 - 4	Classifi-cation	$L_{620-670}$	0.8*	19.8%*	2039 1	Koponen et al., 2004
2004	US	Gulf of Mexico	MODIS	DOS	TSS	~1 - 55	LR	$L_{620-670}$	0.89	2.18mg.l^{-1}	52	Miller & McKee, 2004
2003	Australia	Moreton Bay	Hyperion	MODTRAN	Chl *a*	1.0 - 19.9	Analytical	Matrix inversion algorithm	-	-	-	Brando & Dekker, 2003
					a_{CDOM}	0.13 - 0.75	Analytical	Matrix inversion algorithm	-	-	-	
					TSS	3.4 - 46.3	Analytical	Matrix inversion algorithm	-	-	-	
2003	Netherlands	Lakes IJssel and Marken	SeaWiFS	SeaDAS	Chl *a*	~ 5 - 160	Analytical	2 step SeaWiFS algorithm	-	27	14	Vos et al., 2003
					TSS	~10 - 250	Analytical	3 step SeaWiFS algorithm	-	38	14	
2002	Netherlands	Lake Veluwe	Hyperspect ral scanner	MODTRAN	Chl *a*	6.4 - 10.6	Analytical	Matrix inversion algorithm	-	-	9	Hakvoort et al., 2002
					TSS	6.0 - 43.2	Analytical	Matrix inversion algorithm	-	-	9	
2000	Germany	Mecklenburg Lake District	LISS-III	MODTRAN	Chl *a*	~2 - 63	LSU	LISS1; LISS2; LISS3	0.85	3.6mg.m^{-3}	11	Thiemann & Kaufmann, 2000
1999	Netherlands	Lakes, rivers and estuaries	Spec.	None	Chl *a*	3 - 185	Semi-analytical	R704/R672	0.95	3mg.m^{-3}	114	Gons, 1999
1998	US	Nebraska Sand Hills Lakes	Spec.	Empirical	Chl *a*	1 - 171	MLR	dR429+dR695+(dR429*dR695)	0.5	-	19	(Fraser, 1998)
					TURB	1 - 82	MLR	dR429+dR628+d695	0.69	-	30	
1998	US	Carter Lake	Spec.	None	Chl *a*	20 - 280	LR	$RLH_{670-850}$	0.86	±5.3mg.m^{-3}	35	Schalles et al., 1998
					Chl *a*	21 - 280	LR	$SUM_{670-850}$	0.87	±5.3mg.m^{-4}	36	
1994	US	Tennessee Reservoirs	AMMS	None	Chl *a*	2 - 79	LR	R700/R680	0.95	2.19mg.m^{-3}	29	Dierberg & Carriker, 1994
					Chl *a*	2 - 79	LR	$FLH_{663-700}$	0.85	2.76mg.m^{-3}	29	
					TURB	1.1 - 11	LR	R700/R680	0.88	0.93NTU	29	
			CASI	None	Chl *a*	1 - 46	LR	L694/L679	0.84	2mg.m^{-3}	34	
					Chl *a*	1 - 46	LR	$SLH_{665-752}$	0.86	1.9mg.m^{-3}	34	

Year	*Country*	*Study area*	*Data type[1]*	*Atmospheric correction*	*WQPs[2]*	*Data range[3]*	*Statistical technique*	*Bands/algorithm[4]*	*r^2*	*RMSE[5] (%)*	*N*	*Reference*
					TURB	1.1 - 10	LR	L694/L679	0.77	1.0NTU	34	
1994	Israel	Lake Kinneret	Spec.	None	Chl *a*	3.1 - 7.3	LR	$SUM_{670-730}$	0.84	0.69mg.m^{-3}	20	Gitelson et al., 1994
					Chl *a*	3.1 - 7.3	LR	$FLH_{670-730}$	>0.73	0.77mg.m^{-3}	20	
1993	Europe	>20 Inland water bodies	Spec.	None	Chl *a*	0.1 - 350	NLR	R700/R675	>0.88	<2mg.m^{-3}	>383	Gitelson et al., 1993
					TSS	0.1 - 66	MLR	(R560-R520)/ (R560+R520)	0.86	1.79mg.l^{-1}	66	
					a_{CDOM}	0.1 - 12	MLR	((R480-R700/R675)-R520)/((R480+R700/R675)+R520))	0.9	0.25mgC.m^{-3}	-	
			Sl. LS MSS	None	Chl *a*	30 - 150	MLR	MSS6/MSS4+MSS5 +MSS6	0.88	<4.47mg.m^{-3}	134	
1992	*Germany*	*Laboratory, rivers and lakes*	*Spec.*	*None*	*Chl a*	*5 - 350*	*MLR*	*L705/L670*	*0.98*	-	*94*	Mittenzwey et al., 1992

Postscripts
* total classification accuracy/error.
[1]Sl. means simulated.
[2] WQPs = Water Quality Parameters
[3] Units for Chl a = mg.m^{-3}; TSS, SPIM = mg.l^{-1}; a_{CDOM} = m^{-1}; SD = m; TURB = NTU, unless otherwise indicated.
[4] Lx = radiance at wavelength x; Rx =reflectance at wavelength x; DN = Digital Number; Satellite bands are prefixed by the abbreviated sensor's name. Note: coefficients of determination and variables other than spectral bands have not been included. Only algorithms with highest performing correlation coefficients are presented.
[5] RMSE= Root Mean Square Error. In percentage unless otherwise indicated.

List of Abbreviations		
Data type	Chl *a* = Chlorophyll *a*	**Statistical technique**
AISA = Airborne Imaging Spectrometer for Applications	COD = Chemical Oxygen Demand	ANN = Artificial Neural Network
ALI = Advanced Land Imager	PC = Phycocyanin pigment	BOM =Bio-Optical Model
AMMS = Airborne Multispectral Measurement System	SD = Secchi Disk depth	CHROM = Chromaticity analysis
CASI = Compact Airborne Spectrographic Imager	SPIM = Suspended Particulate Inorganic Material	GEGA = Grammatical Evolution Genetic Algorithm
CHRIS = Compact High Resolution Imaging Spectrometer	TOC = Total Organic Carbon	LMM = Linear Mixture Modelling
DS-1260 MSS = Airborne Daedalus Multi Spectral Scanner	TSS = Total Suspended Solids	LR = Linear Regression
LS 7 ETM+ = Landsat 7 Enhanced Thematic Mapper	TURB = Turbidity	LSU = Linear Spectral Unmixing
LS TM = Landsat Thematic Mapper		LT-LR = Log-Transformed Linear Regression
LISS III = Linear Imaging Self-Scanning Sensor		LT-MLR = Log-Transformed Multiple Linear Regression
MERIS = Medium Resolution Imaging Spectrometer	**Atmospheric correction**	LT-MLSR = Log-Transformed Multiple Linear Stepwise Regression
MIVIS = Multispectral Infrared and Visible Imaging Spectrometer	6S = Second Simulation of the Satellite Signal in the Solar Spectrum (Vermote et al., 1997)	MIP = Modular Inversion and Processing System
MODIS = Moderate Resolution Imaging Spectrometer	DDV = Dense Dark Vegetation	MLR = Multiple Linear Regression
ROSIS = Reflective Optics System Imaging Spectrometer	DOS = Dark Object Subtraction	MLSR = Multiple Linear Stepwise Regression
SeaWiFS = Sea-viewing Wide Field-of-view Sensor	ELM = Empirical Line Method (Moran et al., 2001)	NLR =Non-Linear Regression
Spec. = Spectroradiometer	LOWTRAN = Low Resolution Atmospheric Transmittance Code	PCA = Principal Component Analysis
SPOT HRV = Le Systeme Pour l'Observation de la Terra High Resolution Visible	MODTRAN = Moderate Resolution Atmospheric Transmittance Code	SAM = Spectral Angle Mapper
	RTC = Radiative Transfer Code	UC = Unsupervised Classification
Water Quality Parameters (WQPs)		
a_{CDOM} = absorption by Coloured Dissolved Organic Matter		
BOD = Biological Oxygen Demand		